

This PDF was created from the British Library's microfilm copy of the original thesis. As such the images are greyscale and no colour was captured.

Due to the scanning process, an area greater than the page area is recorded and extraneous details can be captured.

This is the best available copy

D75209/87

Attention is drawn to the fact that the copyright of this thesis rests with its author.

This copy of the thesis has been supplied on condition that anyone who consults it is understood to recognise that its copyright rests with its author and that no quotation from the thesis and no information derived from it may be published without the author's prior written consent.

237

*

D75209/87

ANDREWS.D.A.

Plates
Clean Plates.

237

CITY OF LONDON Poly
(CNA)

**AN INVESTIGATION INTO THE USE OF GROUP VI ELEMENTS AS DOPANTS
IN III-V MATERIALS PREPARED BY MOLECULAR BEAM EPITAXY.**

by DAVID ARTHUR ANDREWS, M.Phil.

Submitted to the Council for National Academic Awards in
partial fulfilment of the requirements for the degree of Doctor
of Philosophy.

Study performed at British Telecom Research Laboratories in
conjunction with the City of London Polytechnic.

Submitted April 1987.

**AN INVESTIGATION INTO THE USE OF GROUP VI ELEMENTS AS DOPANTS
IN III-V MATERIALS PREPARED BY MOLECULAR BEAM EPITAXY.**

by D.A.ANDREWS.

ABSTRACT

An electrochemical cell Pt/Ag/AgI/Ag₂X/Pt (X=S,Se) has been used as a highly controllable source of S₂ or Se₂ molecules for n-type doping of GaAs and GaAlAs grown by Molecular Beam Epitaxy (MBE). This source produces a pure beam of chalcogen dimers at low temperature (200-300°C) and is simply programmed by an applied emf. The response time of the cell is of the order of one second enabling complicated doping profiles to be achieved.

The behaviour of S and Se generated in this way and incorporated into MBE GaAs and GaAlAs has been determined and is simple at low growth temperatures (<580°C). The dopant species are incorporated and electrically activated with constant high efficiency and behave simply as shallow donors as expected from their use in other areas of GaAs technology. No evidence for anomalous diffusion or segregation has been observed.

The incorporation reaction is described via the interaction of S and Se with arsenic vacancies within a thermodynamic framework. Calculation reveals that this incorporation reaction is strongly favoured under MBE growth conditions as observed, but extension of the model reveals that reactions resulting in the formation of volatile Ga₂S and Ga₂Se are also favoured. At elevated growth temperatures, the incorporation efficiency of S and Se into GaAs is observed to be reduced, and to a lesser extent in GaAlAs, although the loss of dopant may be overcome by increasing the incident chalcogen or arsenic flux. This behaviour is modelled in terms of the kinetic hindrance to volatile gallium chalcogenide formation at low temperature being overcome as the growth temperature is raised and the surface stoichiometry of the growing layer is changed. The thermodynamic model predicts that the Aluminium sub-chalcogenides should not be volatile under MBE conditions and explains the observed reduced loss in the case of GaAlAs.

Some results are presented on devices grown using S and Se doping of MBE layers where enhanced performance and novel properties are observed. These include a hyperabrupt varactor with a linear frequency-voltage characteristic and the observation of the integral and fractional quantised Hall effect in two-dimensional electron gas structures. The potential of chalcogen dopants as arsenic vacancy, and hence DX centre, getters is investigated and discussed. The facility with which sulphur and selenium may be incorporated into practical device structures, including heterostructures, is emphasised.

ACKNOWLEDGEMENTS

Acknowledgement is made to the Director of Research, British Telecom Research Laboratories for permission to publish this work and to Dr R.Heckingbottom for the provision of facilities in the Materials Division. Thanks are also due to Dr G.J.Davies of BTRL for his supervision of the MBE project and to Dr E.H.C.Parker of City of London Polytechnic for his encouragement and critical reading of the manuscript. Appreciation is also extended to the members of the MBE group at BTRL for helpful discussions, particularly Dr K.A.Prior for initiating the author into thermodynamics. Except where specifically acknowledged in the text, the work presented here is that of the author.

CONTENTS

Abstract.

Acknowledgements.

1	Introduction.	1
1.1	Molecular Beam Epitaxy.	1
1.2	Low Dimensional Structures.	3
1.3	MBE Dopants and Motivation for Studying the Chalcogens.	4
1.4	References.	10
2	Experimental.	12
2.1	Apparatus.	12
2.1.1	The MBE System.	12
2.1.2	The High Temperature Knudsen Cells.	15
2.2	Pre-Growth Procedures.	17
2.2.1	MB288 Operation.	17
2.2.2	Flux Calibrations.	18
2.2.3	Substrate Temperature Measurement.	19
2.2.4	Substrate Preparation.	20
2.3	Growth Procedures.	21
2.4	References.	24
3	Electrochemical Chalcogen Sources.	25
3.1	Introduction.	25

3.2	Principles of Operation.	25
3.3	Cell Construction.	30
3.4	Cell Performance.	32
3.5	References.	38
4	The Growth of High Purity GaAs.	39
4.1	Introduction.	39
4.2	Material Properties.	40
4.2.1	Morphology.	40
4.2.2	Background Carrier Concentration.	40
4.2.3	Deliberately Doped Material.	42
4.2.4	Electron Mobilities.	43
4.2.5	Luminescence Properties.	43
4.3	Conclusions.	45
4.4	References.	46
5	Thermodynamic Framework.	47
5.1	Introduction.	47
5.2	The Thermodynamic Method.	49
5.3	The Dopant Incorporation Model.	49
5.4	Dopant Incorporation Calculations.	53
5.4.1	The Simplest Case: Condensation.	53
5.4.2	VPE Extrapolation: Sulphur Doping of GaAs.	54
5.4.3	LPE Extrapolation: Tellurium Doping of GaAs.	56
5.4.4	Selenium Doping of GaAs.	58
5.4.5	Chalcogen Doping of InP.	59
5.5	Conclusions.	62
5.6	References.	63

6	Sulphur and Selenium Doping of MBE GaAs.	65
6.1	Introduction.	65
6.2	Material Properties.	65
6.3	Sulphur Incorporation Behaviour.	66
6.4	Selenium Incorporation Behaviour.	67
6.5	Discussion.	71
	6.5.1 Thermodynamic Model.	71
	6.5.2 Stability of Gallium Sulphides.	74
	6.5.3 Stability of Gallium Selenides and Tellurides.	78
	6.5.4 Kinetic Aspects.	80
6.6	Conclusions.	81
6.7	References.	83
7	Sulphur and Selenium Doping of MBE AlGaAs.	84
7.1	Introduction.	84
7.2	Experimental Results.	85
7.3	Discussion.	92
7.4	Summary of Reactions and Thermodynamic Predictions.	98
	7.4.1 Simplifying Assumptions.	98
	7.4.2 Gallium Sulphide Reactions.	99
	7.4.3 Gallium Selenide Reactions.	99
	7.4.4 Aluminium Sulphide Reactions.	100
	7.4.5 Aluminium Selenide Reactions.	100
7.5	Conclusions.	100
7.6	References.	102

8	Chalcogen Doped Devices.	103
8.1	Introduction.	103
8.2	Hyperabrupt Varactor Diode.	103
8.3	Guided Wave Devices.	105
8.4	Laser Structures.	107
8.5	Low Dimensional Structures.	108
8.6	Postscript on DX Centres.	112
8.7	Conclusions.	113
8.8	References.	114
9	Conclusions and Suggestions for Further Work.	116
9.1	Conclusions and Suggestions.	116
9.2	References.	121
10	Publications.	122

CHAPTER 1: INTRODUCTION.

1.1: Molecular Beam Epitaxy.

Molecular Beam Epitaxy (MBE) is a well established crystal growth technique with demonstrated access to a wide range of material systems (1). It is essentially a vacuum evaporation technique. A heated single crystal substrate is maintained clean on the atomic level under conditions of ultra-high vacuum where the impingement rate of species from the background gases ($P < 10^{-10}$ Torr) is considered to be negligible. Figure 1.1 shows a schematic of the growth environment. Molecular beams, generated from individual thermal Knudsen evaporation sources, supply the constituent elements for epitaxial growth at fluxes corresponding to beam equivalent pressures of 10^{-6} Torr. This produces deposition rates of the order of one atomic layer per second which equates to approximately one micron per hour. The flux of evaporant is regulated via the relationship between the Knudsen cell temperature and the equilibrium vapour pressure of the source material in the crucible through a geometric factor including the orifice area and the distance to the substrate (1). Thus,

$$J = (1.1 \times 10^{22}) \cdot P \cdot A / L^2 \cdot (M \cdot T)^{1/2}$$

where

J is flux in molecules $\text{cm}^{-2} \text{s}^{-1}$,

P is the source pressure in Torr,

A is the source orifice area in cm^2 ,

L is the distance from the orifice to the substrate in cm,

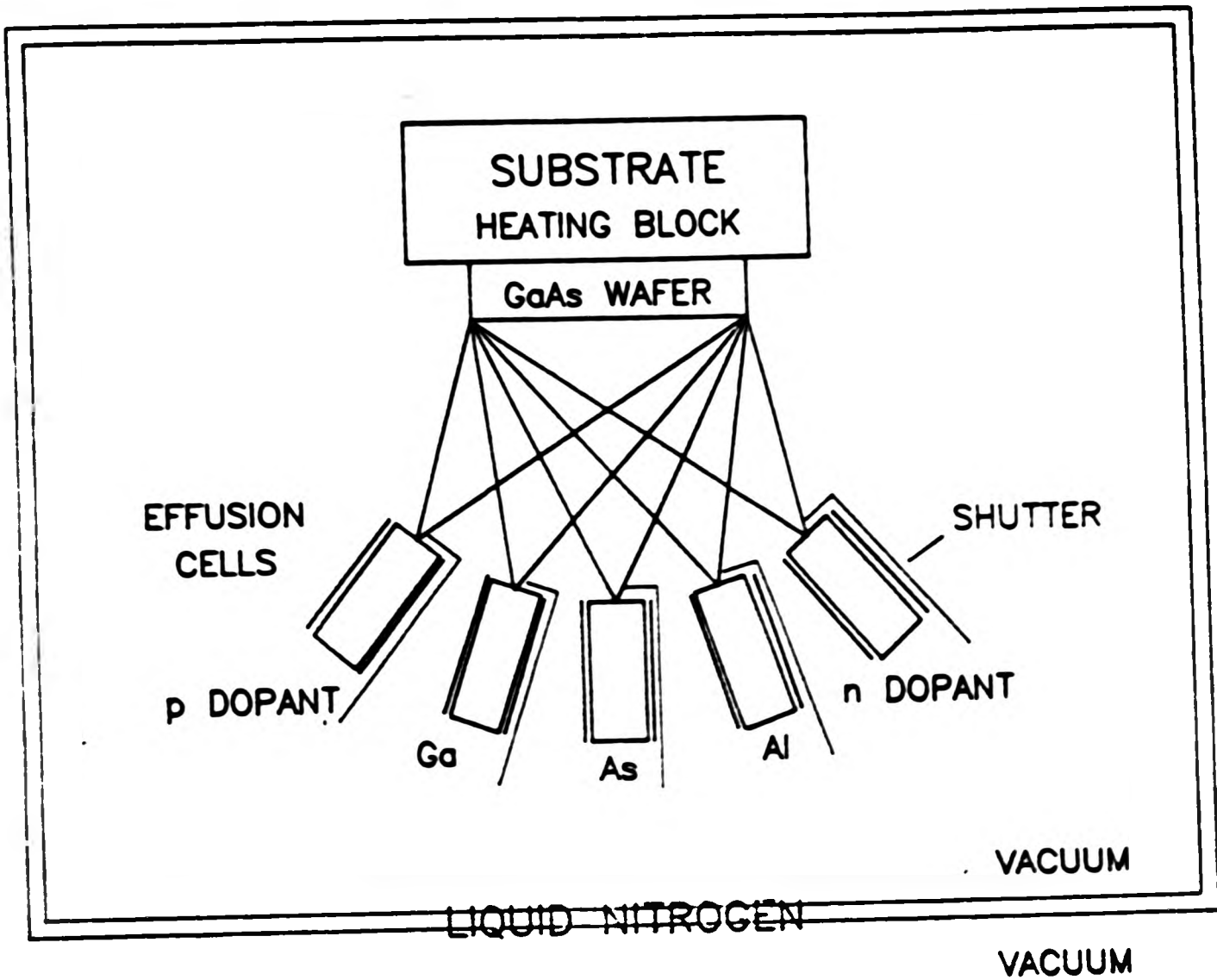


FIGURE 1.1: Schematic of the MBE growth environment and principal components.

M is the molecular weight of the effusing species in gm mol^{-1} ,
 T is the absolute temperature in the source in K.

The beam pressures are low enough so that the flow from cell to substrate is molecular rather than hydrodynamic so the interposition of a line-of-sight shutter is sufficient to stop the beams reaching the substrate. In this way, the composition of the epitaxial layer may be changed simply by shuttering or uncovering individual Knudsen cells. Shutter operation times are typically \ll λ so thickness control and doping abruptness may be on the atomic level. Growth temperatures are typically lower than the classically equilibrium techniques of liquid or vapour phase epitaxy (LPE and VPE) giving potentially reduced interdiffusion of dopants and matrix elements. The UHV environment also allows in-situ monitoring of the substrate and grown layers before, during and after growth so that growth conditions may be optimised. These features conspire to provide an ultra-clean environment for the growth of semiconductors under well controlled conditions.

Of the III-V semiconductors, most of the MBE activity has been on the GaAs/Ga_{1-x}Al_xAs heteroepitaxial system. The high electron mobility in GaAs facilitates fast logic and microwave applications while its direct bandgap is useful for optoelectronic devices. The combination of these properties allows the possibility of integrated circuits which combine both optical and electrical processing on one chip, a feature which is not available in silicon technology. A particularly attractive feature of this materials system is that GaAs and AlAs have very similar lattice parameters so the whole composition range $0 < x < 1$ may be explored in epitaxial structures

under lattice-matched conditions. For this reason it is probably the simplest heteroepitaxial system to study and, notwithstanding the important technological applications mentioned above, is therefore valuable as a testing ground for device and materials studies before launching into more advanced materials where the lattice matching criterion is more stringent.

1.2: Low Dimensional Structures.

The development of advanced semiconductor crystal growth techniques such as MBE, with its ability to produce uniform, thin layers with abrupt interfaces, has recently been coupled with novel ideas in semiconductor physics. The study of transport and optical properties in these ultra-thin semiconductor layers has resulted in hitherto unobserved phenomena.

It is the band structure of a semiconductor which largely determines its optical and electronic properties and this in turn is predominantly influenced by the ion core potential of the constituent atoms and the lattice periodicity. The introduction of perturbations to this potential or periodicity results in modifications to the properties of the semiconductor. The behaviour of some impurity atoms as dopants and the modification of the bandgap as a function of composition in GaAlAs/GaAs structures (which have nearly identical lattice parameters) are two simple examples of the effect of perturbations to the ion core potential. Modifications due to pressure are the most obvious effects of changes in lattice

parameter alone.

The atomic layer depth control of MBE allows the introduction of new periodicities into semiconductor structures, by periodic doping and/or by the growth of heterostructures with band-edge discontinuity periodicities between one lattice spacing and the electron wavelength ($\sim 500\text{\AA}$).

The range of activities in this area of Low Dimensional Structures (LDS) covers the whole spectrum from fundamental physics studies to practical applications and commercially available devices with enhanced performance. Both these categories are described in more detail in chapter 8 where the High Electron Mobility Transistor (HEMT) structures are studied.

1.3: MBE Dopants and Motivation for Studying the Chalcogens.

The extremely thin layers and abrupt interfaces required for the observation of low-dimensional effects means that diffusion of matrix elements and dopants must be particularly well controlled. The species for crystal growth are delivered to the growing layers under extremely good control in MBE and the growth temperatures are generally the lowest amongst the epitaxial techniques. It is however vital that any dopant used in MBE growth of LDS materials has a simple and well characterised incorporation behaviour.

Conventionally, the donor species used to dope MBE GaAs and GaAlAs n-type have been drawn from group IV of the periodic

table (1). Silicon, germanium and tin have all been successful to varying degrees but all suffer from complications in practice. Tin shows marked surface segregation during growth, making abrupt profiles difficult to achieve (2). Germanium shows marked amphoteric behaviour implicit in all group IV dopants, being a donor or acceptor according to whether it is incorporated in the gallium or arsenic sublattice, and is therefore very sensitive to the precise growth conditions used (3-6). Silicon is probably the best characterised MBE dopant for MBE GaAs and GaAlAs but still shows amphoteric behaviour (albeit much less so than germanium) over a wide range of doping levels and in fact converts from a net donor to net acceptor at high concentrations but below the solubility limit (7). Silicon is also quite involatile and care must be taken in the design of suitable sources to ensure that the necessary high temperatures required do not result in the unintentional generation of impurities (8).

Much of the work on LDS worldwide has been on Si-doped MBE-grown GaAs/GaAlAs heterostructures and the successful realisation of useful devices has been hindered by the characteristics of the so-called DX centre which has been widely observed in this material system. The deliberately introduced silicon impurity atoms seem to form both shallow and deep donors in $\text{Ga}_{1-x}\text{Al}_x\text{As}$. The deep donor has been labelled the DX centre in the belief that it corresponds to a complex formed between the silicon donor atoms and a species X, with X postulated as an arsenic vacancy V_{As} (16). The shallow donor seems to dominate for $x < 0.2$ but the deep donor dominates in the technologically important region $0.2 < x < 0.4$ (17). In this latter range, the DX centre manifests itself at low temperature via

photoconductivity which persists after the removal of light and a drastic, sometimes total, reduction in the free electron concentration upon cooling from room temperature. Since HEMTs may in principle be operated at low temperatures to take advantage of the enhanced mobility due to suppression of phonon scattering, the DX centre-related phenomena need understanding. Even at room temperature, the presence of traps or deep donors may be troublesome for device operation if carrier capture and emission rates are comparable to the operating frequencies. At cryogenic temperatures, these phenomena are disastrous for FETs based on HEMT structures and lead to a catastrophic collapse in the drain current which may only be recovered upon warming to room temperature or illumination. Such modes of operation are not preferred for practical devices.

The reduction of DX centre concentrations in GaAs/GaAlAs heterostructures is therefore of great importance for the practical application of low dimensional structures to devices. At the time of this work, a possible route to such a reduction in DX centre concentration was suggested by the then popular arsenic vacancy model. If X were really related to arsenic vacancies, then a reduction in the concentration of V_{As} should produce a corresponding reduction in the concentration of DX. A simple means of doing this would be to "getter" the vacancies by using a chalcogen dopant occupying the arsenic sublattice. This idea is tested in chapter 8 and discussed in the light of more recent work.

The chalcogens S, Se and Te have been largely ignored as dopants in MBE although they have several potential advantages over the group IV elements, the main feature being their unambiguous

donor character. Although diffusion may be a problem at the temperatures used in LPE, VPE and for the activation of ion-implanted dopants, lower growth temperatures generally pertain in MBE. The prospect of a higher upper limit to practical n-type doping than that set by silicon type-conversion is also attractive for low resistance contacts and power devices. Higher mobilities may also be achievable with chalcogen dopants due to reduced compensation as compared to silicon-doped material. There are further benefits to be gained by the use of a non-amphoteric dopant in the antimonide material system where silicon produces only closely compensated p-type material (18).

These deficiencies in the currently available n-type dopants available for use in MBE prompted a wider survey of potential dopants for MBE (9) which suggested that the chalcogens deserved further study, especially in the light of the potential benefits outlined above.

The general reluctance to commit serious effort to the use of chalcogen dopants in MBE stems from two reasons, both related to their high volatility. The first is a feeling that materials with a high elemental vapour pressure at the MBE growth temperatures are intrinsically unsuitable since they would not be incorporated efficiently. The second is the practical difficulty of constructing a suitable source that is UHV compatible since sulphur selenium and tellurium in elemental form all have high vapour pressures at bakeout temperatures and are significantly volatile even at room temperature. These initial reservations cannot be substantiated as calculations have shown that the interaction between the GaAs lattice and the Group VI dopants is strong enough to guarantee a route for

incorporation (9). The difficulties of constructing UHV compatible chalcogen sources has been tackled by several workers using compound sources.

Some promising initial results were reported by Wood (10) who used PbS and PbSe sources which gave successful incorporation of sulphur and selenium and n-type layers with negligible Pb content. Collins (11,12) used SnTe to incorporate both Sn and Te but observed complicated behaviour including the expected segregation of both elements. Cho and Arthur (2) obtained a very high donor concentration with Te but again observed Te segregation. Smith (13) used SnSe₂ to achieve incorporation of Se but not Sn but with decreasing incorporation efficiency or dopant activation at levels above 10^{17}cm^{-3} . H₂S has been used for the incorporation of sulphur in GaAs, GaAlAs (14) and InGaSb (15) grown by MBE but exhibits behaviour that is not simple. Relatively high pressures of H₂S are required and lead to undesirable memory effects in the MBE system as it is pumped only slowly (like H₂O) making abrupt doping changes difficult to achieve and making frequent baking of the system necessary.

This body of work suggests that, although Te is probably not very useful in MBE GaAs and GaAlAs due to its segregation behaviour, sulphur and selenium may be useful n-type dopants if a simple, UHV compatible source of elemental S and Se could be constructed.

This thesis is concerned with the design and development of such a novel source of S and Se molecules and its use for the characterisation and modelling of the incorporation behaviour of S and Se into GaAs and GaAlAs grown by MBE.

Chapter 2 covers the experimental apparatus and procedures used to grow GaAs and GaAlAs layers by MBE. Chapter 3 gives details of the principles of operation and construction of the electrochemical dopant sources and the results of some experiments illustrating the successful incorporation of S and Se into GaAs. The growth of high purity GaAs is described in chapter 4 using mobility and photoluminescence data as a demonstration of the reliability of the MBE system and growth procedures used, and as a vindication of the use of diffusion pumps in MBE systems. Chapter 5 outlines the thermodynamic framework used for the description of the MBE growth and doping processes and demonstrates that a thermodynamically preferred incorporation route for S, Se and Te in GaAs does exist. The incorporation of S and Se into GaAs is investigated in greater detail in chapter 6 where more complicated behaviour than in chapter 3 is observed under certain conditions. The thermodynamic model is expanded to explain the competition between incorporation and loss reactions. Chapter 7 extends the experimental study to the incorporation behaviour of S and Se into GaAlAs alloys and the thermodynamic calculations are again used successfully to interpret the results. Chapter 8 highlights some examples where S and Se, generated by the electrochemical dopant sources have been used as successful dopants in device structures yielding enhanced performance and novel phenomena. Chapter 9 draws conclusions from the work presented here and offers suggestions for further work.

1.4: References.

- 1) See for example the review articles in "The Technology and Physics of MBE", edited by E.H.C.Parker, Plenum Press, New York & London, (1985).
- 2) A.Y.Cho and J.R.Arthur, Prog.Sol.St.Chem., 10, 157, (1975).
- 3) A.Y.Cho and I.Hayashi, J.Appl.Phys., 42, 4422, (1971).
- 4) C.E.C.Wood, J.Woodcock and J.J.Harris, in Proceedings of the 7th International Symposium on GaAs, Institute of Physics, London, (1978).
- 5) K.Ploog, A.Fischer and H.Kunzel, Appl.Phys., 18, 353, (1979).
- 6) R.Heckingbottom and G.J.Davies, J.Cryst.Growth, 50, 644, (1980).
- 7) Y.G.Chai, R.Chow and C.E.C.Wood, Appl.Phys.Lett., 39, 800, (1981).
- 8) E.H.C.Parker, R.A.Kubiak, R.M.King and J.D.Granger, J.Phys.D., 14, 1853, (1981).
- 9) R.Heckingbottom, C.J.Todd and G.J.Davies, J.Electrochem.Soc., 127, 444, (1980).
- 10) C.E.C.Wood, Appl.Phys.Lett., 33, 770, (1978).
- 11) D.M.Collins, Appl.Phys.Lett., 35, 67, (1979).
- 12) D.M.Collins, J.N.Miller, Y.G.Chai and R.Chow, J.Appl.Phys., 53, 3010, (1982).
- 13) R.S.Smith, P.M.Ganser and H.Ennen, J.Appl.Phys., 53, 9210, (1982).
- 14) F.Briones, D.Golmayo, L.Gonzalez and J.L. de Miguel, Appl.Phys., A36, 147, (1985).
- 15) H.Gotoh, T.Yamamoto and M.Kimata, Jap.J.Appl.Phys., 21, L767, (1982).
- 16) D.V.Lang, R.A.Logan and M.Jaros, Phys.Rev.B, 19, 1015,

(1979).

- 17) E.F.Schubert and K.Ploog, Phys.Rev.B, 30, 7021,(1984).
- 18) T.M.Kerr, T.D.Maclean, J.D.Grange and D.I.Westwood, J.Vac.Sci.Technol., B3, (1985).

CHAPTER 2: EXPERIMENTAL.

2.1: Apparatus.

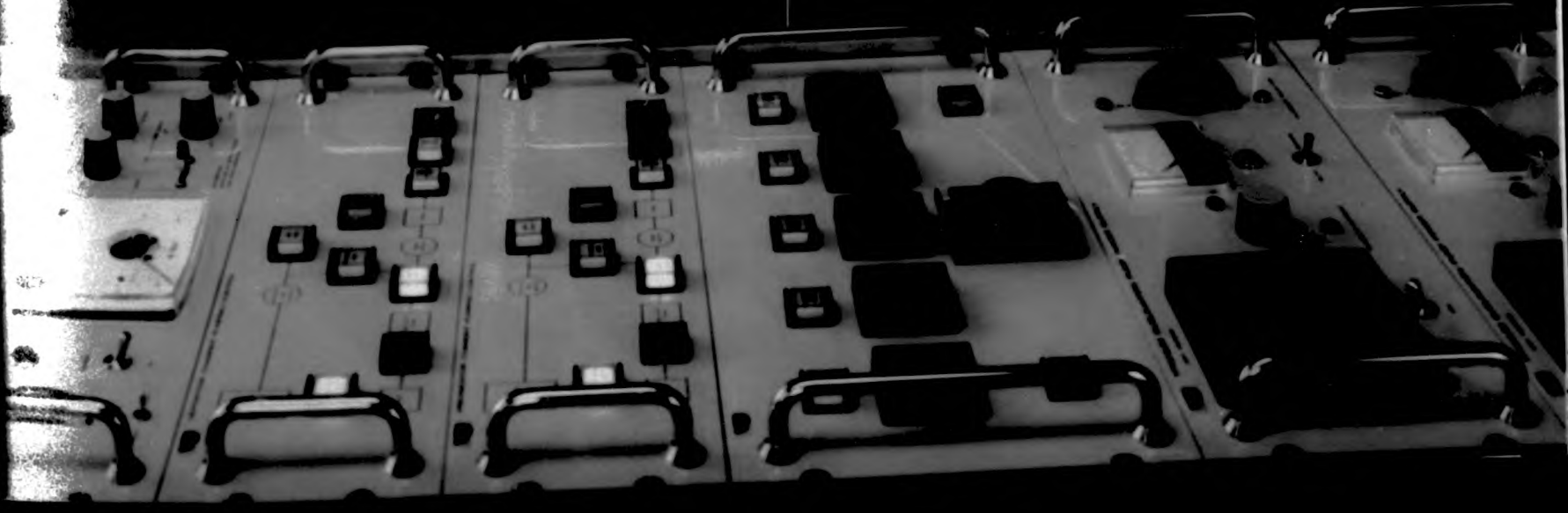
2.1.1: MBE System.

The experimental work was carried out in a Vacuum Generators MB288 three chamber MBE system, shown in figures 2.1 and 2.2. This system featured a fast-entry airlock, a preparation chamber and a growth chamber, isolated from each other by six-inch internal diameter gate valves. The growth and preparation chambers were independently pumped by diffusion pumps filled with a poly-phenyl ether oil (Santovac 5) and fitted with liquid nitrogen cooled, chevron baffled traps and pneumatically operated isolation valves. Each diffusion pump was backed by a large ballast volume which was periodically evacuated by a molecular sieve trapped (10 μ) rotary pump which was set to operate when the backing pressure exceeded 0.05 torr: under UHV conditions this occurred approximately once every 24 hours. The backing and diffusion pump isolation valves were pneumatically operated and configured to return the system to a fail-safe condition on power or cooling water failure. Additional pumping was provided in the growth and preparation chambers by liquid nitrogen shrouded titanium sublimation pumps. The fast entry lock was evacuated to rough vacua by a trapped rotary pump and to higher vacua via a side arm to the preparation chamber diffusion pump.

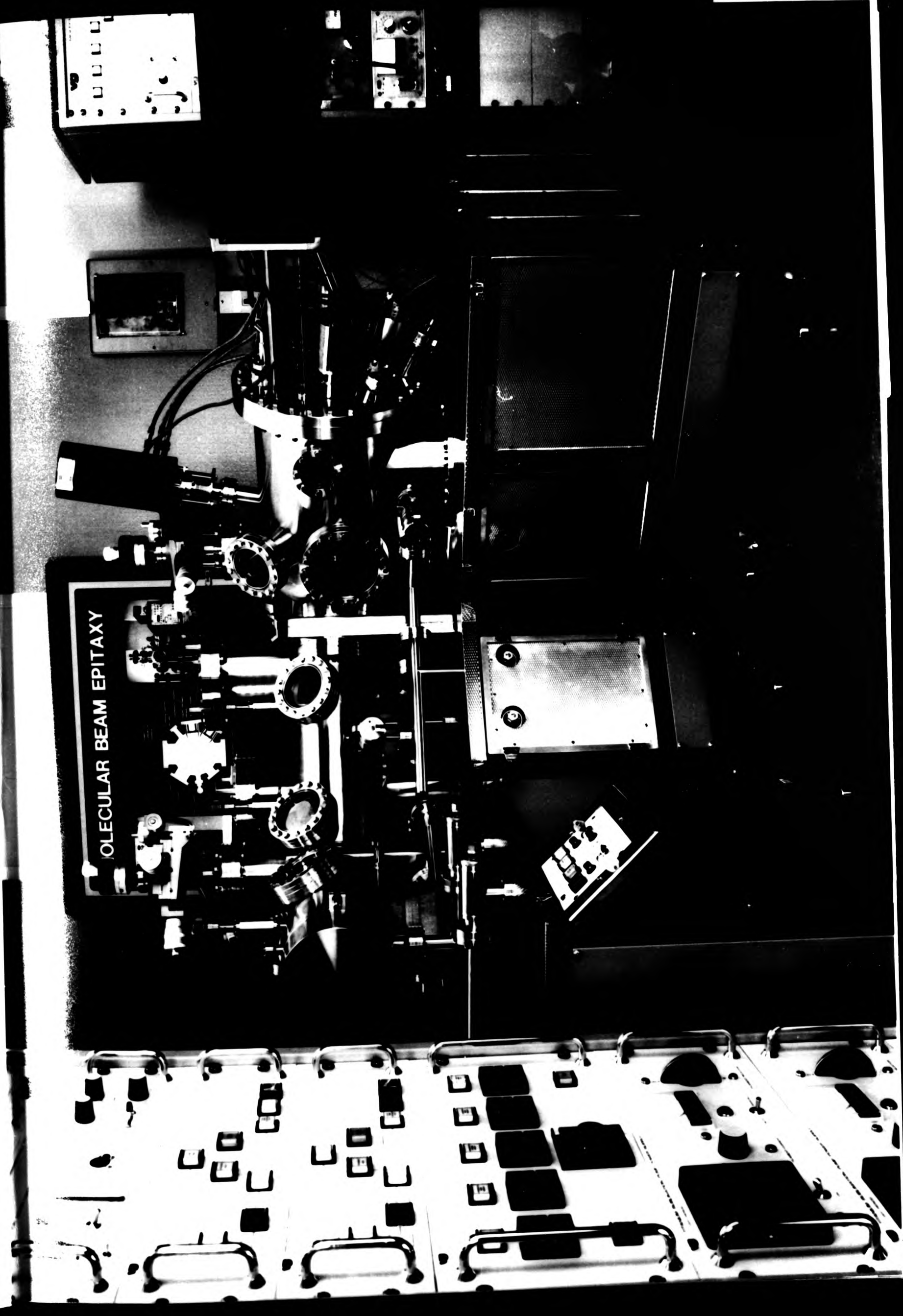
Substrates up to two inches in diameter could be accommodated on

FIGURE 2.1: MB288 system photograph. (Overleaf).

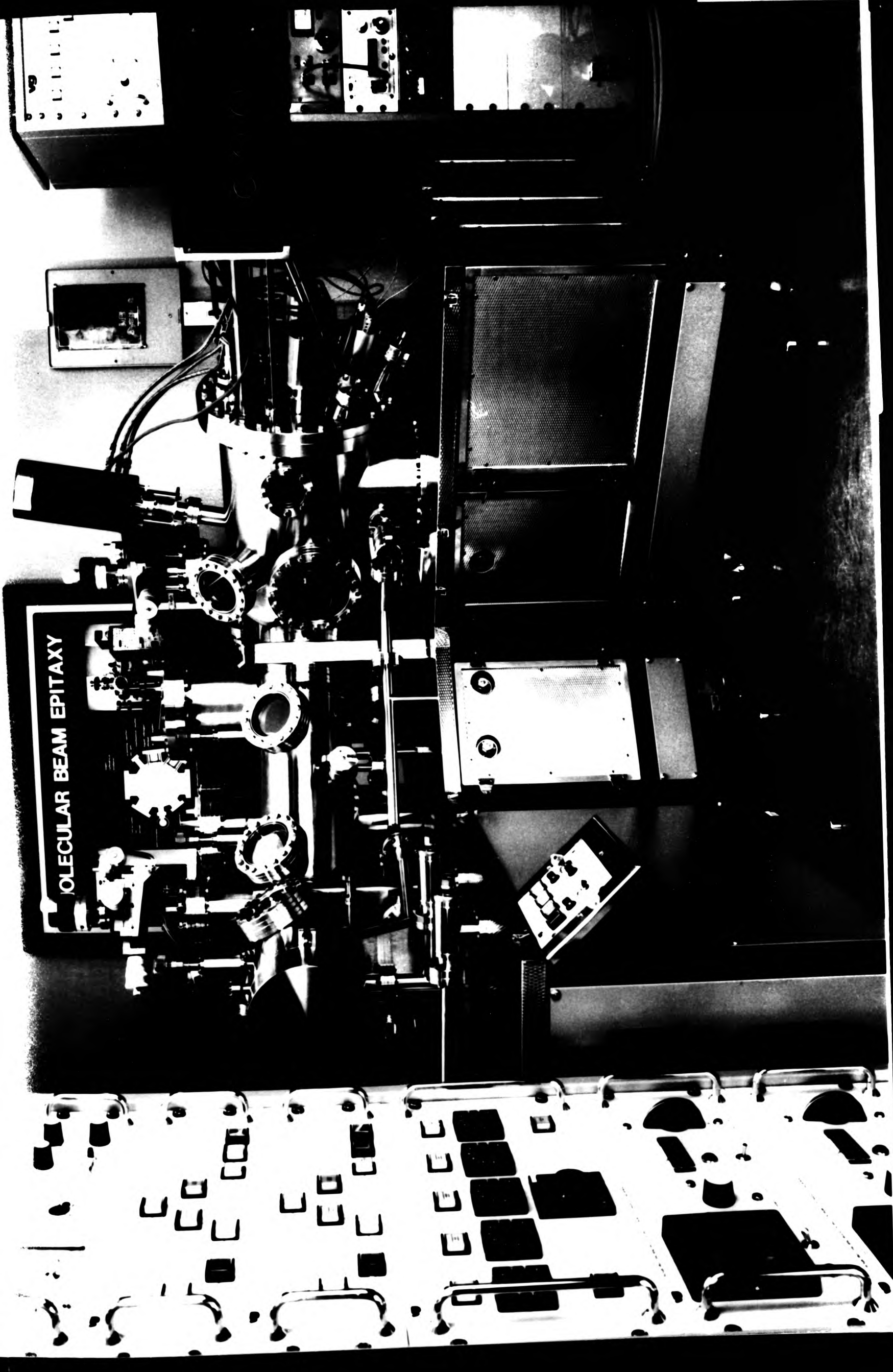
MOLECULAR BEAM EPITAXY



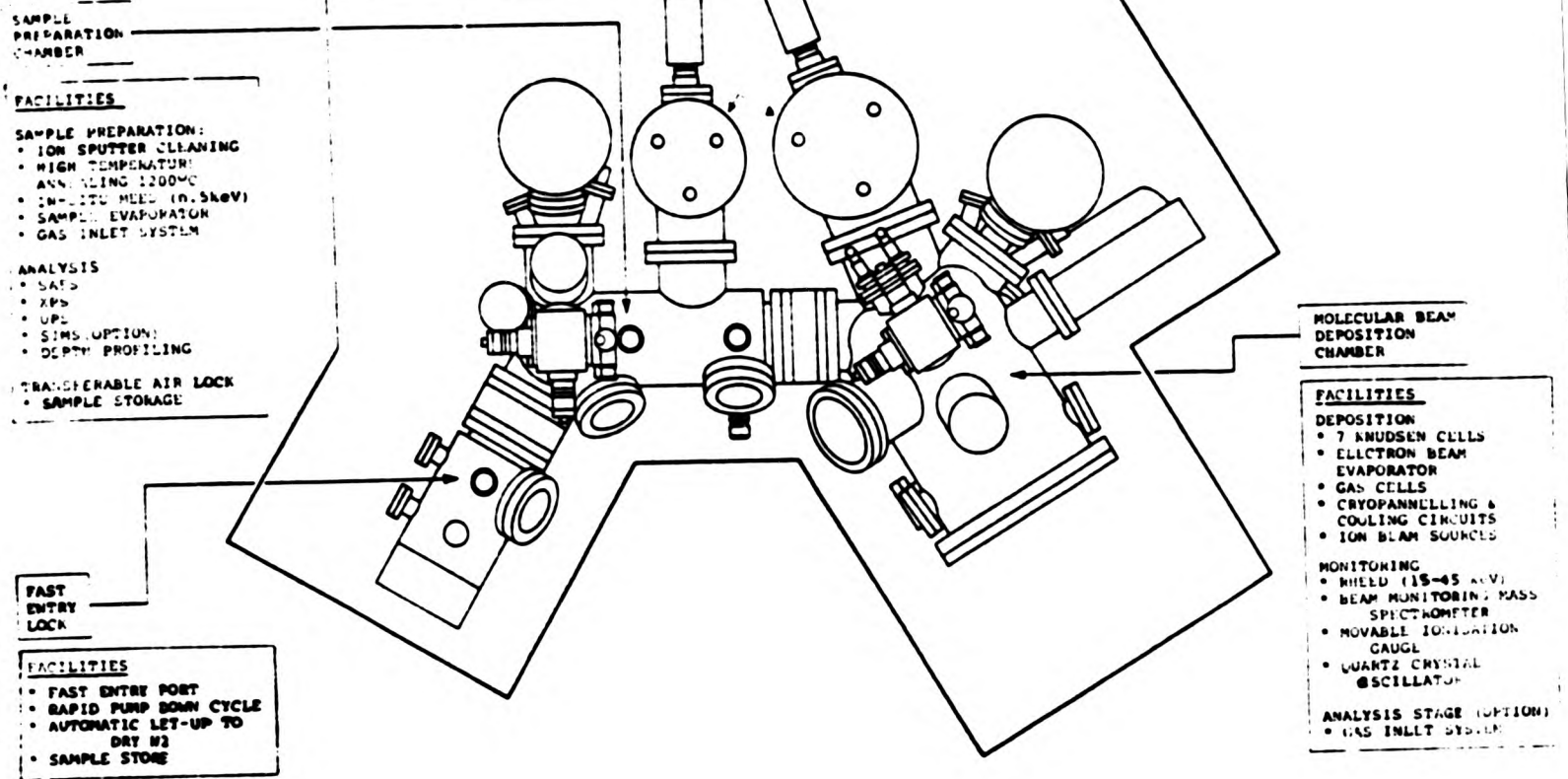
MOLECULAR BEAM EPITAXY



MOLECULAR BEAM EPITAXY



MOLECULAR BEAM DEPOSITION SYSTEM FACILITIES



MOLECULAR BEAM EPITAXY CHAMBER FACILITIES

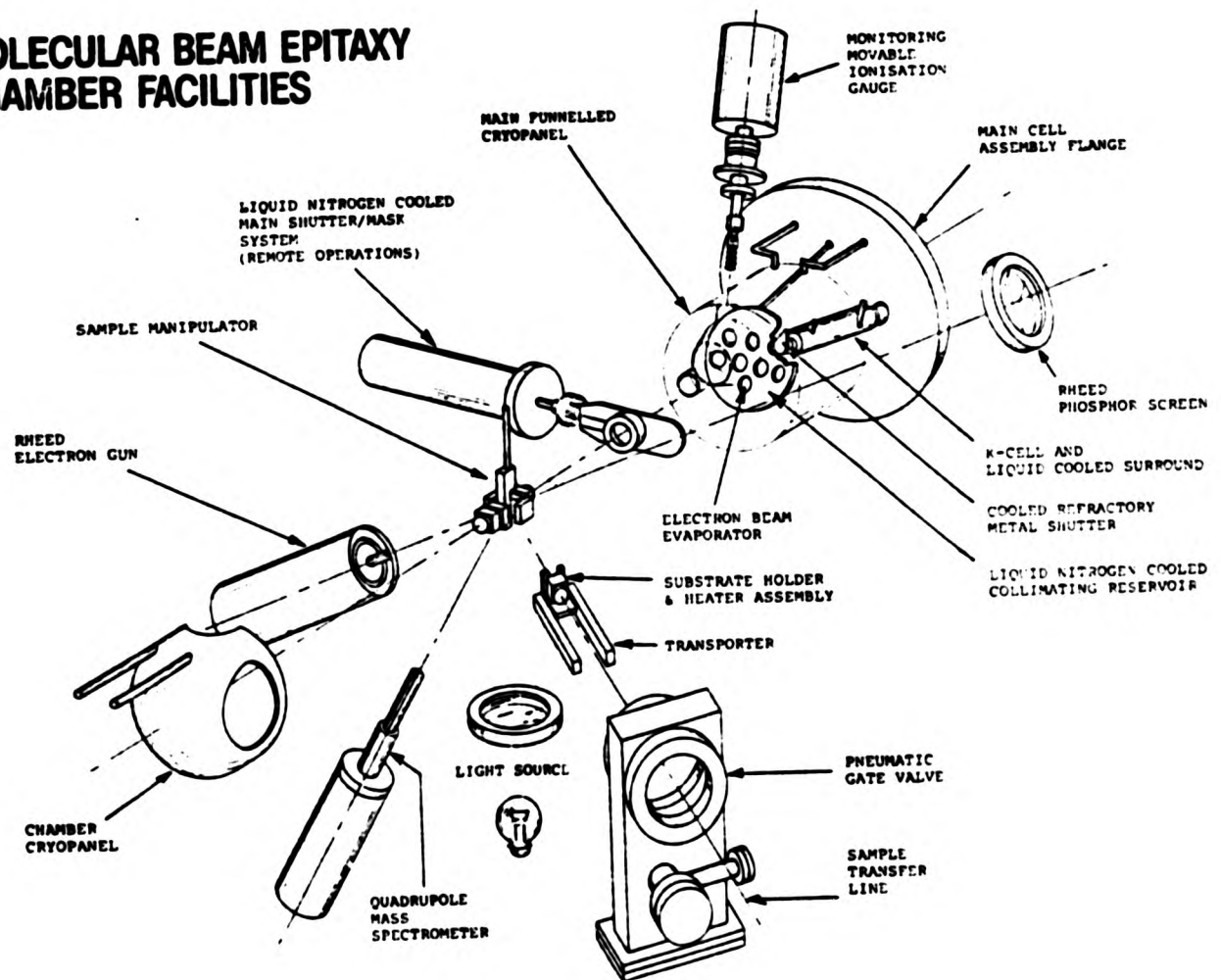


FIGURE 2.2: MB288 system schematic.

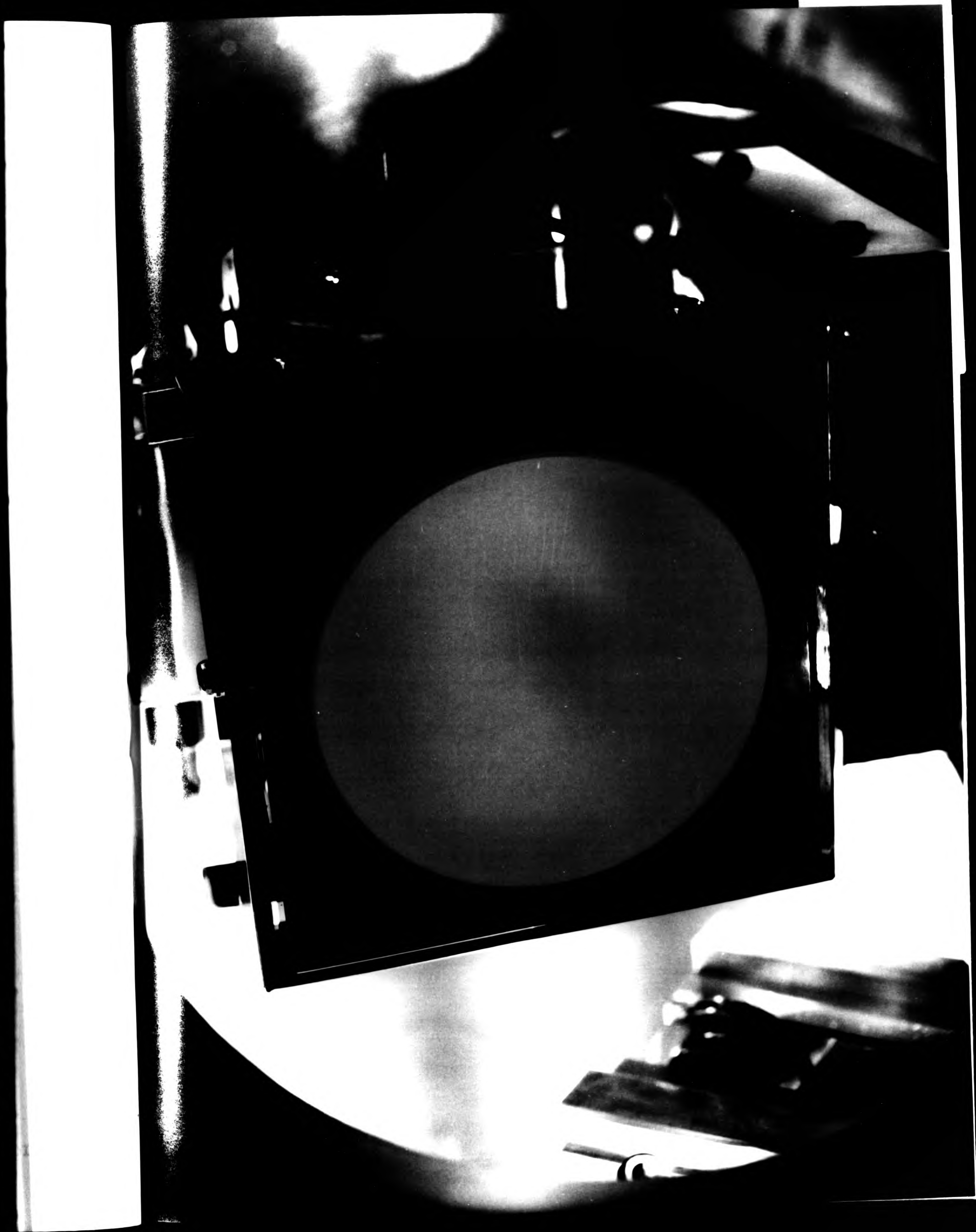
the demountable sample holders which were unusual in that they contained an integral heater and thermocouple assembly, figure 2.3. This combined unit could be transferred between chambers through the gate valves on a trolley driven by a rack and pinion system and plugged into acceptors on high precision manipulators in the growth and preparation chambers. Connection to the heater and thermocouple were achieved via pins on the sample holder and sprung finger contacts on the manipulator assembly.

The provision of the preparation chamber between the airlock and the growth chamber allowed samples to be transferred into the growth chamber under UHV conditions. The preparation chamber also contained facilities for sample treatment and analysis. A Varian 3kV CMA Auger analyser and argon ion sputtering gun were fitted for surface analysis and depth profiling but this chamber was mainly used to outgas the sample and holder in UHV prior to growth without introducing contamination into the growth chamber.

The growth chamber itself was quasi-horizontally configured with ports for eight effusion cells whose axes met at a point near the sample surface. The effusion distance from the cell orifices to the sample was 18cm. Each cell was surrounded by a tube which could be cooled by either water or liquid nitrogen. The arsenic and electrochemical cells were water-cooled while the rest were liquid nitrogen cooled. In front of each cell a tantalum shutter was fitted which was cooled by conduction from the tube via tungsten braid and actuated via a system of gears inside the vacuum by a bellows sealed pushrod which was driven by a pneumatic cylinder outside the system. A perforated dished

FIGURE 2.3: Substrate holder photograph. (Overleaf).





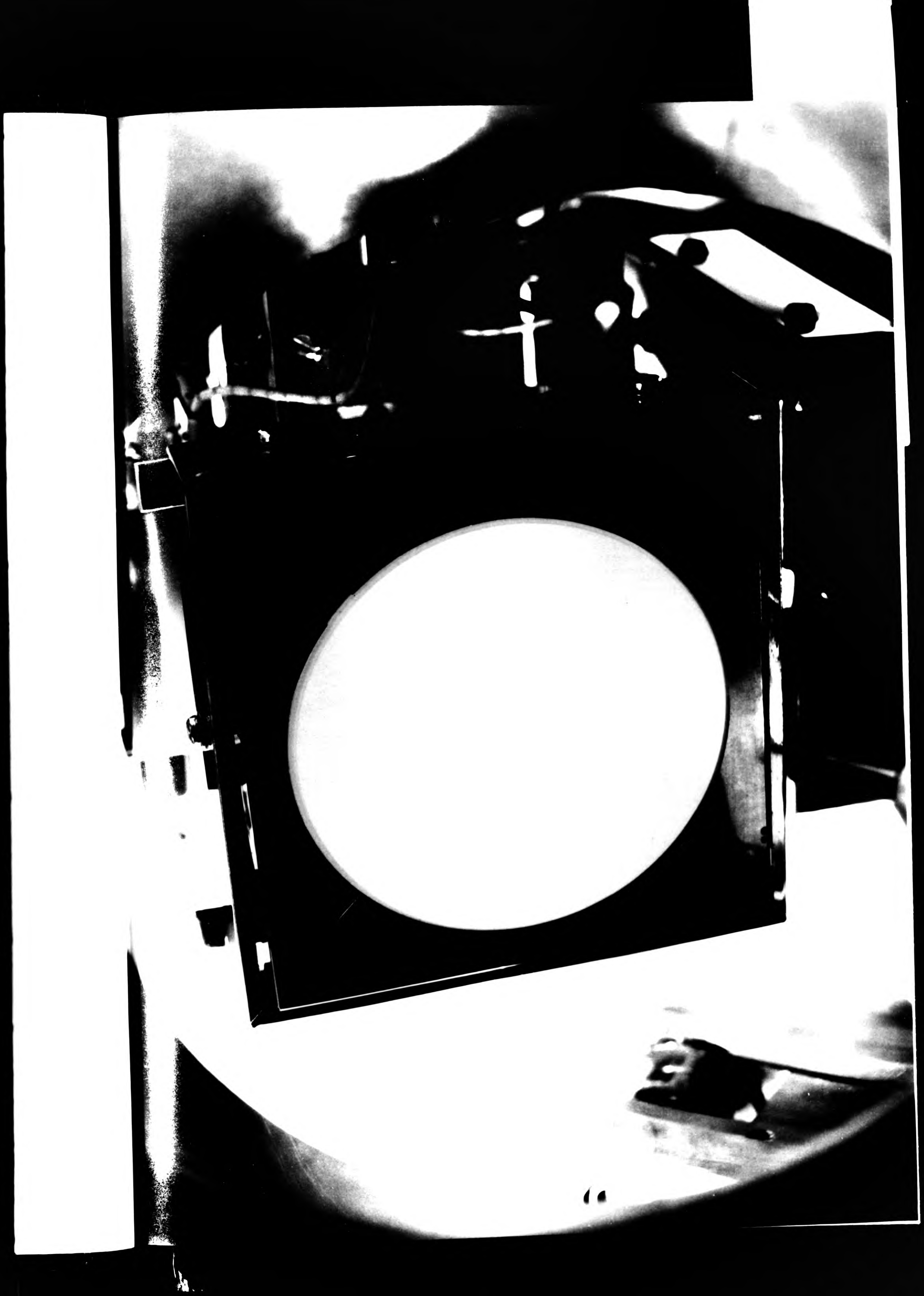


FIGURE 2.4: Photograph of the growth environment. (Overleaf).





cryopanel was situated between the cell shutters and the sample to collimate the molecular beams and to ensure that only the cell orifices were in line of sight of the sample. This liquid nitrogen cooled cryopanel also served to reduce cross-contamination between the cells. This entire multiple source assembly was surrounded by a large liquid nitrogen cooled cryotank with a two inch diameter hole at the sample end. This hole was shuttered by a liquid nitrogen cooled, pneumatically operated main shutter which closed just in front of the sample. This configuration effectively provided a vacuum system within a vacuum system and ensured that from the sample position during growth, only the hot orifices of the effusion cells and liquid nitrogen cooled surfaces were visible, so providing a potentially extremely clean growth environment. A further cryopanel behind the sample provided extra cryopumping and completed the double walled nature of the growth chamber.

A pneumatically retractable moveable ion gauge (MIG) was fitted which could be inserted into the source region to monitor the source fluxes prior to growth while being shielded from the sample by the main shutter. A 1-300 amu Q8 quadrupole mass spectrometer (V.G. Gas Analysis) was mounted so as to intercept a fraction of the molecular beams from each cell. However this soon became coated with GaAs and was retracted by 2cm out of line of sight of the sources and used primarily for residual gas analysis and leak detection. Finally, the growth chamber was equipped with a 15kV electron gun (V.G. Scientific LEG110) and a phosphor screen to facilitate reflection high energy electron diffraction (RHEED) studies of the sample in the growth position. The interior of the growth chamber is shown in figure 2.4 with the main cryoshield removed. The moveable ion

gauge, substrate holder socket (horizontal slot), liquid nitrogen cooled collimator and quadrupole mass spectrometer are all visible.

2.1.2: The High Temperature Knudsen Cells.

The high temperature effusion cells used for the gallium, aluminium and indium sources were constructed by the author with special attention to the materials used to ensure that the molecular beams were of the highest purity. In particular pyrolytic boron nitride (Fulmer Research Institute) and tantalum (Goodfellow Metals) were used wherever possible. It has been shown that it is preferable to avoid the use of alumina in the construction of effusion sources for MBE (1). In these sources the only alumina used was of a high purity (Degussa AL23 grade >99.7% pure). This was twin-bore tubing for the thermocouple insulator and was placed at the rear of the crucible, well out of line of sight of the sample and with a convoluted gas path out of the cell. The thermocouple alloys were tungsten-rhenium 5% and tungsten-rhenium 26%. These alloys were chosen for their resistance to corrosion at elevated temperatures and purity of composition. Chromel-alumel thermocouples were found to deteriorate rapidly above 1000°C but were used in the low temperature arsenic and electrochemical cells.

The overall construction of the high temperature cells is shown in figure 2.5. The heater was made from 0.4mm tantalum wire threaded through boron nitride tubes which ran up and down the length of the crucible. This assembly was wrapped with

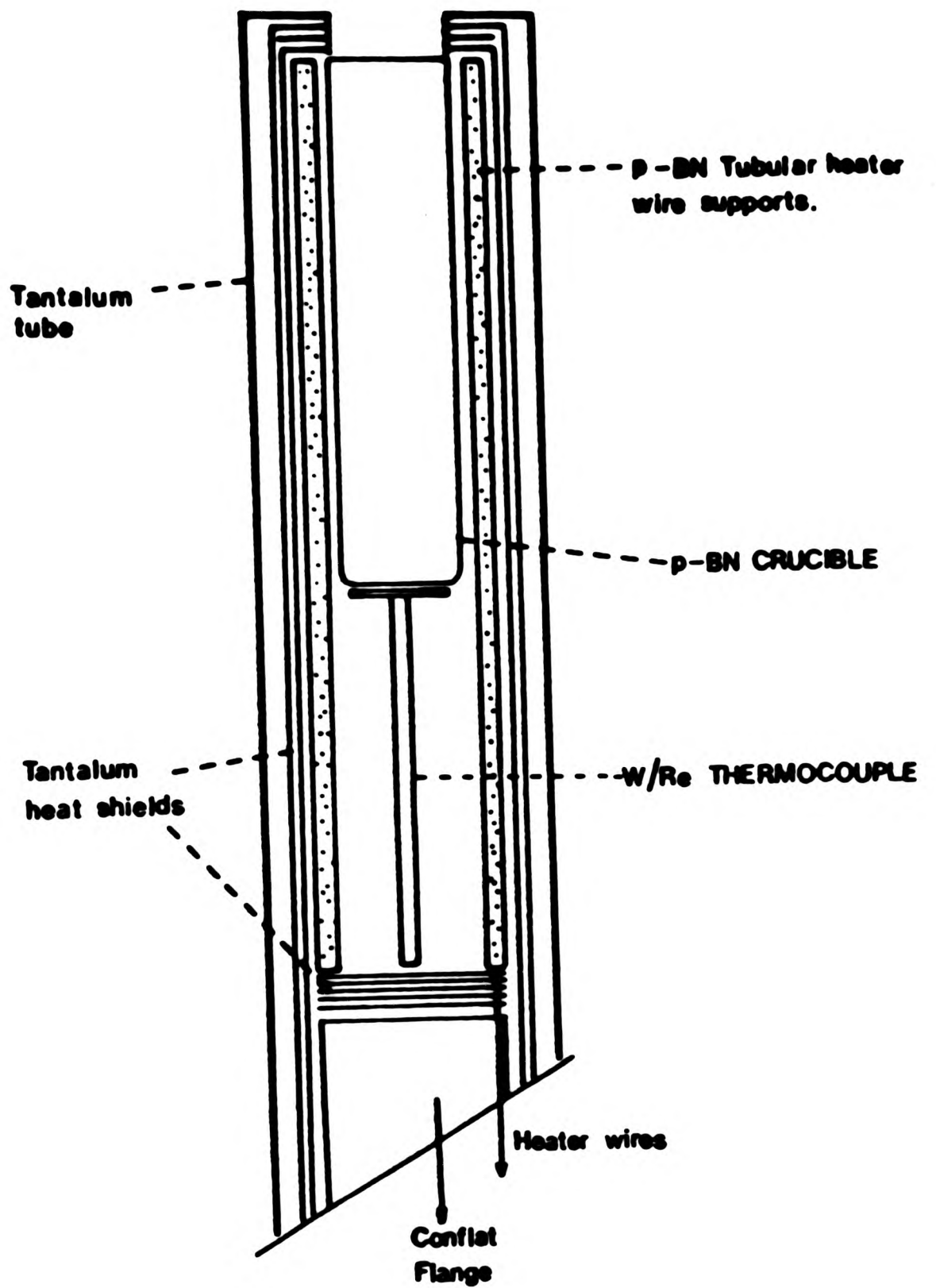


FIGURE 2.5: High temperature effusion cells schematic.

approximately 8-10 turns of crinkled 0.0125mm tantalum foil to act as a heat shield. The base of the heater was fitted with 8, disc shaped, heat shields made from the same foil to reduce radiation loss from the rear of the cell. The crucible was shorter than the heated volume and the thermocouple was introduced through the disc heat shields and brought into contact with the base of the crucible.

Several detailed designs of the front of the cell were tried in an effort to minimise "spitting" (7,8) from the gallium cell. In particular, lipped and unlipped crucibles and varying degrees of heat shielding at the front were used. In addition, extra heating to the front of the cell to prevent the formation of gallium droplets in the cell mouth was attempted. The results of these modifications were inconclusive and the final cells featured lipped crucibles in the Al and In cells and unlipped ones in the gallium cell. Rigorous outgassing of the gallium source was subsequently found to effect the most profound improvement in the density of "spit" type defects in grown layers.

The arsenic cell was of similar construction but with a much larger crucible which was made of high purity graphite rather than boron nitride. The heater tubes were made of AL23 alumina which was quite suitable for low temperature operation.

2.2: Pre-Growth Procedures.

2.2.1: MB288 Operation.

In addition to being operated in accordance with conventional UHV practices, the following precautions were also taken. Bakes were typically conducted overnight at 175°C for 10 hours with the diffusion pumps outside the bakeout region and with their cold-traps filled with liquid nitrogen. The cells were generally kept at 200°C during the bake. Subsequent to this, the diffusion pump traps were kept filled while the chamber isolation valves were open. If the system was unattended for more than 15 hours, the isolation valves were closed and the system pumped by a 60 litre per second ion pump which maintained a base pressure of better than 10^{-8} mB. The diffusion pump traps were periodically baked using heating tape into the diffusion pumps with the isolation valves closed.

Up-to-air times were minimised in an effort to reduce system contamination and oxidation of source materials. Further, filtered dry nitrogen from the vapourisation of liquid nitrogen was used to backfill the system to maintain a slight positive pressure in the chambers.

The source materials were loaded with no pretreatment. The aluminium cell was only filled with sufficient aluminium to just outlast the arsenic cell so as to reduce the strain on the boron nitride crucible on solidification (2). 7N pure gallium from Canyonlands Corporation was used. The 7N arsenic was purchased from both Canyonlands and Johnson Matthey. The indium

was 7N pure from MCP and the aluminium 6N pure from Metals Crystals Ltd. Typical cell charges were Ga-20g, Al-3g, In-20g, As-60g.

2.2.2: Flux Calibrations.

Calibration of source fluxes were made from measurements of the composition and thicknesses of layers grown through masks under the assumption that the growth rate was determined by the total group III flux at growth temperatures where group III loss from the substrate was negligible. The pressures in the molecular beams were measured with the moveable ion gauge. The ion gauge collector current was measured with a Keithley model 610 electrometer and correction made for the background pressure by making measurements with the source shutter open and closed. For the group III cells the flux was allowed to stabilise for 2 minutes as the front of the cell cooled when the heat reflected back into the cell was removed by the action of opening the shutter. The arsenic flux was measured on the assumption that As_4 had the same ionisation cross-section as gallium since arsenic has a similar atomic number. Correction was also made in calculating fluxes from measured pressures for the fact that the ionisation gauge measures density rather than pressure by allowing for the different velocities of the molecular beams (3). Arsenic flux measurement was simplified in the MB288 by virtue of the large amount of liquid nitrogen cryopaneling which greatly reduced the amount of As_4 reflected back through the gauge in multiple passes by condensing it out.

2.2.3: Substrate Temperature Measurement.

The sample holder was equipped with a thermocouple which was in contact with the back of the molybdenum mounting block. To assess the accuracy of the thermocouple, the temperature of the front surface of this block was measured by several means. A dual wavelength infra-red pyrometer (Vanzetti Systems, USA) was used to observe the block in vacuo through a freshly cleaned viewport. Compensation for the differential absorption of the two pyrometer wavelengths by the window was corrected for, to a first approximation, by inserting a second window in the path of the detector, noting the temperature error introduced, and then doubling it. For a GaAs sample soldered to the block with indium, the pyrometer indicated that at the typical growth temperature of 600°C the thermocouple was reading some 30°C high. This was confirmed routinely by observing the melting point of aluminium wire (660°C) clipped to the block after it had been cleaned of indium to prevent the formation of any indium-aluminium alloy. The melting point observed in this way was between 690°C and 700°C. The most useful calibration point for the substrate temperature came from the observation of the clean-up and subsequent surface reconstruction of GaAs in an arsenic flux prior to growth as observed by RHEED. This usually took place at a temperature indicated by the thermocouple of 630°C. Correcting for the estimated error gives a figure of 600°C which is in good agreement with the usually quoted figures of 580°C-600°C(4).

2.2.4: Substrate Preparation.

Layers were generally grown on both n-type and semi-insulating (100) GaAs substrates simultaneously. The wafers were supplied chemo-mechanically polished on both sides. The n-type GaAs from MCP was silicon doped at 10^{18}cm^{-3} while the semi-insulating GaAs was nominally undoped and supplied by Wacker. The n-type InP was either sulphur doped at 10^{19}cm^{-3} or tin doped at 10^{18}cm^{-3} and the semi-insulating InP was iron doped from Metals Research. Substrate thicknesses of 0.35mm were typical. All reagents used for degreasing or etching were Aristar grade and the glassware was all high purity silica. The processes were carried out in a laminar flow chemical work station.

The polished wafers were reflux washed for 30 minutes in hot acetone, trichloroethylene and finally propanol. After blow drying in filtered dry nitrogen, they were etched for 2 minutes in hot (90°C) 15:2:2 $\text{H}_2\text{SO}_4:\text{H}_2\text{O}_2:\text{H}_2\text{O}$ (5). The etch was quenched in 18 $\text{M}\Omega\text{cm}$ deionised filtered water from a Milli-Q 4-bowl pure water system (6). After two minutes of rinsing, the slices were blown dry taking care not to leave drying stains.

The substrates were mounted on the substrate holder with pure indium solder at 175°C . The backs of the slices were well wetted by floating them on excess In on the heated substrate holder. The slices were then removed and replaced until a uniform layer of In had adhered. Excess In was then removed from the holder and the slices remounted. Finally the substrate holder was loaded into the fast entry lock on the MBE system. Pumpdown and transfer into the preparation chamber typically took 10 minutes. The substrates and the holder were then stored

overnight at 100°C for growth the next day or immediately outgassed at 200°C (InP) or 350°C (GaAs) for 1-2 hours prior to growth until the preparation chamber pressure had fallen below 10^{-9} mB.

2.3: Growth Procedures.

Before growth was commenced, the liquid nitrogen flow around the cell surrounds and the cryopanel was started. Once the cryopanel was chilled and the flow stabilised, the gallium, indium and aluminium cells were heated to their operating temperatures.

When the cell temperatures had stabilised, the fluxes from each cell were measured. The flux measurements were made with the moveable ion gauge once the flux had equilibrated after the shutter was opened. The shutter was then closed and the background pressure noted and subtracted. The cell temperatures were then adjusted to give the required fluxes for the growth. The following calibration points were determined from measurements of the thickness and composition of grown layers. One micron per hour growth of GaAs was achieved for a gallium beam current of approximately 2×10^{-8} A measured at 1 mA emission. The corresponding figures for AlAs and InAs were 1.1×10^{-8} A and 4×10^{-8} A.

The point at which the incident arsenic atom flux equalled the gallium flux was judged by the current ratio at which the grown GaAs became covered in Ga droplets and occurred for an arsenic beam current of approximately 6×10^{-8} A. The arsenic flux was

always kept in excess of the total group III flux during growth and in terms of current ratios was typically of the order of 5-10:1 for GaAs and GaAlAs and 20-50:1 for indium containing alloys. When the required fluxes had been set, the moveable ion gauge was retracted from the growth position and its filament extinguished.

At this point the outgassed samples were transferred from the preparation chamber to the growth chamber with the main shutter closed. The substrate was then rotated to the growth position facing the cells and the main shutter opened. The arsenic shutter was then opened and the GaAs substrate heated to 620°C in the arsenic flux desired for growth.

During this process the RHEED pattern from the $\langle 110 \rangle$ and $\langle \bar{1}10 \rangle$ azimuths was observed. For GaAs, below 500°C the diffraction pattern was generally diffuse with only the zero order streak discernible. At ~500°C the contrast of the pattern improved considerably giving a 1x1 pattern. At approximately 600°C the pattern strengthened again in intensity and 1/4 and 1/2 order streaks could be discerned in the $\langle \bar{1}10 \rangle$ and $\langle 110 \rangle$ azimuths respectively. The substrate was then kept at 620°C for one or two minutes during which time this reconstructed (2x4) pattern usually improved further in contrast and brightness. On certain occasions temperatures up to 650°C were required to produce the (2x4) reconstruction but this could usually be correlated with poor wetting of the rear of the slice with indium and subsequent inefficient heat transfer.

The desired growth temperature was then set and growth initiated by opening the group III shutter(s). The practical

upper limit of growth temperature could be judged by observing the RHEED pattern as the substrate temperature was raised. For GaAs/GaAlAs, the 2/4 order streaks in the $\langle 110 \rangle$ azimuth faded first leaving only the 1/4, 3/4 and 5/4 streaks. When the 2/4 streaks had disappeared, the $n/4$ (n odd) order streaks were faint and almost merged with the integral orders. In the $\langle 110 \rangle$ azimuth, the 1/2 order streaks were somewhat reduced in intensity and somewhat diffuse. Some 10°C above the extinction temperature of the 2/4 streaks in the $\langle 110 \rangle$ azimuth, the $n/4$ (n odd) streaks also faded leaving only the integer order streaks in this azimuth and faint 1/2 order streaks in the $\langle 110 \rangle$ azimuth. A further rise of 10°C resulted in the total loss of fractional order intensity and a spotty 1×1 pattern which usually correlated with a very rough grown surface. Further increase in temperature produced group III droplets on the surface. The GaAs (100) (4×2) pattern characteristic of the gallium stabilised surface was not observed.

After the required growth sequence, the growth was terminated by closing all but the arsenic shutter. The substrate heating was then turned off and the substrate cooled in an arsenic flux. The arsenic shutter was closed when the sample had cooled below 300°C . When the temperature had fallen below 200°C , the sample was removed from the system and a new one loaded for the next growth.

2.4: References.

- 1) R.F.C.Farrow and G.M.Williams, Thin Solid Films, 55, p303, (1978).
- 2) R.W.Lashway, U.S.Patent No 3,986,822, (1976).
- 3) C.E.C.Wood, D.Desimone, K.Singer and G.W.Wicks, J.Appl.Phys., 53, p4230, (1982).
- 4) M.Heilblum, E.E.Mendez and L.Osterling, J.Appl.Phys., 54, p6982, (1983)
- 5) G.J.Davies, D.A.Andrews and R.Heckingbottom, J.Appl.Phys., 52, p7214, (1981).
- 6) Millipore (UK) Ltd., Millipore House, 11-15 Peterborough Road, Harrow, Middlesex.
- 7) C.E.C.Wood, L.Rathburn, H.Ohno and D.DeSimone, J.Crystal Growth, 51, p299, (1981).
- 8) M.Bafleur, A.Munoz-Yague and A.Rocher, J.Crystal Growth, 59, p531, (1982).

CHAPTER 3: ELECTROCHEMICAL CHALCOGEN SOURCES.

3.1: Introduction.

The electrochemical generation of chalcogen species has been used previously for adsorption studies (1), investigation of chalcogenide composition and electrical properties (2) and mass spectrometric analyses of chalcogen vapour compositions (3). The adaptation of this technique to produce dopant sources for MBE (4) provides a novel and convenient solution to the problems of UHV incompatibility and uncertainty of beam composition inherent in thermal evaporation from elemental or compound sources.

3.2: Principles of Operation.

The principles of operation will be described in terms of the sulphur cell. The selenium cell is substantially similar but differences will be outlined in a following section.

The key to the operation of the electrochemical chalcogen sources lies in the properties the silver chalcogenides. These compounds all exhibit a defected crystal structure and can exist over a range of compositions close to stoichiometry. The large immobile anions (S,Se) are generally disposed on a well defined lattice (body centred cubic for the high temperature forms of the sulphide and selenide (10)) with the silver ions distributed randomly among a large number of nearly equivalent lattice sites. The phase diagram for silver sulphide (Ag_2S) is

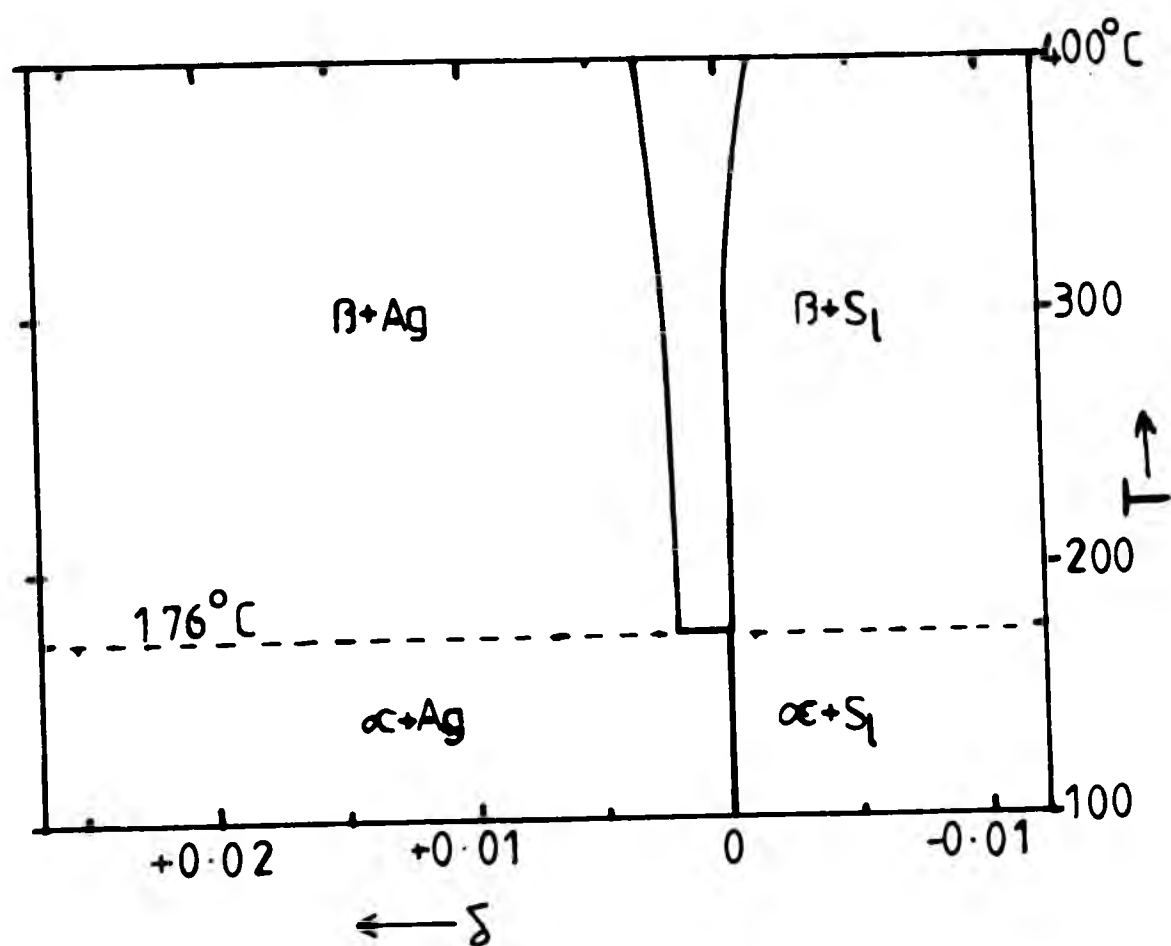


FIGURE 3.1: Phase diagram for $\text{Ag}_{(2+d)}\text{S}$. The deviation from stoichiometry, d , is plotted on the horizontal axis and the temperature on the vertical axis. The alpha-beta phase transition takes place at about 176°C . The important point is that the range of non-stoichiometry is much larger for the beta phase and that it extends from the the two extremes of silver precipitation to sulphur precipitation.

shown in figure 3.1. In the high temperature phase, above 175°C, the composition range is quite substantial: at 200°C it ranges from a silver excess of 2×10^{-3} mol Ag/mol Ag₂S in equilibrium with elemental silver to near ideal stoichiometry when the sulphide is in equilibrium with liquid sulphur (5). Clearly, the sulphur vapour pressure in equilibrium with the sulphide will be depressed from that of elemental sulphur at the silver deficient end of its composition, to a very low value in the silver rich region. Therefore, by varying the composition of the sulphide, one may explore a very wide range of sulphur vapour pressures. A suitable means of adjusting the composition is by taking advantage of the easy interdiffusion of silver ions through the open cation sublattice in the sulphide, and adding or subtracting silver ions electrolytically.

Consider the cell Pt/Ag/AgI/Ag₂S/Pt. The silver iodide is used as an electrolyte and is an almost purely ionic conductor in its high temperature phase. Above 146°C its Ag⁺ ion conductivity is high: 1.31 (ohm.cm)⁻¹ at 146°C, 2.1 (ohm.cm)⁻¹ at 350°C and 2.6 (ohm.cm)⁻¹ at 500°C while its electronic component is much smaller 10^{-6} (ohm.cm)⁻¹ (6,7). Passage of a current through the cell causes migration of Ag⁺ ions through the AgI which either enrich or deplete the silver mole fraction of the sulphide, depending on the direction of current flow. The AgI is necessary as the sulphide is a mixed electronic and ionic conductor (7). The emf of the above cell provides a direct measure of the chemical potential of the silver in the silver sulphide. From this, the silver and hence sulphur activities can be deduced. Under conditions where the Ag₂S is in equilibrium with sulphur vapour (in a Knudsen cell for

example) there is therefore a direct relationship between the cell emf and the partial pressures PS_x of the different sulphur molecules. This may be expressed as (8):

$$PS_x = PS_{x'} \cdot \exp(2x(E-E')F/RT) \quad (1),$$

where PS_x is the partial pressure of the molecular species S_x over Ag_2S , $PS_{x'}$ is the equilibrium partial pressure of species S_x over liquid sulphur, E is the emf of the cell, E' the cell emf in equilibrium with liquid sulphur, R is the gas constant, T the absolute temperature and F Faradays constant. E' has been measured as 0.23V at 200°C and 0.243V at 300°C (2) and the $PS_{x'}$ tabulated (8).

It is clear from this equation that the $\{PS_x\}$ are all less than the $\{PS_{x'}\}$. Also, as E is reduced, the species with high values of x have their vapour pressure reduced much more rapidly than those with low values. The consequence of this is that while for $E=E'$ (cell in equilibrium with liquid sulphur) S_8 rings are the predominant gas phase species, for values of E sufficiently smaller than E' , S_2 dimers have the higher vapour pressure. Atomic sulphur has a very low elemental partial pressure at the temperatures we are considering and although it is favoured by the exponential term, the very small value of PS_1 means that the monomer does not have a significant partial pressure in our operating range. The relationship between the partial pressures for the different sulphur species and the cell emf is plotted in figure 3.2. Clearly, operation at a cell emf lower than 200mV guarantees that dimers will be the predominant species.

The combination of this electrochemical cell with a Knudsen

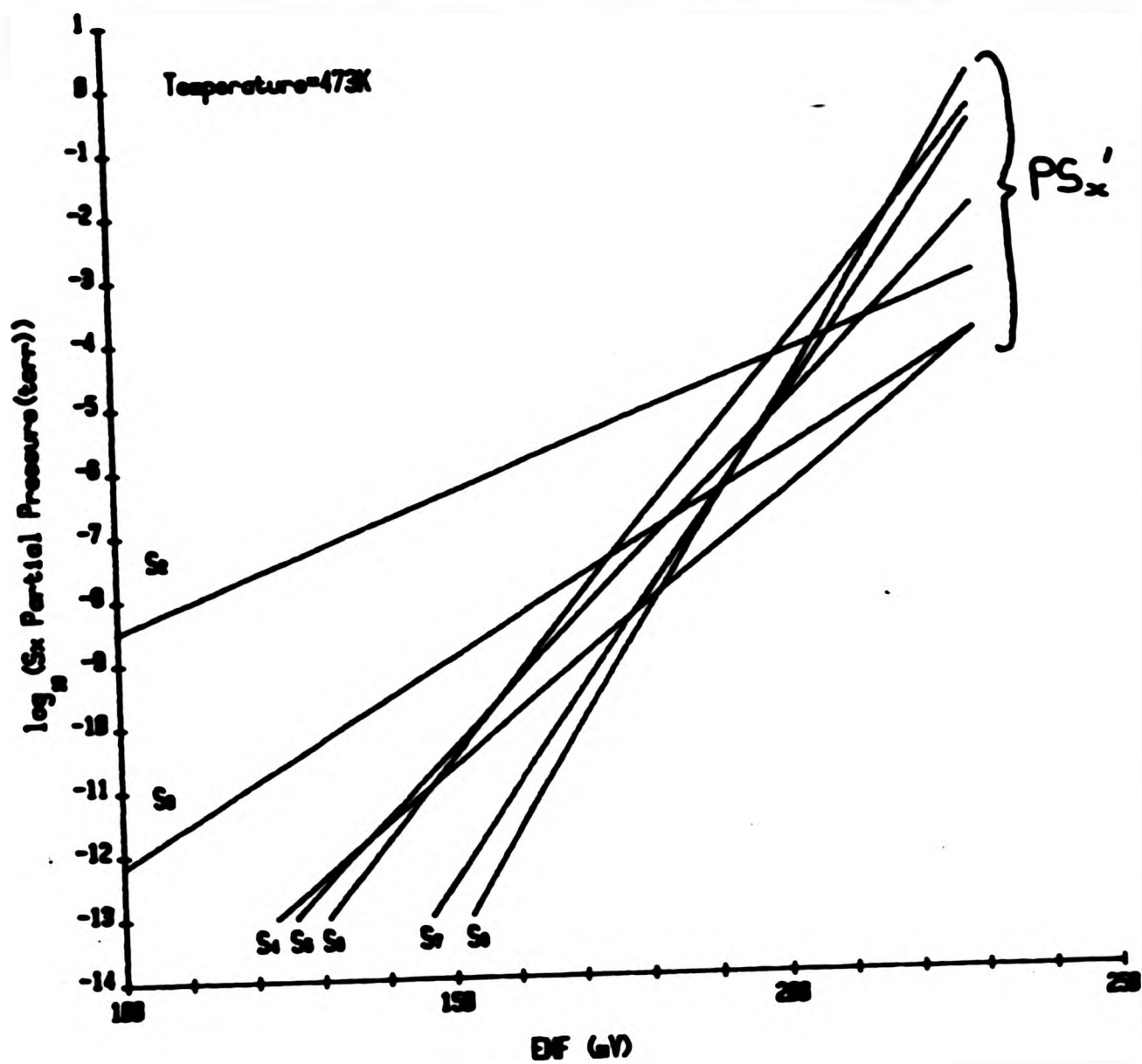


FIGURE 3.2: Sulphur partial pressure over Ag_2S versus cell emf.

cell results in a most convenient, controllable source of sulphur dimers since the flux effusing from such a cell is proportional to the sulphur vapour pressure which is directly accessible via the cell emf. Under conditions of equilibrium, at any particular cell emf E , the rate of loss of sulphur from the effusion cell is exactly balanced by the extraction of Ag^+ ions from the sulphide via the AgI . This is measurable as a current through the cell. It is possible to drive the cell with a current source, making use of Faraday's law to calculate the current for the required flux, with the proviso that the vapour pressure demanded by the operating temperature and Knudsen cell geometry does not place the Ag_2S too near the sulphur rich end of the composition range. However, changing to a new flux and hence current would entail a long wait as the rate of change of the sulphide composition (and hence the sulphur vapour pressure) is fixed by the applied current which transports the Ag^+ ions to or from the Ag_2S . The currents that correspond to MBE doping fluxes are small and equilibration times using this mode of operation may be of the order of hours.

If the cell is driven from a voltage source, the cell may be charged or discharged between operating emfs at a current limited only by the internal resistance of the cell. The current through the cell will then settle down to one corresponding to the effusing flux after a short period of time when the sulphide has achieved the required composition. These equilibration times are of the order of one or two seconds (2) for cells operated at 200°C , ie where both the Ag_2S and the AgI are in their high temperature phases and where the diffusion of Ag through the Ag_2S and the ionic conductivity of the AgI are high. If this rapid response is to be achieved, it is important

that the impedance of the voltage source driving the cell is low compared with the internal resistance of the cell, otherwise the charging or discharging current will create a significant voltage drop across this impedance and the desired emf will never be reached. Unfortunately the insertion resistance of most current measuring devices sufficiently sensitive to measure the equilibrium currents involved ($\sim 10^{-6}$ A) are too large.

In practice a Datel model DVC 8500 digital voltage source was used which had a current limit of 25mA and an output impedance less than 10 milliohms. This was connected directly to the cell with no current monitoring device. One final aspect that may have an influence on the cell response time is the free volume of the Knudsen cell. The time taken for this volume to fill or empty on changing the flux may be calculated to be significantly less than one second for any practical design.

The electrochemical Knudsen cell clearly has advantages in terms of purity of beam composition, low temperature operation and speed of response. In fact, the response time should be rapid enough for the entire MBE doping range (10^{14} cm⁻³ to 10^{19} cm⁻³) to be traversed by the cell in a time comparable to that required to deposit one monolayer of GaAs during MBE growth, comparable to the operation time of a mechanical shutter. More importantly, step changes between two different doping levels are possible with just one source, unlike conventional thermal effusion sources where heating and cooling times are much longer. This rapid programmability is particularly appropriate for doping in superlattice structures where thicknesses can be counted in atomic layers.

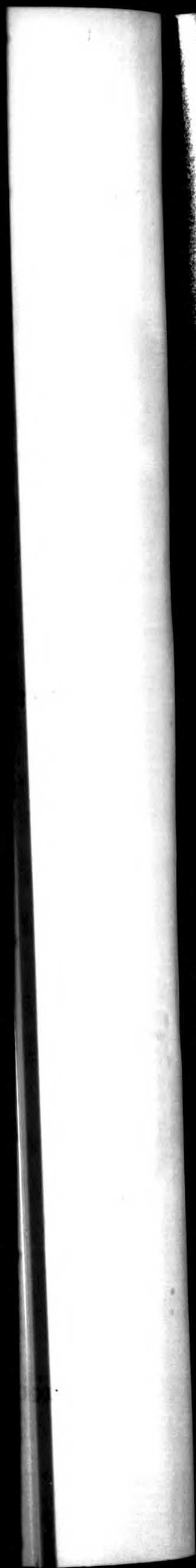
3.3: Cell Construction.

The electrochemical sulphur cell is shown assembled in figure 3.3 and schematically in figure 3.4. The electrochemical cell was formed by pressing 7mm diameter pellets of the powdered materials (Koch-Light Ltd.) in a Beckman infra-red sample preparation die. The AgI pellet was pressed first and then the Ag₂S added to the die and pressed on top of the AgI to form a single pellet. This was then inserted into the machinable glass ceramic Knudsen cell and held in contact with the silver disc and the platinum electrodes by a tungsten spring. The cell orifice was 1mm. A 0.25mm tantalum wire heater was wound on a double spiral groove machined in the cell body and trapped in position by a machinable glass ceramic sleeve. A chromel-alumel thermocouple in contact with the silver electrode served to measure the temperature. The cell assembly was supported on a stainless steel rod on an FC64 flange and mounted in the MBE system on a cell flange with a water-cooled surround and shutter.

After bakeout, the cell was heated to 250°C to outgas it and then lowered to 200°C after one hour. The cell was maintained at this temperature, being cooled to room temperature only when the system was let up to air. When not actively being used for doping, the cell was discharged to 100mV and left in an open-circuit condition.

A slightly different form of construction was used for the selenium cell which was assembled from alumina tube and plate stock components for convenience. The pellet was formed in the

FIGURE 3.3: The electrochemical sulphur cell. (Overleaf).





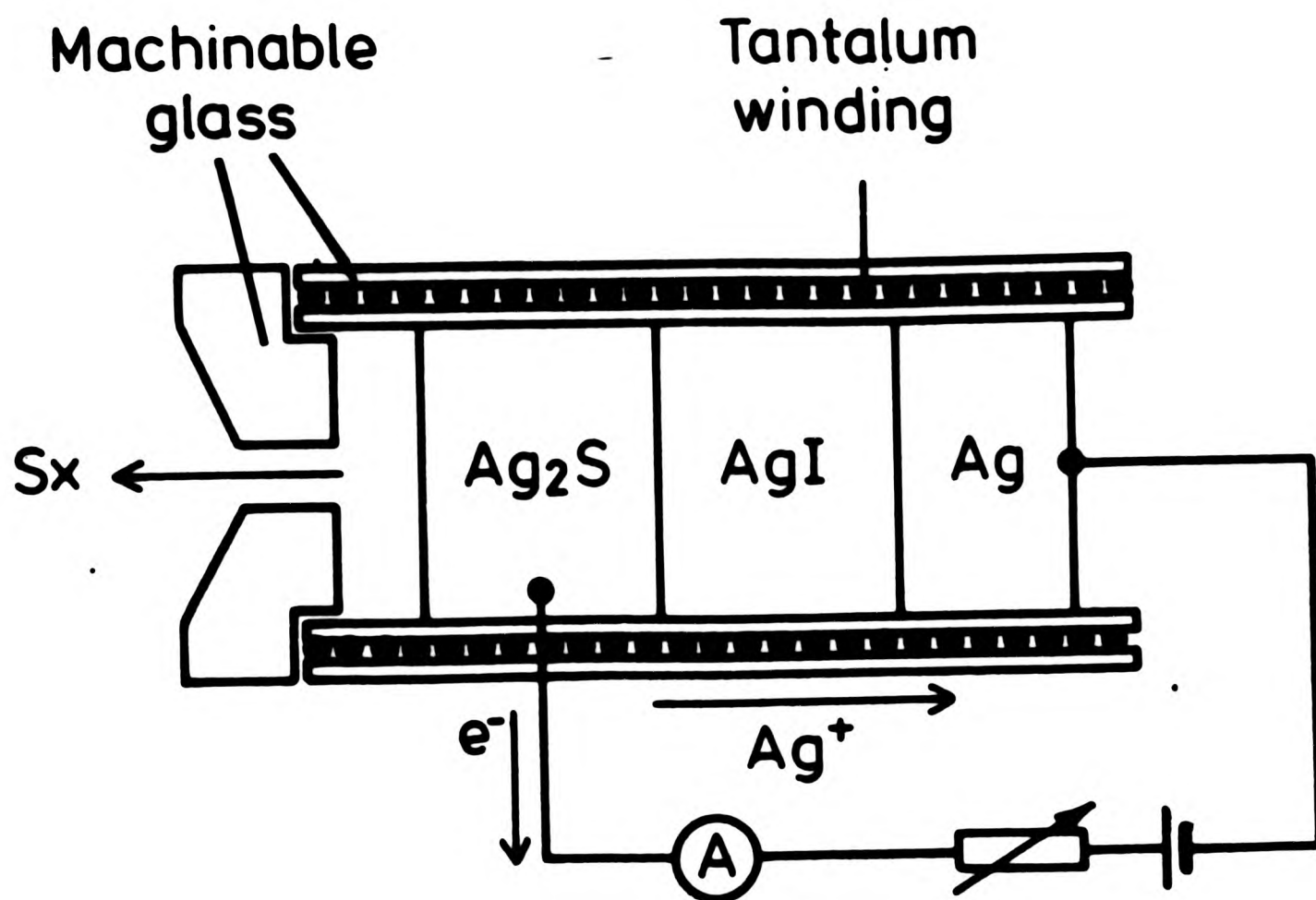
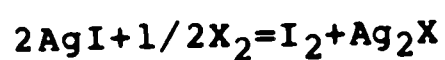


FIGURE 3.4: Sulphur cell schematic.

same way as for the sulphur cell, with the simple substitution of silver selenide (Lancaster Synthesis) for the sulphide. The selenium cell has to be operated at a higher temperature as selenium is less volatile than sulphur: typically, cell temperatures of 300°C were used. E' for the selenium cell has been measured as 0.273V at 150°C (9).

Certain difficulties were experienced when the selenium cell was being tried out. On heating from room temperature to 300°C for the first time, the cell would go short-circuit internally and discharge. This was not due to any mechanical short on the connecting wires either inside or outside the vacuum system and happened for the first two or three cells constructed. Examination of the electrolyte pellet revealed that the AgI had become coated with a layer of what appeared to be Ag₂Se when analysed by EDAX in the scanning electron microscope. Ag₂Se has a relatively high electronic conductivity and it was this that was causing the cell short. The problem was overcome by deliberately discharging the cell at room temperature and keeping it short circuited while it was heated to 300°C for the first time. This keeps the selenide at the silver rich end of its composition and so prevents the evolution of large quantities of selenium as the cell is heated if the as-received selenide is at the selenium rich end of its composition range. The shorting problem thus solved however, tended to reappear after a period ranging from days to months, with the same degradation of the silver iodide. An explanation may be sought by considering the reaction:



(2),

where X=S or Se. Calculation of the equilibrium constant $k=P(I_2)/(PS_2)^{1/2}$ from standard thermochemical data (10) shows that at 200°C the reaction lies almost completely to the left, giving $k=10^{-6} \text{ atm}^{1/2}$, consistent with the stability of the sulphur cell. At 300°C however, substantial decomposition of the iodide is predicted, with $k \sim 0.5 \text{ atm}^{1/2}$. The reaction is limited by the amount of chalcogen vapour available, so heavily used cells would be expected to deteriorate more quickly. Fortunately, if the pellet is a good fit in the cell tube, access of the chalcogen to the silver iodide is restricted and the cell life prolonged. In future designs, larger orifices should be used to facilitate lower operating temperatures: increasing the orifice to 5mm should permit the cell to be operated below 250°C.

3.4: Electrochemical Cell performance.

In order to evaluate the electrochemical cells, an effort was made to measure the dopant fluxes using the moveable ion gauge flux monitor. Although producing fluxes for doping very much smaller than the matrix element fluxes used for growth, and for which the moveable ion gauge was normally used, by operating only the electrochemical cells and minimising outgassing through thorough liquid nitrogen cooling of the system, it was possible to lower the system background pressure to below 1×10^{-10} mbar. With this low background, it was possible to observe directly the fluxes emitted from the electrochemical cells as a function of the applied emf. Figures 3.5 and 3.6 show the results of this experiment for the sulphur and selenium cells respectively. The rate of change of the measured pressure on

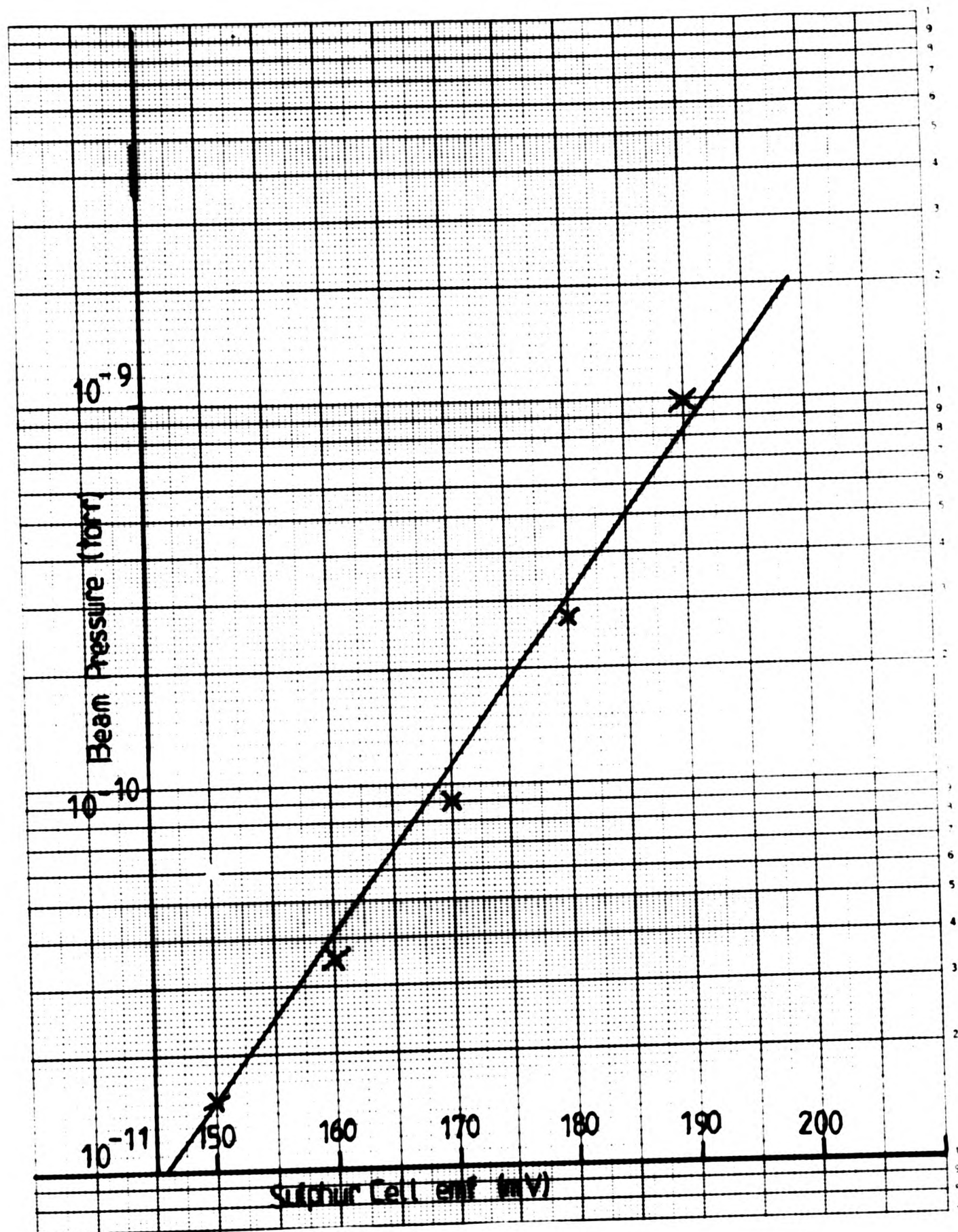


FIGURE 3.5: Plot of sulphur pressure vs applied emf measured on the moveable ion gauge.

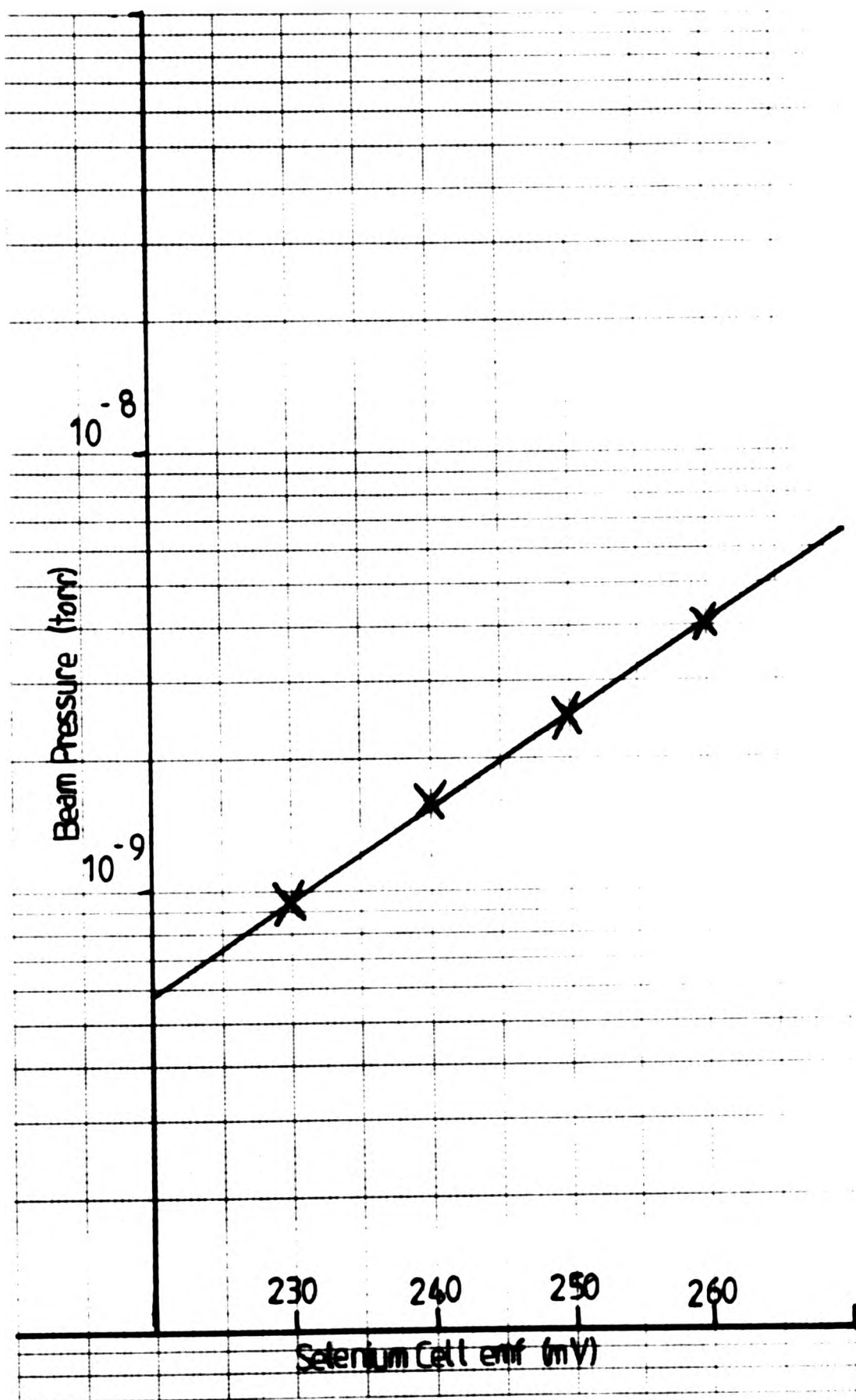


FIGURE 3.6: Plot of selenium pressure vs applied emf measured on the moveable ion gauge.

the moveable ion gauge in response to changes in the emf applied to the electrochemical cells appeared to be limited by the rise-time of the gauge electronics themselves and was of the order of 1-5 seconds.

The straight-line behaviour of the $\log(\text{pressure})$ versus applied emf plots confirms the predicted behaviour from equation (1). Further, it is possible to deduce the polyatomicity, x , of the effusing chalcogen species S_x or Se_x from the slope since

$$x = \text{Slope}(\text{decades per volt}) \cdot R.T / 2.F.\log_{10}e \quad (3).$$

For the sulphur cell, substituting $T=200^\circ\text{C}$ produces the result $x=1.9$, in excellent agreement with the prediction from figure 3.2 and equation (1) that dimers should predominate in the beam over this range of emf.

For the selenium cell, the agreement is less good. It is noted that the plot still exhibits straight-line behaviour, but the slope suggests an apparent value of $x=1.2$. Consideration of the decomposition of Se_2 to monatomic Se using thermochemical data reveals that the atomic species should not be present to any significant degree so that the value of x is not likely to be an average over several integral values. The other possibility is that of an error in the cell temperature measurement. However, for the slope measured to correspond to $x=2$, a temperature of 680°C must be assumed, some 380°C in error, which is rather larger than can be accounted for. However, if not all the applied emf actually appears across the selenide, then the slope will be altered. If the applied emf is V and that part appearing across the selenide is $E=K.V$, equation 1

becomes :

$$P_{Se_x} = P_{Se_x'} \cdot \exp(2 \cdot x \cdot (K \cdot V - E') \cdot F / RT) \quad (4).$$

Taking logs and differentiating with respect to the experimentally applied variable V gives:

$$x = \text{Slope}(\text{decades per volt}) \cdot R \cdot T / 2 \cdot K \cdot F \cdot \log_{10} e \quad (5),$$

thus yielding the same straight-line behaviour but with modified slope. For $x=2$, a value of $K=0.6$ is implied, ie. only 60% of the applied voltage actually appears across the selenide. This voltage drop presumably takes place across the AgI. It is not apparent in the sulphur cell ^{which} despite the lower temperature should give higher resistance (6,7) due to the lower Ag^+ ion conductivity. A likely explanation is that the degradation of the AgI through coating with Ag_2Se , referred to earlier, results in an electronic conduction path and the corresponding potential divider effect. Indeed, other experiments plotting pressure, C-V carrier concentration and SIMS measurements, all show linear behaviour but with slopes varying between 1-2 according to the age of the Se cell, consistent with a gradual degradation.

Figures 3.7 and 3.8 show a C-V and SIMS (13) depth profile through a GaAs layer staircase-doped with sulphur. The growth temperature was $550^\circ C$ with a As_4/Ga flux ratio of 3:1. The steps are well resolved by both techniques with the carrier concentration and elemental concentration agreeing to within a factor of 2. The C-V and SIMS results are plotted together in figure 3.9. At the higher levels, ($>1.10^{17} cm^{-3}$), the slope of

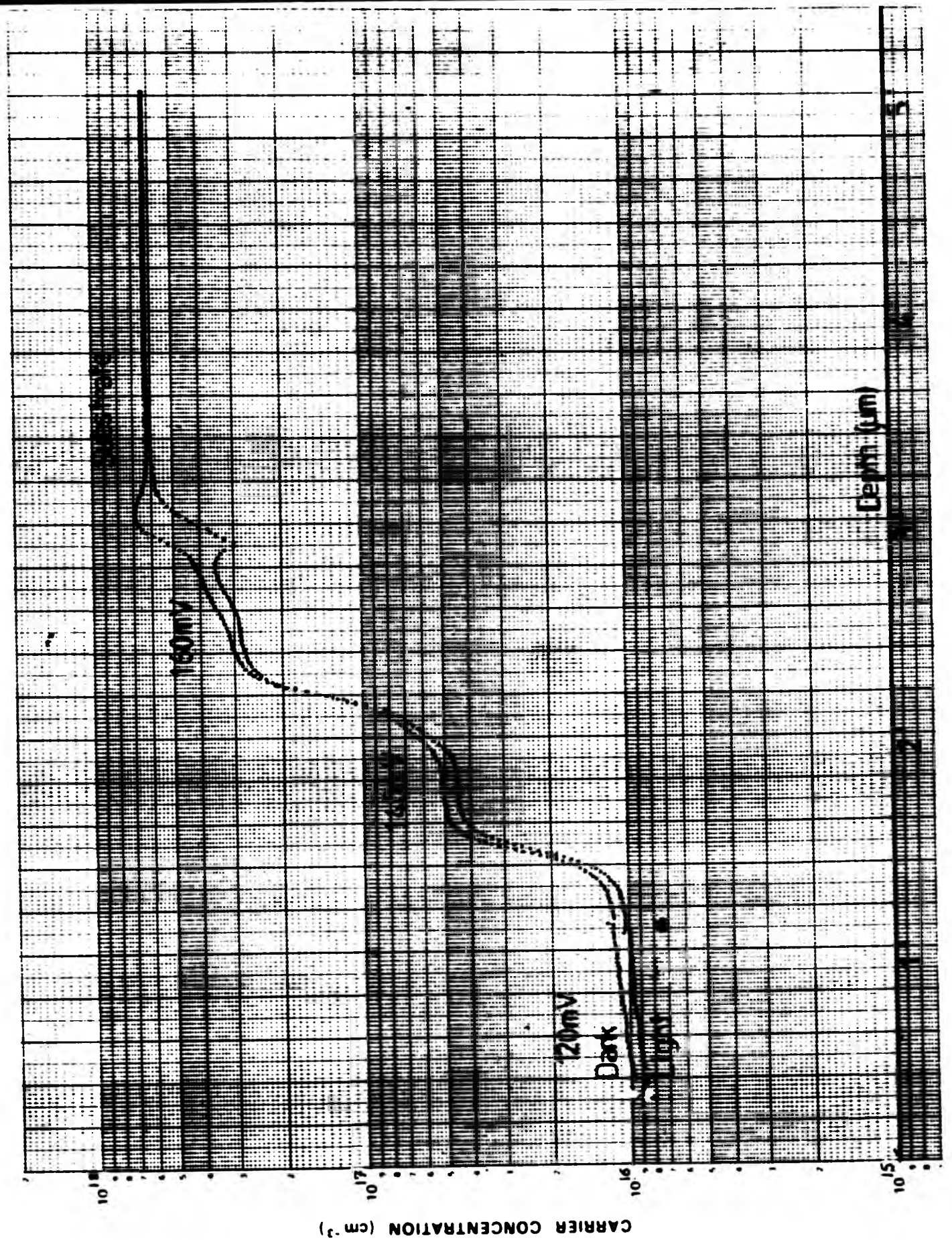


FIGURE 3.7: An electrochemical C-V depth profile through a GaAs layer staircase-doped with sulphur. Measurements of carrier concentration were made both in the dark between dissolution steps and under illumination during dissolution. Both are plotted.

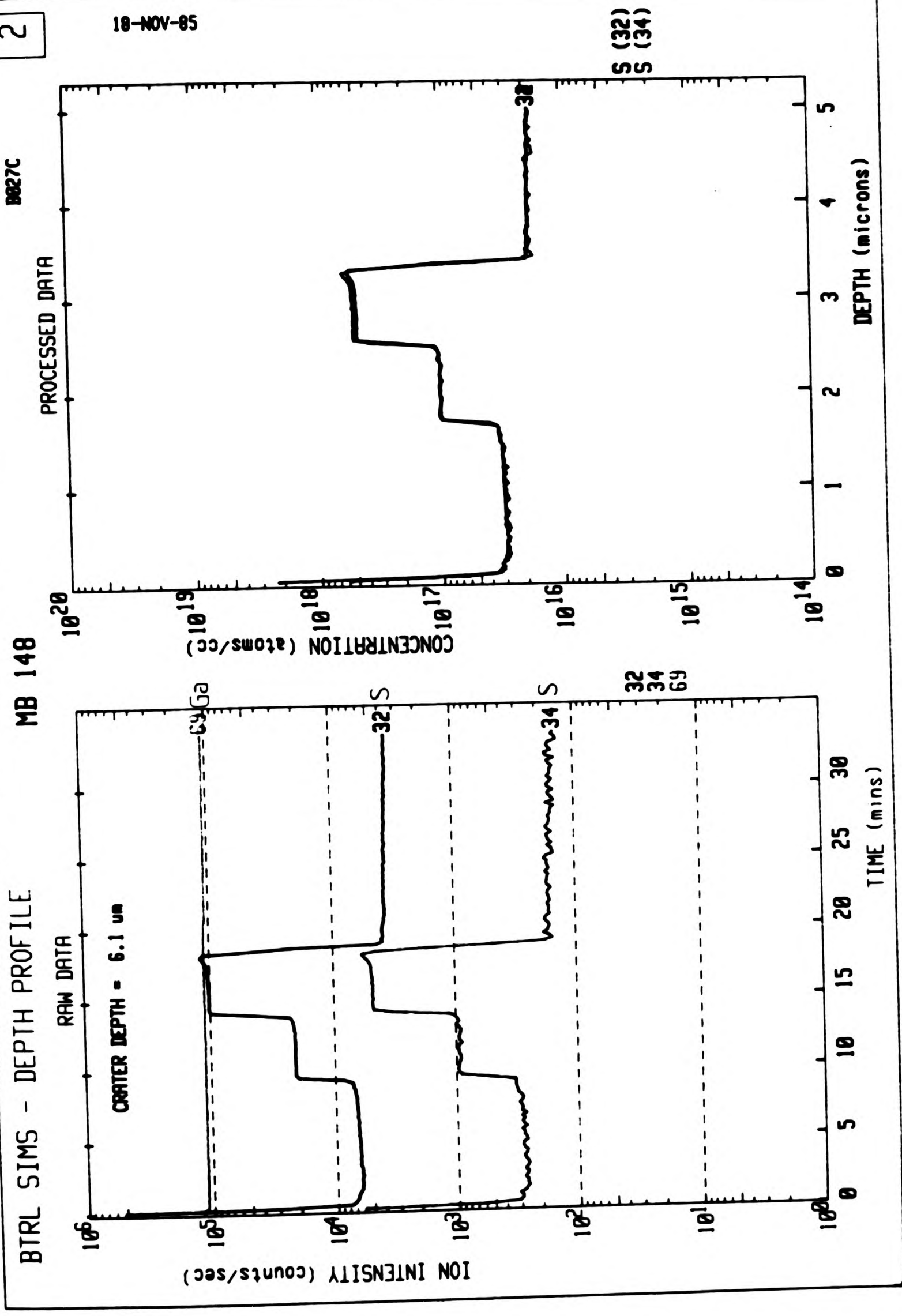


FIGURE 3.8: SIMS profile through the sulphur doped layer in figure 3.7.

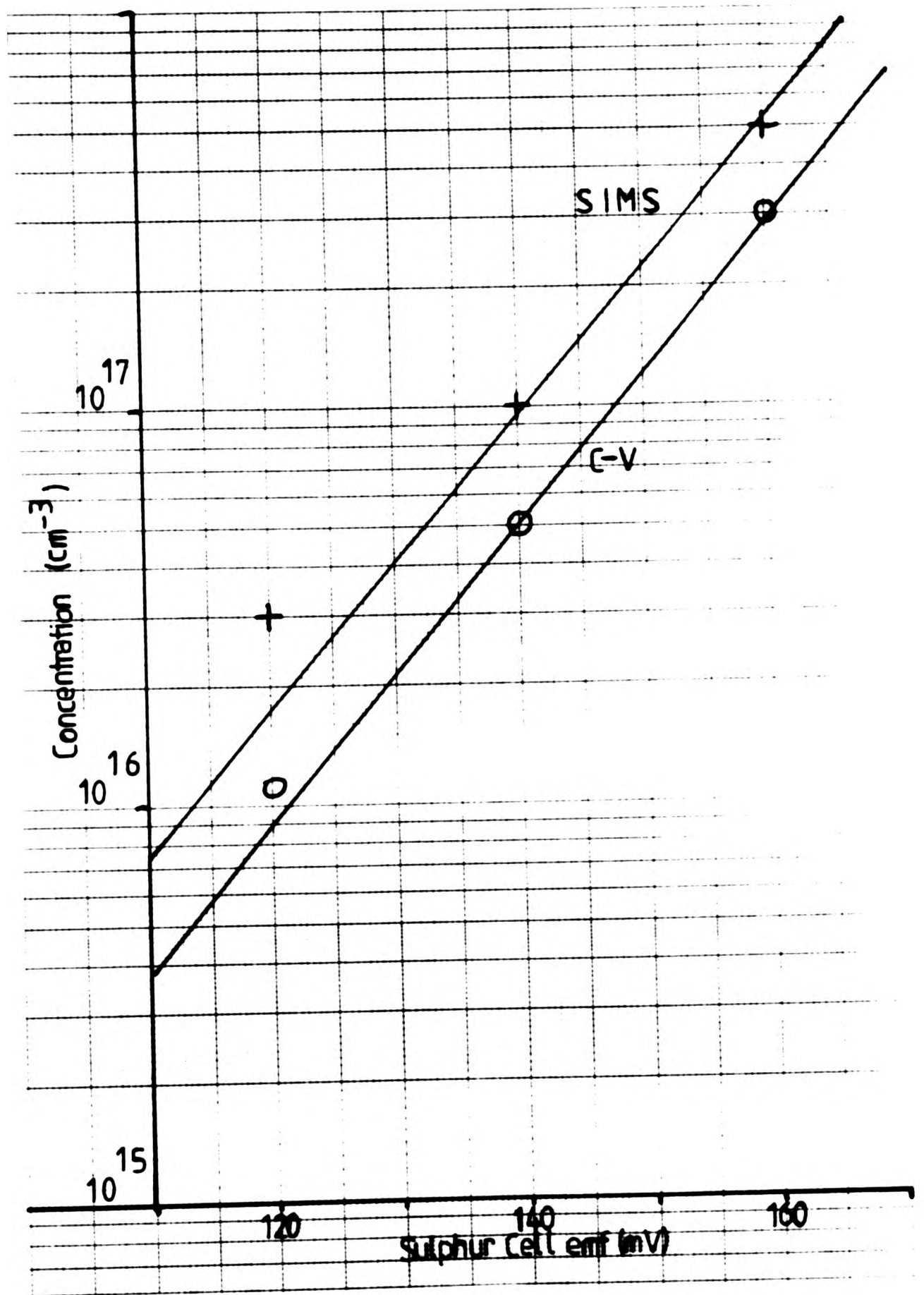


FIGURE 3.9: Sulphur concentrations deduced from C-V and SIMS measurements plotted vs applied emf from figures 3.7 and 3.8.

both lines agrees with that from the moveable ion gauge experiments giving $x=2.1$ in both cases. Below $5 \cdot 10^{16} \text{cm}^{-3}$ however, a residual background sulphur doping concentration ($\sim 1 \cdot 10^{16} \text{cm}^{-3}$), which is believed to come from the arsenic batch used, gives a deviation from the expected straight-line behaviour.

The steepness of the risers and the flatness of the plateaux, in the SIMS profile of figure 3.8 in particular, reveal simple incorporation behaviour under these growth conditions. In the C-V profile, the measurements in both the light and dark are plotted and agree well over the entire doping range; a deviation is observed at the interface with the substrate which may be due to incomplete surface oxide removal prior to growth giving an enhanced trap concentration.

Figures 3.10 and 3.11 show C-V and SIMS (13) profiles through a GaAs layer staircase-doped with selenium. The growth temperature was 610°C and the As_4/Ga flux ratio 3:1. Again the steps are well resolved and the concentrations agree to within a factor of 1.5. Figure 3.12 shows the SIMS and C-V concentrations plotted versus emf where the lines have the same slope suggesting $x=1.6$ in both cases again consistent with the moveable ion gauge data. The relationship holds to lower concentrations than for the sulphur experiment revealing a much lower S and Se background doping concentration of $< 1 \cdot 10^{15} \text{cm}^{-3}$ in this instance.

For both sulphur and selenium then, the well resolved staircase profiles show that the electrochemical cells have a fast response and a simple relationship between applied emf and

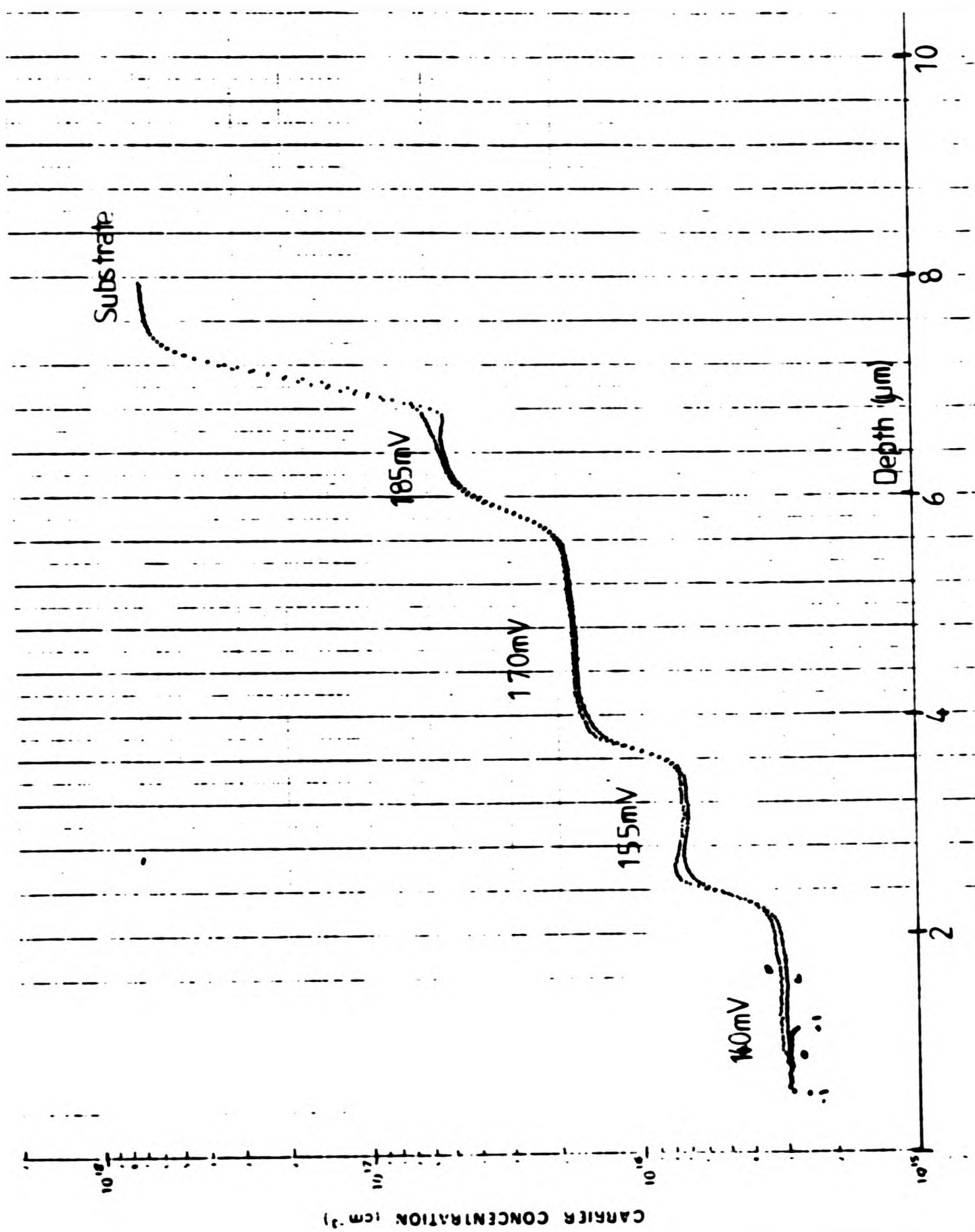


FIGURE 3.10: An electrochemical C-V depth profile through a GaAs layer staircase-doped with selenium. Light and dark measurements are plotted together.

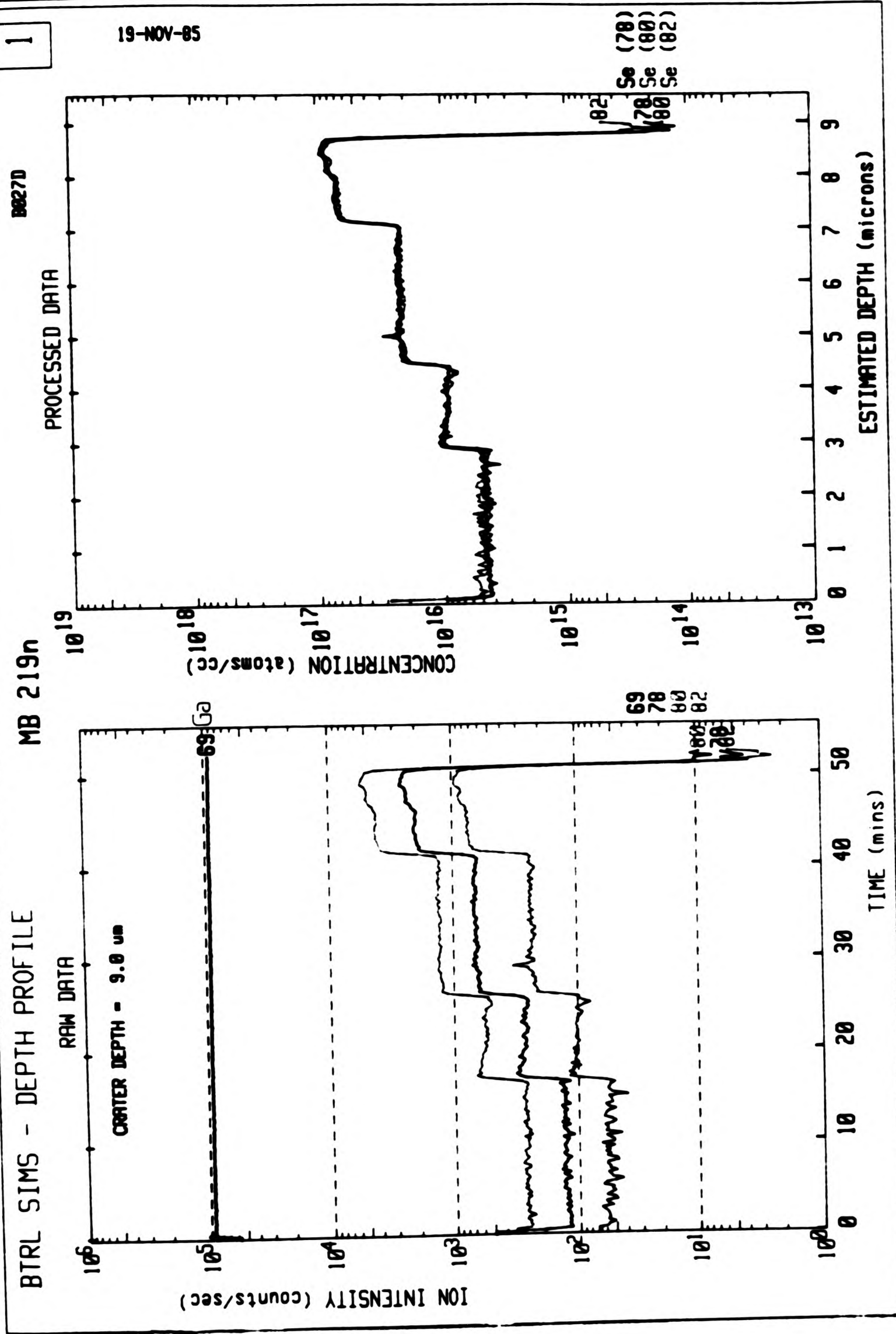


FIGURE 3.11: SIMS profile through the selenium doped layer in figure 3.10.

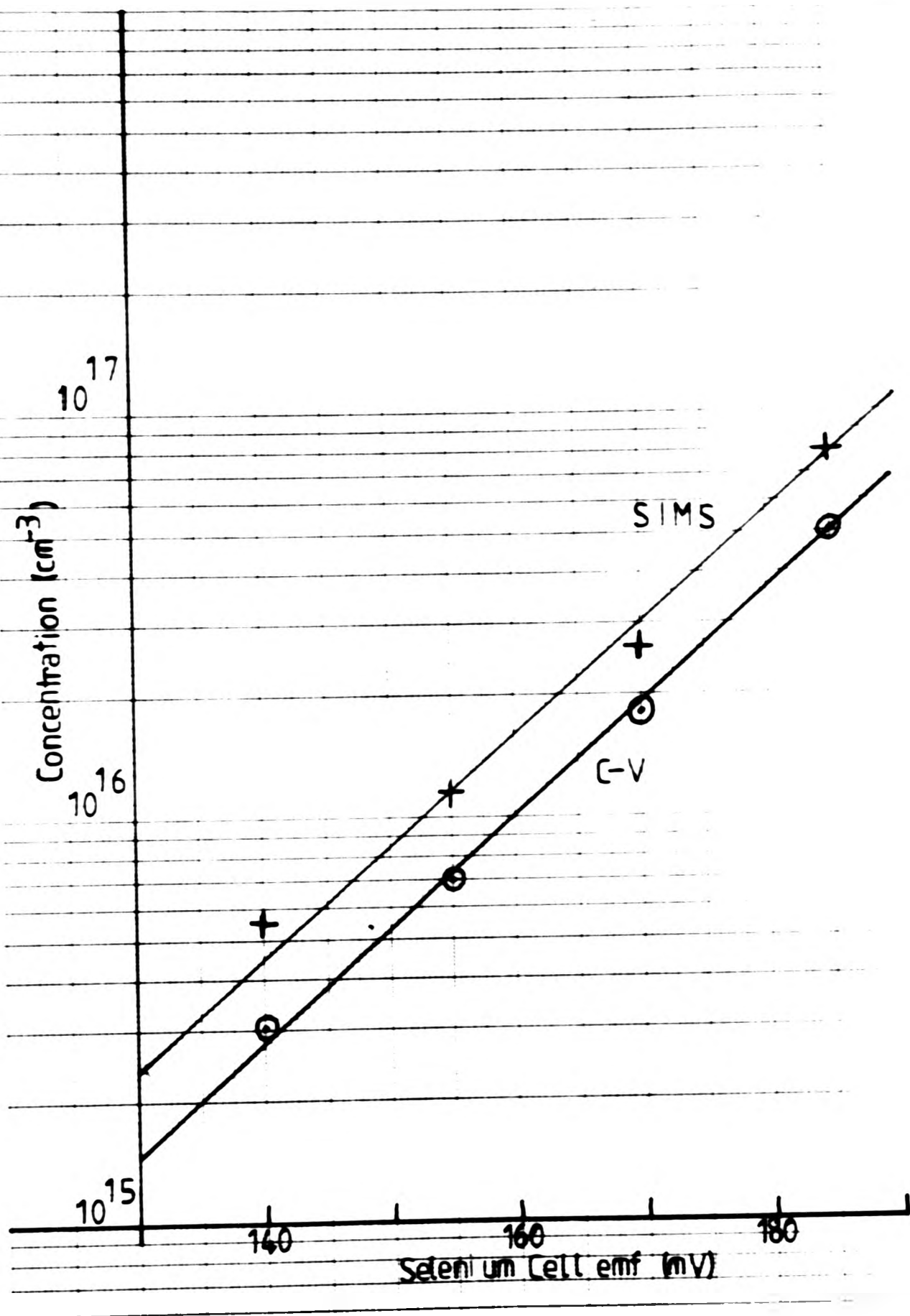


FIGURE 3.12: Selenium concentrations deduced from SIMS and C-V measurements plotted vs applied emf from figures 3.10 and 3.11.

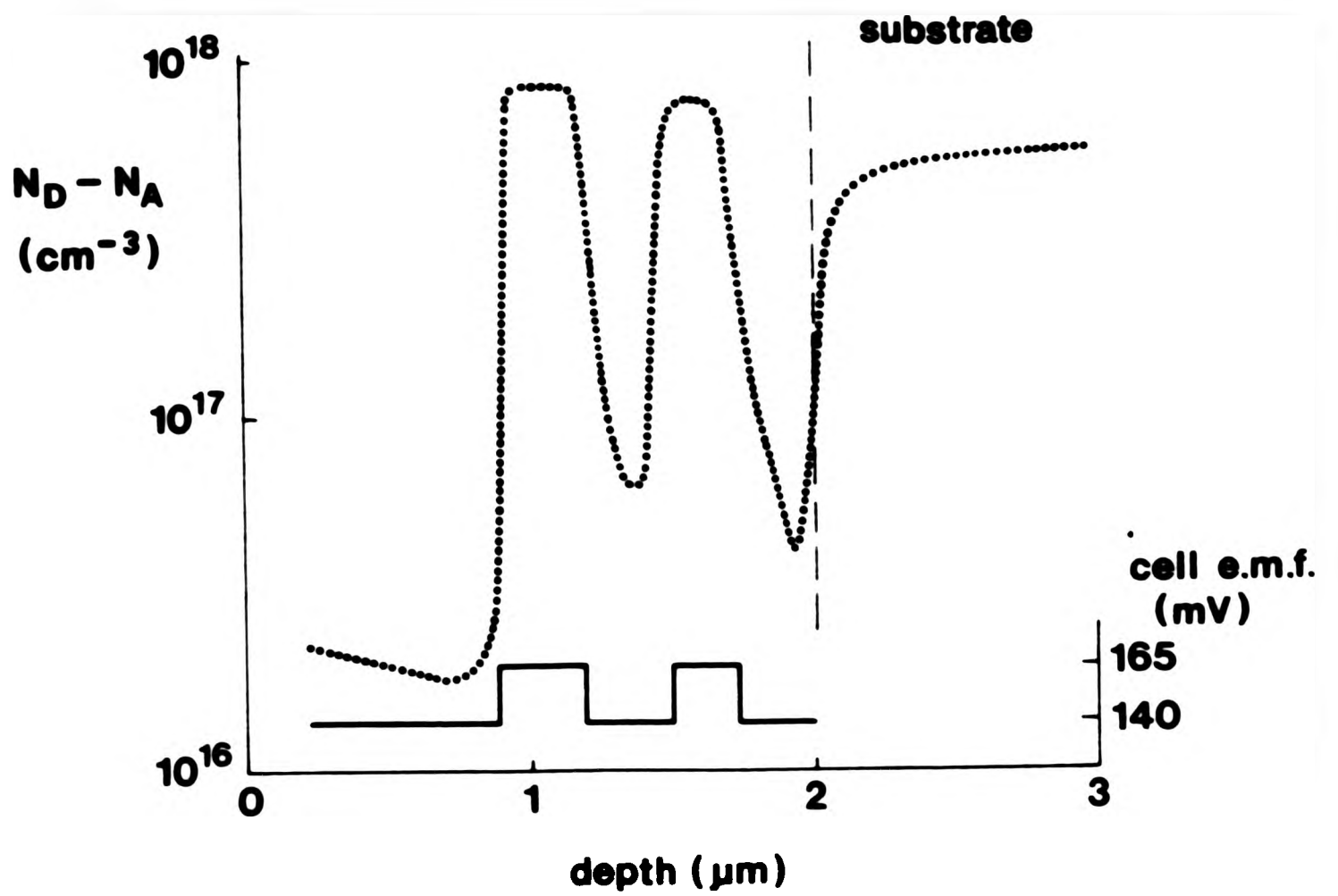


FIGURE 3.13: Free carrier profile of a HI-LO-HI-LO doping sequence in a sulphur doped GaAs layer.

dopant flux. Further, the fact that the incorporated concentration shows the same emf dependence as the measured flux indicates that the incorporation process for both dopants is simple and first order. Also, under the above growth conditions, no evidence was found for discernible segregation, diffusion or incomplete activation phenomena within the sensitivity of the techniques used.

In a further experiment, the speed of response of the electrochemical cell and the lack of memory effects in the system were demonstrated when a HI-LO-HI-LO structure was deliberately grown by switching between two emfs. The electrochemical C-V profile through this structure is shown in figure 3.13. The crucial interface for the assessment of the response time is the one nearest the surface which is encountered first by the electrochemical C-V profiler. The change in free carrier concentration is of the order of two orders of magnitude and occurs within approximately 40nm. This is close to the Debye length for GaAs at this doping level and represents the limit of the depth resolution of the C-V profiling technique (11). This type of structure is particularly taxing to profile as it is very sensitive to the uniformity of the dissolution of the GaAs which depends in turn on the uniformity of the light source used to activate the dissolution process in n-type material (11). The loss of depth resolution with increasing depth into the profile is then expected and may explain the irreproducibility of the measured doping level in the troughs corresponding to the LO regions. As an independent check, SIMS analysis of the layer was carried out (12) and revealed the repeatability of the HI and LO doping levels obscured in the C-V measurement. This also suggests that

memory effects, which might be expected if the sulphur incident on the system walls reevaporated, are negligible. No evidence was found for an enhanced residual doping level even after highly doped layers had been grown and the cryopanel allowed to thaw overnight. It seems that any sulphur condensed on the cryopanel is trapped by the GaAs that also impinges.

As a final demonstration of the utility of the electrochemical cells, a sulphur doped GaAs layer was grown with the electrochemical cell programming voltage provided by a sinusoidal function generator. Figure 3.14 shows the result of a C-V profile through the layer. Since the sulphur flux is exponentially related to the applied emf, the log plot reproduces the applied sinusoid. The damping in the profile with increasing depth is almost certainly due to nonuniform illumination during dissolution. Such a carrier profile would be difficult to achieve with a conventional thermal Knudsen source due to the long thermal time constants of a high thermal capacity cell.

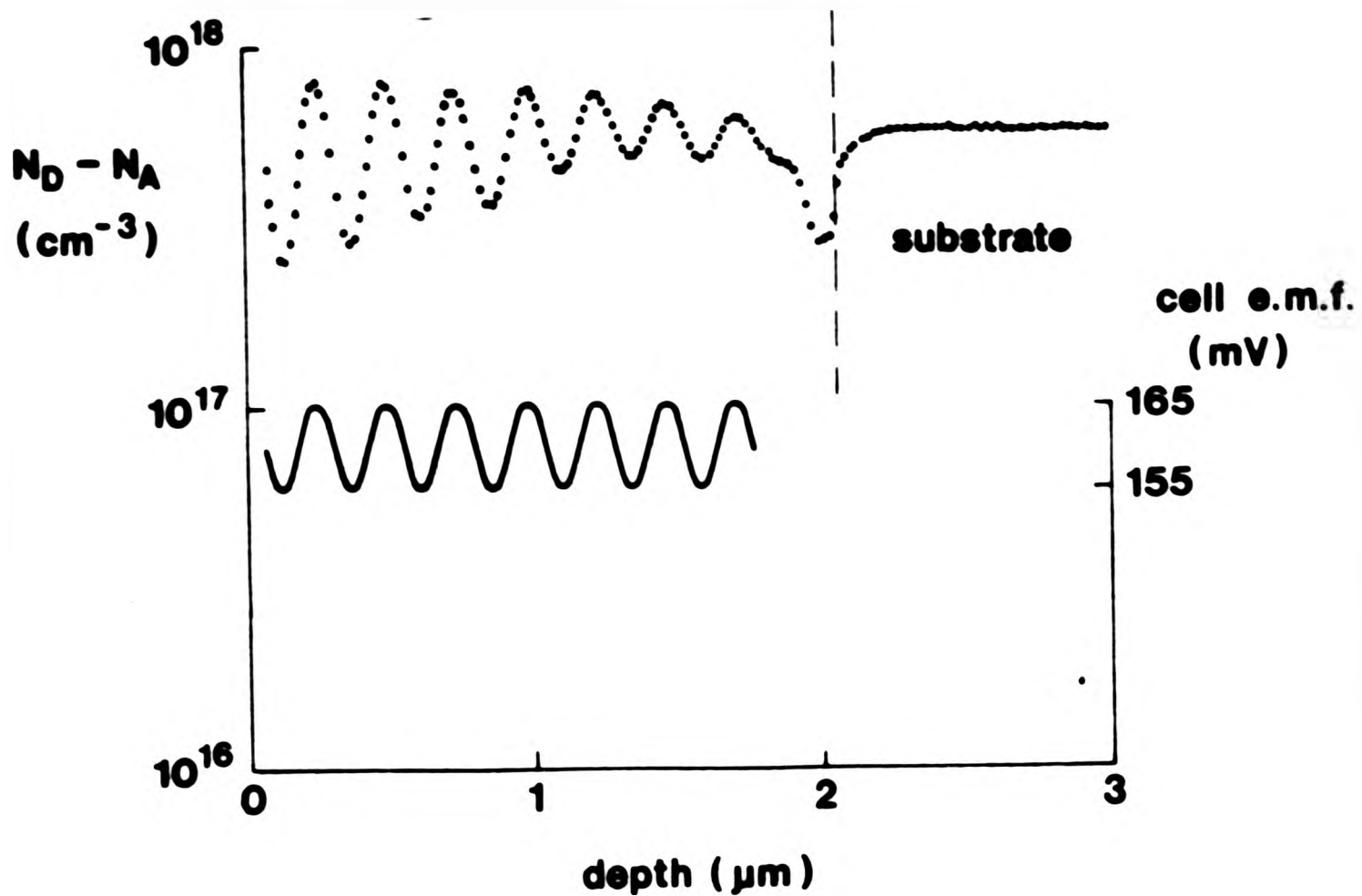


FIGURE 3.14: Sinusoidal free carrier profile generated by programming the sulphur cell with a low frequency sine wave.

3.5: References.

- 1) Ch.Park, H.M.Kramer and E.Bauer, Surface Science, 115, pl, (1982).
- W.Heegeman, K.H.Meister, E.Bechtold and K.Hayek, Surface Science, 49, p161, (1975).
- K.Schwaha, N.D.Spencer and R.M.Lambert, Surface Science, 81, p273, (1979).
- 2) C.Wagner, J.Chem.Phys., 21, p1819, (1953).
- 3) D.Detry, J.Drowart, P.Goldfinger, H.Keller and H.Rickert, Zeit.Phys.Chem., 55, p314, (1967).
- 4) G.J.Davies, D.A.Andrews and R.Heckingbottom, J.Appl.Phys., 52, p7214, (1981).
- 5) K.Mitteilung, Zeits.fur.Physik.Chem.Neue Folge, 119, p251, (1980).
- 6) K.O.Hever in Physics of Electrolytes, edited by J.Hladik (Academic, New York, 1972), Volume 2, p809
- 7) R.T.Foley, J.Electrochem.Soc., 116, p13C, (1969).
- 8) H.Rickert in reference 6, p519.
- 9) N.Valverde, Zeit.fur.Physik.Chem.Neue Folge, 70, pl13, (1970).
- 10) O.Kubaschewski and C.B.Alcock, Metallurgical Thermochemistry, 5th edition, (Pergammon, London, 1979)
- 11) T.Ambridge, J.L.Stevenson and R.M.Redstall, J.Electrochem.Soc., 127, p222, (1980).
- 12) SIMS analysis by Charles Evans and Associates, San Mateo, California.
- 13) SIMS analysis by G.Spiller, R3.1.1, BTRL.

CHAPTER 4: THE GROWTH OF HIGH PURITY GaAs.

4.1: Introduction.

Before embarking on dopant studies it was necessary to establish the credibility of both the MBE system hardware and the growth procedures used in terms of the residual impurities in the grown layers. This is particularly so since the MB288 is in something of a minority among other MBE systems worldwide in being diffusion pumped, and especially in the light of suggestions (1,2) in the literature that oil diffusion pumps prove deleterious to resulting electrical and optical properties of MBE-grown semiconductors. There are however very good reasons for choosing suitably trapped diffusion pumps. They are especially appropriate where gaseous feedstocks such as arsine and phosphine are used: large quantities of hydrogen are liberated which are difficult to pump by other methods. Also, in conjunction with a liquid nitrogen cold trap, a diffusion pump may be used to advantage in systems that handle elemental phosphorus. This is all in addition to their natural advantages of high pumping speeds, ability to pump all gases and lack of memory effects.

In this chapter we demonstrate that GaAs grown in the MB288 system using the procedures described in chapter 2 is of excellent quality.

4.2: Material Properties.

A series of deliberately doped samples were grown in order to assess their electrical properties. The layers were grown on n+ and undoped substrates simultaneously to facilitate capacitance-voltage and mobility measurements respectively. The layers were grown at 1um per hour with thicknesses between 2um and 7um depending on the doping level.

4.2.1: Morphology

The surface morphology was in general very good with total defect densities $<1000 \text{ cm}^{-3}$. The defects were of two main kinds: gallium droplet or "spit" type defects and "oval" defects. The concentration of these defects was consistently reduced to the levels quoted by rigorous outgassing of the gallium effusion cell before growth at 1200°C for 30 minutes.

4.2.2: Background Carrier Concentration.

Nominally undoped layers were n-type with free carrier densities of the order of $5 \times 10^{14} \text{ cm}^{-3}$. This background doping level is believed to arise from residual chalcogen impurities in the arsenic source charge.

Figures 4.1a-c show SIMS profiles through a nominally undoped GaAs layer grown at 580°C where the arsenic cell temperature was varied as indicated (9). The approximate As_4/Ga flux ratios are marked. The arsenic was 6N pure according to the

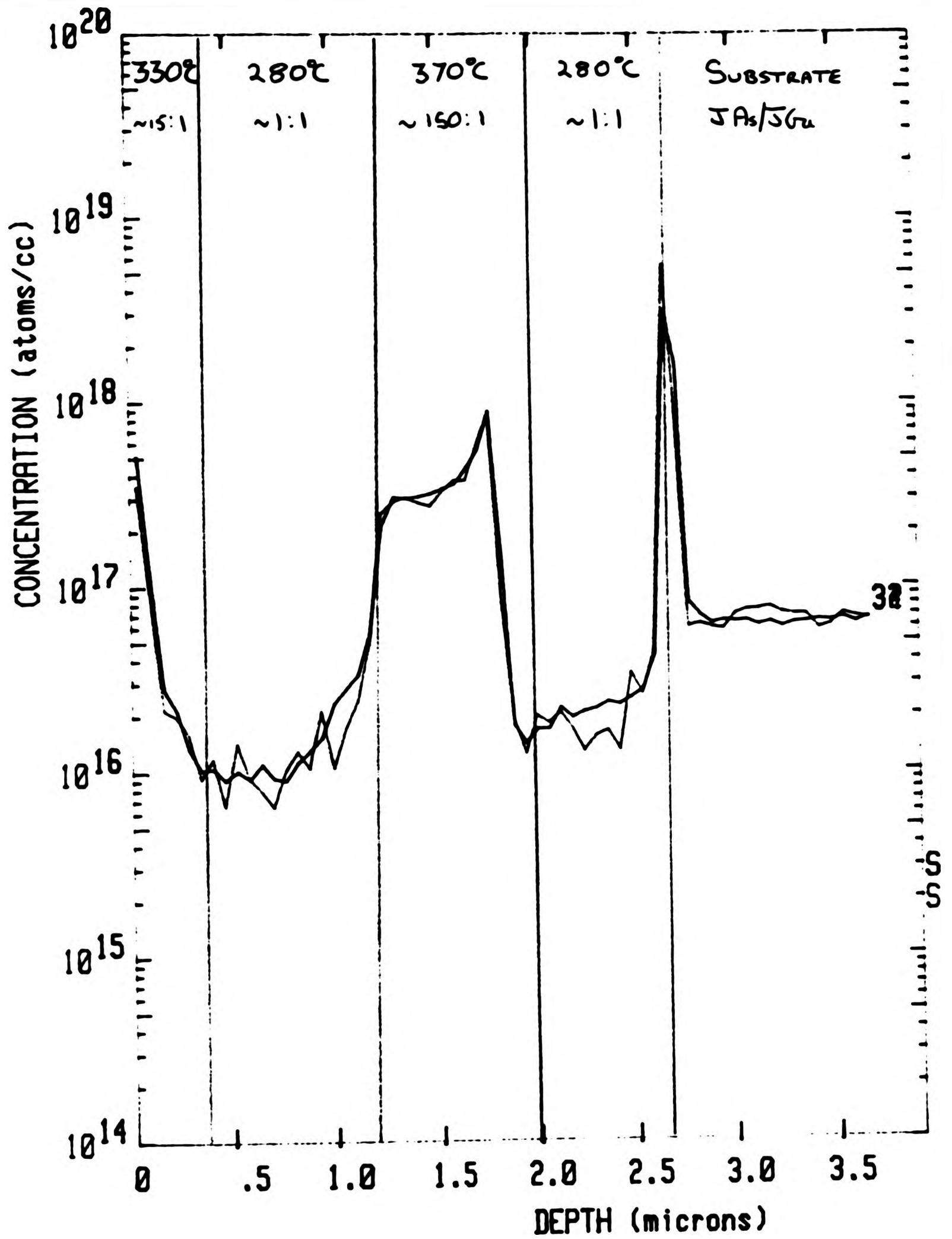


FIGURE 4.1a: Sulphur (mass 32&34 isotopes) SIMS profile of a nominally undoped GaAs layer where the arsenic cell temperature and As_4/Ga flux ratio were varied as indicated.

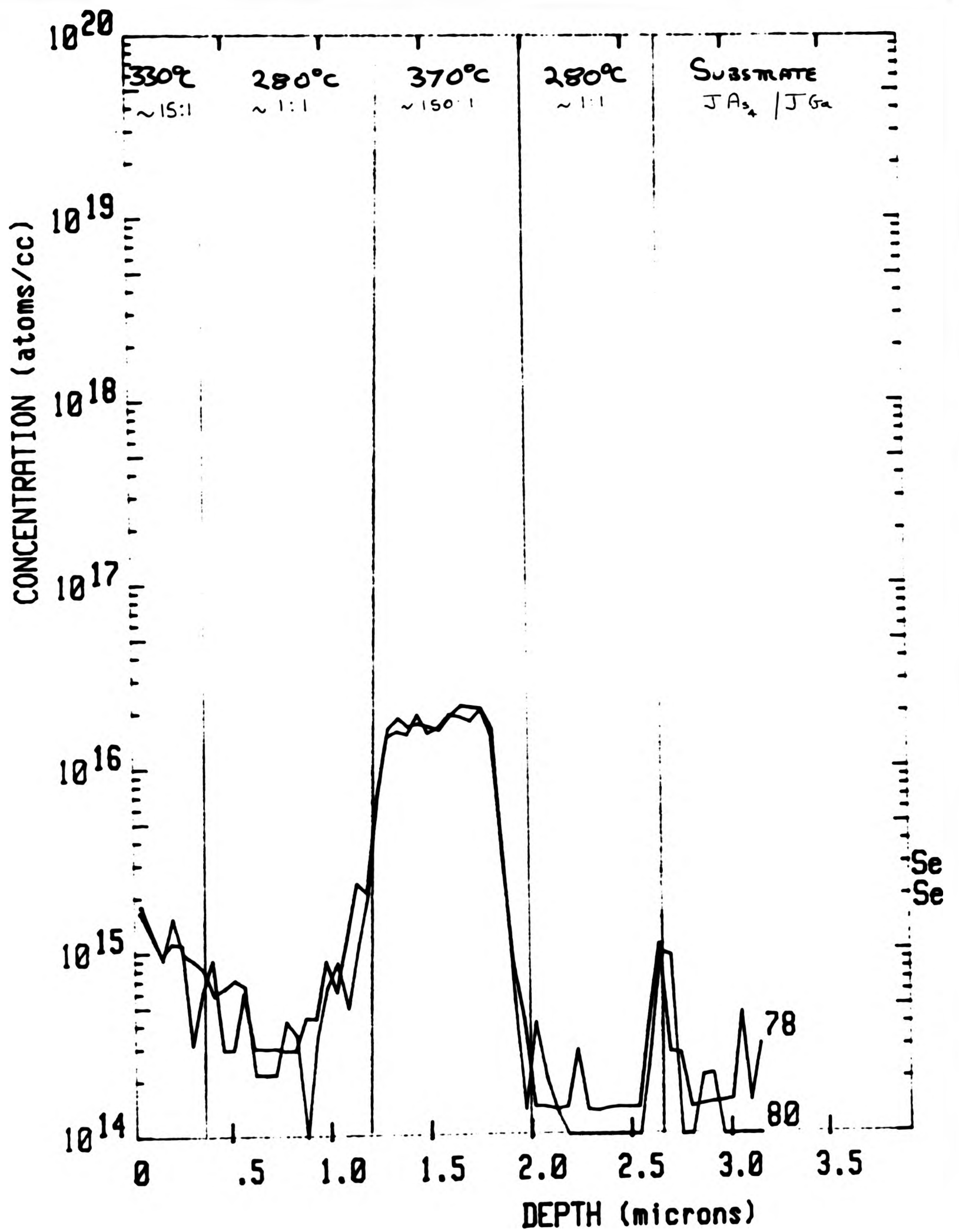


FIGURE 4.1b: Selenium (mass 78&80 isotopes) SIMS profile of a nominally undoped GaAs layer where the arsenic cell temperature and As₄/Ga flux ratio were varied as indicated.

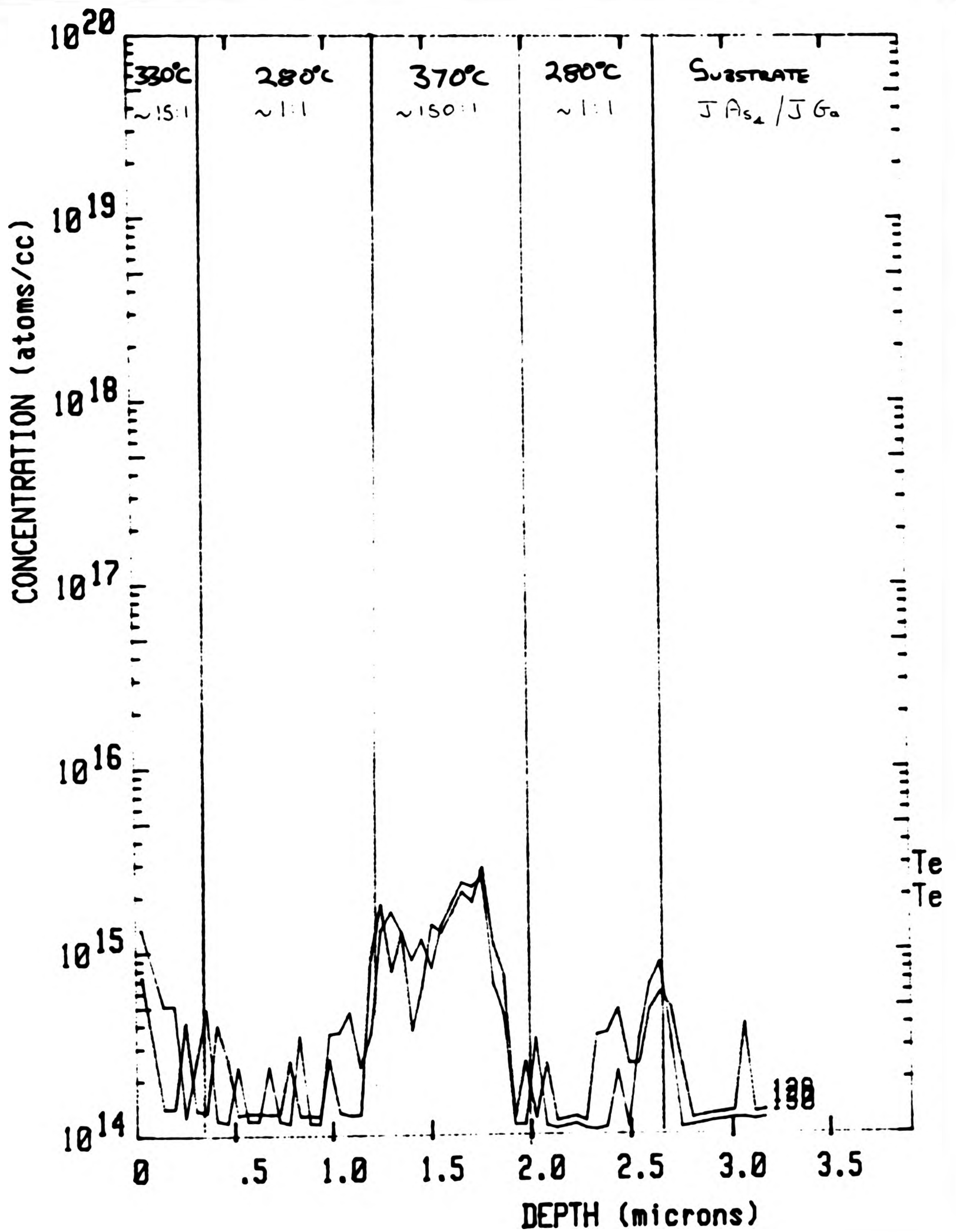


FIGURE 4.1c: Tellurium (mass 128&130 isotopes) SIMS profile of a nominally undoped GaAs layer where the arsenic cell temperature and As_4/Ga flux ratio were varied as indicated.

manufacturer. It is clear that in each case sulphur, selenium and tellurium are incorporated at higher concentrations at the higher arsenic temperatures. The spike at the layer/substrate interface may be due to chalcogen indiffusion during the surface cleanup under the stabilising arsenic flux. The incorporated concentrations of the chalcogens are in the same order as would be expected from the relative volatilities i.e sulphur, the most volatile, has the highest concentration. If we consider that the chalcogens are present in arsenic in dilute solid solution and evaporate as the elements, we may estimate their concentrations in the arsenic source material.

Let

$X = S, Se \text{ or } Te.$

$[X]$ = concentration of X in the arsenic charge.

PX° = elemental equilibrium vapour pressure of X.

PX = actual vapour pressure of species X in the arsenic cell.

PX_b = pressure of X in the molecular beam.

PAs_b = pressure of As_4 in the molecular beam.

PGa_b = pressure of Ga in the molecular beam.

$[GaAs]$ = density of GaAs.

$R = PAs_4 / PGa =$ flux ratio at the surface.

$T =$ temperature of the arsenic cell.

$n(X) =$ measured concentration of X in the grown GaAs.

Then $PX = PX^{\circ} \cdot [X]$ and

$$n(X) \cdot PX_b / [GaAs] \cdot PGa_b = PX_b \cdot R / PAs_b$$

Since $PX_b / PAs_b = PX / PAs^{\circ}$, we have

Species	Sulphur		Selenium		Tellurium	
T. (°C)	280	370	280	370	280	370
PX ^o	20	200	4x10 ⁻²	1	4x10 ⁻⁵	6x10 ⁻³
PAs ^o	1.5x10 ⁻³	0.2				
R	~1	~150				
n(X)	10 ¹⁶	5x10 ¹⁷	10 ¹⁵	2x10 ¹⁶	<10 ¹⁴	10 ¹⁵
[X]	3.5x10 ⁻¹¹	1.5x10 ⁻¹⁰	1.7x10 ⁻⁹	1.2x10 ⁻⁹	<10 ⁻⁷	10 ⁻⁸

TABLE 4.1: Chalcogen impurity concentration in the arsenic source material calculated from the data in figure 4.1.

$$[X] = \frac{P_X}{P_X^0} = \frac{P_{As^0} \cdot P_{X_b}}{P_X^0 \cdot P_{As_b}} = \frac{P_{As^0} \cdot n(X)}{P_X^0 \cdot R} \text{ [GaAs]}.$$

The results of this calculation are shown in tabular form in table 4.1 where it may be seen that the concentrations are all very low and certainly below most normally quoted detection limits on certificates of analysis for arsenic. One particular batch of nominally 7N pure arsenic produced GaAs layers unintentionally doped to greater than 10^{17} cm^{-3} (these are the filled circle data in figure 4.3). This was traced by wet chemical analysis (4) to tellurium contamination of the arsenic of the order of 10ppm, consistent with the above calculations. Chalcogen contamination of the arsenic is clearly a problem, especially since the chalcogens are chemically similar to arsenic (or indeed phosphorus) and are therefore difficult to extract chemically or identify spectroscopically. Different suppliers of arsenic were tried (MCP, Johnson Matthey, Cominco and Canyonlands) but there appeared to be as much variation between batch numbers from the same supplier as between suppliers. Gallium from each of the above suppliers was also tried but with no effect on the background doping level.

4.2.3: Deliberately Doped Material.

A C-V depth profile through a typical low-doped layer is shown in figure 4.2. The free carrier concentration is plotted against depth, both under illumination during electrochemical dissolution and in the dark between dissolution steps. The lack of any significant separation under these two conditions is indicative of high material quality: specifically there are no significant concentrations of deep levels which would generate

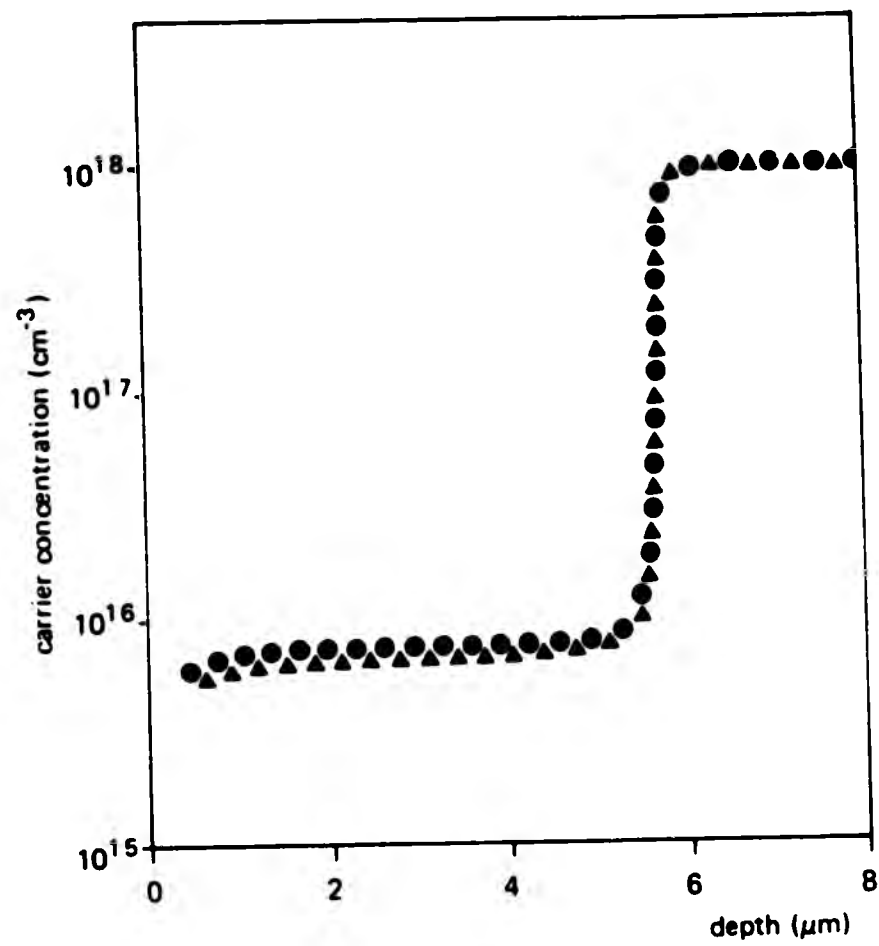


FIGURE 4.2: A C-V depth profile through a lightly sulphur-doped GaAs layer. ● = measured under illumination during dissolution, ▲ = measured in the dark between dissolution steps.

or trap carriers under illumination and affect the measurement of free carrier level. In addition, the abrupt interface with the substrate indicates that the dissolution is extremely uniform implying a low concentration of crystal defects which would otherwise tend to preferentially etch (5). There is also no evidence for trap states at the interface which would cause a dip in the plot at this point implying that the substrate was well cleaned before growth was initiated.

4.2.4: Electron Mobilities.

Hall mobility measurements were made on 6mm square samples with tin dots alloyed into the corners. In a few instances, proper Van der Pauw patterns were defined and showed that in every case the simple corner geometry led to an under estimate of the mobility as illustrated in table 4.2. The Hall mobility data at 300K and 77K are shown in figure 4.3 superimposed on published data from several other commercial MBE systems, all of which use ion pumps. The data is taken from the manufacturers literature. It is clear from this figure that there are no identifiable deleterious effects on mobility which could be attributed to the use of diffusion pumps, at least for free electron concentrations in excess of $1 \times 10^{15} \text{cm}^{-3}$.

4.2.5: Luminescence Properties.

The luminescence properties of semiconductor material provide another good test of material quality. In particular, one of the main arguments against the use of diffusion pumps is that

Sample	Nd-Na (cm^{-3})	Mobility ($\text{cm}^2\text{V}^{-1}\text{s}^{-1}$)			
		300K		77K	
		Without Van de Pauw	With Van de Pauw	Without Van de Pauw	With Van de Pauw
MB155	3.3×10^{16}	4380	5617	9000	11400
MB177	2.5×10^{15}	6300	7700	42000	45000
MB191	1.3×10^{17}	4100	4500	5200	-----
MB206	1.7×10^{15}	5850	6600	-----	-----

TABLE 4.2: Comparison of mobility measurements made using tin dots and Van der Pauw mesas. Measurements made at room temperature and 77K.

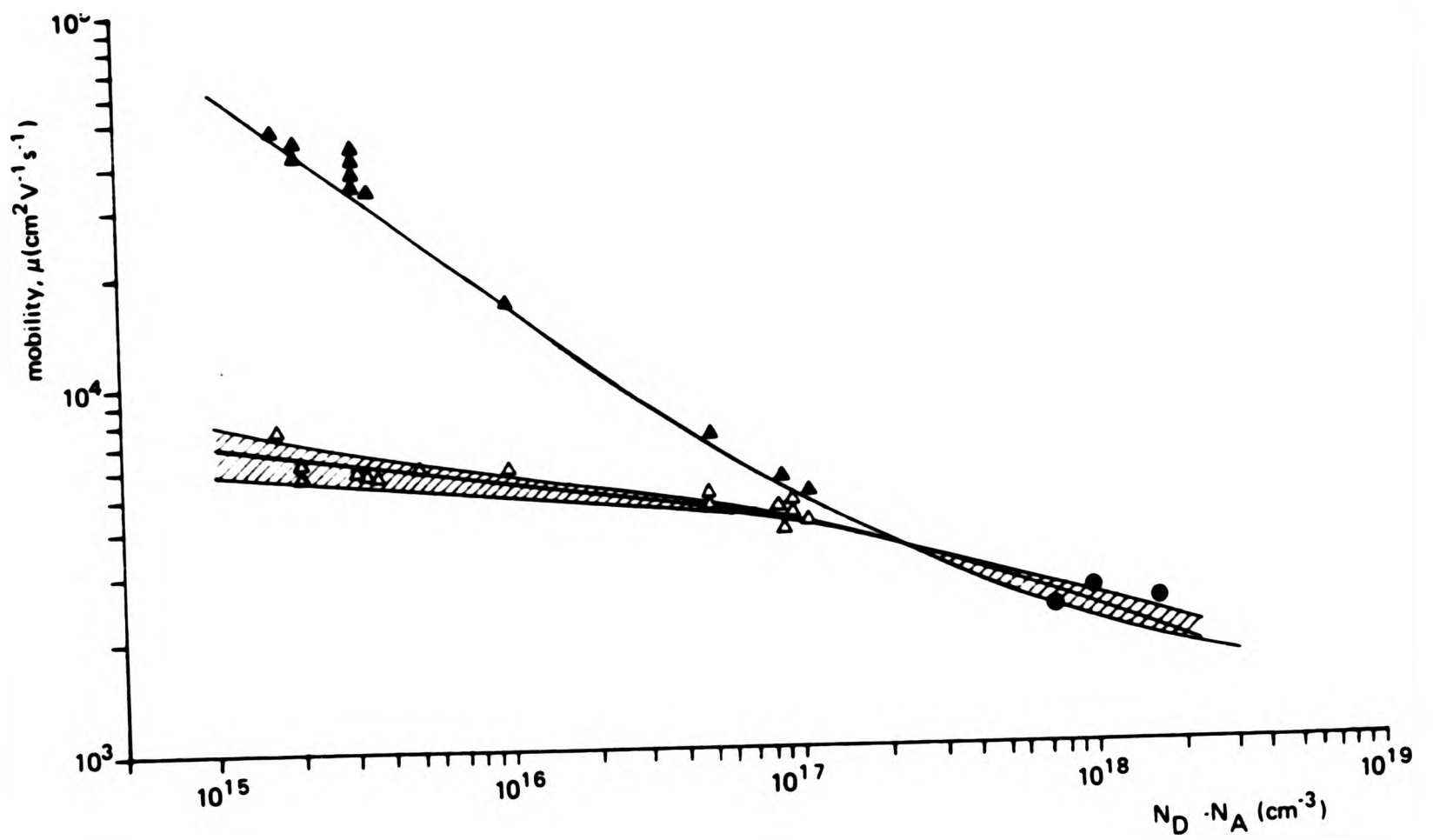


FIGURE 4.3: Comparison of mobility for a range of donor concentrations for commercial MBE systems made by Varian, PHI and RIBER (solid lines, silicon or tin doped) and the MB288 system (sulphur doped: - \blacktriangle = 77K, \triangle = 300K, tellurium doped: - \bullet = 300K).

backstreaming of diffusion pump oil leads to an enhanced incorporation of carbon, which is an acceptor in GaAs. To test the carbon levels in the GaAs grown in the MB288 system the 4K cathodoluminescence spectra of nominally similar high purity GaAs samples grown in a variety of systems were compared (6). Table 4.3 shows the results of such a comparison where it may be seen that the luminescence due to the presence of carbon acceptors is of a similar intensity among the different MBE systems. It should be emphasised that the luminescent intensity is not necessarily an accurate indicator of elemental concentration. However, the samples were measured side-by-side in the same C-L system on the same day and the distinct similarity in intensities over several samples and MBE systems does indicate that the incorporation of carbon is relatively independent of pumping system. This is perhaps not entirely unexpected since these MBE systems possess large amounts of cryopanelling which serve to create an environment within the vacuum system effectively isolated from the primary pumps.

In addition, high resolution 4.2K photoluminescence spectra (7) from the MB288 material were at least as well resolved in the excitonic region as would be expected from the donor concentrations as indicated in figure 4.4. However, the background doping level means that the fine structure on the D^0X and A^0X peaks reported elsewhere (8) for the highest purity MBE material ($n \sim 10^{14} \text{ cm}^{-3}$) may not be resolved on the MB288 material.

Sample	MB164	MB168	35	63	98	1109
300K						
Relative Luminescence Intensity	72	140	76	100	11	100
Doping ($\times 10^{15}$)	1.0 n	2.0 n	1.2 n	1.7 n	0.4 p	???
4K						
Relative Intensity (Donors)	85	250	140	105	17	150
Relative Intensity (Carbon)	21	26	34	40	11	38

MB164 and MB168 were grown on the VG MB288 system. The rest were grown on Varian 360 and Gen II systems. All the samples were measured by cathodoluminescence under nominally identical conditions.

TABLE 4.3: Comparison of the luminescence intensities from GaAs grown in diffusion and ion pumped MBE systems.

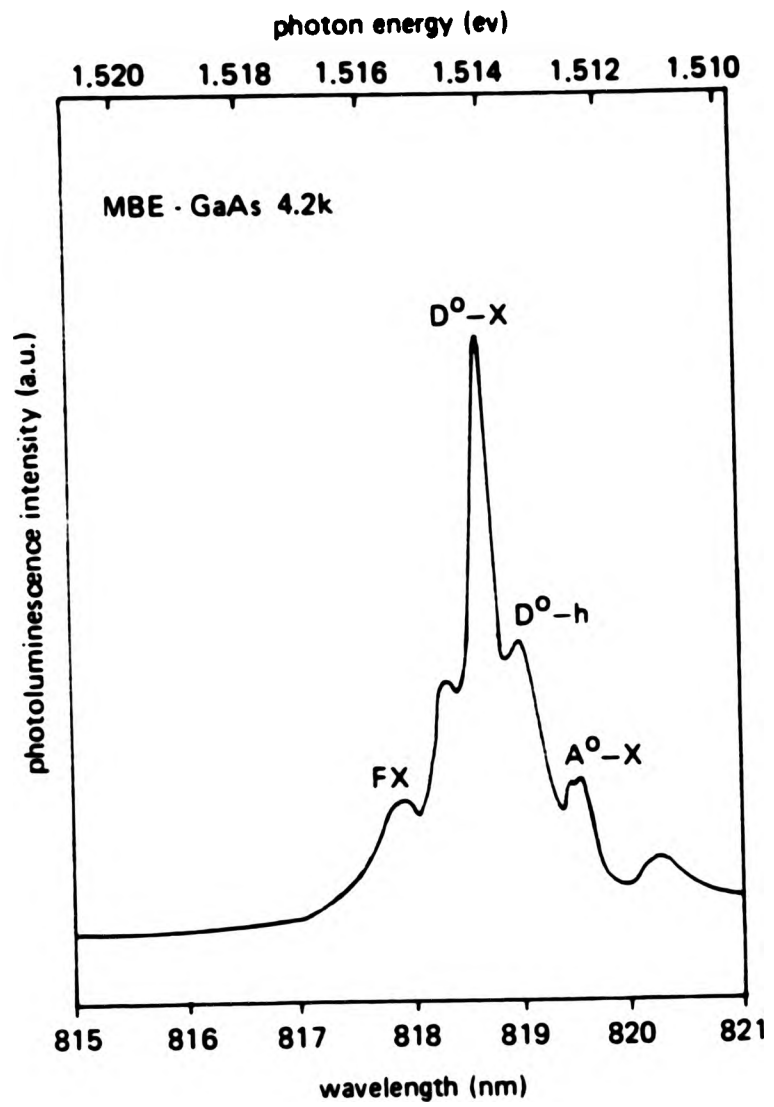


FIGURE 4.4: 4.2K photoluminescence spectrum of nominally undoped GaAs, $n \sim 8 \times 10^{14} \text{cm}^{-3}$.

4.3: Conclusions.

It is clear that the MB288 system, used in conjunction with the procedures outlined in chapter 2, is capable of producing GaAs of very high quality, comparable with any other commercial machine. In particular, there are no identifiable deleterious effects that could be attributed to the use of diffusion pumps. The limiting factor on residual doping seems to be the purity of the source materials available, particularly the arsenic.

4.4: References.

- 1) M.B.Panish, J.Electrochem.Soc., 127, p2729, (1980).
- 2) R.A.Kubiak, P.Driscoll and E.H.C.Parker, J.Vac.Sci.Tech., 20, p252, (1982).
- 3) O.Kubaschewski and C.B.Alcock, Metallurgical Thermochemistry, 5th ed., (Pergammon, Oxford, 1979).
- 4) Chemical analysis performed by Johnson Matthey Chemicals Ltd., Royston, England.
- 5) T.Ambridge, J.L.Stevenson and R.M.Redstall, J.Electrochem.Soc., 127, p222, (1980).
- 6) Samples kindly supplied by Dr.G.Weimann, FTZ, Darmstadt, W.Germany. Cathodoluminescence studies performed by B.Wakefield R3.1.1, BTRL.
- 7) High resolution photoluminescence study by M.Skolnick of RSRE, Malvern.
- 8) R.Dingle, C.Weisbuch, H.L.Stormer, H.Morkoc and A.Y.Cho, Appl.Phys.Lett., 40, 507, (1982).
- 9) G.D.T.Spiller and D.A.Andrews, Vacuum, 36, p991, (1986).

CHAPTER 5: THERMODYNAMIC FRAMEWORK.

5.1: Introduction.

Historically, the MBE process has been described mainly in terms of the kinetics of the growth and doping reactions (1). This preference, and the corresponding assumption of the low relevance of thermodynamic considerations may be readily appreciated.

Much of the early growth of GaAs by MBE took place with the substrate supercooled by some 100°C with respect to the equilibrium position dictated by the applied reactant pressures. For example, for a typical growth rate of $1\mu\text{m}\cdot\text{hr}^{-1}$ and $P(\text{Ga})=P(\text{As})=10^{-6}$ torr, the equilibrium substrate temperature may be deduced from Arthur's vapour pressure data (2) as $T_s=680^{\circ}\text{C}$ whereas much MBE GaAs growth takes place at $T_s=580-600^{\circ}\text{C}$ (3). The reactants are therefore in excess with respect to equilibrium values and there is a large overpotential for growth. Also, in an MBE apparatus, the reactants appear to make only one collision with the growing surface before being pumped away.

However, it has been demonstrated that the species leaving the substrate have acquired its temperature (4) and incorporated species may therefore be considered to be at the substrate temperature. Further, for a $1\mu\text{m}\cdot\text{hr}^{-1}$ growth rate, the incorporated species are in the surface layer for approximately one second before being buried by the next atomic layer. For $T_s=600^{\circ}\text{C}$ and a 1eV surface binding energy, an atom may sample

approximately 10^6 sites with plenty of opportunity for reaching its preferred position.

The strongest argument for the relevance of thermodynamics to MBE growth comes from the fact that material grown by MBE is of a similar quality, in terms of low concentrations of non-equilibrium defects, to that obtained by LPE or VPE. These growth techniques are well described by a thermodynamic framework that assumes that growth occurs under near-equilibrium conditions. The conclusion must be that the kinetic processes relevant to MBE are sufficiently facile to allow equilibrium to be reached without significant hindrance. With the current trend to higher growth temperatures in MBE (5), and the consequent reduction in overpotential for growth, this conclusion should be even more valid.

In a recent body of work (6-9), the thermodynamic framework for the description of MBE processes has been outlined and a critical study of the importance of kinetic influences made. It has been shown that, in the majority of cases, thermodynamic considerations are most successful in predicting behaviour (ie equilibrium is reached), and allow the relatively few instances when kinetic hindrances do intrude to be identified. In the following sections, the thermodynamic framework will be described and the method for extrapolating from VPE and LPE conditions to MBE growth conditions, outlined in reference (6), will be illustrated in detail for sulphur and tellurium incorporation in GaAs. The model is then applied to selenium doping of VPE-grown GaAs and sulphur selenium and tellurium doping of LPE-grown InP.

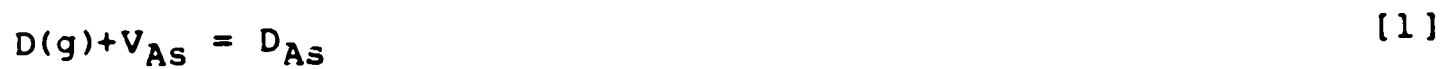
5.2: The Thermodynamic Method.

In the situation where the growth kinetics are facile, a fairly complete picture of the growth process may be obtained by considering the equilibrium positions of all relevant reactions under the conditions imposed during MBE. The equilibrium position of a reaction, measured by its equilibrium constant $K(T)$, may be obtained by considering the free energies of reactants and products. For a reaction to occur spontaneously, the products must have a lower free energy than the reactants. In this case the thermodynamic prediction is only that the reaction is permitted; only if the kinetics are facile may equilibrium be reached. In the reverse situation, the prediction that the reaction is forbidden comes entirely from the thermodynamics, without any recourse to kinetic arguments. Additionally, the experimental observation that a thermodynamically predicted reaction does not occur provides a clear indication of the intrusion of hindered, as opposed to facile, kinetics. It is, however, important to be aware that a particular reaction may not be observed simply due to competition from a second side reaction whose products are energetically more favoured. It is therefore necessary to consider all likely routes before invoking kinetics as the culprit for the non-observation of a reaction.

5.3: The Dopant Incorporation Model.

The generally accepted approach to describing the incorporation of substitutional dopants is via the interaction between the

dopant species and the lattice vacancies (6). Consider the case of a donor impurity occupying a site on the arsenic sublattice in GaAs. The incorporation reaction is:-



with corresponding free energy change G_1 . The incorporated donor atoms are then ionised according to



to yield the overall reaction



where $D(g)$ is a donor atom in the gas phase, D_{As} and D_{As}^+ are the neutral and ionised donor atoms incorporated onto sites in the arsenic sublattice, V_{As} is a vacant arsenic site and e^- is an electron in the conduction band of the bulk GaAs. The relationship between the free energy change for a reaction and its equilibrium constant may be expressed as, using reaction [1] as an example,

$$K_1(T) = \exp(-G_1/RT) \quad [4]$$

in which R is the gas constant, T the absolute temperature, G_1 the free energy change for reaction [1] and K_1 the corresponding equilibrium constant which may also be expressed in terms of the mass action law as

$$K_1 = [D_{As}] / P_D \cdot [V_{As}] \quad [5]$$

where $[\]$ represents concentration and P the pressure in atmospheres. Activity coefficients of unity are assumed. Similarly,

$$K_2 = n \cdot [D_{As}^+] / [D_{As}] \text{ where } n = [e^-] \quad [6]$$

$$K_3 = K_1 \cdot K_2 = n \cdot [D_{As}^+] / P_D \cdot [V_{As}] \quad [7]$$

If we assume that all the electrons in the conduction band arise from reaction [2], we may substitute $n = [D_{As}^+]$ into equation [7] to yield

$$[D_{As}^+] = n = K_3^{1/2} \cdot P_D^{1/2} \cdot [V_{As}]^{1/2} \quad [8]$$

The native defect concentration $[V_{As}]$ is conventionally described by the equation

$$1/4 As_4 + V_{As} = 0 \quad [9]$$

and by fixing the conditions for this reaction to give a particular value of $[V_{As}]$, we may access a range of carrier concentrations in the grown GaAs by varying P_D and would expect a $P_D^{1/2}$ dependence of n . In fact this relationship is not observed, rather a linear one seems to apply (10,11,12,13) with n proportional to the activity of the dopant species (P_D in VPE and a_D in LPE). This dependence subsists in LPE and VPE reports on dopants from groups II, IV and VI of the periodic table incorporated onto both sublattices. The required linear behaviour may be obtained if we assume that n is not determined during growth by reaction [2] but is instead fixed at some high

constant value. Rearranging equation [7] then yields

$$[D_{As}^+] = K3 \cdot P_D \cdot [V_{As}] / n \quad [10]$$

$$[D_{As}^+] = K3' \cdot P_D \cdot [V_{As}] \quad [11]$$

where $K3' = K3/n$, n constant.

Arsenic is usually supplied as As_4 by evaporation from the solid so we may account for the $[V_{As}]$ term via equation [9] thus

$$K9 = 1/PAs_4^{1/4} \cdot [V_{As}]$$

$$[V_{As}] = 1/K9 \cdot PAs_4^{1/4}$$

and substituting in [11] gives

$$[D_{As}^+] = K3'' \cdot P_D \cdot PAs_4^{-1/4} \quad [12]$$

where $K3'' = K3'/K9$.

While it is worth noting that the required high constant value of n during growth may not be obtained by thermal excitation of electrons in the valence band across the energy gap, the precise details are not crucial to the following discussion. At least two models have been proposed (11,13), the latter suggesting that ionisation of a shallow native defect, such as V_{As} , at the growth temperature may be responsible. However, in view of the apparent widespread validity of the linear dependence of $[D^+]$ on P_D or a_D for VPE and LPE growth using a

wide variety of dopants, we may extrapolate to MBE conditions with some-confidence.

5.4: Dopant Incorporation Calculations.

In determining whether the incorporation of a particular dopant is likely, we need to establish some values for the terms in equation [12]. The key issue is to determine whether the dopant pressure P_D required above the growing GaAs to achieve suitable doping levels is accessible under MBE conditions.

5.4.1: The Simplest Case, Condensation.

In the kinetic limit of all impinging dopant atoms being incorporated, P_D is the equivalent pressure of the molecular beam flux, so that

$$P_D/P_{Ga} = J_D/J_{Ga} = n/[GaAs]$$

where the $\{J\}$ are the dopant and gallium fluxes arriving at the substrate and $[GaAs]$ is the density of GaAs. Dopant species such as silicon which have a negligible elemental vapour pressure at the growth temperature would condense under these conditions anyway and do not require any more detailed consideration of their interaction with the GaAs lattice. So for a gallium beam pressure of 10^{-6} torr and a doping level of $2.2 \times 10^{16} \text{cm}^{-3}$ (1ppm), we would require a dopant pressure in the molecular beam of 10^{-12} torr.

The chalcogen dopants S, Se and Te on the other hand, all have large elemental vapour pressures at the growth temperature and consideration of their interaction with the GaAs lattice is crucial.

Direct calculation of $[V_{As}]$ and K_3'' for substitution into equation [12] is difficult due to the paucity of thermochemical data for the relevant species. However, by using data on doping from VPE and LPE experiments, one may calculate the equivalent P_D for the case if the VPE or LPE processes were to take place under MBE conditions of temperature and pressure.

5.4.2: VPE Extrapolation, Sulphur Doping of GaAs.

For a typical VPE experiment (14) sulphur doping is achieved by the introduction of H_2S in an excess of H_2 at 1 atm. For a pressure ratio of $PH_2S/PH_2=10^{-7}$, a doping level $[S_{As}^+]=10^{17}cm^{-3}$ may be achieved at $750^\circ C$. Consider the reaction



G for this reaction may be expressed as (18)

$$G=-41360+23.61T \text{ calories } (298K<T<1800K) \quad [14]$$

This evaluates to $-22.54Kcal$ at $600^\circ C$. The equilibrium constant is

$$K_{13}=(PH_2S)^2/PS_2.PH_2^2 \quad [15]$$

Using [4] and rearranging [15] gives

$$P_{S_2} = (P_{H_2S}/P_{H_2})^2 \cdot K_3^{-1} \quad [16]$$

$$P_{S_2} = (P_{H_2S}/P_{H_2})^2 \cdot \exp G/RT \quad [17]$$

At 600°C this gives $P_{S_2} = 2.25 \times 10^{-20}$ atm or 1.71×10^{-17} torr. This is the partial pressure of S_2 that would be produced by the decomposition of 0.1ppm H_2S in 1 atmosphere of H_2 at the MBE growth temperature of 600°C.

Rewriting equation [12] for diatomic sulphur we have

$$[S_{As}^+] = K_3'' \cdot P_{S_2}^{1/2} \cdot P_{As_4}^{-1/4} \quad [18]$$

Assuming K_3'' to be a weak function of temperature (typically varying by a factor of 3 between 660°C and 760°C (19)) we may substitute for a typical VPE value of $P_{As_4} = 1.5 \times 10^{-3}$ atm (15,19) into equation [18] to give $K_3'' = 1.31 \times 10^{26} \text{ cm}^{-3} \cdot \text{atm}^{-1/4}$. Therefore, under MBE conditions of $n = 10^{17} \text{ cm}^{-3}$, $T = 600^\circ\text{C}$ and $P_{As_4} = 2 \times 10^{-6}$ torr, we may calculate from equation [18] that $P_{S_2} = 2.99 \times 10^{-23}$ atm or 2.27×10^{-20} torr.

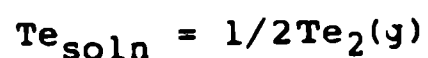
The pressure calculated above is the vapour pressure of S_2 gas in equilibrium with arsenic vacancies in GaAs under MBE growth conditions. If we consider a range of intended donor concentrations from $1 \times 10^{15} \text{ cm}^{-3}$ to $1 \times 10^{19} \text{ cm}^{-3}$, we may calculate the required range of sulphur pressures to be $2.27 \times 10^{-24} < P_{S_2} < 2.27 \times 10^{-16}$ torr. These small values cause the situation to degenerate to that for silicon where every dopant

atom impinging on the GaAs surface is predicted to be incorporated. The incorporation is therefore limited by the rate of supply of dopant from the molecular beam flux. The calculated pressure is also small enough by a large enough margin to make the prediction that incorporation is favoured and relatively insensitive to the precise values of the data used in the calculation. The enormous difference between the above pressures and the elemental vapour pressure of sulphur at 600°C emphasises the importance of considering the interaction of the dopant with the GaAs lattice.

5.4.3: LPE Extrapolation, Tellurium Doping of GaAs.

As an example of the method, the case for tellurium will be demonstrated. In this case we extrapolate from LPE data. Under typical LPE growth conditions, a donor concentration $[Te_{As}^+] = 1 \times 10^{-6} = 2.2 \times 10^{16} \text{ cm}^{-3}$ may be achieved with a concentration in the melt of $[Te_{soln}] = 2.85 \times 10^{-6}$ at 1000°C (16). This corresponds to a segregation coefficient of 0.35. By extrapolating from the data of Greene (17), the segregation coefficient may be estimated to have increased to of the order of 40 at the typical MBE growth temperature of 600°C. The required value of $[Te_{soln}]$ is therefore approximately 2×10^{-8} at this temperature.

To deduce the equivalent pressure of Te_2 in equilibrium with the melt at 600°C, we consider the evaporation of $Te_2(g)$ from liquid tellurium. Thus,



[19]

$$K_{19} = P_{Te_2}^{1/2} / [Te_{soln}] \quad [20]$$

If we assume that the Te-Ga system forms an ideal solution and neglect any stabilising interaction between the two components, we may use Raoult's law to estimate K_{19} . The vapour pressure of $Te_2(g)$ over liquid tellurium may be expressed as (18)

$$\log_{10}(P_{Te_2}) = 22.59 - (7830/T) - (4.27 \times \log_{10}(T)) \quad [21]$$

Therefore, for liquid tellurium at $600^\circ C$ we have $P_{Te_2} = 5.75$ torr. Substituting this in [20] gives

$$K_{19} = P^{\circ}Te_2^{1/2} / [1] = 8.7 \times 10^{-2} \text{ atm}^{1/2}$$

where $P^{\circ}Te_2$ ($=K_{19}^2$) is the vapour pressure of Te_2 in equilibrium with pure liquid tellurium.

Then for dilute solutions of tellurium, the vapour pressure will be reduced according to the degree of dilution thus,

$$P_{Te_2}^{1/2} = [Te_{soln}] \cdot P^{\circ}Te_2^{1/2} \quad [22]$$

Rewriting equation [12] for Te_2 we have,

$$[Te_{As}^+] = K_{3'''} \cdot P_{Te_2}^{1/2} \cdot P_{As_4}^{-1/4} \quad [23]$$

Since the MBE experiment takes place under a lower arsenic pressure than LPE, an overestimate of the equilibrium pressure of $Te_2(g)$ over GaAs under MBE conditions may be obtained by neglecting the arsenic pressure dependence and writing

$K_3'''' = K_3''' \cdot P_{As_4}^{-1/4}$. Then

$$[Te_{As}^+] = K_3'''' \cdot P_{Te_2}^{1/2} \quad [24]$$

Substituting $[Te_{soln}] = 2 \times 10^{-8}$, $P_{Te_2}^0 = 5.8$ torr at $600^\circ C$ and the doping level of $2.2 \times 10^{16} \text{ cm}^{-3}$ gives a value for $K_3'''' = 5.72 \times 10^2 \text{ atm}^{-1/2}$. Therefore, for an intended doping range between 1×10^{15} and $1 \times 10^{19} \text{ cm}^{-3}$, the equilibrium pressure of tellurium lies in the range $4.75 \times 10^{-18} < P_{Te_2} < 4.75 \times 10^{-10}$ torr.

The situation is the same as predicted for sulphur; the interaction between tellurium and the GaAs lattice is strong enough to ensure incorporation under MBE conditions limited only by the rate of supply from the molecular beam flux.

5.4.4: Selenium Doping of GaAs.

There is rather less data for selenium doping of GaAs, although sufficient to suggest strongly that it has similar behaviour to sulphur and tellurium, as would be expected from its chemical similarity. Hollan et al (19) have compared the electronic and optical properties of GaAs grown by VPE and doped at high concentrations with sulphur and selenium. Using pickup from elemental S and Se sources they achieve n-type doping at 10^{17} cm^{-3} for source temperatures of $50^\circ C$ and $80^\circ C$ respectively. This translates to equilibrium source pressures of 4×10^{-5} torr for sulphur and 10^{-8} torr for selenium. We note that their growth temperature of $760^\circ C$ and arsenic mole fraction of 10^{-3} atm are very close to those in reference (14) from which the data for the sulphur incorporation reaction was taken.

Unfortunately Hollan et al do not describe their sources in detail so we have to assume that they operate with similar efficiencies of dopant pickup. In this case, the equilibrium pressures of sulphur and selenium over the growing GaAs surface will be in a similar ratio to the source pressures. Even allowing for differences in source construction, it is clear that for the same doping level a substantially lower selenium pressure is required than for sulphur. The implication is that the interaction between arsenic vacancies and selenium vapour is at least as strong, if not much stronger, than for sulphur vapour. This is supported by the observation of a higher solubility limit for selenium (19). Therefore, the equilibrium pressures required for selenium doping of GaAs grown by MBE are likely to be comparable with or lower than those calculated for sulphur earlier. The conclusion is that for selenium, as for sulphur and tellurium, the incorporation reaction should go to completion restricted only by the rate of supply from the molecular beams.

5.4.5: Chalcogen Doping of InP.

The general point about chalcogen doping in MBE may be further illustrated by considering the data for InP grown by LPE. Here, the extrapolation is rather easier since LPE growth temperatures for InP are typically between 600°C and 700°C and are therefore much closer to typical MBE InP growth temperatures (450°C-550°C) than for GaAs (1000°C vs 600°C). This means that, to a first order approximation, we may neglect changes in segregation coefficient with temperature in extrapolating between the two techniques.

Brown (20) has published the melt concentrations for S, Se and Te doping of InP during LPE growth at temperatures between 620°C and 670°C. For an electron concentration of 10^{18} cm^{-3} he used melt concentrations of

$$[S_{\text{soln}}]=2 \times 10^{-5}, [Se_{\text{soln}}]=2 \times 10^{-5} \text{ and } [Te_{\text{soln}}]=10^{-4}.$$

Rewriting equation [24] we obtain

$$[X_p^+] = K_3'''' \cdot [X_{\text{soln}}] \cdot P^{\circ} X_2^{1/2} \text{ where } X=S, Se, Te.$$

For Te which is predominantly dimeric in the gas phase we may use the vapour pressure relation [21] as before from reference (18), but for S and Se, which have several polyatomic species in equilibrium with the molten element, we must estimate the PX_2 from their heats of formation (23). This results in elemental dimer pressures at an MBE growth temperature of 500°C of:-

$$P^{\circ} S_2 = 430 \text{ torr}, P^{\circ} Se_2 = 27 \text{ torr and } P^{\circ} Te_2 = 0.7 \text{ torr.}$$

Substituting $[X_p^+] = 4.5 \times 10^{-5}$ for 10^{18} cm^{-3} doping we obtain:-

$$K_3'''' = 3 \text{ atm}^{1/2}, 12 \text{ atm}^{1/2} \text{ and } 15 \text{ atm}^{1/2} \text{ for S, Se and Te.}$$

Therefore, for a doping range of $10^{15} \text{ cm}^{-3} < n < 10^{19} \text{ cm}^{-3}$ we obtain the following ranges of PX_2 :-

$$1.7 \times 10^{-13} \text{ torr} < PS_2 < 1.7 \times 10^{-5} \text{ torr}, \\ 1.1 \times 10^{-14} \text{ torr} < PSe_2 < 1.1 \times 10^{-6} \text{ torr and}$$

$$7 \times 10^{-15} \text{ torr} < \text{PTe}_2 < 7 \times 10^{-7} \text{ torr.}$$

These figures, although order of magnitude estimates only, are clearly comparable with the arriving dopant molecular beam pressures in MBE. This contrasts with the situation just demonstrated for GaAs where the equilibrium pressures were much smaller. The situation is rather borderline to make a definite prediction about the likely efficiency of incorporation of the chalcogens in MBE InP, except that sulphur may have the lowest and tellurium the highest probability of incorporation. Significant reevaporation of each dopant seems probable at the highest doping levels.

However, there is very clear evidence that sulphur, for which the lowest doping efficiency is predicted, may be incorporated into InP grown by MBE (21,22). Unintentional sulphur doping has been observed from sulphur-contaminated phosphorus source material and the electrochemical sulphur cell has also been used to deliberately incorporate sulphur into MBE InP over a wide range of concentrations $10^{16} \text{ cm}^{-3} < n < 6 \times 10^{19} \text{ cm}^{-3}$ (21,22). It is significant however that in both cases some dopant reevaporation is observed at elevated growth temperatures. Whether this is due to the borderline position of the doping equilibria described above or to some competing loss reaction is not clear. On the basis of the experimental results and the calculations above, it seems likely that doping with Se or Te should also be possible, perhaps with reduced loss for the less volatile species.

5.5: Conclusions.

We therefore have a clear prediction that the chalcogens S, Se and Te should be incorporated in GaAs and InP grown by MBE. This conclusion was reached by a simple consideration of the free energies of the reactants and products of the incorporation reaction [3] using data extrapolated from VPE and LPE experiments. For GaAs, the predicted dopant pressures required for incorporation are several orders of magnitude lower than the kinetic supply limit imposed in MBE, making the prediction relatively insensitive to the precise values of the thermodynamic data used. For InP the prediction is less firm and this is reflected to some extent in the limited experimental data available to date.

However, there is the possibility that other reaction pathways may compete with the incorporation reaction. In particular, there are several volatile group III chalcogenides such as Ga₂S and Ga₂Se which may not only be stable, but also have vapour pressures substantially greater than 1×10^{-6} torr under MBE growth conditions (18). In the following chapters, we show that chalcogen incorporation into III-V semiconductors by MBE is possible and identify several competing reactions that may lead to loss of dopant from the growing semiconductor surface under certain conditions.

5.6: References.

- 1) A.Y.Cho and J.R.Arthur, in "Progress in Solid State Chemistry", 10, G.Somorgai and J.McCaldin, Editors, Pergamon Press, Oxford, (1975).
- 2) J.R.Arthur, J.Phys.Chem.Sol., 28, 2257, (1967).
- 3) J.C.M.Hwang, T.M.Brennan and A.Y.Cho, J.Electrochem.Soc., 130, 493, (1983).
- 4) J.R.Arthur and T.R.Brown, J.Vac.Sci.Tech., 12, 200, (1975).
- 5) F.Capasso, W.T.Tsang, A.L.Hutchinson and G.F.Williams, Appl.Phys.Lett., 40, 38, (1982).
- 6) R.Heckingbottom, C.J.Todd and G.J.Davies, J.Electrochem.Soc., 127, 444, (1980).
- 7) R.Heckingbottom and G.J.Davies, J.Cryst.Growth, 50, 644, (1980).
- 8) R.Heckingbottom, G.J.Davies and K.A.Prior, Surface Science, 132, 375, (1983).
- 9) K.A.Prior, G.J.Davies and R.Heckingbottom, J.Cryst.Growth, 66, 55, (1984).
- 10) J.B.Mullin, J.Cryst.Growth, 42, 77, (1977).
- 11) D.T.J.Hurle, "Proc. 6th Int. Symposium on GaAs and Related Compounds", Institute of Physics Conference Series, 33a, 113, (1977).
- 12) M.Heyen, H.Bruch, K.H.Bachem and P.Balk, J.Cryst.Growth, 42, 127, (1977).
- 13) H.C.Casey and M.B.Panish, J.Cryst.Growth, 13/14, 818, (1972).
- 14) M.A.Savva, J.Electrochem.Soc., 123, 1498, (1976).
- 15) D.J.Ashen, P.J.Dean, D.T.J.Hurle, J.B.Mullin, A.M.White and P.D.Greene, J.Phys.Chem.Sol., 36, 1041, (1975).
- 16) H.C.Casey, M.B.Panish and K.B.Wolfstirn, J.Phys.Chem.Sol.,

32, 571, (1971).

17) P.D. Greene, *Sol.St.Comm.*, **9**, 1299, (1971).

18) O. Kubaschewski and C.B. Alcock, *Metallurgical Thermochemistry*, 5th ed., Pergamon Press, Oxford, (1979).

19) L. Hollan, M. Bouloué and J.P. Chane, *J.Elect.Mats.*, **10**, 193, (1981).

20) K.E. Brown, *Sol.St.Electr.*, **17**, 507, (1974).

21) T. Martin, C.R. Stanley, A. Iliadis, C.R. Whitehouse and D.E. Sykes, *Appl.Phys.Lett.*, **46**, 994, (1985).

22) A. Iliadis, K.A. Prior, C.R. Stanley, T. Martin and G.J. Davies, *J.Appl.Phys.*, **60**, 213, (1986).

23) K.C. Mills. "Thermodynamic data for inorganic S, Se, and Te compounds", Butterworth, London, (1974).

6.1: Introduction.

The successful doping of GaAs with sulphur and selenium described in chapter 3 was achieved at relatively low substrate temperatures $\sim 570^{\circ}\text{C}$ where the incorporation behaviour was facile. In this region, the sulphur and selenium were incorporated with effectively 100% efficiency with no evidence of segregation or diffusion. However, the move towards higher growth temperatures for enhanced crystal quality in general, and photoluminescence yields in particular, reveals slightly more complicated behaviour as will now be described. A number of samples were prepared and grown according to the procedures outlined in chapter 2. The effect of substrate temperature, arsenic overpressure and dopant flux on the the incorporation behaviour was investigated for both sulphur and selenium.

6.2: Material Properties.

Mobility data for sulphur doped layers were presented in figure 4.5 in chapter 4 where similar results to layers grown using Si or Sn were achieved. Uniformly selenium doped GaAs layers with $2 \times 10^{15} < N_d - N_a < 2 \times 10^{18} \text{cm}^{-3}$ showed excellent electrical properties and morphology. Mobilities of 6350 and $25000 \text{cm}^2 \text{V}^{-1} \text{s}^{-1}$ at 300K and 77K respectively, were achieved for $N_d - N_a = 8 \times 10^{15} \text{cm}^{-3}$. Surface morphology was in general excellent with defect densities of the order of 10^3cm^{-2} , comparable with the etch pit densities of the substrates used.

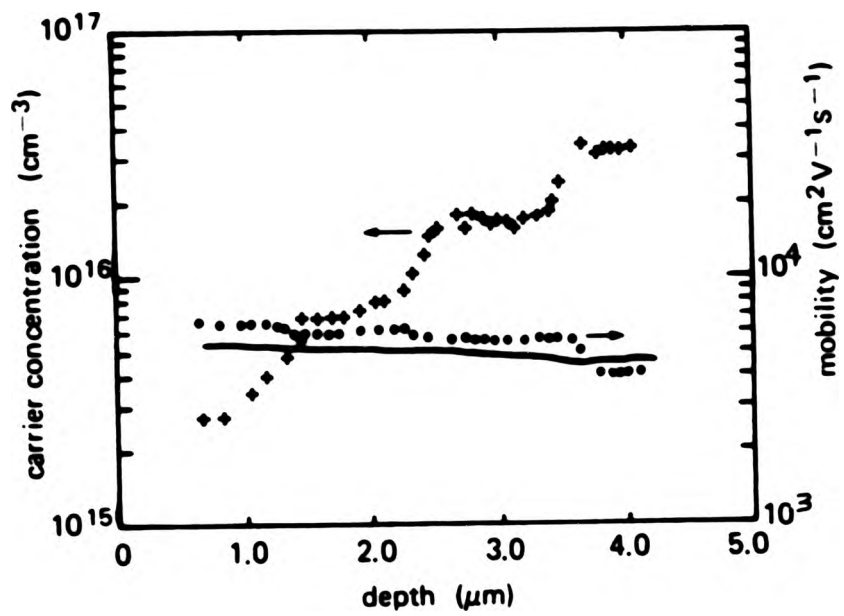


FIGURE 6.1: A combined C-V and Hall mobility depth profile of a four layer Se-doped GaAs film. The crosses show the local carrier concentration, the circles the local Hall mobility and the solid line the sheet mobility.

Figure 6.1 shows a combined carrier concentration and Hall mobility profile through a GaAs layer grown with a four step selenium staircase doping profile. The layer was grown on an undoped substrate and fabricated into Van der Pauw mesas for mobility measurement. The measurement technique (1) makes use of an electrolytic Schottky contact to give controlled dissolution of the layer and a depth profile of the local carrier concentration (upper curve), local Hall mobility (middle curve) and sheet mobility (lower curve). The changes in carrier concentration are clearly resolved and are reflected in the local mobility curve. On the other hand, the sheet mobility reveals little information thus highlighting the utility of the modulation technique for extracting local information. The mobilities from this figure compare well with those from chapter 4.

6.3: Dependence of Sulphur Incorporation on MBE Parameters.

Figure 6.2A shows the result of varying the substrate temperature during the growth of sulphur doped GaAs. The sulphur flux was maintained constant by applying an emf of 155mV to the sulphur cell while the arsenic to gallium flux ratio was held at 2:1. It may be seen from figure 3.9 that this corresponds to a doping level of $\sim 3 \times 10^{17} \text{cm}^{-3}$ in the low temperature regime where the doping efficiency is effectively 100%. The substrate temperature was increased during growth in four steps from 590°C to 680°C. It is evident from the C-V depth profile that there is a decrease in carrier concentration with increasing substrate temperature. That this is due to a

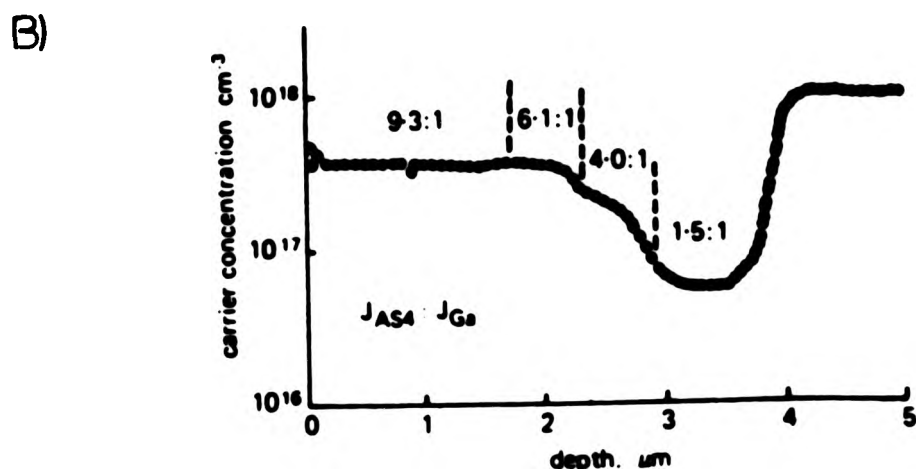
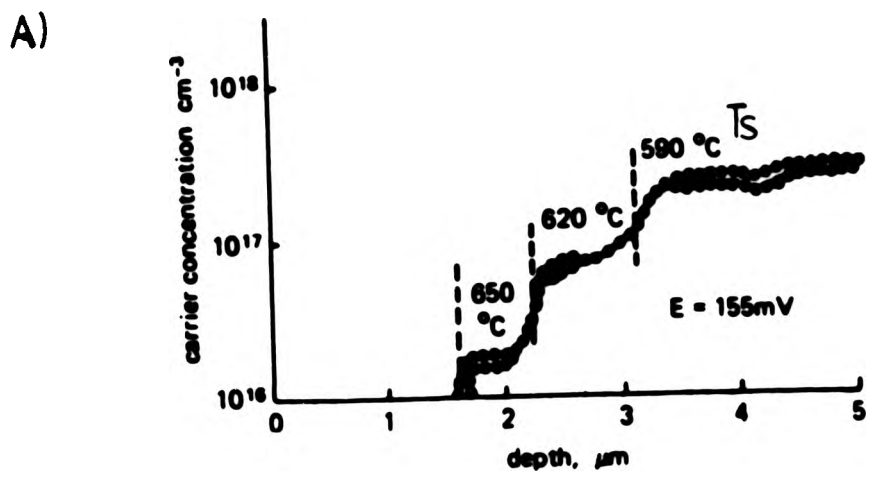


FIGURE 6.2: (A) C-V depth profile of a four layer S-doped GaAs film. The figure shows the decrease in S incorporation with increasing temperature. (B) C-V depth profile of a four layer S-doped GaAs film where the As_4 :Ga beam flux ratio was changed as indicated in the figure.

decreasing sulphur atom concentration is borne out by results from SIMS (2). This loss of sulphur may be offset by increasing the arsenic overpressure. Figure 6.2B shows a C-V depth profile through a layer grown with the same incident sulphur flux as above but at a constant substrate temperature of 615°C where significant loss of sulphur was apparent from figure 6.2A. The arsenic to gallium flux ratio was varied from 1.5:1 to 9.3:1 in four steps as indicated in the diagram. The higher levels of arsenic overpressure may be clearly seen to suppress the loss of sulphur.

Figure 6.3 shows the carrier concentration from C-V measurements of many separate layers grown over a period of several months at 610°C under conditions of sulphur loss. The behaviour of the carrier concentration when plotted against emf is linear, as in chapter 3, with a slope that predicts that the incident species S_x is S_2 ($x=2.0$) as before. This indicates that, even under conditions where some loss is occurring, the electrochemical sulphur cell is a well controlled dopant source and that the sulphur incorporation behaviour is still simple and first order under these conditions. Thus in practical terms, higher growth temperatures may be used and any sulphur loss compensated for by simply increasing the applied flux.

6.4: Dependence of Selenium Incorporation on MBE Parameters.

The effect of varying the substrate temperature (T_s) during the growth of Se doped layers is shown in figure 6.4A. The selenium flux was kept constant by applying a fixed emf (210mV) to the electrochemical cell. The arsenic to gallium flux ratio

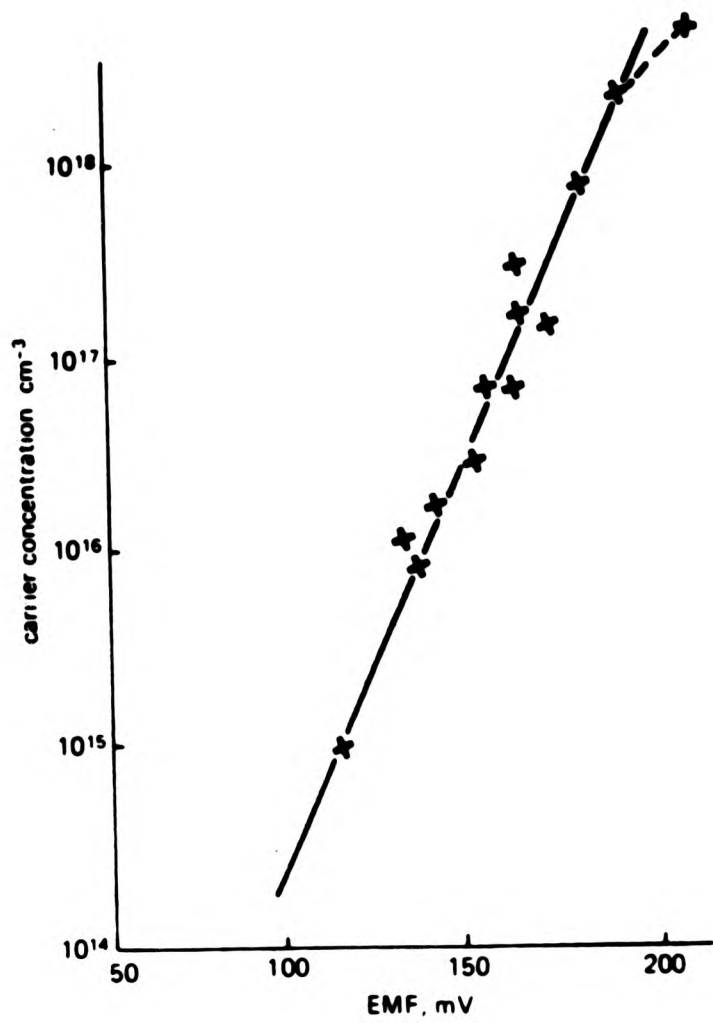


FIGURE 6.3: Plot of carrier concentration of sulphur doping in GaAs (measured by the C-V method) against emf applied to the electrochemical sulphur cell. Layers grown under conditions of sulphur loss.

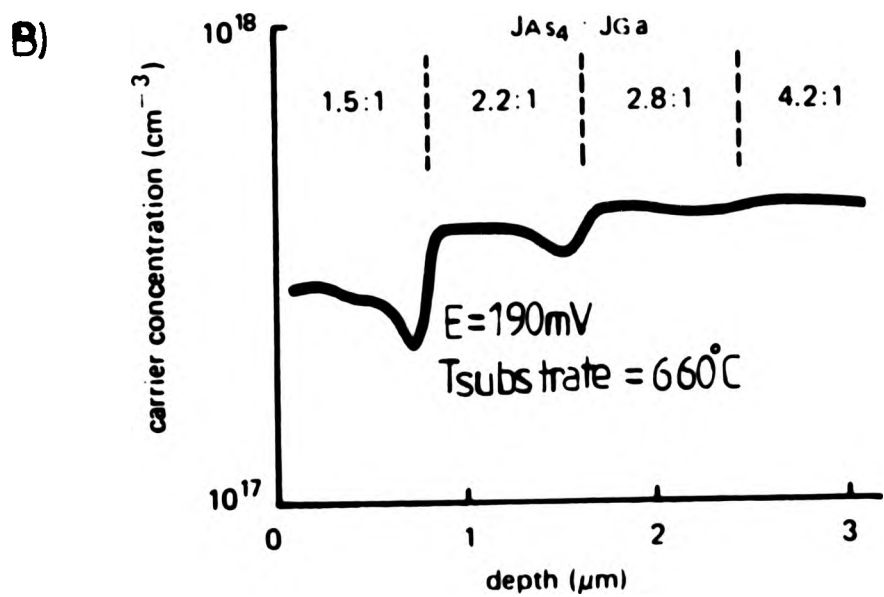
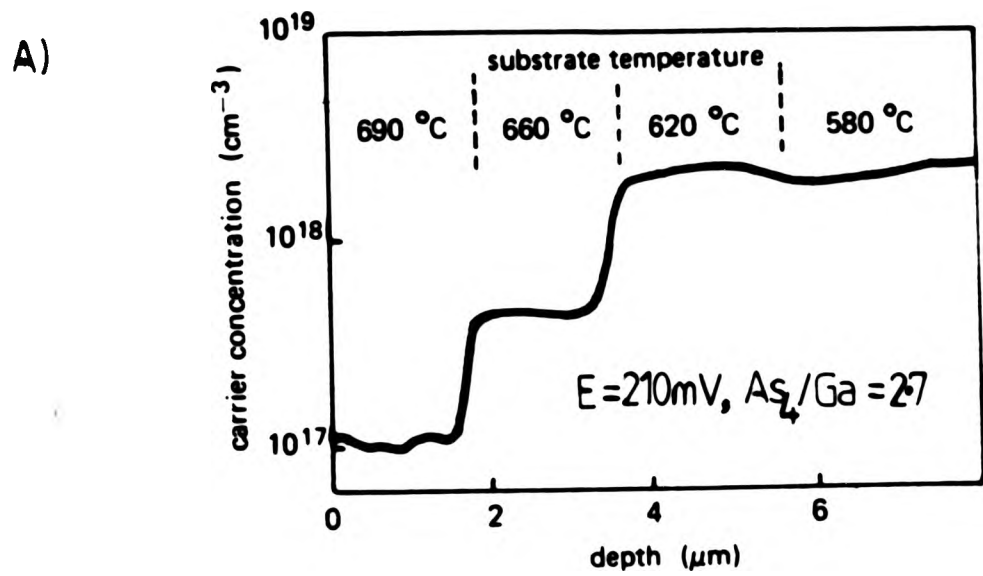


FIGURE 6.4: (A) C-V depth profile of a four layer Se-doped GaAs film. The figure shows the decrease in Se incorporation with increasing substrate temperature. (B) C-V depth profile of a four layer Se-doped GaAs film where the As₄:Ga beam flux ratio was changed as indicated in the figure.

(JAs_4/JGa) was kept constant at 2.7:1 while T_s was increased in four steps from $580^\circ C$ at the interface to $690^\circ C$ at the surface.

It is readily apparent that there are two domains of behaviour. At or below $620^\circ C$, the carrier concentration is a weak function of growth temperature, while above $620^\circ C$ it decreases rapidly with increasing T_s . The corresponding SIMS profile is shown in figure 6.5 (2). This agrees well with the C-V measurements in terms of concentration, showing clearly that the drop in free electron concentration is due to a loss of selenium, and reveals a difference in the two lowest temperature layers that has become blurred in the electrochemical C-V plot. This loss of resolution was probably due to non-uniform illumination of the sample during etching and resulting in uneven dissolution.

In a separate experiment, a selenium-doped layer was grown at a T_s where Se loss was observed and the effect of varying the arsenic overpressure during growth studied. At a T_s of $660^\circ C$ and a Se-cell emf of 190mV, corresponding to a nominal doping level of $4 \times 10^{17} \text{cm}^{-3}$ (assuming unity sticking coefficient), JAs_4/JGa was varied in four steps from 4.2:1 to 1.5:1. It may be seen from figure 6.4B that selenium loss is suppressed at the higher arsenic overpressures. The dips in the profile at the changes in overpressure are believed to be due to the dynamic response of the arsenic effusion cell, which was different to that used for the sulphur experiments due to the amount of heat shielding surrounding the cell heaters. Although the temperature response of the effusion cell was critically damped, the flux response measured by the moveable ion gauge showed some overshoot, presumably due to temperature gradients within the cell resulting in thermal lag.

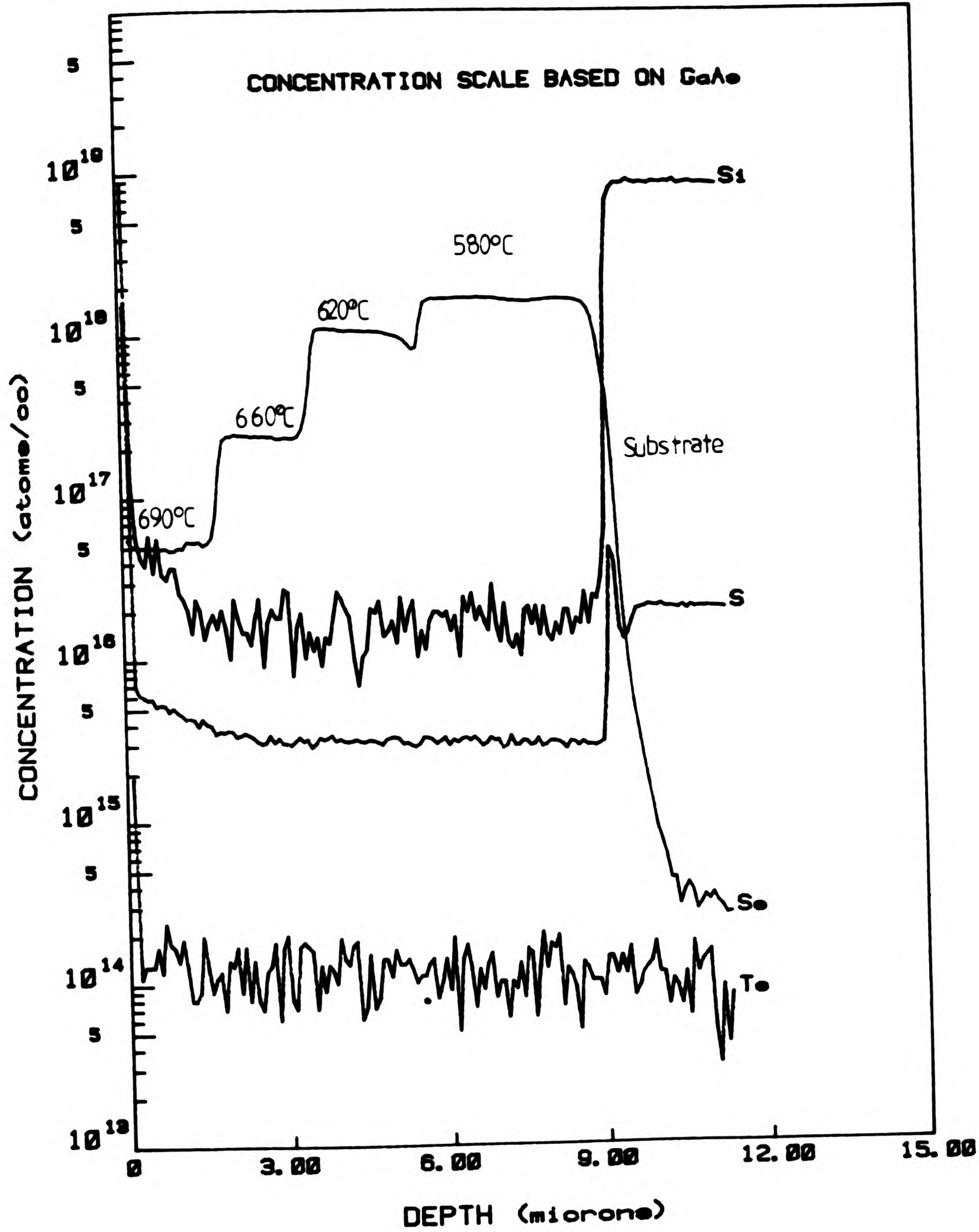


FIGURE 6.5: SIMS profile of the layer shown in figure 6.4A.

It should be noted that the rather high growth temperatures and reduced arsenic overpressures required to induce selenium loss place the growing surface very close to becoming gallium rich. The RHEED pattern from such surfaces is generally rather diffuse, certainly well away from the As-rich (2x4) pattern and more characteristic of the (3x1) phase.

In a further experiment, the incorporation of selenium into GaAs was investigated as a function of arriving Se flux. A growth temperature of 560°C was used, with a J_{As_4}/J_{Ga} ratio of 3.5:1 and the electrochemical cell driving emf varied in six steps from 180mV to 250mV. The resulting C-V depth profile is shown in figure 6.6, the SIMS profile (16) in figure 6.7 and the carrier and elemental concentrations plotted against emf in figure 6.8. The SIMS concentrations were deduced from an ion implanted standard at $2 \times 10^{19} \text{cm}^{-3}$. The C-V profile becomes confused above $2 \times 10^{18} \text{cm}^{-3}$ since at this level the electrolytic Schottky junction is rather leaky electrically which causes errors in the capacitance measurement from which the carrier concentration is derived. However, as far as it goes, the C-V depth profile is linear with respect to emf, showing simple behaviour. The SIMS data is extremely well resolved up to the maximum doping level and at the surface agrees with the C-V data to within a factor of two. The elemental concentration revealed by SIMS is also linear with respect to emf, even up to $3 \times 10^{19} \text{cm}^{-3}$ showing no evidence of saturation effects or gross precipitation which would tend to alter the SIMS yield. This would suggest that the saturation solubility is in excess of $3 \times 10^{19} \text{cm}^{-3}$. There is also no evidence for surface segregation effects under these growth conditions, consistent

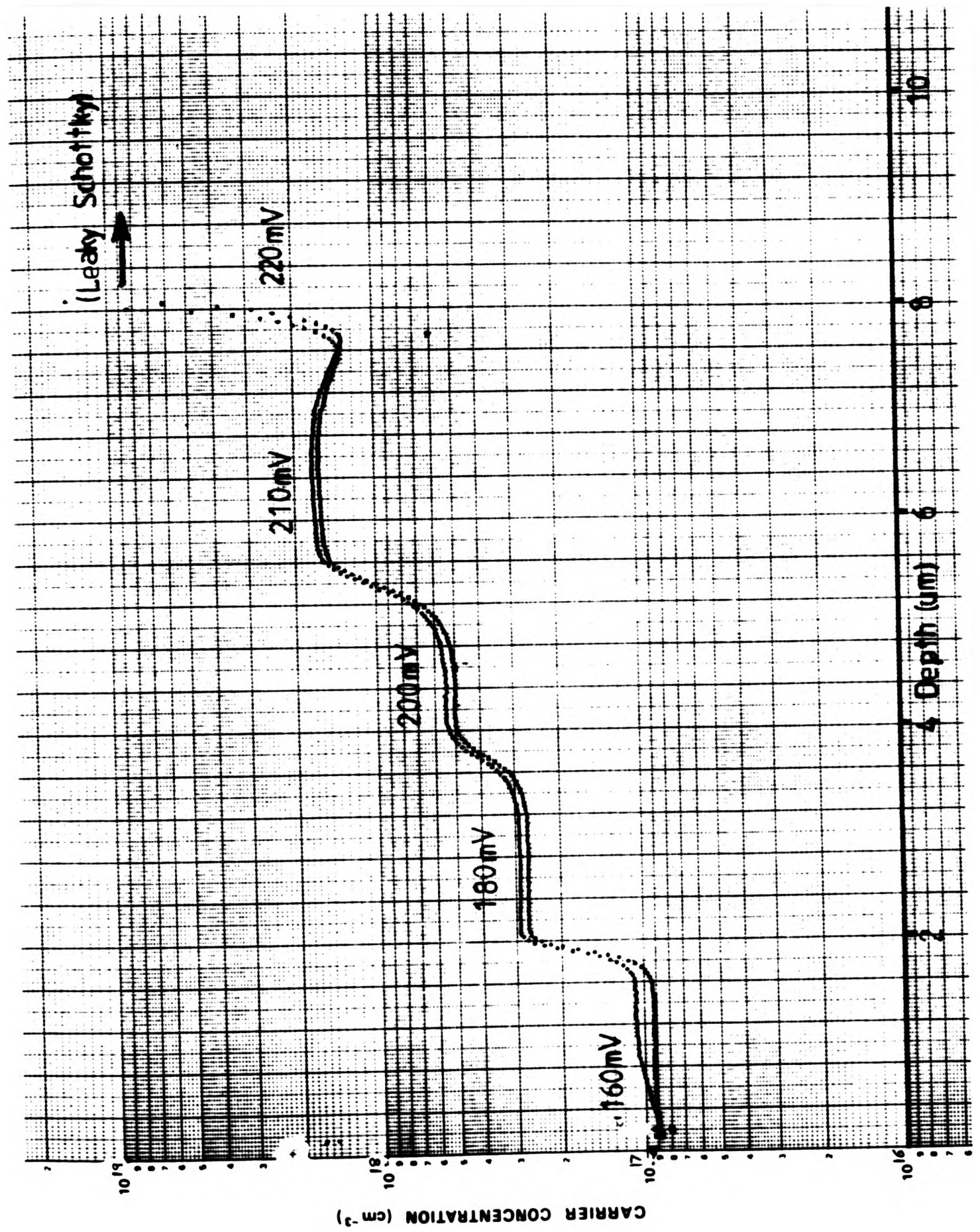


FIGURE 6.6: A C-V depth profile of a six layer Se-doped GaAs film where the EMF applied to the electrochemical Se source is varied as indicated in the figure. $T_s=560^{\circ}\text{C}$, $\text{JAs}_4:\text{JGa}=3.5:1$.

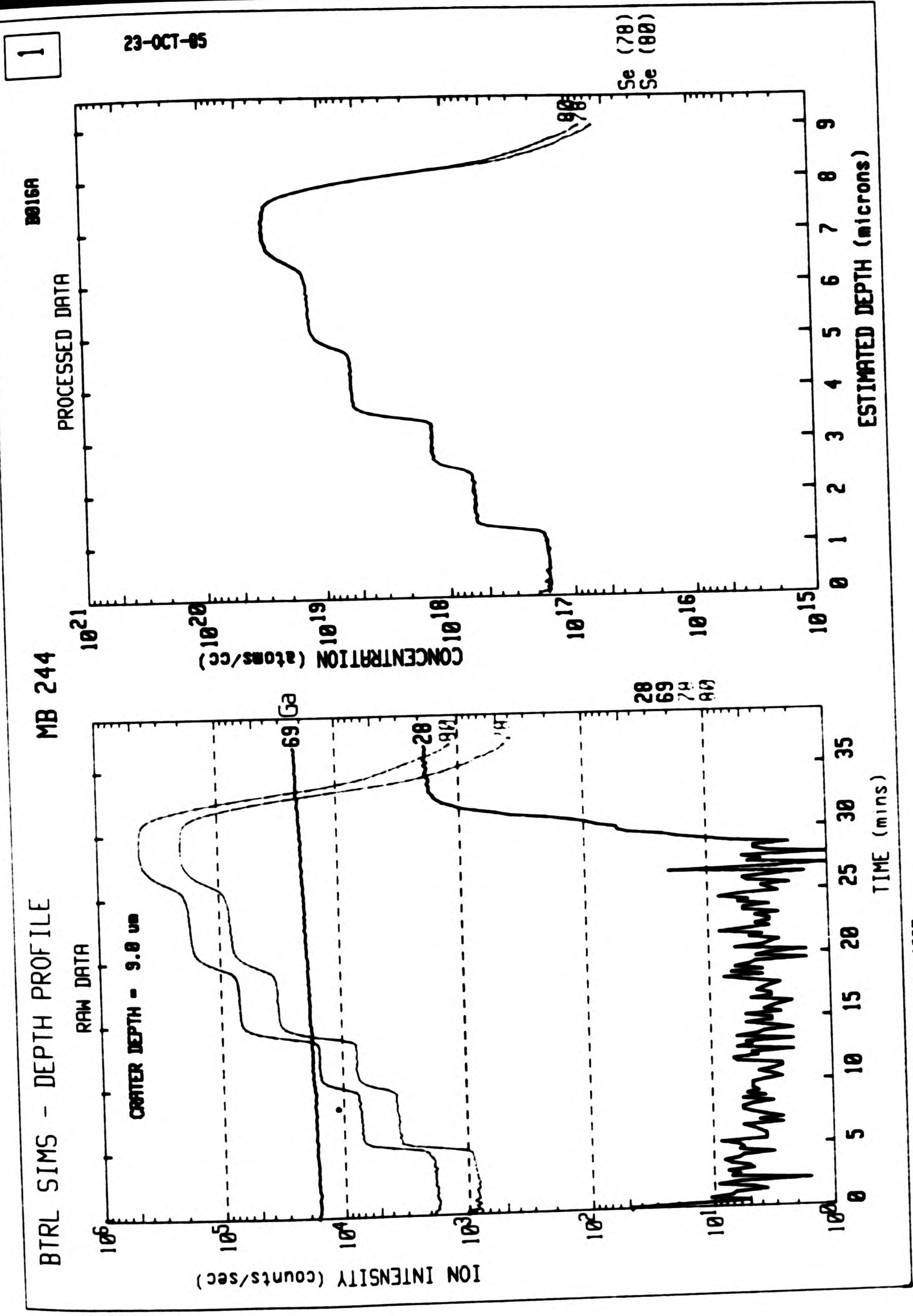


FIGURE 6.7: SIMS profile of the layer shown in figure 6.6.

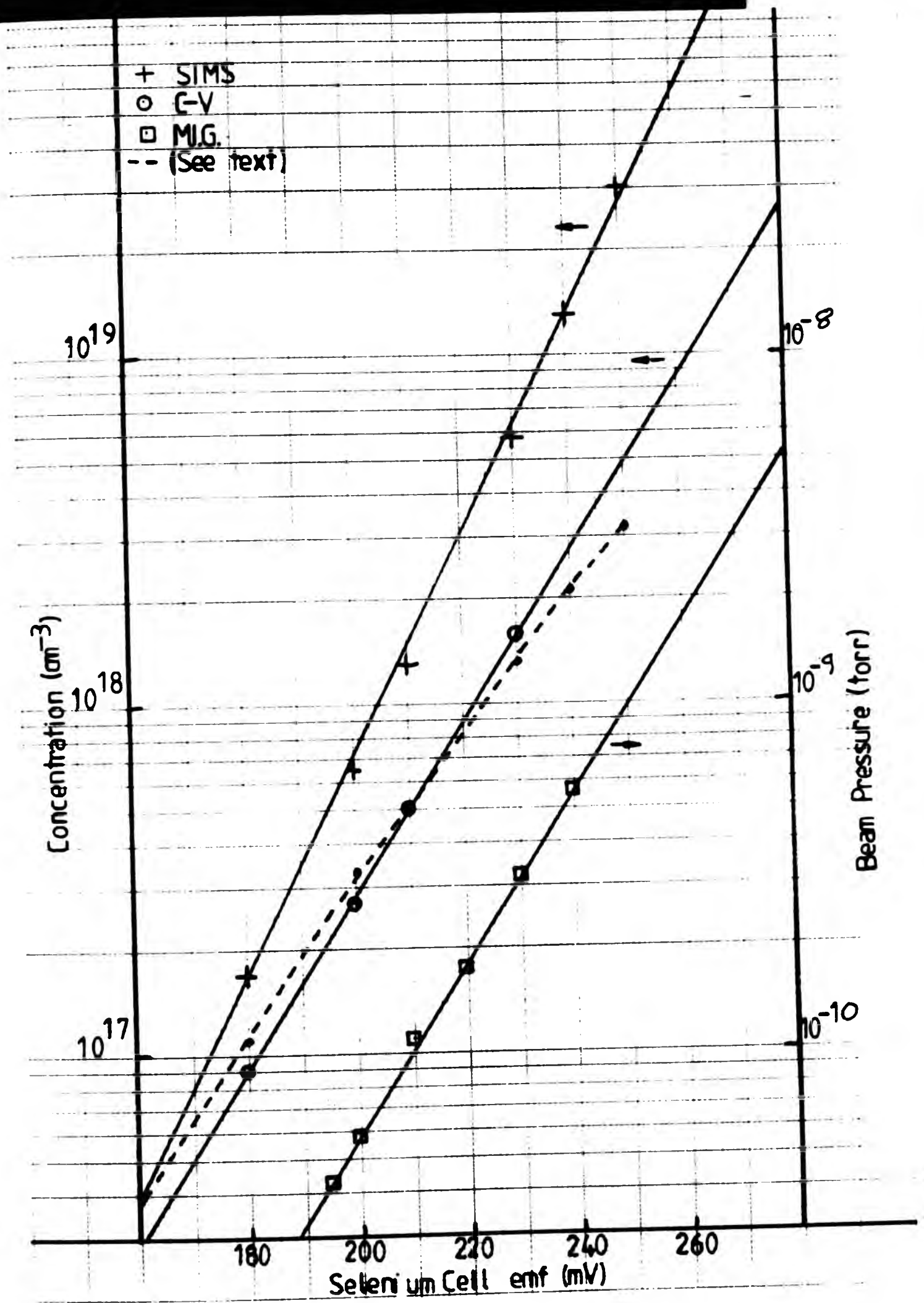


FIGURE 6.8: SIMS and C-V concentrations plotted against Se-cell emf. Other lines are explained in the text.

with the data of Smith et al (4).

However, there is a worsening discrepancy between the SIMS and C-V data as the profile progresses through the higher doped layers. This is apparent in figure 6.8 where the SIMS and C-V lines have different slopes; the SIMS data gives $x=1.9$ and the C-V data $x=1.4$. Smith et al (4) have observed similar, although not identical, behaviour. They used the non-congruent evaporation of SnSe_2 to produce Se doped GaAs layers by MBE. Below 10^{17}cm^{-3} , they observed a linear dependence of carrier concentration (from C-V measurements) against reciprocal dopant cell temperature (with the correct activation energy) but above this level found the carrier concentration depressed from the value predicted by extrapolation from lower levels. They proposed that not all of their incorporated selenium was electrically active but did not make SIMS measurements. The difference in slopes between the lines is clearly evident, as is the good linearity in each case. The dashed line shows the effect of scaling the SIMS concentration by the amount predicted by Smith et al's data. Although the concentration is depressed by approximately the correct amount, the linear behaviour of the C-V data is not reproduced suggesting that this explanation may not be wholly correct.

Similar saturation effects are observed in Te doped GaAs using SnTe (5) but not PbTe (14) which indicates that the effect may be due to the evaporation behaviour of the particular selenide or telluride used rather than an effect intrinsic to selenium or tellurium.

To account for this discrepancy through reduced activation at

high concentrations, it is necessary to postulate a power law dependence of the activation of the form $n=k[\text{Se}]^i$, $i=0.75$. Although there are some suggestions in the literature that selenium may form electrically inactive complexes such as $\text{V}_{\text{Ga}}\text{Se}_3$ (15), we have insufficient data to pursue this possibility further.

However, there is a further piece of data which must be considered. The lower line in figure 6.8 is a plot of the selenium flux arriving at the substrate, shown as a function of the applied emf. This was measured on the moveable ion gauge flux monitor the day before the high doped staircase was grown. This has the expected straight line behaviour but has the same slope as the C-V measurements. If this is correct, it implies a constant, if not total, activation of the incorporated selenium and a non-linearity in the SIMS yield from Se in GaAs as a function of concentration. The concentrations involved, even at the highest levels $\sim 0.1\%$, are believed to be too low for any significant matrix effects on the SIMS yield (16). Such a discrepancy certainly deserves further study to confirm the credibility of the SIMS technique in this material system.

6.5: Discussion.

6.5.1: Thermodynamic Model.

The temperature dependence of the incorporation behaviour of the common chalcogen dopants S, Se and Te into MBE GaAs is summarised in figure 6.9. The sulfur and selenium data are our

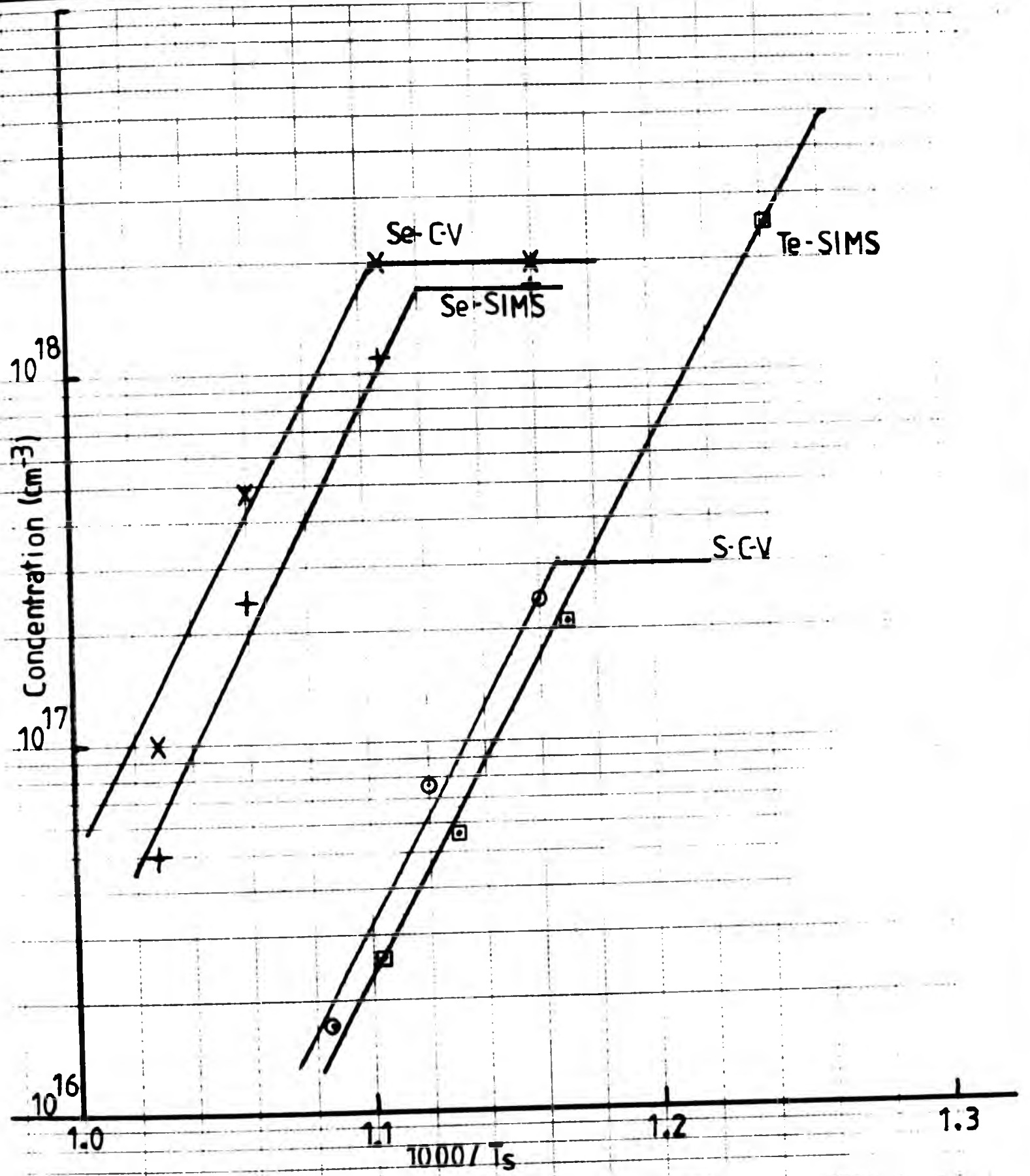


FIGURE 6.9: Incorporated dopant concentration from figures 6.2, 6.4 and 6.5 plotted vs. reciprocal substrate temperature. \circ : -S (C-V), \times : -Se (C-V), $+$: -Se (SIMS), \square : -Te (SIMS, data from ref 5).

own and the tellurium data is drawn from the work of Collins et al (5). In this figure, reciprocal substrate temperature is plotted along the horizontal axis and donor concentration on the vertical axis. Sulfur, selenium and tellurium both exhibit very similar behaviour, and the activation energy for desorption derived from the slope of the high temperature portion of the graph is similar at 70kcal.mol^{-1} .

In chapter 5, we showed that the reaction



(where X is S, Se or Te, (g) indicates the gas phase, V_{As} is an arsenic vacancy in GaAs, X_{As}^+ an ionised atom on an arsenic site in GaAs and e^- an electron in the conduction band of GaAs) goes essentially to completion under MBE conditions. Earlier results on chalcogen doping of GaAs by MBE using thermal evaporation from compound sources (6) indicated that there were no loss reactions of significance at a growth temperature of 560°C and this was confirmed by the results presented in chapters 3 and 4. In addition we note that the prediction that reaction [1] above lies to the right was firm enough for the situation not to change over the range of temperatures and arsenic overpressures explored in MBE. Indeed, the experimental behaviour is opposite to that predicted from any likely temperature or arsenic overpressure dependence of the arsenic vacancy concentration.

In seeking an explanation for the loss of chalcogen dopant observed at elevated growth temperatures, we therefore consider the possible reaction routes competing with [1] above and

involving the production of volatile chalcogenide compounds at the growing surface. Since the gallium chalcogenides generally have more negative heats of formation than the arsenic chalcogenides (7), and especially since the chalcogens are incorporated on the arsenic site in GaAs, we may consider that the gallium chalcogenides are the most likely to be formed.

A very simple model will be used to illustrate the GaAs-chalcogen interaction. The gallium, arsenic and chalcogen reactants are incident upon the substrate in gaseous form. Impinging on the substrate, they are adsorbed and assumed to equilibrate to the substrate temperature. In this adsorbed layer, which has less than one monolayer effective thickness, the atoms have a high surface mobility, as evidenced by the ability to grow GaAs with very small deviations from stoichiometry and consequently low defect concentrations suitable for electro-optic devices, and growth takes place via the interaction between the adsorbed layer and the substrate. The situation is conceptually rather similar to growth from the liquid phase (LPE) where the solution depth has been reduced to ~ 1 monolayer. The species present in this adsorbed layer are assumed to be in equilibrium with the bulk layer, the adsorbed atom mobilities being high enough to make the reaction kinetics facile. Those reactions resulting in solid products are assumed to lead to incorporation, while gaseous products result in desorption. The reactant pressures calculated for the incorporation reaction in chapter 5 obtain at the interface between the adsorbed layer and the substrate, while the beam pressures obtain at the interface between the vacuum and the adsorbed layer. These pressures represent the maximum and minimum values for substitution into the relevant expressions

for equilibrium constant calculations.

Mass spectrometric studies of the dissociative evaporation of solid gallium chalcogenides (8) have revealed that the main stable species at or near MBE pressures and temperatures are of the form $\text{Ga}_2\text{X}_3(\text{s})$ and $\text{Ga}_2\text{X}(\text{g})$ where $\text{X}=\text{S}, \text{Se}$ or Te . Using standard thermochemical data for these species (7,9), the equilibria between the GaAs surface, the incident chalcogen species $\text{X}_2(\text{g})$ and the solid and gaseous gallium chalcogenides may be explored within the framework of the simple model outlined above. If, for a particular set of growth conditions, the solid form is predicted to be stable with respect to the gaseous form, we may expect doping to proceed via reaction [1] of chapter 5. Alternatively, if the gaseous form is the thermodynamically predicted product, (or rather if its equilibrium vapour pressure is comparable with or exceeds the incident chalcogen pressure), a potential route for the loss of dopant will have been identified. The extent to which such a loss reaction may proceed and compete with [1] is determined by the detailed kinetics of the growing surface.

6.5.2: Stability of Gallium Sulphides.

Consider the formation of the volatile species $\text{Ga}_2\text{S}(\text{g})$.



Using enthalpy and entropy values from (7) we may calculate the free-energy change for this reaction to be:

$$G_2 = -10,325 - 22.45xT \text{ calories/mol.}$$

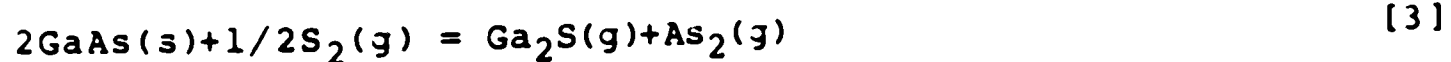
The equilibrium constant is therefore

$$K_2 = P_{Ga_2S} / (P_{S_2})^{1/2} = \exp(-G_2/RT)$$

This evaluates to $K_2 = 6.7 \times 10^7 \text{ atm}^{-1/2}$ at 500°C , $3.1 \times 10^7 \text{ atm}^{-1/2}$ at 600°C and $1.7 \times 10^7 \text{ atm}^{-1/2}$ at 700°C .

We may consider that equation [2] reflects the conditions at the growing surface since growth does take place near the Ga liquidus (10), and substitute typical MBE values of $T = 500-700^\circ\text{C}$ and $P_{S_2} = 6 \times 10^{-14} \text{ atm}$ (the incident flux for $n = 2 \times 10^{18} \text{ cm}^{-3}$ doping) to yield values of P_{Ga_2S} of 16.4 atm, 7.6 atm and 4.2 atm at 500, 600 and 700°C respectively. Clearly, this exceeds any applied sulphur pressure practical under MBE conditions over a wide range of temperature and doping level.

To include the effect of Ga being present in the form of GaAs, we may take a different reaction for our model thus:-



This leads to $G_3 = 81495 - 68.9xT$ calories/mol and

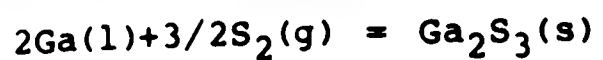
$$K_3 = P_{As_2} \cdot P_{Ga_2S} / P_{S_2}^{1/2} = \exp(-G_3/RT)$$

For $P_{As_2} = 2 \times 10^{-6} \text{ torr}$ and other values as in the previous example, we obtain $P_{Ga_2S} = 9.6 \times 10^{-7} \text{ atm}$ at 500°C , $4.2 \times 10^{-4} \text{ atm}$ at 600°C and $5.2 \times 10^{-2} \text{ atm}$ at 700°C , all greatly in excess of the applied P_{S_2} .

It may be argued that, since reaction [3] deals with the solid GaAs rather than just the gallium component in [2], the equilibrium PS_2 values deduced from chapter 5 should be used. Thus, for the same doping level of $n=2 \times 10^{18} \text{ cm}^{-3}$, $PS_2=1.2 \times 10^{-20} \text{ atm}$. Therefore the predicted values for PGa_2S become $4.3 \times 10^{-10} \text{ atm}$ at 500°C , $1.9 \times 10^{-7} \text{ atm}$ at 600°C and $2.3 \times 10^{-5} \text{ atm}$ at 700°C , which again exceed the applied PS_2 by several orders of magnitude.

Reaction [3] would appear to be a more realistic choice for modelling the behaviour than reaction [2] as it does include the effect of the arsenic overpressure. Indeed, it does show the correct trend in predicting reduced loss at low temperatures and elevated arsenic pressures. However, the predicted dependence on PAs_2 is much weaker than observed experimentally. In addition, the experimental data was gathered using As_4 , and although the equilibrium between the tetrameric and dimeric arsenic species may be easily calculated, it is well known that the decomposition of As_4 to As_2 is kinetically hindered under typical GaAs MBE growth conditions. In the following therefore, the simpler form [2] will be used with the justification that growth takes place near the liquidus (10). The role of the arsenic overpressure will now become apparent later.

The important point is that $Ga_2S(g)$ is predicted to be a stable species under MBE conditions with an equilibrium pressure greatly in excess of the applied dopant flux. Similarly, we may consider the formation of the solid sulphide $Ga_2S_3(s)$ thus:-



[4]

$$G_4 = -168,925 + 67.95xT$$

$$K_4 = (\text{PS}_2)^{-3/2} = \exp(-G_4/RT) \text{ and}$$

$$\text{PS}_2 = (\exp(G_4/RT))^{2/3} = 1.1 \times 10^{-22} \text{ atm at } 500^\circ\text{C}, 5 \times 10^{-19} \text{ atm at } 600^\circ\text{C}$$

and $3.9 \times 10^{-16} \text{ atm at } 700^\circ\text{C}.$

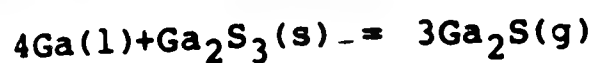
These values are low in comparison with the applied flux but of the same order as the calculated equilibrium sulphur pressure from chapter 5.

Interestingly, if we substitute these equilibrium pressures into equation [18] of chapter 5, we find that they correspond to doping levels in the range $10^{17} < n < 10^{19} \text{ cm}^{-3}$. Although detailed agreement is to some extent fortuitous in the light of the simple thermodynamic approximations used in the calculation, the predicted doping levels do correspond approximately to the known saturation doping level ($\sim 10^{19} \text{ cm}^{-3}$) of sulphur in GaAs (11), where $\text{Ga}_2\text{S}_3(s)$ would be precipitated. This agreement suggests that a certain confidence in the validity of the method is justified.

Therefore, both $\text{Ga}_2\text{S}(g)$ and $\text{Ga}_2\text{S}_3(s)$ are expected to be formed under MBE conditions. To determine which of the forms is most stable, the equilibrium between the solid and gaseous forms must be considered. There are two possible reactions:-



[5]



[6]

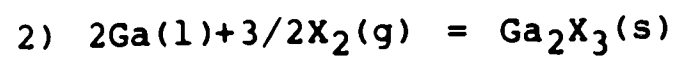
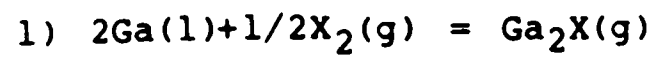
Reaction [5] is the principal route by which $\text{Ga}_2\text{S}_3(s)$ evaporates (8), but it is important to take into account the fact that the growing surface contains a great excess of Ga as far as the chalcogenide is concerned since doping typically takes place on the ppm scale. Therefore reaction [6] may be of importance. Using the values $P_{\text{S}_2} = 6 \times 10^{-14} \text{ atm}$ $T = 600^\circ\text{C}$ and assuming that the activities of Ga_2S_3 are unity (near saturation doping and growth near the Ga liquidus) the equilibrium pressure of $P_{\text{Ga}_2\text{S}}$ is calculated to be $8.5 \times 10^{-19} \text{ atm}$ for reaction [5] ($4.3 \times 10^{-12} \text{ atm}$ using chapter 5 values for P_{S_2}) and $2 \times 10^{-2} \text{ atm}$ for reaction [6]. The former result is consistent with negligible evaporation of Ga_2S_3 below 897K (8), while the latter indicates that the Ga_2S_3 may indeed be reduced quite readily under Ga-rich conditions to volatile Ga_2S .

Therefore, not only is the gaseous sulphide predicted to be formed in the growing surface under MBE conditions, leading to a net loss of sulphur dopant, but also the sulphur in the GaAs lattice (modelled as Ga_2S_3 near the solubility limit) is unstable with respect to the gaseous form via reduction by gallium.

6.5.3: Gallium Selenides and Tellurides.

The calculations for the other two chalcogens Se and Te follow the same framework and the results are depicted in table 1. In each case, the gaseous form $\text{Ga}_2\text{X}(g)$ ($X = \text{S}, \text{Se}, \text{Te}$) is predicted to

REACTIONS



PREDICTED PRESSURES(atm)

	X	S	Se	Te
1) $P_{\text{Ga}_2\text{X}}$		7.0	4.4×10^{-3}	2.6×10^{-12}
2) P_{X_2}		4.5×10^{-19}	4.6×10^{-6}	2.6×10^{-12}
3) $P_{\text{Ga}_2\text{X}}$		8.5×10^{-19}	2.9×10^{-6}	9.2×10^{-10}
4) $P_{\text{Ga}_2\text{X}}$		2.0×10^{-2}	4.1×10^{-4}	9.4×10^{-5}

TABLE 6.1: Likely reactions and predicted equilibrium pressures for the gallium chalcogenides under MBE growth conditions.

form at the growth temperature under the incident fluxes and the solid phase $\text{Ga}_2\text{X}_3(\text{s})$, if formed, is predicted to be unstable with respect to the gaseous phase. In addition, the calculated equilibrium $\text{Ga}_2\text{X}(\text{g})$ pressures exceed the incident $\text{X}_2(\text{g})$ flux leading to a predicted net loss of dopant from the growing surface over a wide range of growth temperatures, doping levels and beam pressures. The successful achievement of chalcogen doping via reaction [1] must therefore only be possible by virtue of kinetic hindrance to the loss reaction in table 1.

In the above, formation of volatile Ga_2X is identified as a possible route for the loss of chalcogen. The equilibrium with Ga_2X_3 is used to determine the stability of any Ga_2X so formed. However, it is not suggested that the chalcogens are actually present in GaAs as Ga_2X_3 , except at the solubility limit, only that in considering the equilibria between the chalcogenide species, Ga_2X_3 is a convenient analogy for the chalcogen environment for which thermochemical data are readily available. The calculations are therefore strictly only valid at the solubility limit (hence the choice of a high doping level) and at lower concentrations the activity of the Ga_2X_3 would be reduced. However, the predictions regarding the formation of Ga_2X are sufficiently strong that they remain valid over a wide range of doping. The actual incorporation reaction is still believed to be governed by equation (1), notwithstanding the analogy with Ga_2X_3 .

6.5.4: Kinetic Aspects.

It is evident from figure 6.9 that S, Se and Te all have similar temperature dependences in the regime where loss is significant. The calculated activation energy for the desorption process is of the order of 70kcal.mol^{-1} in each case. Additionally, in each case the effect of increasing the substrate temperature may be offset by an increase in the As_4/Ga ratio impinging on the substrate as shown in figures 6.2B and 6.4B for S and Se and by Collins (5) for Te.

A similar temperature behaviour and activation energy have been reported by Panish (12) for the $\text{GaAs}(100)(2\times 4)\text{-GaAs}(100)(3\times 1)$ arsenic stabilised surface structure phase transformation observed by RHEED, as a function of As_2/Ga ratio. This is shown in figure 6.10. The similar activation energies suggest a common reaction mechanism and it seems likely that it is the surface arsenic population that plays a key role in the kinetics of the loss reaction in the same way as it does for the surface structure. Therefore, at elevated temperatures, loss of arsenic not only leads to the formation of new surface structures, but also results in an increasing Ga population (gallium droplets in the limit) free to bond to chalcogen dopant atoms and so to form the volatile dopant species $\text{Ga}_2\text{X}(g)$ ($\text{X}=\text{S}, \text{Se}, \text{Te}$). Increased arsenic overpressures decrease the surface free gallium population available for chalcogenide formation. The behaviour may therefore be explained by a change in the relative rates of the competing incorporation and loss reactions. At lower temperatures the kinetic barrier to the loss reactions reduces the formation of volatile $\text{Ga}_2\text{X}(g)$ to a negligible amount, allowing the incorporation reaction to

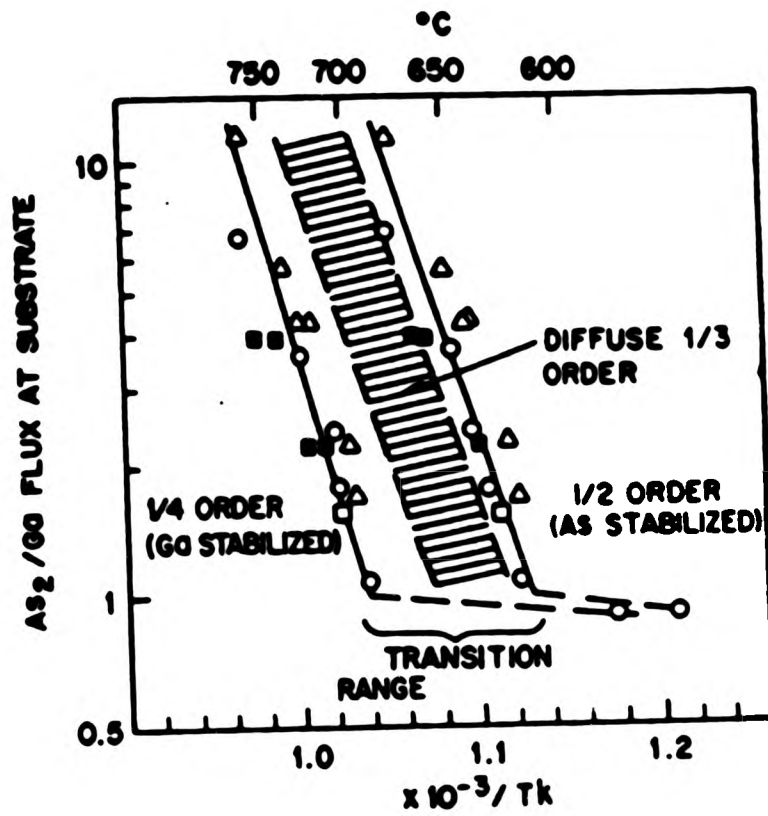


FIGURE 6.10: Temperature dependence of GaAs surface structures as a function of arsenic to gallium flux ratio. After reference (12).

dominate, unimpeded by any detected kinetic barriers.

The selenium results however show that not all the features of the chalcogen-GaAs interaction may be explained. The actual loss rate for this dopant is the lowest of the three chalcogens under otherwise similar conditions, the plateau region in figure 6.9 extending to higher temperatures ; although the case with Te is not strictly comparable owing to the interaction with Sn (5). Se lies in the middle of the group VI series and its enhanced stability as a dopant with respect to S and Te which lie above and below it in the periodic table contradicts the usual monotonic trend in properties as such a column is descended. There is no clue from the thermodynamic calculations, indeed the relative stabilities of the solid chalcogenides would predict the opposite trend to that observed. The explanation for its enhanced stability in the lattice is not known but it is noted that Se does lie next to As in the periodic table whose site it occupies in the GaAs lattice. The effect of dopant atom size and the strain effects induced by substitutional doping are well known in highly doped III-V semiconductors (13) but there is insufficient data to pursue this avenue further. What is clear is the technological importance of this enhanced stability. Se may be used as a dopant for GaAs at higher growth temperatures and with low As/Ga ratios consistent with the growth of the highest quality GaAs layers.

6.6: Conclusions.

Sulphur and selenium have been used successfully to dope MBE

GaAs. Both dopants are incorporated in a facile manner and with effectively 100% efficiency at low temperatures. However, at elevated temperatures, $>590^{\circ}\text{C}$ for sulphur and $>620^{\circ}\text{C}$ for selenium, incorporation at useful levels may still be achieved but an increasing loss of dopant is observed. This loss is interpreted in terms of competition between the incorporation reaction and the formation of volatile gallium chalcogenides $\text{Ga}_2\text{X}(\text{g})$ ($\text{X}=\text{S}, \text{Se}, \text{Te}$) which are increasingly favoured at elevated growth temperatures and restricted arsenic fluxes. A model has been presented for the GaAs-chalcogen interaction and it has been demonstrated that the loss reactions are thermodynamically favoured over the entire MBE range of growth conditions and that successful doping at low temperatures may only be achieved due to a kinetic barrier to the formation of the Ga_2X species. It is postulated that it is the surface gallium population, mediated by the substrate temperature and arsenic overpressure, that plays a key role in the kinetics of the loss reaction. Analogies with reported data on Te doping and surface structure phase transformations support this theory. It has been shown that, of the chalcogens, selenium shows an enhanced stability which, although not explained by the simple model presented here, makes it the most technologically useful chalcogen dopant for high quality MBE GaAs.

6.7: References.

- 1) T.Ambridge and C.J.Allen. Electronics Letters, 15, 648, (1979). Hall Profile performed by C.J.Allen, R3.1.4, BTRL.
- 2) SIMS analysis by Charles Evans and Associates, San Mateo, California, USA.
- 3) H.Rickert, Physics of Electrolytes, edited by J.Hladik, (Academic New York), 2, 519, (1972).
- 4) R.S.Smith, P.M.Ganser and H.Ennen. J.Appl.Phys., 53, 9210, (1982).
- 5) D.M.Collins, J.N.Miller, Y.G.Chai and R.Chow. J.Appl.Phys., 53, 3010, (1982).
- 6) C.E.C.Wood. Appl.Phys.Lett., 33, 770, (1978).
- 7) O.Kubaschewski and C.B.Alcock, Metallurgical Thermochemistry 5th Ed, Pergamon Press London (1979).
- 8) O.M.Uy, D.W.Muenow, P.J.Ficalora and J.L.Margrave, Trans. Faraday Soc., 64, 2998, (1968).
- 9) K.C.Mills. Thermodynamic data for inorganic S, Se and Te compounds, Butterworth London (1974).
- 10) J.R.Arthur. J.Phys.Chem.Sol., 28, 2257, (1967).
- 11) E.Veuhoff, M.Maier, K.H.Bachem and P.Balk. J.Cryst.Growth., 53, 598, (1981).
- 12) M.B.Panish. J.Electrochem.Soc., 127, 2729, (1980).
- 13) L.Suchow. Mat.Res.Bull., 17, 1401, (1982).
- 14) Jiang De-Sheng, Y.Makita, K.Ploog and H.J.Queisser, J.Appl.Phys., 53, 999, (1982).
- 15) L.J.Vieland and I.Kudman. J.Phys.Chem.Sol., 24, 437, (1963).
- 16) SIMS Analysis by G.Spiller, BTRL SIMS facility.

7.1: Introduction.

In the preceding chapters, it has been demonstrated that sulphur and selenium may be successfully incorporated into GaAs during MBE growth in a facile manner at moderate growth temperatures. At elevated temperatures, near the practical maximum for MBE GaAs, a reduced doping efficiency has been observed and explained in terms of the formation of volatile gallium chalcogenides on the basis of a thermodynamic model. This model and the experimental study are extended in this chapter to the incorporation of S and Se in $\text{Ga}_{1-x}\text{Al}_x\text{As}$. Layers of this material with the best optical and electrical characteristics are obtained at

restricted arsenic overpressures and at growth temperatures some 100°C higher than for typical GaAs growth (1). It might seem therefore, from the evidence for GaAs, that these growth conditions would preclude the successful incorporation of chalcogen dopants in MBE $\text{Ga}_{1-x}\text{Al}_x\text{As}$. In the following, it is demonstrated that S and Se may be successfully incorporated and the thermodynamic framework is expanded to include the stability of aluminium chalcogenides. The experimental results are then discussed in the light of the results from the thermodynamic calculations.

A number of structures were grown to explore the incorporation behaviour of sulphur and selenium in $\text{Ga}_{1-x}\text{Al}_x\text{As}$ as a function of growth temperature, arsenic overpressure, incident chalcogen flux and aluminium content x . The grown layers were

characterised by several techniques including SIMS and electrochemical C-V profiling to determine dopant and free-electron concentrations and photovoltage spectroscopy (PVS) for measurements of aluminium content. Unfortunately, the range of experiments using selenium is rather more limited than for sulphur due to the premature failure of the selenium electrochemical cell by the mechanism described in chapter 3.

7.2: Experimental Results.

Figures 7.1 and 7.2 show C-V and SIMS profiles respectively through a layer of $\text{Ga}_{0.75}\text{Al}_{0.25}\text{As}$ deliberately doped with sulphur at a range of growth temperatures as indicated. The As_4/Ga flux ratio was ~2:1 and the sulphur cell emf of 165mV corresponded to a doping level of $3-5 \times 10^{17} \text{cm}^{-3}$ in GaAs at low growth temperatures. PVS spectra taken at intervals through the C-V profile revealed that the aluminium concentration was constant at 25% throughout the layer.

At growth temperatures of 630°C and 660°C, the SIMS and C-V concentrations agree to within a factor of two, although the SIMS concentration scale was based on ion implanted GaAs standards and is therefore subject to some uncertainty. Both figures are in broad agreement with the doping level expected for GaAs for this cell emf at low growth temperatures. Additionally, at 630°C and 660°C, there is no evidence for the substantial loss of sulphur that would certainly be expected from GaAs at these elevated temperatures. The addition of 25% aluminium to GaAs then, appears to stabilise the incorporation of sulphur up to 660°C.

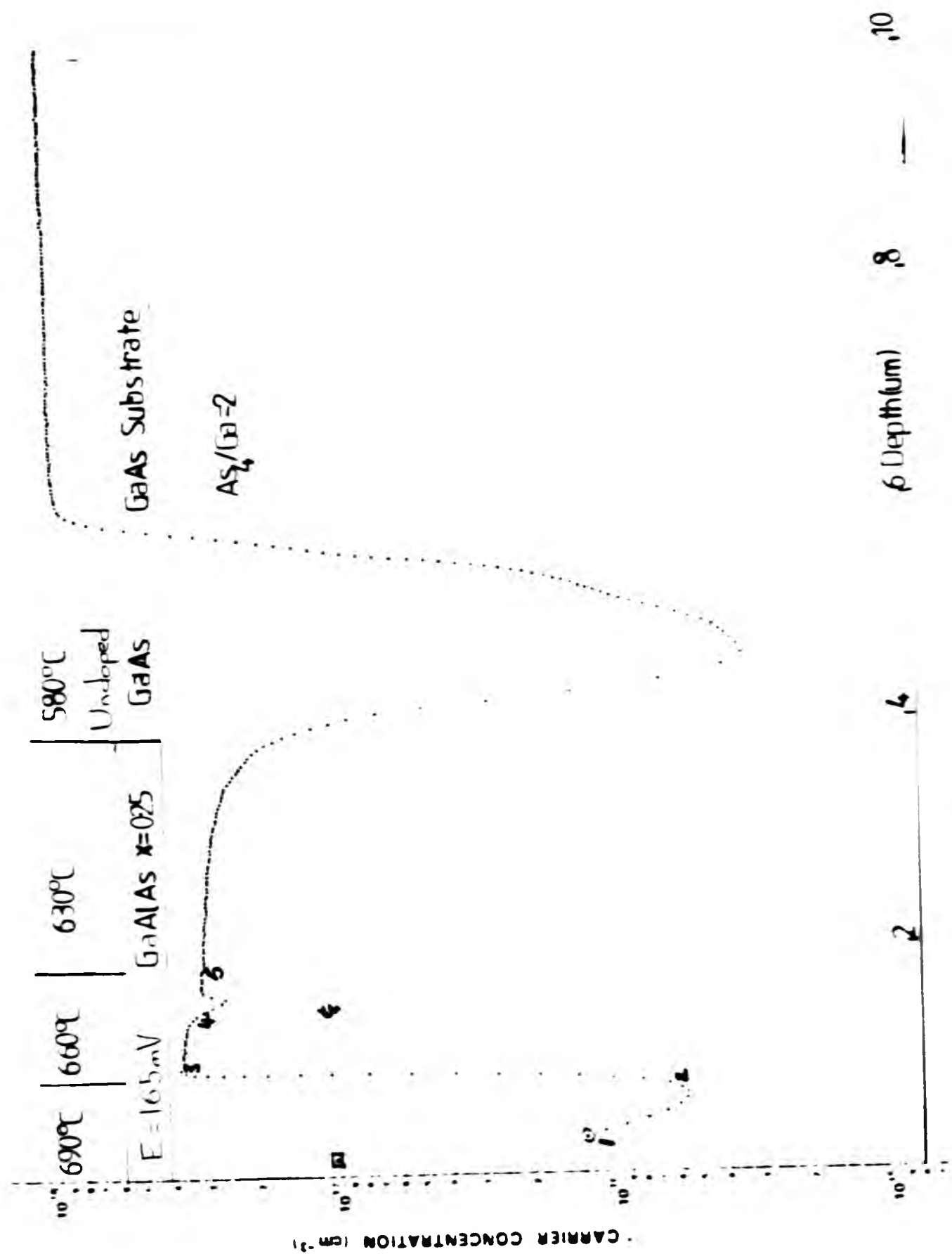


FIGURE 7.1: Electrochemical C-V profile through a layer of Ga_{0.75}Al_{0.25}As doped with sulphur where the growth temperature was varied as indicated.

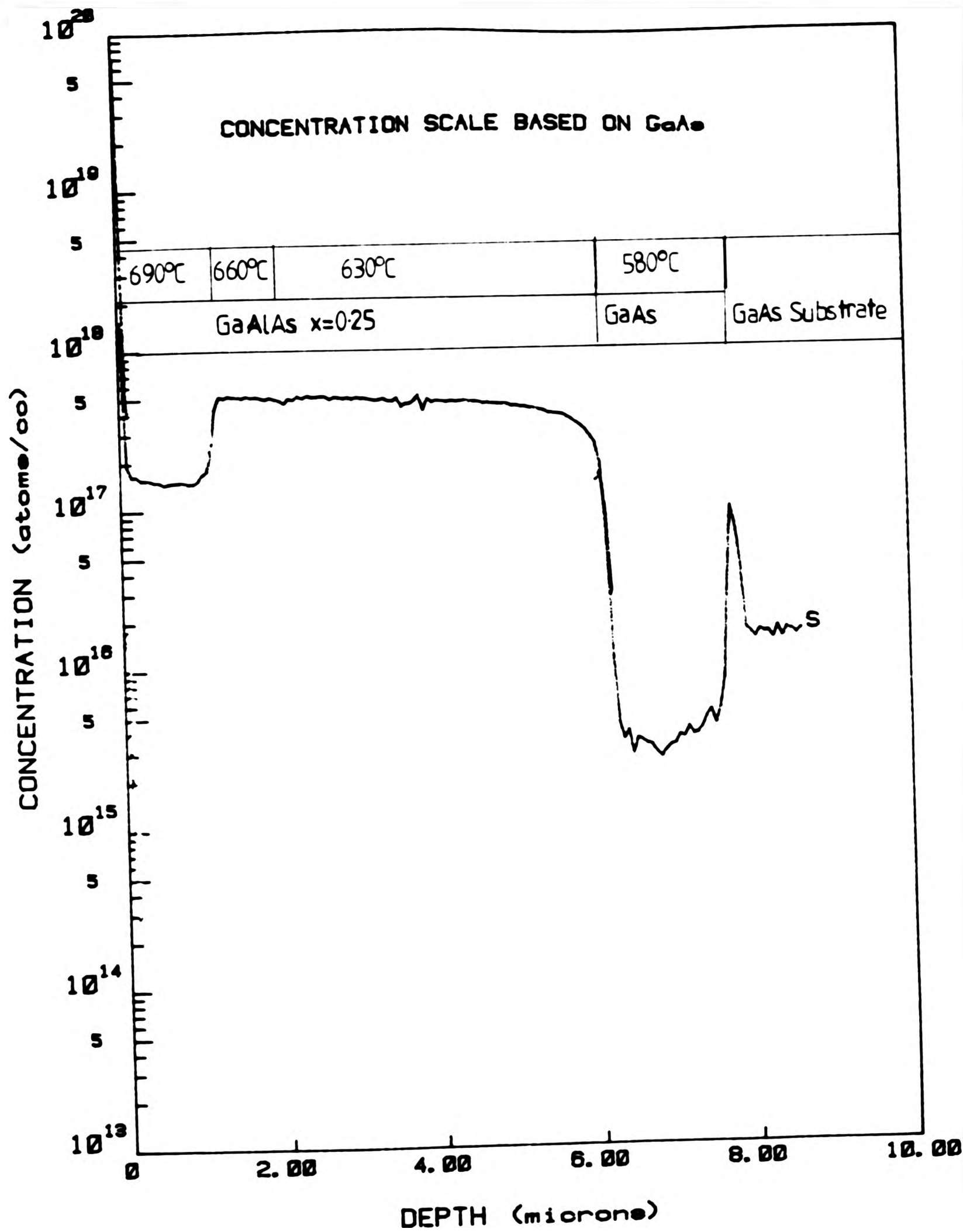


FIGURE 7.2: SIMS profile of the layer in figure 7.1.

At 690°C however, as both the SIMS and C-V profiles bear out, some loss of sulphur does occur. The C-V data shows a reduced concentration compared with the SIMS data which is probably due to the capture of electrons by deep traps which are characteristic of MBE GaAlAs grown under non-optimum conditions. Nominally undoped GaAlAs is usually semi-insulating, especially when grown at low temperatures (<600°C) due either to the high reactivity of aluminium with oxygen containing species in the system ambient gas background or to its relatively low surface mobility which stems from its high surface binding energy. The dip at ~1.6µm from the surface is probably due to the fact that the C-V profile was stopped at this point for a PVS measurement and does not appear in the SIMS profile.

Figures 7.3 and 7.4 show C-V and SIMS profiles respectively of a Ga_{0.7}Al_{0.3}As layer staircase doped with selenium. The growth temperature was 620°C and the As₄/Ga flux ratio was 2.5:1. Again, PVS spectra revealed a constant Al content throughout the layer. The three separate doping levels are clearly resolved in both figures with a factor of two agreement between the electrical and elemental concentrations. Again the SIMS concentrations are based on ion implanted GaAs standards. The measured concentrations also agree with those predicted from the doping of GaAs under conditions of no loss; cf figure 6.10. Although temperatures high enough to induce Se desorption were not used in this experiment, it seems that selenium has very similar incorporation behaviour at moderate temperatures in both GaAs and Ga_{0.7}Al_{0.3}As.

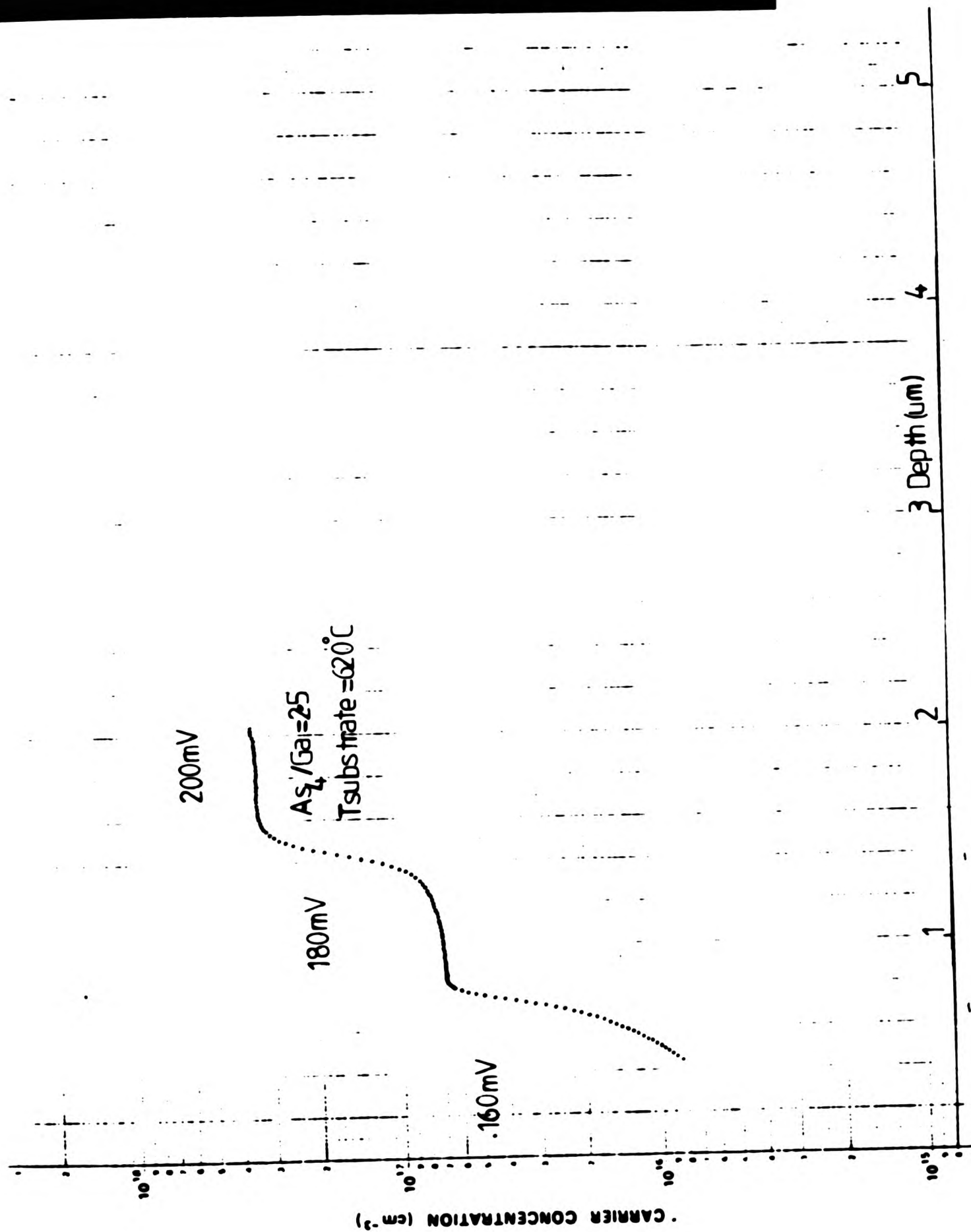


FIGURE 7.3: Electrochemical C-V profile through a Ga_{0.7}Al_{0.3}As layer staircase doped with selenium.

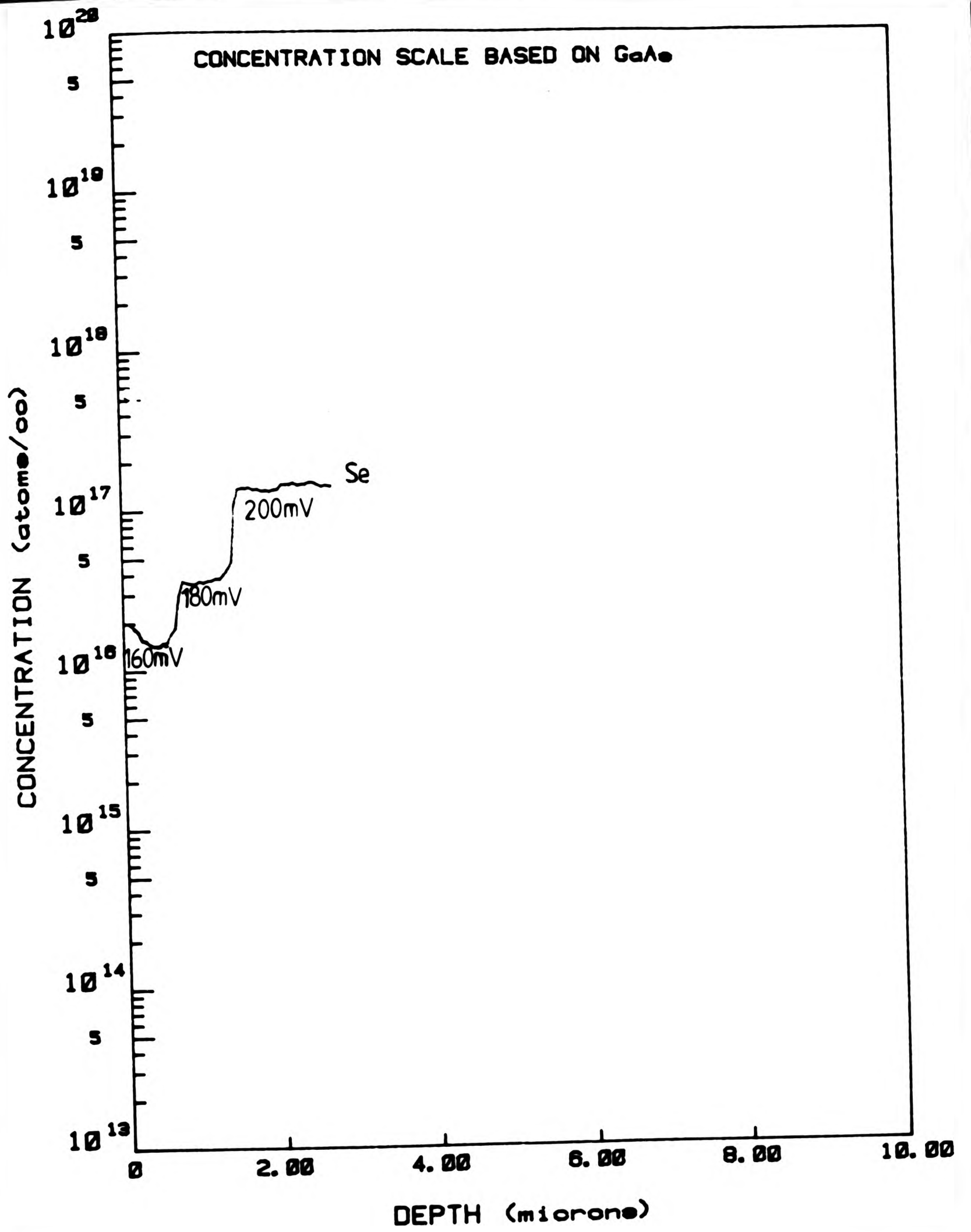


FIGURE 7.4: SIMS profile of the layer in figure 7.3.

The slope of the selenium concentration versus emf curve from the SIMS data gives Se_x $x=1.5$, a similar value to that for Se in GaAs from chapters 3 and 6 and non-integer for the reasons described therein.

Figure 7.5 shows a SIMS profile through a multilayer structure deliberately doped simultaneously with sulphur and selenium. The surface layer is GaAs while deeper layers contain an increasing amount of aluminium which was intended to range from ~2%-25%. The growth temperature was 640°C and the As_4/Ga flux ratio ~3:1. The sulphur and selenium cell emfs were 165mV and 200mV respectively corresponding to intended doping levels (based on 100% incorporation) of $3-5 \times 10^{17} cm^{-3}$ in both cases. The intention was to illustrate any differences in the incorporation behaviour of sulphur and selenium as a function of aluminium content under conditions where loss of both would be expected from GaAs. Unfortunately, the Se cell went short circuit shortly after this experiment and failed to operate. This is manifest in the SIMS profile as a reduced Se concentration against that which was expected. The cause of the transient in the Se concentration at 3-4 μm from the surface is unknown but may be due to the impending cell malfunction, especially as it appears to be asynchronous with the changes in Al concentration. In the light of these two deficiencies, the rest of the Se profile is probably suspect. However, it does show a slightly increased concentration of Se in the first two Al-containing layers as compared with the surface GaAs layer from which a small loss is expected from the results in chapter 6.

For the case of sulphur however, the trend is clearer. There is

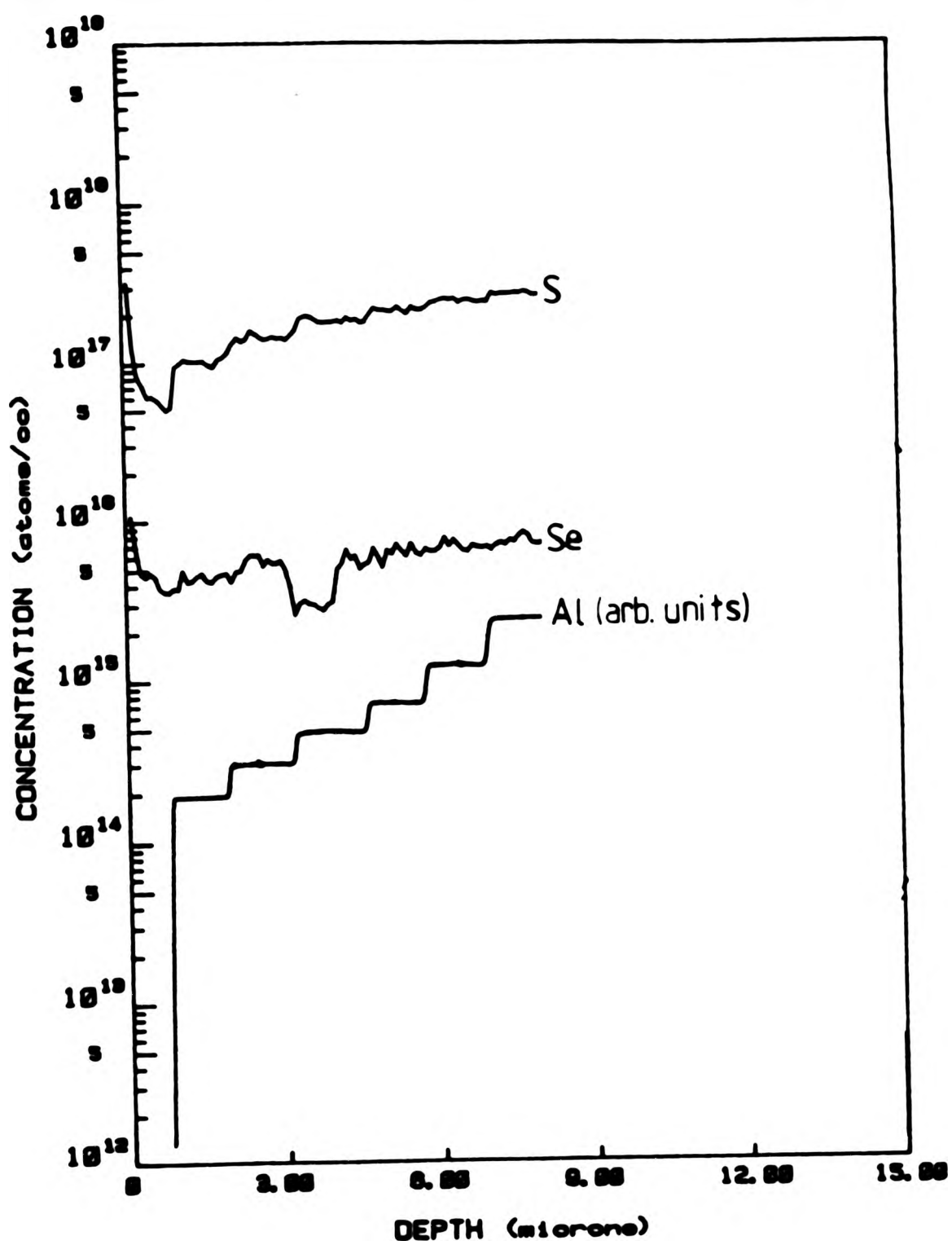


FIGURE 7.5: SIMS profile of a $\text{Ga}_{1-x}\text{Al}_x\text{As}$ $0.02 < x < 0.25$ multilayer simultaneously doped with sulphur and selenium.

a definite increase of approximately a factor of two on going from the GaAs layer to the first Al containing (~2%) layer and the sulphur concentration increases synchronously with the Al steps up to $\sim 3 \times 10^{17} \text{cm}^{-3}$ at ~25% Al. This again suggests the increasing ability of aluminium to suppress loss of sulphur.

Figure 7.6 shows a C-V profile through the same structure and the trend and carrier concentrations are in broad agreement with the SIMS elemental concentrations.

The preceding experiments indicate that when sulphur and/or selenium are incorporated into GaAlAs, they are efficiently activated as donors, producing well behaved electrolytic Schottky junctions allowing C-V analysis. The electrical and elemental concentrations show good agreement and the SIMS profiles show little evidence for segregation or diffusion under the conditions explored. Although the case for selenium is uncertain, it is clear that the presence of aluminium in the GaAlAs has a significant stabilising effect on the incorporation of sulphur, suppressing reevaporation at temperatures up to 80°C higher than in GaAs.

Two further multi-layer structures were grown to investigate in detail the incorporation behaviour of sulphur in $\text{Ga}_{1-x}\text{Al}_x\text{As}$. The first was designed to explore a range of Al concentrations ($x=0.03, 0.075$ and 0.15) and growth temperatures for a fixed incident sulphur and arsenic flux. The second explored Al concentration and $\text{As}_4/\text{total Group III}$ flux ratio at fixed sulphur flux and growth temperature. The sulphur flux used corresponded to an intended doping level of $n=2 \times 10^{17} \text{cm}^{-3}$. The resulting layers were analysed by SIMS (2). The changes in Al

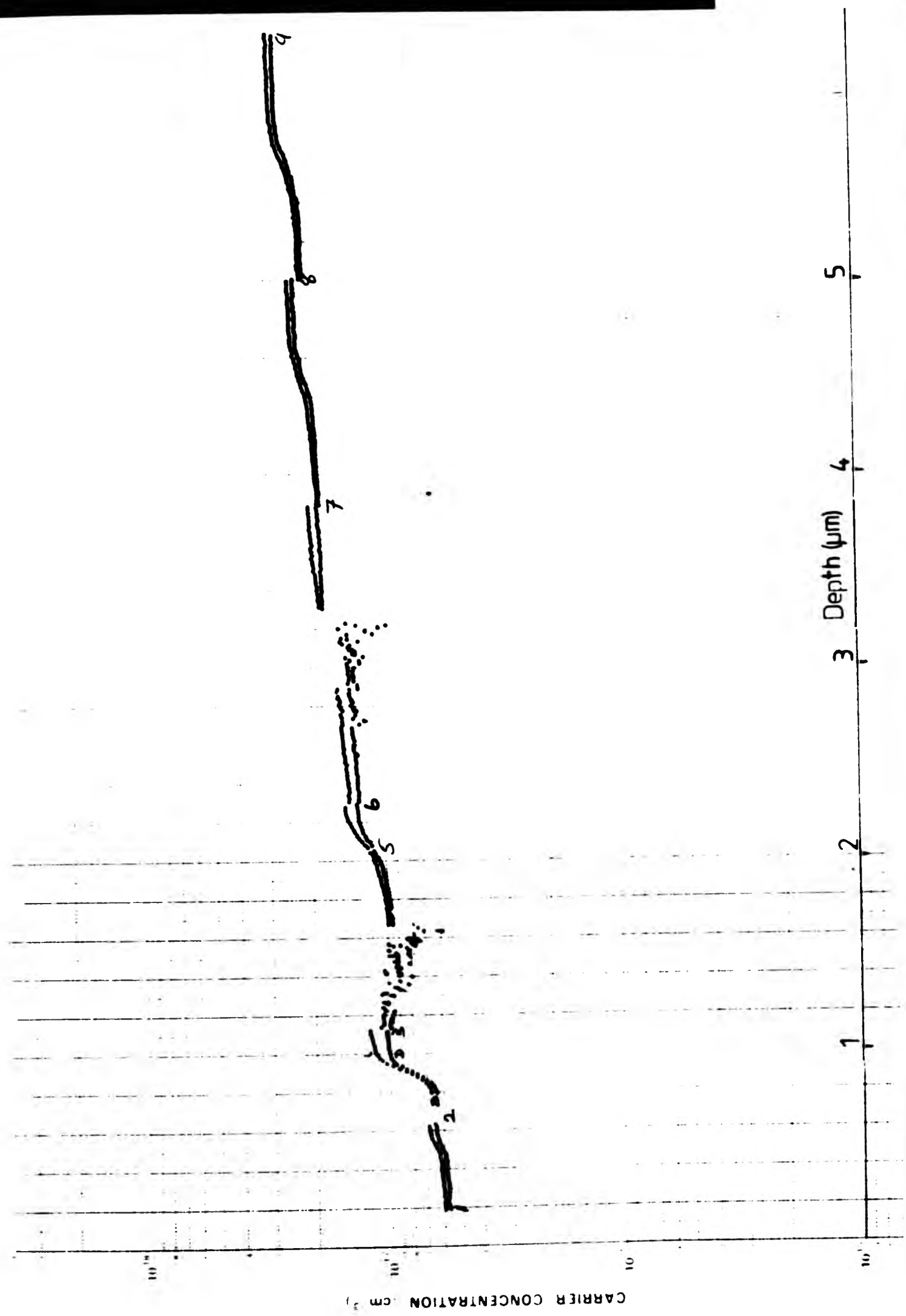


FIGURE 7.6: Electrochemical C-V profile of the layer in figure 7.5.

concentration were used as markers in the SIMS depth profile for the expected response in the sulphur concentration.

The SIMS data are presented in the form of raw data with ion count rates rather than concentrations. This is because there are many effects which make the quantification of absolute concentrations difficult in heterostructures. Both the ion emission rate and the sputter rate are functions of the matrix compositions and at the time of the measurements, neither Charles Evans and Associates or Loughborough Consultants who performed the SIMS analyses had access to concentration standards for GaAlAs. In some instances, GaAs standards were available but the use of these would ignore the above-mentioned matrix effects. In order to overcome the difficulties of measuring absolute concentrations in alloys of different compositions, the growth experiments were designed to include built in references so that comparison could be made between the ion count rate from alloys of the same composition under different growth conditions. Figures 7.7 and 7.10 illustrate the layer sequences used. In practice, for the relatively low aluminium concentrations used (<15% AlAs), the matrix effects seem to be weak and of the same order as the concentration changes due to the increased growth rate for GaAlAs over GaAs when a single shuttered aluminium source is used.

Figures 7.7 and 7.8 show the growth sequence and SIMS profile of the substrate temperature experiment respectively. There is an overall curvature to the sulphur depth profile which is believed to be due to an instrumental effect in the SIMS measurement rather than a direct indication of a changing sulphur concentration and may be due to a variation in the

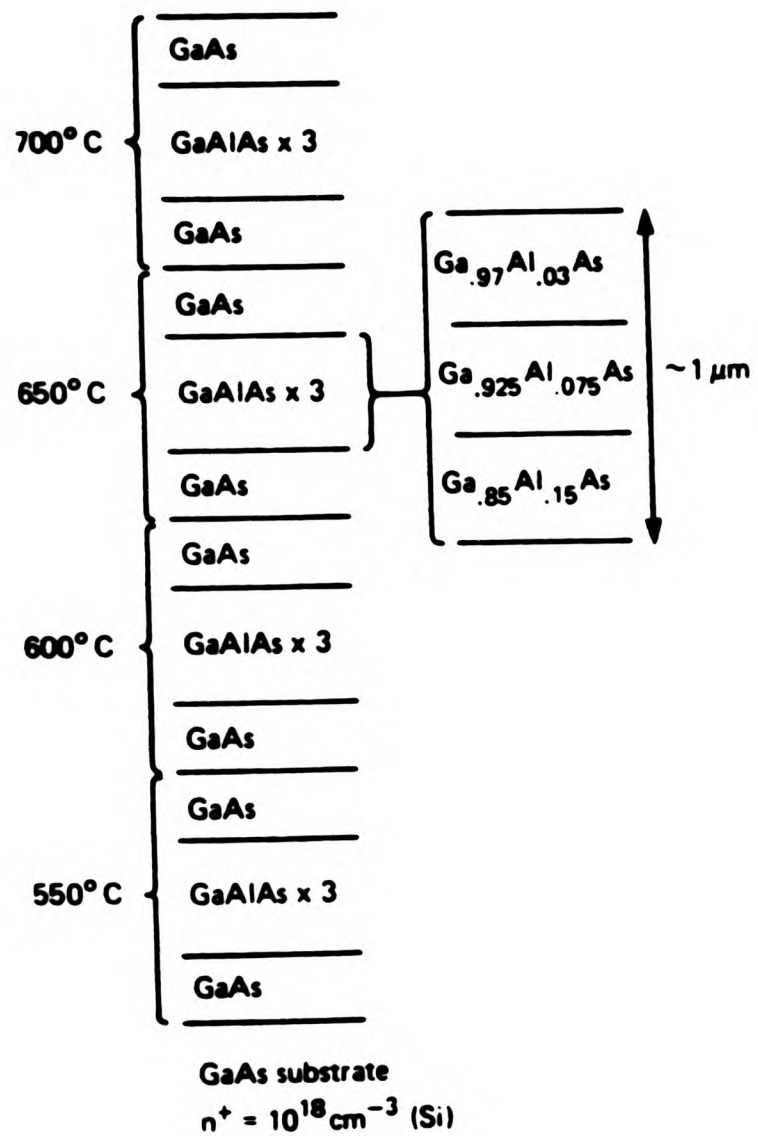


FIGURE 7.7. Growth sequence for the study of sulphur incorporation in $\text{Ga}_{1-x}\text{Al}_x\text{As}$ as a function of x and growth temperature.

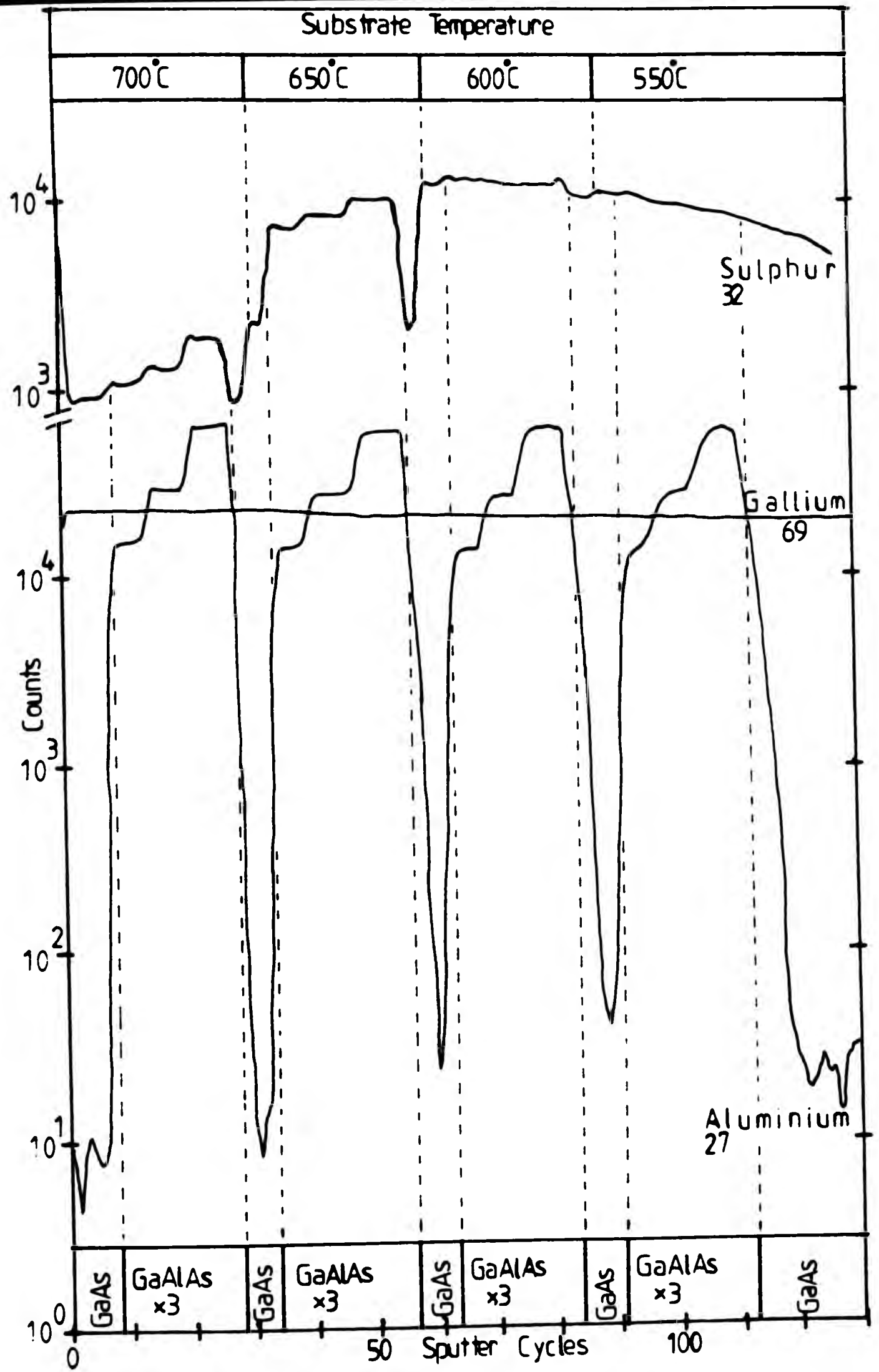


FIGURE 7.8. SIMS depth profile of the structure illustrated in figure 7.7.

sulphur background signal from the ambient gas background of the unbaked SIMS system. However, it is the changes stimulated by the steps in the aluminium profile and the growth temperature, and synchronous with them, that are of most interest. At 550°C the addition of aluminium to GaAs to form $\text{Ga}_{.85}\text{Al}_{.15}\text{As}$ has no effect on the SIMS mass 34 or 32 sulphur signal. There are two possible effects that might be expected; a change in the rate of any sulphur loss and a change in the emission rate of ionised species from the SIMS process due to the change in the aluminium content of the $\text{Ga}_{1-x}\text{Al}_x\text{As}$ and the subsequent sputter rate and matrix effects. The lack of any observed change in ion count rate argues strongly for both no change in sulphur loss and no change in SIMS yield for sulphur 32 and 34 species for $\text{Ga}_{1-x}\text{Al}_x\text{As}$ ($x < 0.15$). The alternative explanation is that the change in any sulphur loss rate is exactly balanced by a change in the SIMS sensitivity as the elemental composition of the $\text{Ga}_{1-x}\text{Al}_x\text{As}$ is changed.

In the GaAs region where the temperature was raised from 550°C to 600°C, a small sulphur loss is observed at the higher temperature. This loss is completely suppressed at the initiation of the $\text{Ga}_{.85}\text{Al}_{.15}\text{As}$ layer and remains undetectable down to the lowest aluminium concentration of $\text{Ga}_{.97}\text{Al}_{.03}\text{As}$. The loss reappears however in the GaAs layer grown before the temperature was raised to 650°C. At this higher temperature, the sulphur loss from the GaAs becomes much more significant but is again suppressed by the addition of aluminium to form $\text{Ga}_{.85}\text{Al}_{.15}\text{As}$. This time however there is still some residual loss from the $\text{Ga}_{1-x}\text{Al}_x\text{As}$ which becomes greater as x is reduced. Note again that the degree of sulphur loss is identical for the two GaAs layers grown at the same temperature

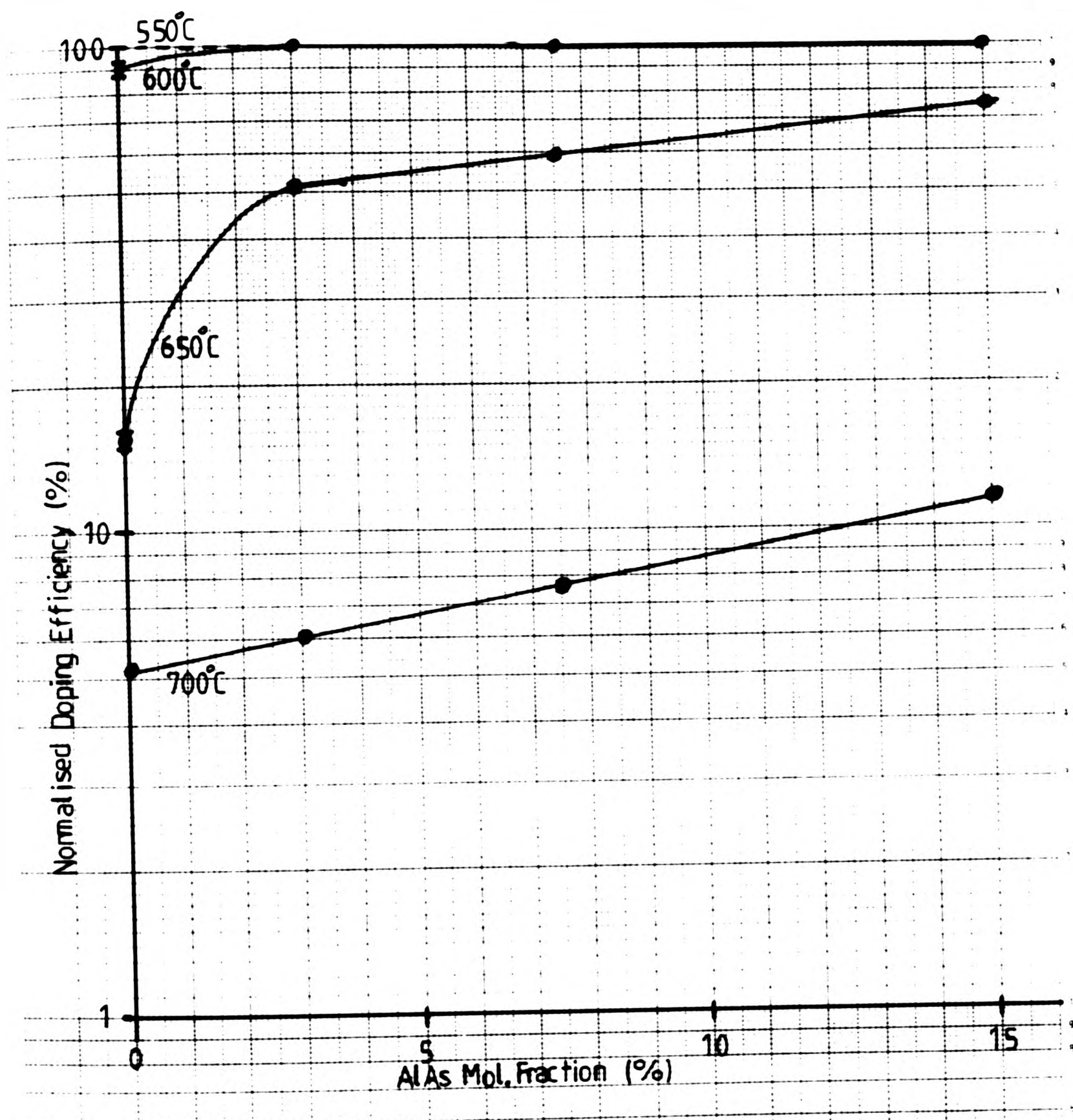


FIGURE 7.9. Incorporated sulphur concentration in $Ga_{1-x}Al_xAs$ as a function of x and growth temperature.

either side of the $\text{Ga}_{1-x}\text{Al}_x\text{As}$ layers. As the temperature is raised further to 700°C , less than 10% of the sulphur remains in the GaAs. This figure may be smaller as the background level for the SIMS machine is unknown. At this elevated temperature, the addition of Al results in a much smaller but still significant suppression of the sulphur loss.

These results are summarised in figure 7.9 where the sulphur ion count rates have been ratioed to give a relative incorporation efficiency which is plotted against AlAs content for the different growth temperatures. At 550°C the efficiency is independent of aluminium content corresponding to no loss. At 600°C approximately 15% of the arriving sulphur is lost from GaAs and this is reduced to an unmeasurable amount in the case of $\text{Ga}_{.97}\text{Al}_{.03}\text{As}$. At 650°C , the doping efficiency was of the order of 15% for GaAs, compared with the case at 550°C , rising rapidly to 50% for $\text{Ga}_{.97}\text{Al}_{.03}\text{As}$ and more slowly to 75% for $\text{Ga}_{.85}\text{Al}_{.15}\text{As}$. At 700°C , the suppression of sulphur loss was more gradual. The doping efficiency rose from of the order of 5% in GaAs to 15% in $\text{Ga}_{.85}\text{Al}_{.15}\text{As}$. This loss seems severe but extrapolation suggests that the doping efficiency could rise to ~50% for the higher aluminium content of layers used in many devices such as lasers and HEMTs where $\text{Ga}_{.7}\text{Al}_{.3}\text{As}$ is commonly used. This could be usefully established in future experiments.

Figures 7.10 and 7.11 show the grown structure and the corresponding SIMS profile for the investigation of the effects of the arsenic overpressure on sulphur loss from $\text{Ga}_{1-x}\text{Al}_x\text{As}$. A growth temperature of 650°C was used, corresponding to a region where sulphur loss had been observed to take place from the previous experiment. Starting from the substrate, GaAs was

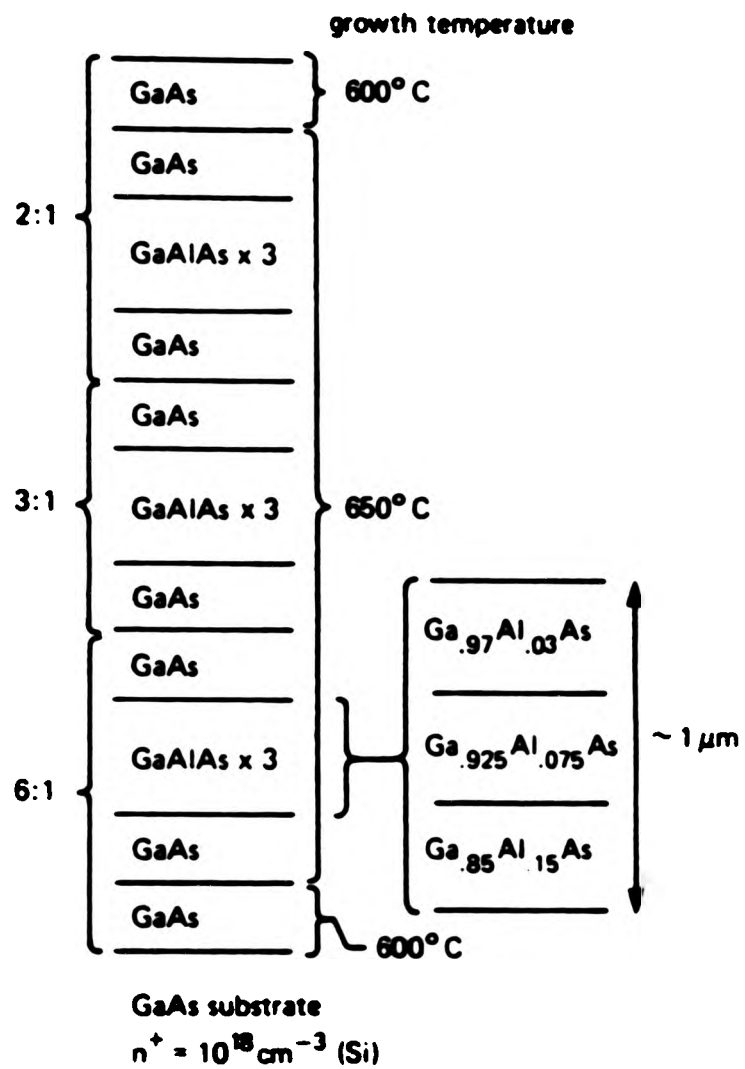


FIGURE 7.10. Growth sequence for the study of sulphur incorporation in $\text{Ga}_{1-x}\text{Al}_x\text{As}$ as a function of x and arsenic overpressure.

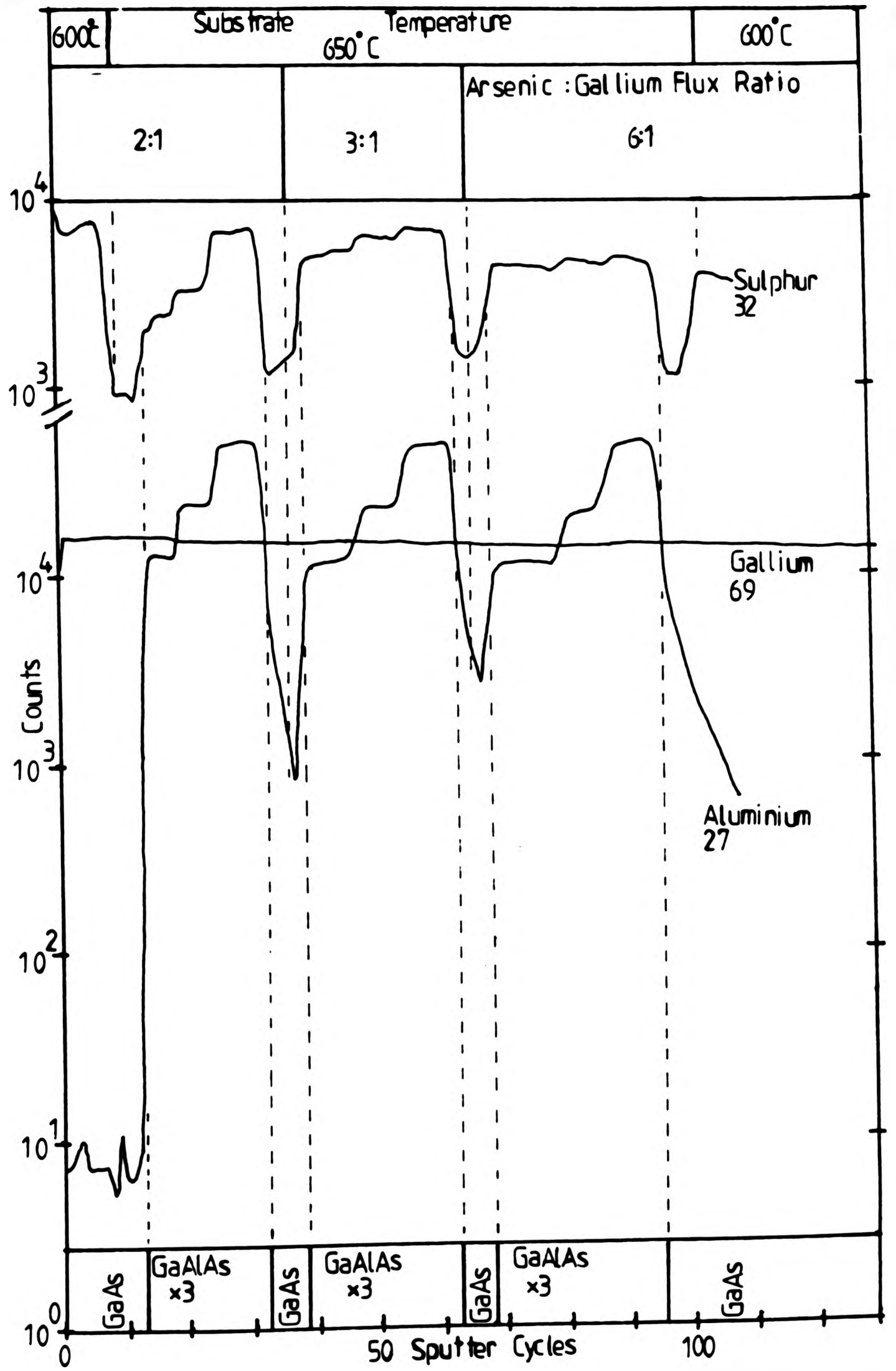


FIGURE 7.11. SIMS depth profile of the structure illustrated in figure 7.10.

grown at 600°C under an arsenic overpressure J_V/J_{III} of 6:1 where minimal sulphur loss was expected. As the substrate temperature is raised to 650°C, a degree of sulphur loss is observed. This is suppressed by the commencement of growth of the $Ga_{.85}Al_{.15}As$ and to a lesser extent by the layers containing less aluminium.

The overall behaviour is shown in figure 7.12 where sulphur ion count rate is plotted against AlAs content for the three arsenic overpressures. As in the previous experiment, the percentage change in sulphur intensity brought about by the change in the Al flux has been used to determine a relative incorporation efficiency, thus compensating for any instrumental drift. For $J_V/J_{III}=6:1$, the sulphur loss from GaAs is rapidly suppressed on going to $Ga_{.97}Al_{.03}As$ with almost no increase in doping efficiency as the aluminium content is increased further. For $J_V/J_{III}=3:1$, the doping efficiency rises slightly more slowly and saturates a little later. For $J_V/J_{III}=2:1$ the sulphur loss is suppressed much more slowly at low aluminium contents but the doping efficiency has still risen to more than 80% in $Ga_{.85}Al_{.15}As$. In this respect the $Ga_{1-x}Al_xAs$ mirrors the behaviour of GaAs in that sulphur is incorporated with greater efficiency as the growth conditions move away from the group III rich surface structures towards higher As_4 fluxes.

7.3: Discussion.

In chapter 5, thermodynamic calculations showed that the interaction between the GaAs lattice and the chalcogen dopants

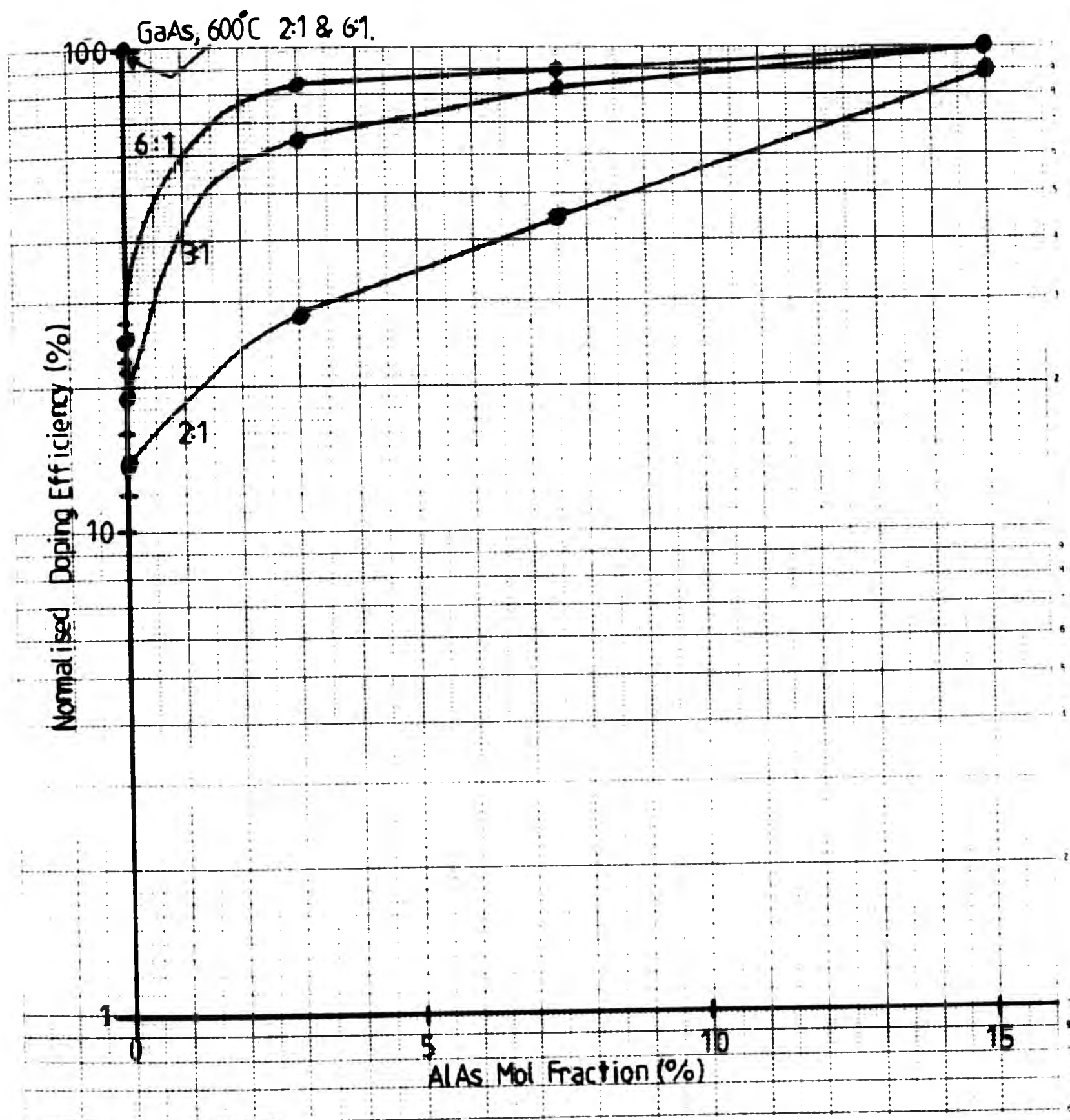


FIGURE 7.12. Incorporated sulphur concentration in $Ga_{1-x}Al_xAs$ as a function of x and arsenic overpressure.

S, Se and Te is strong enough to lead to their incorporation rather than evaporation under MBE conditions. Thus the reaction



(where X is S, Se or Te, (g) indicates the gas phase, V_{As} is an arsenic vacancy in the GaAs lattice, X_{As}^+ is an ionised dopant atom on an arsenic site in GaAs and e^- is an electron in the conduction band in GaAs) is well to the right under MBE conditions. Further consideration in chapter 6 revealed that competing reactions are even more preferred thermodynamically but are kinetically hindered at low growth temperatures. As the growth temperature is raised, these reactions become more important and result in the loss of chalcogen dopant from the growing surface in the form of the volatile gallium chalcogenides $Ga_2X(g)$. Thus the reaction



also lies well to the right under all practical MBE conditions with equilibrium pressures $P(Ga_2X)$ of 7atm, 4.4×10^{-3} atm and 2.6×10^{-12} atm for X=S, Se and Te respectively. These pressures were calculated for an intended doping level of $2 \times 10^{18} \text{cm}^{-3}$ and are not accessible in the MBE regime, except for Te where fewer than 1% of the Te is predicted to be incorporated. In addition, the equilibrium between the gaseous and solid forms of the gallium chalcogenides favours loss and the reaction



also lies well to the right with an equilibrium pressure

$P(\text{Ga}_2\text{S})$ of the order of 2×10^{-2} atm at 600°C .

The situation is somewhat different for the interaction of sulphur with AlAs. Firstly, there are at least three species of gaseous aluminium sulphide for which thermodynamic data are available:- $\text{AlS}(\text{g})$, $\text{Al}_2\text{S}_2(\text{g})$ and $\text{Al}_2\text{S}(\text{g})$. Although the following is described in terms of $\text{Al}_2\text{S}(\text{g})$ for purposes of comparison with $\text{Ga}_2\text{S}(\text{g})$, the other species produce very similar equilibrium pressures. Rewriting equation (2) for aluminium produces



and substitution of standard thermochemical data (3,4) reveals that for a doping level of $2 \times 10^{18} \text{cm}^{-3}$, the equilibrium Al_2S pressure is of the order of 8×10^{-12} atm at 600°C rising to 2.3×10^{-10} atm at 750°C which compares with the incident PS_2 of 6×10^{-14} atm. Although these pressures are many orders of magnitude lower than for the gallium chalcogenides, they still predict a borderline doping efficiency of the order of less than 0.1%.

The key difference between the predicted behaviour of sulphur incorporation in AlAs and GaAs becomes clear when the aluminium analogue of reaction (3) is considered. Whereas $\text{Ga}_2\text{S}_3(\text{s})$ (sulphur in the GaAs lattice) is unstable with respect to the gaseous form $\text{Ga}_2\text{S}(\text{g})$, Al_2S_3 (sulphur in the AlAs lattice) is predicted to be stable under MBE conditions of pressure and temperature. Hence, the reaction



lies substantially to the left with a predicted $P(\text{Al}_2\text{S})$ less than 1.71×10^{-18} atm at 600°C . This is much less than the corresponding figure for $P(\text{Ga}_2\text{S})$ of 2×10^{-2} atm.

Although the values of the predicted pressures are not precise due to the approximation of considering Al_2S_3 for S_{As} , the uncertainty in the thermodynamic data and the simple two-term approximation used for the free-energy calculations, there is a clear difference in the predicted behaviour for the relative stabilities of the gallium and aluminium chalcogenides. It seems likely, therefore, that the observed difference in the doping behaviour between GaAs and $\text{Ga}_{1-x}\text{Al}_x\text{As}$ is strongly related to these relative stabilities.

Therefore, although the incorporation of sulphur into GaAs is only possible due to a kinetic barrier to the formation of volatile Ga_2S , the equivalent loss reactions are not favoured for the interaction of sulphur with AlAs, since the Al_2S is likely to decompose to Al_2S_3 , and the behaviour in this case may be explained from purely thermodynamic considerations without recourse to hindered kinetics.

In considering the behaviour for $\text{Ga}_{1-x}\text{Al}_x\text{As}$, we may model the GaAs and AlAs components separately since they have little heat of mixing and the activity coefficients for GaAs and AlAs are near unity (5). The aluminium activity therefore scales as x , the concentration of the AlAs component. However, the predicted difference in behaviour is strong enough (16 orders of magnitude) that between 600°C and 700°C sulphur should be incorporated even for $\text{Ga}_{1-x}\text{Al}_x\text{As}$ very dilute in AlAs ($x \ll 1$)

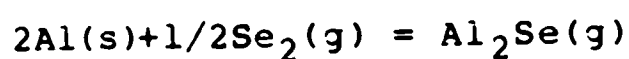
where the activity of the Al is much reduced.

However, our data suggests that something slightly different is happening in practice. At low AlAs concentrations (<10%), some sulphur continues to be lost. It is assumed that this loss occurs as Ga_2S and of course in the limit of zero aluminium content this is indeed so. High crystal quality implies significant atom mobility in the growing surface layer and there will therefore be competition for the sulphur atoms in this layer between the free aluminium and gallium atoms. Although the reaction is heavily in favour of bonding to the aluminium in the lattice (leading to incorporation), for low Al concentrations there is a higher probability that a sulphur atom will encounter two Ga atoms with the subsequent options of incorporation or kinetically hindered desorption as Ga_2S in the same way as for GaAs. Higher overpressures of As_4 therefore increase the sulphur doping efficiency by suppressing the loss reaction through control of the surface arsenic and hence gallium concentrations. The balance between the various thermodynamically allowed reaction pathways is critically dependent on the details of the surface kinetics. A simple model, requiring a sulphur atom to have two Ga atom nearest neighbours for Ga_2S formation, would predict an incorporation efficiency proportional to $1-(1-x)^2$, where x is the AlAs mole fraction. This has approximately the correct form but takes no account of surface diffusion. Further modelling would require a wider experimental database to elucidate the kinetics in more detail, but the situation for $\text{Ga}_{1-x}\text{Al}_x\text{As}$ is clearly intermediate between GaAs and AlAs.

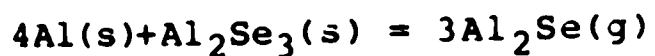
For the case of selenium, it was shown in chapter 6 that it

exhibits an excess of stability over sulphur at elevated growth temperatures when used to dope MBE GaAs. This is believed to be due to a kinetic barrier to the formation of $\text{Ga}_2\text{Se}(\text{g})$ in the same way as for sulphur. In fact, $\text{Ga}_2\text{Se}_3(\text{s})$ is predicted to be less stable with respect to $\text{Ga}_2\text{Se}(\text{g})$ under MBE conditions than $\text{Ga}_2\text{S}_3(\text{s})$ is with respect to $\text{Ga}_2\text{S}(\text{g})$ (Table 1, chapter 6) so the apparent enhanced stability remains largely unexplained.

In considering the incorporation of Se in AlAs, $\text{Al}_2\text{Se}(\text{g})$ is predicted to be formed, thus the reaction



lies to the right with $P_{\text{Al}_2\text{Se}} \sim 4.4 \times 10^{-3} \text{ atm}$ indicating a strong potential for Se loss via this route. In addition, $\text{Al}_2\text{Se}_3(\text{s})$ is barely stable at 600°C growth temperature and $n = 2 \times 10^{18} \text{ cm}^{-3}$ doping, and significant decomposition to volatile $\text{Al}_2\text{Se}(\text{g})$ is expected. Thus for the reaction



the equilibrium pressure of Al_2Se is predicted to be of the order of $3 \times 10^{-14} \text{ atm}$, comparable with the incident selenium flux ($P_{\text{Se}_2} = 6 \times 10^{-14} \text{ atm}$). In this respect, the stabilising effect of the solid aluminium chalcogenides that act to encourage sulphur incorporation into AlAs does not appear to operate for selenium. The successful incorporation of Se into GaAlAs alloys is therefore probably due to the existence of kinetic barriers to the formation of Ga_2Se in the same way as for its incorporation into GaAs. The addition of aluminium to selenium-doped GaAs is therefore predicted to have less of a stabilising

effect at elevated growth temperatures than for sulphur doping. Preliminary results indicate that Se may be successfully incorporated into GaAlAs at GaAs growth temperatures as illustrated in figures 7.3 and 7.4 for the selenium doping staircase. However, data at higher temperatures and other compositions is limited but indicates that incorporation may be less reliable. It is not clear whether this is due to the chemical effects predicted above or the deterioration in the electrochemical selenium cell which failed while this was being investigated.

7.4: Summary of Reactions and Thermodynamic Predictions.

In this section, the reactions considered are listed together with the pressures predicted. The method of calculation has been covered in the preceding chapters.

7.4.1: Simplifying Assumptions.

The conditions assumed for the calculations are as follows:

- a) Growth temperature = 600°C for comparison with typical GaAs growth temperatures.
- b) $P_{X_2} = 6 \times 10^{-14} \text{ atm}$ ($X = \text{S, Se}$) for $2 \times 10^{18} \text{ cm}^{-3}$ doping.
- c) $[M]^{-1}$ ($M = \text{Ga(l), Al(s)}$) since MBE growth takes place near the Group III liquidus.

d) $[M_2X_3]^{-1}$. The doping level of $2 \times 10^{18} \text{ cm}^{-3}$ is assumed to be close to the solid solubility of the chalcogen dopant in GaAs and AlAs.

These conditions were chosen since they allow the activities of the solid components to be approximated to unity and in some respects are a calculational device since practical growth under these conditions would almost certainly produce poor morphology material. However they do allow comparisons to be drawn between the different material systems. It should be emphasised that the calculated values are order of magnitude estimates only, relying as they do on a simple two-term evaluation of the free-energy change and particularly on the modelling of $X_{As} = M_2X_3$.

7.4.2: Gallium Sulphide Reactions.

- 1) $2\text{Ga}(l) + 1/2\text{S}_2(g) = \text{Ga}_2\text{S}(g) \dots \dots P_{\text{Ga}_2\text{S}} = 7 \text{ atm.}$
- 2) $2\text{Ga}(l) + 3/2\text{S}_2(g) = \text{Ga}_2\text{S}_3(s) \dots \dots P_{\text{S}_2} = 4.5 \times 10^{-19} \text{ atm.}$
- 3) $\text{Ga}_2\text{S}(g) + \text{S}_2(g) = \text{Ga}_2\text{S}_3(s) \dots \dots P_{\text{Ga}_2\text{S}} = 8.5 \times 10^{-19} \text{ atm.}$
- 4) $4\text{Ga}(l) + \text{Ga}_2\text{S}_3(s) = 3\text{Ga}_2\text{S}(g) \dots \dots P_{\text{Ga}_2\text{S}} = 2 \times 10^{-2} \text{ atm.}$

7.4.3: Gallium Selenide Reactions.

- 5) $2\text{Ga}(l) + 1/2\text{Se}_2(g) = \text{Ga}_2\text{Se}(g) \dots \dots P_{\text{Ga}_2\text{Se}} = 4.4 \times 10^{-3} \text{ atm.}$
- 6) $2\text{Ga}(l) + 3/2\text{Se}_2(g) = \text{Ga}_2\text{Se}_3(s) \dots \dots P_{\text{Se}_2} = 4.6 \times 10^{-16} \text{ atm.}$
- 7) $\text{Ga}_2\text{Se}(g) + \text{Se}_2(g) = \text{Ga}_2\text{Se}_3(s) \dots \dots P_{\text{Ga}_2\text{Se}} = 2.9 \times 10^{-6} \text{ atm.}$
- 8) $4\text{Ga}(l) + \text{Ga}_2\text{Se}_3(s) = 3\text{Ga}_2\text{Se}(g) \dots \dots P_{\text{Ga}_2\text{Se}} = 4.1 \times 10^{-4} \text{ atm.}$

7.4.4: Aluminium Sulphide Reactions.

- 9) $2\text{Al}(s) + 1/2\text{S}_2(g) = \text{Al}_2\text{S}(g) \dots \dots \text{PAl}_2\text{S} = 8 \times 10^{-12} \text{ atm.}$
10) $2\text{Al}(s) + 3/2\text{S}_2(g) = \text{Al}_2\text{S}_3(s) \dots \dots \text{PS}_2 = 2.4 \times 10^{-27} \text{ atm.}$
11) $\text{Al}_2\text{S}(g) + \text{S}_2(g) = \text{Al}_2\text{S}_3(s) \dots \dots \text{PAl}_2\text{S} = 6.5 \times 10^{-32} \text{ atm.}$
12) $4\text{Al}(s) + \text{Al}_2\text{S}_3(s) = 3\text{Al}_2\text{S}(g) \dots \dots \text{PAl}_2\text{S} = 1.7 \times 10^{-18} \text{ atm.}$

7.4.5: Aluminium Selenide Reactions.

- 13) $2\text{Al}(s) + 1/2\text{Se}_2(g) = \text{Al}_2\text{Se}(g) \dots \dots \text{PAl}_2\text{Se} = 4.4 \times 10^{-3} \text{ atm.}$
14) $2\text{Al}(s) + 3/2\text{Se}_2(g) = \text{Al}_2\text{Se}_3(s) \dots \dots \text{PSe}_2 = 2.1 \times 10^{-22} \text{ atm.}$
15) $\text{Al}_2\text{Se}(g) + \text{Se}_2(g) = \text{Al}_2\text{Se}_3(s) \dots \dots \text{PAl}_2\text{Se} = 1.1 \times 10^{-22} \text{ atm.}$
16) $4\text{Al}(s) + \text{Al}_2\text{Se}_3(s) = 3\text{Al}_2\text{Se}(g) \dots \dots \text{PAl}_2\text{Se} = 3.1 \times 10^{-14} \text{ atm.}$

7.5: Conclusions.

An electrochemical cell has been used to dope $\text{Ga}_{1-x}\text{Al}_x\text{As}$ successfully with sulphur and selenium. At low temperatures, $< 600^\circ\text{C}$, the behaviour is facile, as for GaAs. Above this temperature, loss of chalcogen dopant was observed and is believed to be due to the formation of the volatile gallium chalcogenides Ga_2S and Ga_2Se which are the stable species under MBE conditions. Successful doping of GaAlAs is therefore believed to be due to the existence of a kinetic barrier to their formation, possibly mediated by the surface gallium population.

For sulphur doping of AlAs, simple thermodynamic calculations predict that the volatile aluminium sulphides are unstable with respect to the solid form Al_2S_3 (sulphur in the AlAs lattice)

under MBE conditions between 600°C and 700°C. The dopant loss route postulated for sulphur doping in GaAs is therefore not favoured for AlAs. The experimental observations reveal an enhanced stability of sulphur in $\text{Ga}_{1-x}\text{Al}_x\text{As}$ ($x < 0.15$) where the loss is increasingly suppressed at higher values of x . This is interpreted in terms of competition for sulphur between mobile Ga and Al surface atoms with the options of desorption as Ga_2S or incorporation in the AlAs lattice.

The calculations for selenium show a less clear difference between Se incorporation in GaAs and AlAs. In particular, Al_2Se_3 is predicted to have a borderline stability under MBE conditions and the behaviour for $\text{Ga}_{1-x}\text{Al}_x\text{As}$ may not be very different to that for GaAs. However, further work is needed in this area.

For growth of $\text{Ga}_{1-x}\text{Al}_x\text{As}$ at elevated temperatures, sulphur would appear to be the preferred chalcogen dopant, while for devices such as HEMTs (6) and waveguides (7), where GaAs growth temperatures are more usual (6), both have been used successfully, as will be described in chapter 8.

In cases where the chalcogen dopants are chosen for their non-amphoteric behaviour in preference to group IV dopants such as silicon, in the antimony-containing III-V alloys for example (8,9), the above comments regarding the choice of chalcogen dopant for aluminium-containing alloys may be particularly relevant.

7.6: References.

- 1) G.Wicks, W.I.Wang, C.E.C.Wood, L.F.Eastman and L.Rathbun, *J.Appl.Phys.*, **52**, 5792, (1981).
- 2) SIMS analysis performed by Loughborough Consultants Ltd. U.K.
- 3) K.C.Mills, *Thermodynamic Data for Inorganic S, Se and Te Compounds*, (Butterworth, London, 1974).
- 4) O.Kubaschewski and C.B.Alcock, *Metallurgical Thermochemistry*, 5th ed., (Pergamon, London, 1979).
- 5) R.Heckingbottom, *Proceedings of the Third International Conference on MBE, San Francisco 1984*, *J.Vac.Sci.Tech.*, Apr-May, (1985).
- 6) G.Weimann and W.Schlapp, *Appl.Phys.Lett.*, **46**, 411, (1985).
- 7) A.J.N.Houghton, P.M.Rodgers and D.A.Andrews, *Electronics Letters*, **20**, 479, (1984).
- 8) T.M.Kerr, T.D.MacLean, D.I.Westwood, J.D.Medland and C.E.C.Wood, Presented at the 3rd European Workshop on MBE at Aussois, France, March 1985. To be published.
- 9) T.D.Maclean, T.M.Kerr, D.I.Westwood, C.E.C.Wood, D.F.Howell and R.J.Nicholas, Submitted to *J.Appl.Phys.*, (1986).

CHAPTER 8: CHALCOGEN DOPED DEVICES.

8.1: Introduction.

In the preceding chapters, the incorporation behaviour and electrical characteristics of sulphur and selenium in bulk GaAs and AlGaAs MBE layers have been described. The main deviation from ideal dopant behaviour for both elements in both matrices is a tendency to reevaporation at elevated growth temperatures. This loss may be compensated for by increasing the incident dopant flux during growth. Such relatively straightforward behaviour, combined with the main advantages of electrochemical generation of the species (beam purity and rapid response), makes possible the growth of device structures, particularly those with abrupt or complicated doping profiles. Some examples of the successful use of electrochemically generated sulphur and selenium as dopants in MBE grown device structures will be described in the following sections.

8.2: Hyperabrupt Varactor Diode.

An application which made full use of the speed of response and ease of programability of the electrochemical sulphur cell was the growth of a hyperabrupt varactor structure. This device has application as a narrow band microwave tuner. Ideally the n-type region should be graded as $n \propto x^m$, $m = -3/2$, where x is the distance from the junction, since this results in a linear frequency-voltage characteristic when the diode is incorporated in a tuned circuit. This is useful in low distortion frequency

modulators. A further benefit of such a profile is that a wider range of capacitance is achieved before reverse breakdown occurs. Previous attempts have used variable range ion implantation to produce graded doping profiles which only approximate to the power law. In our case, the simple relationship between flux and voltage allowed the emf applied to the electrochemical sulphur cell to be programmed in a series of closely spaced steps to yield the required profile.

In order to optimise the efficiency of a varactor diode, it is necessary to minimise its series resistance and hence maximise the Q of any tuned circuit of which it may form a part. For this reason the device was grown on a highly doped substrate ($n=2 \times 10^{18} \text{cm}^{-3}$) with a buffer layer of similar doping level. The growth temperature was 610°C , corresponding to conditions of some sulphur reevaporation, and the calibration curve shown in figure 6.4 was used to determine the required emf's.

Figure 8.1 shows an electrochemical C-V profile through the grown layer where four separate regions are apparent. Starting from the surface of the layer we have A) a region of constant doping level whose doping-thickness product is calculated to just deplete out when the rectifying contact is formed, B) the hyperabrupt doping profile with exponent $-3/2$, C) a low doped plateau region and D) an abrupt change to the highly doped buffer region and then the n^+ substrate. Figure 8.2 shows the surface C-V characteristic of the electrolytic Schottky junction. The successful realisation of $m=-3/2$ is demonstrated by the straight line behaviour of $C^{-0.5}$ against voltage. Such a structure would be rather more difficult to achieve with a conventional Knudsen cell where time constants rather greater

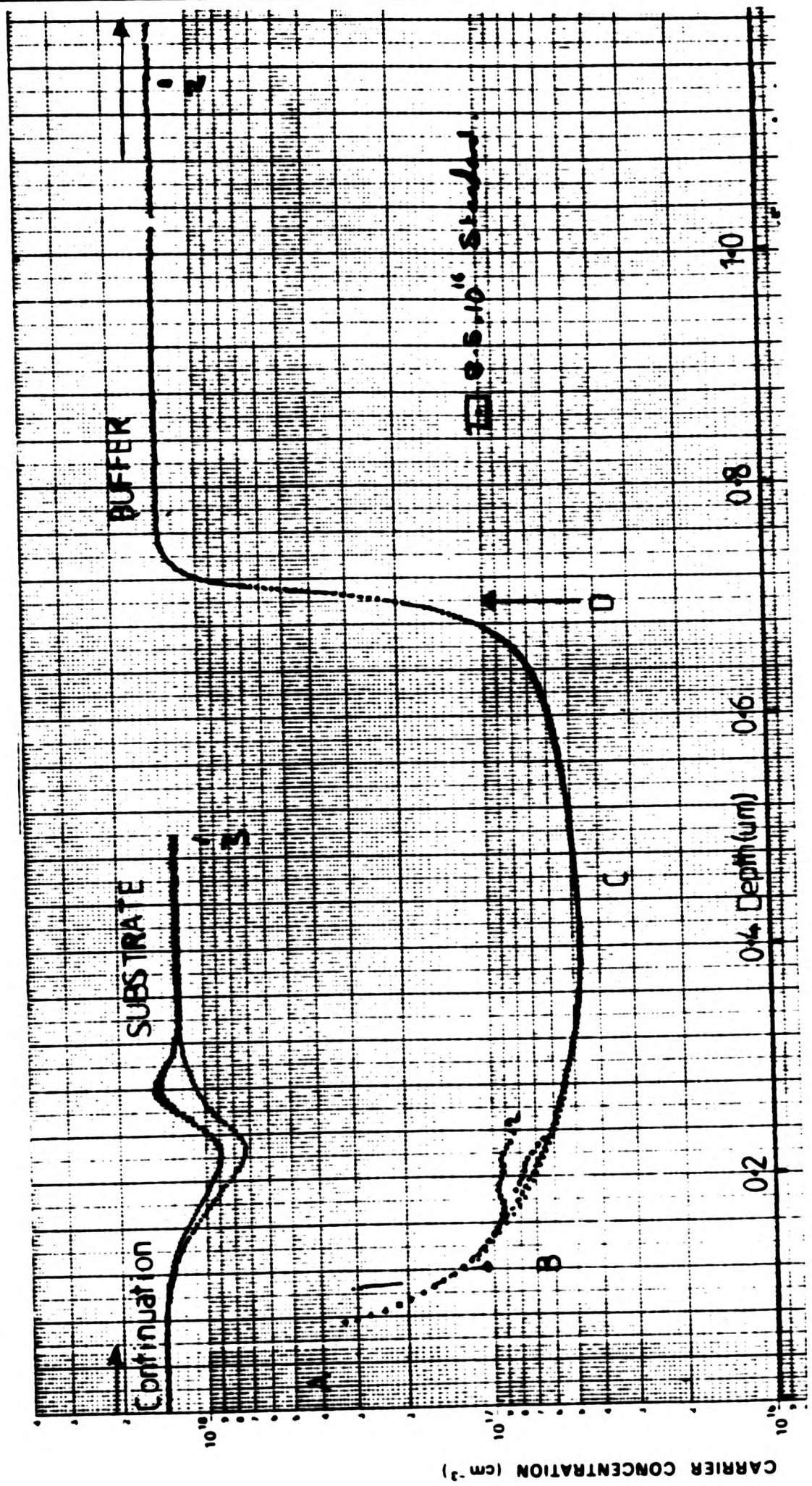


FIGURE 8.1: Electrochemical C-V profile through a hyperabrupt varactor structure. A-D, refer to text.

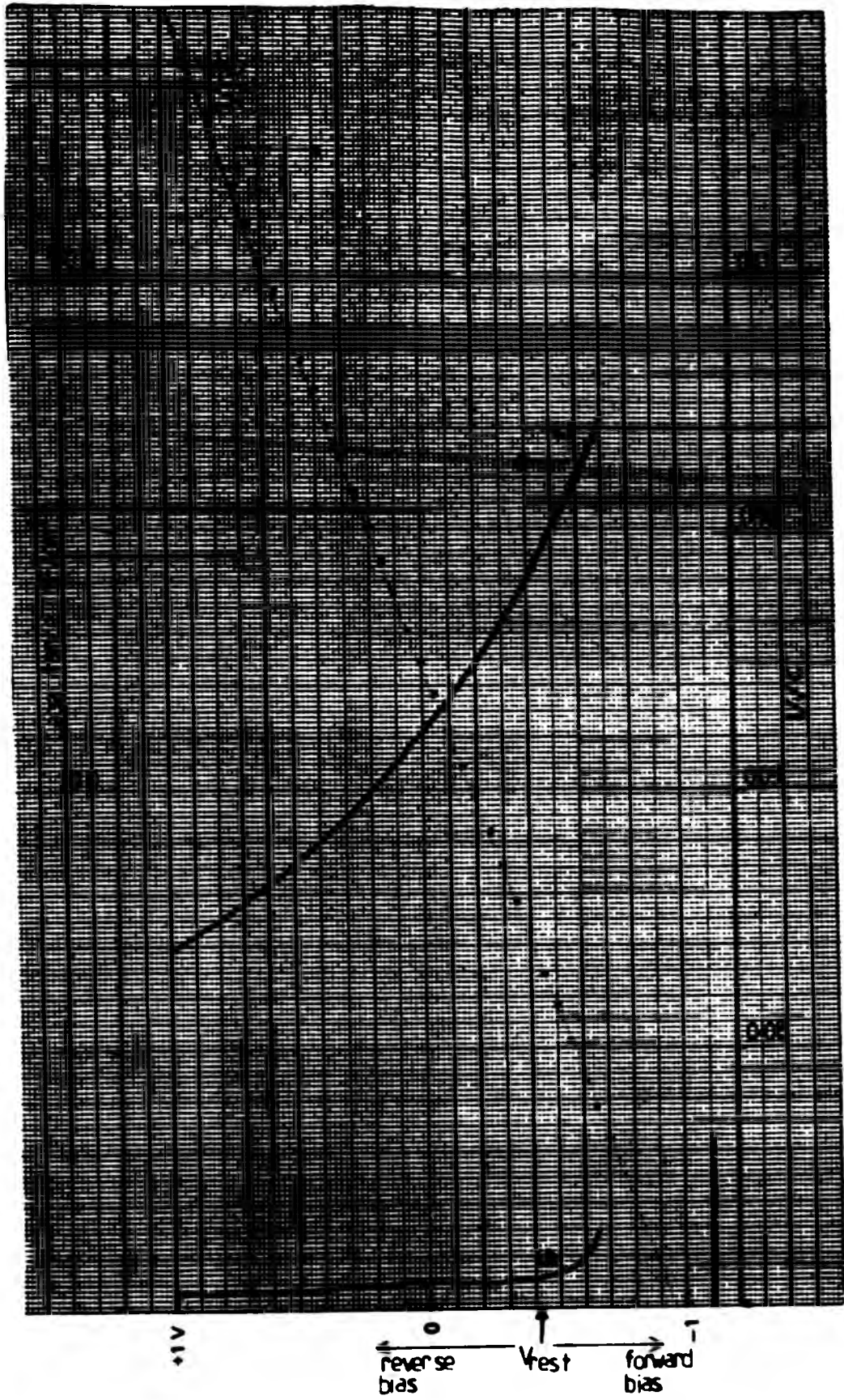


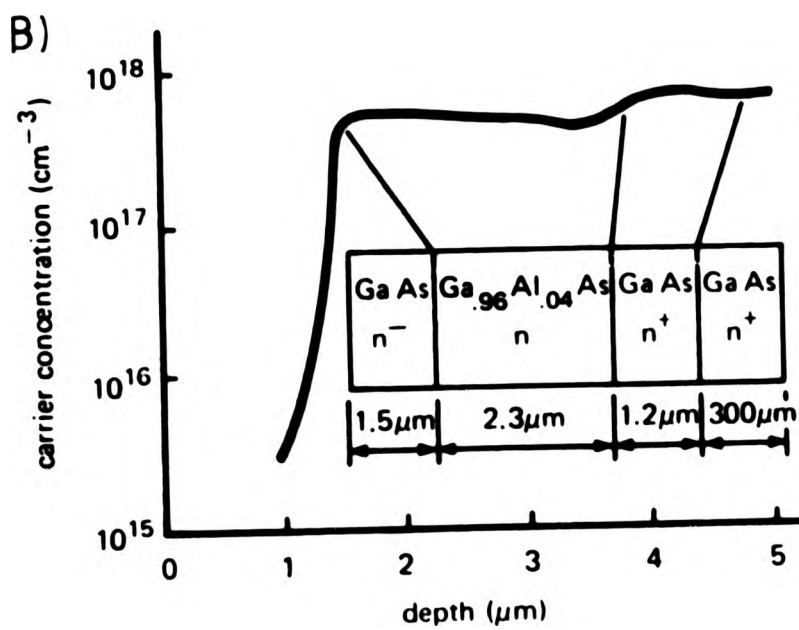
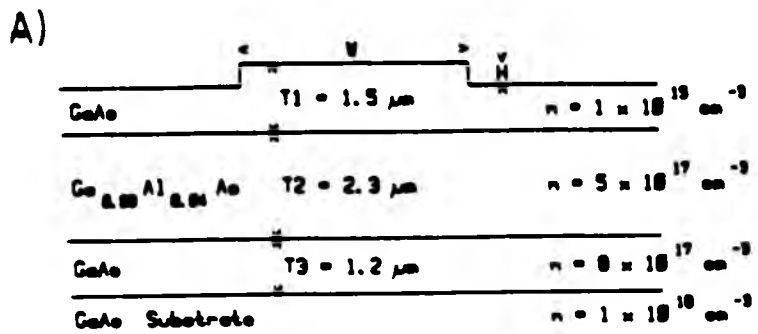
FIGURE 8.2: Capacitance-voltage characteristic of the electrolytic Schottky junction formed on the varactor structure. V_{rest} is the rest potential corresponding to zero bias and G is the resistive component of the AC conductivity.

than the ω characteristic of the electrochemical cell pertain.

When these layers were fabricated into 80 μ m diameter diodes (1), the devices showed the required linear behaviour in a tuned circuit in the 2-18 GHz region. Since the devices were relatively large, the associated capacitance was \sim 4pF with a series resistance of $<$ 10 Ω m (dominated by spreading resistance in the substrate). The capacitance ratio achieved for a 10V change in bias was 14:1.

8.3: Guided Wave Devices.

Guided wave optical devices, and particularly optoelectronic integrated circuits (where information may be processed optically), are of increasing importance as a result of the use of optical fibres in telecommunications systems and cable TV networks. Devices such as directional couplers, phase modulators and amplitude modulators can be made in both semiconductor and dielectric materials but a particular attraction of semiconductor guided wave devices is their inherent potential for integration with light sources and detectors, significantly reducing the problem of interconnection losses associated with hybrid devices. However, semiconductor waveguides have until recently had a reputation for high optical loss (particularly in comparison with their main contender, lithium niobate), which has been attributed at least in part to the presence of free carriers in the guiding material (2). To establish that low loss semiconductor waveguides were feasible, and as a first step towards active



C) RIB WAVEGUIDE PHASE MODULATOR LAYER STRUCTURE

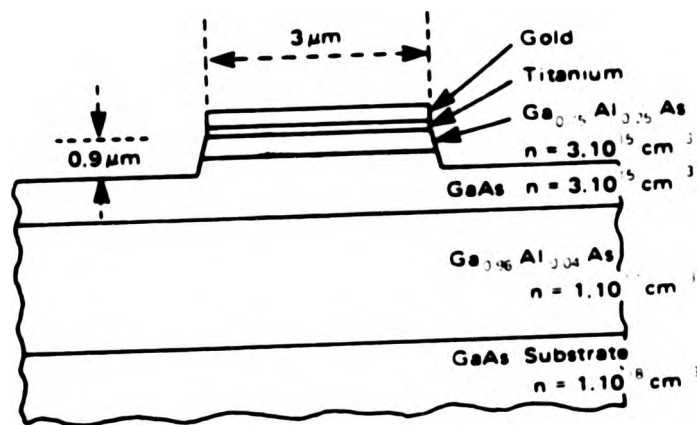


FIGURE 8.3: Semiconductor waveguide structures. A) Low-loss rib waveguide, B) Electrochemical C-V profile through such a structure doped with sulphur, C) Phase modulator structure.

optoelectronic devices capable of optical processing, the following structures were grown.

Figure 8.3 shows a layer structure for a simple semiconductor waveguide. The structure was designed as a precursor to an active device so the lower confining layer of $\text{Ga}_{0.96}\text{Al}_{0.04}\text{As}$ was sulphur doped with the electrochemical sulphur cell to $5 \times 10^{17} \text{cm}^{-3}$. The guiding layer was nominally undoped GaAs, typically $1 \times 10^{15} \text{cm}^{-3}$.

The layers were characterised by fabricating rib waveguides (3). Photoresist stripes were defined and ion beam milling used to produce ribs $\sim 0.2\text{-}0.4 \mu\text{m}$ high and $2\text{-}15 \mu\text{m}$ wide in the top GaAs layer. Loss measurements on guides up to 13.5mm long (to reduce the effect of coupling losses) were made using $1.15 \mu\text{m}$ radiation and gave propagation losses $\sim 2 \text{dB cm}^{-1}$. This low value indicates that integrated optical circuits may be made in which lengths of a few mm are characteristic and where device losses may be less than 1dB .

On the strength of this work, active device layers were subsequently grown where the GaAs guiding layer was capped with low-doped ($n \sim 5 \times 10^{15} \text{cm}^{-3}$) $\text{Ga}_{0.75}\text{Al}_{0.25}\text{As}$ to which a metal Schottky contact could be made. This structure enabled an electric field to be applied across the GaAs guiding layer to change its electro-optic coefficients while keeping optical losses low by minimising the overlap between the guided mode and the electron concentrations in the confining layers. However, in the course of the project, the n-type dopant was changed to silicon and the material from which successful phase modulators and directional couplers were made were so doped

(4,5).

8.4: Laser Structures.

The threshold current density of broad area double heterostructure lasers provides a relatively convenient benchmark for the "quality" of the material grown by a particular technique (6), being a sensitive function of carrier lifetimes, recombination rates and optical losses. Therefore, at an early stage in the study of the growth and sulphur doping of GaAlAs, such a structure was grown as depicted in figure 8.4. This was however a rather optimistic one-shot effort at the structure and evidence from ball-lapping and electrochemical C-V profiling revealed that the doping levels were rather lower and the thicknesses rather different to those intended. Nonetheless, broad area lasers, fabricated by cleaving into 100um wide bars (7) showed threshold current densities in the range $4-6\text{kA.cm}^{-2}$, while a good value might be more like 1kA.cm^{-2} . Much of the high threshold may be attributed to the wide active region and poor optical confinement of the non-ideal structure and the low doping levels giving high contact resistances (7). The successful achievement of lasing action was however most encouraging but indicated that the sulphur doping mechanism was not fully understood and deserved further study.

In another experiment, a GRINSCH (8) laser structure was grown. This structure features a graded refractive index in the guiding region to modify the guided mode to an optimum configuration for launching into an optical fibre. The grading

$1\mu\text{m}, p > 5 \times 10^{18}, \text{GaAs} (p = 5 \times 10^{17}, 0.6\mu\text{m})$
$2.2\mu\text{m}, p = 5 \times 10^{17}, \text{Ga}_{1-x}\text{Al}_x\text{As} (p = 3 \times 10^{16}, 1.7\mu\text{m})$ $x = 0.3 \quad (x = 0.22)$
$0.2\mu\text{m}, n = 10^{16}, \text{GaAs} (n = 10^{16}, 0.4\mu\text{m})$
$2.2\mu\text{m}, n = 5 \times 10^{17}, \text{Ga}_{1-x}\text{Al}_x\text{As} (n = 3 \times 10^{17}, 2.1\mu\text{m})$ $x = 0.3 \quad (x = 0.22)$
$1\mu\text{m}, n = 10^{18}, \text{GaAs} (n = 5 \times 10^{17}, 0.6\mu\text{m})$
$n = 10^{18}, \text{GaAs Substrate}$

FIGURE 8.4: Double-Heterostructure laser layer sequence. The figures in brackets refer to measured values.

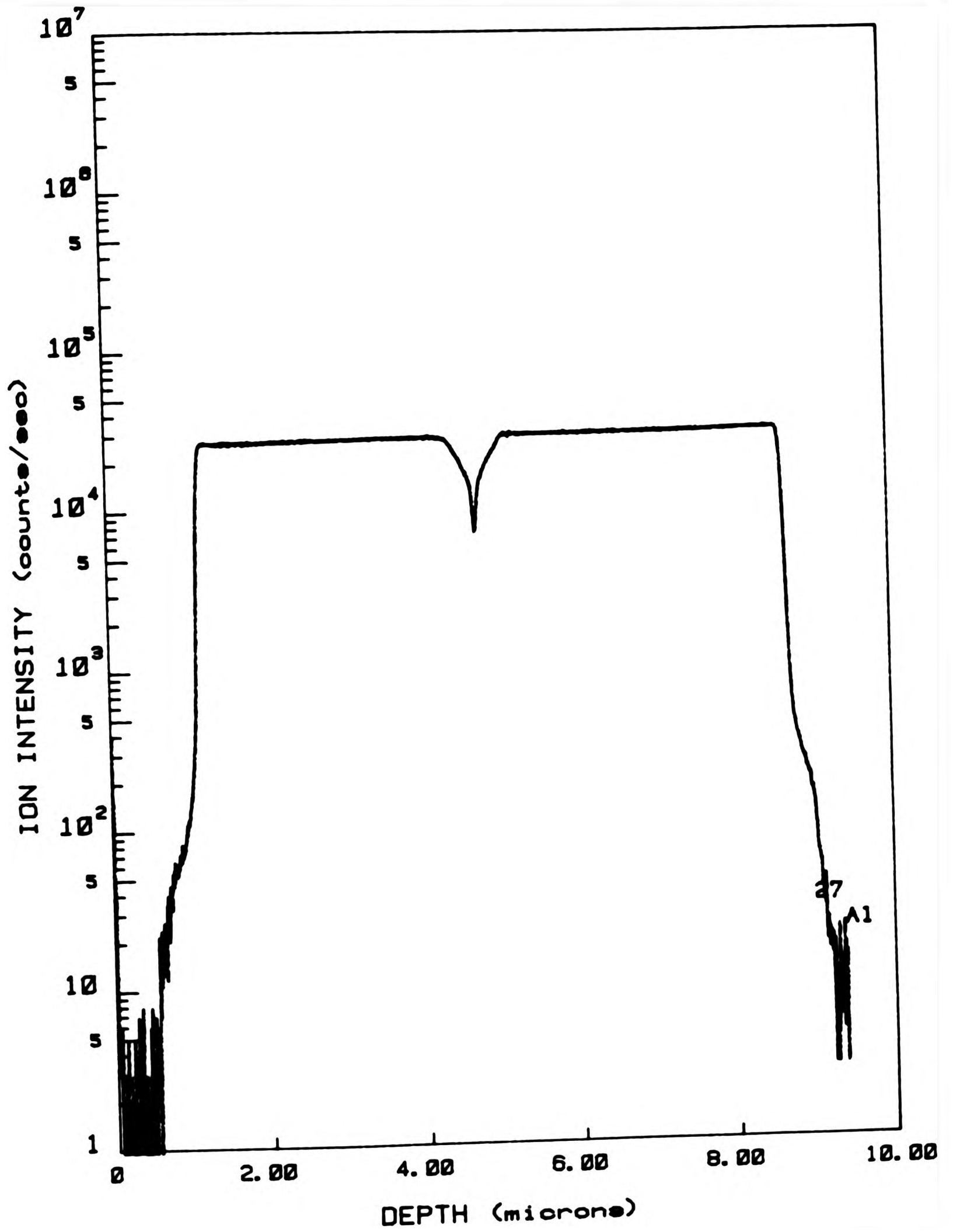


FIGURE 8.5: Aluminium SIMS profile through a GRINSCH laser structure.

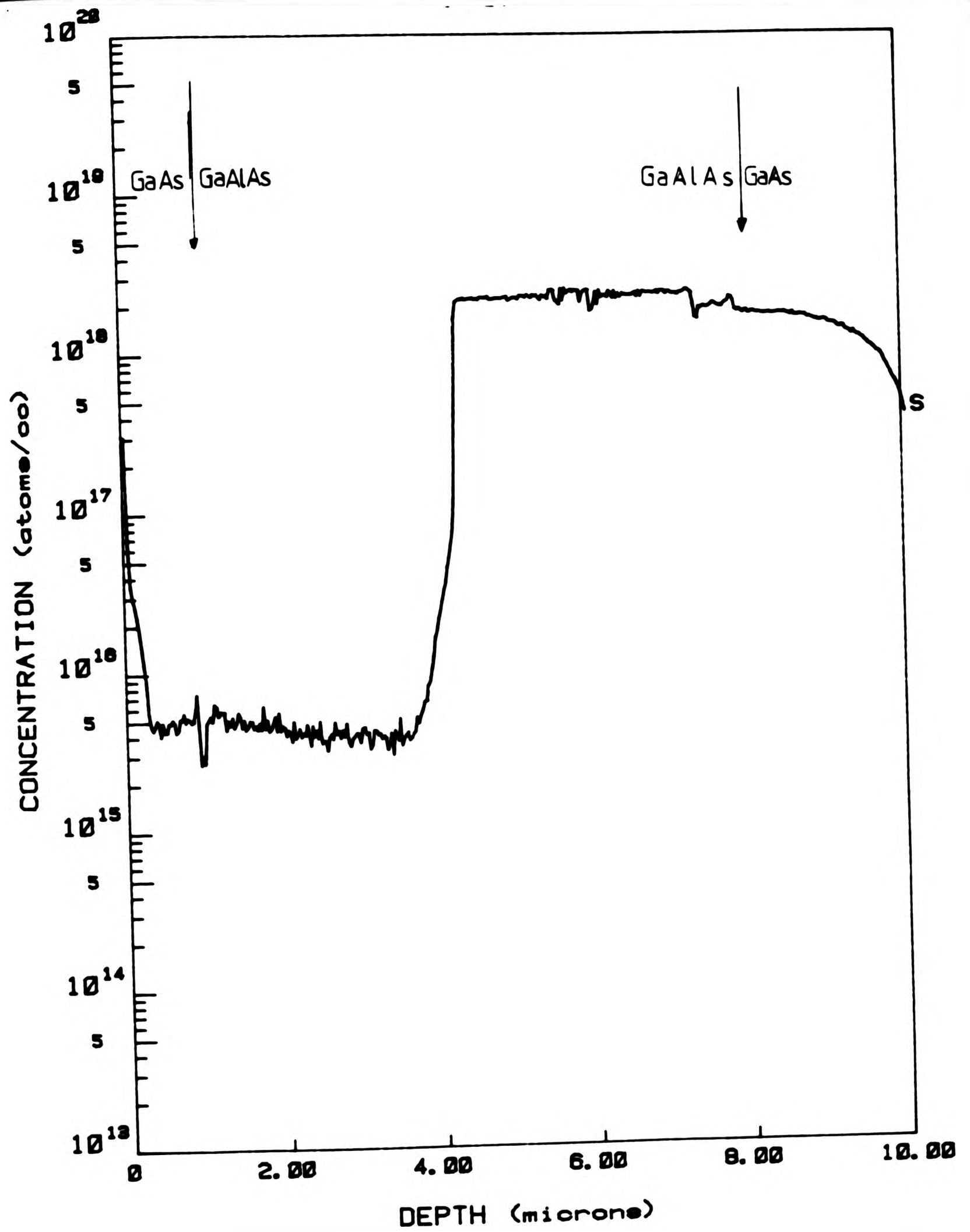


FIGURE 8.6: Sulphur SIMS profile through GRINSCH laser structure.

is achieved by varying the aluminium content of the GaAlAs layers as shown by the aluminium SIMS (9) profile in figure 8.5. The structure was grown with a view to exploring the feasibility of producing such graded layers by MBE rather than with the fabrication of lasers in mind but was deliberately doped like a laser structure nonetheless. The sulphur SIMS profile is shown in figure 8.6. The intended doping profiles are clearly reproduced. Although there is some random noise and a gradual decay on the sulphur trace (whose causes are unknown), the change in doping level is quite abrupt. In particular, the lack of any change in the sulphur count rate synchronous with the transition from GaAs to GaAlAs is consistent with the SIMS analysis of sulphur doped layers in chapter 7.

Unfortunately it was not possible to fabricate broad area lasers from this material since it suffered from a very high density of oval and spit-type defects ($\sim 10^5 \text{cm}^{-2}$). The cause of this was later traced to a defective gallium crucible, rather than being symptomatic of sulphur doping. This means that no optical or electrical data are available. This particular example is of value however in that it indicates that sulphur may be incorporated into a relatively complex structure involving varying Al content and heterojunctions in a simple manner.

8.5: Low Dimensional Structures.

Recently, a new class of materials have been developed which allow access to a whole range of optical and electronic

properties previously unexplored. These are the superlattices or quantum-wells which are heterostructures with band-gap discontinuities so closely spaced that the bulk optical and transport properties are strongly modified. When the layer thicknesses are reduced to below about 500Å, and the electrons are confined in potential wells whose width is comparable to their de Broglie wavelength, new quantum-mechanical states appear. The "bandgap-engineering" facilitated by this process has produced many new device designs with novel and enhanced properties (10).

The high electron mobility transistor (HEMT) (11) is one of the simplest devices to take advantage of low-dimensional effects. Figure 8.7 shows the physical structure and resulting band diagram for such a device in GaAs/GaAlAs. The band-edge discontinuity produces a potential well which dips down below the Fermi level generating an essentially two-dimensional electron gas. The electrons, generated by the donor impurity atoms in the GaAlAs, are confined in the well and travel freely parallel to the interface. The undoped GaAlAs layer acts as an insulating spacer to provide coulombic screening of the carriers from the donor scattering centres. Since the GaAs is undoped and the carriers are separated from their donor atoms, the ionised impurity atom scattering is suppressed and the electrons travel with high mobility. By appropriate choice of doping, this enhanced mobility may be combined with high sheet carrier concentrations to yield fast, low resistance devices. The mobility may be further increased by reducing the temperature and freezing out the phonon scattering processes.

Apart from the practical applications in the area of fast

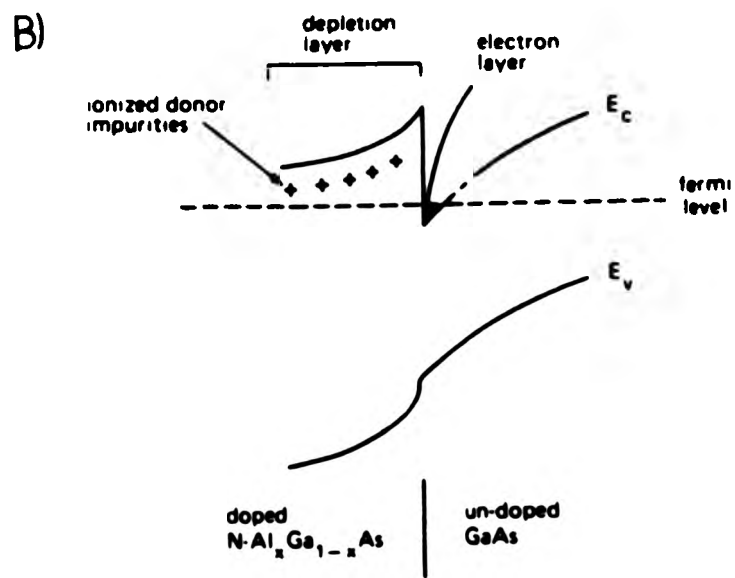
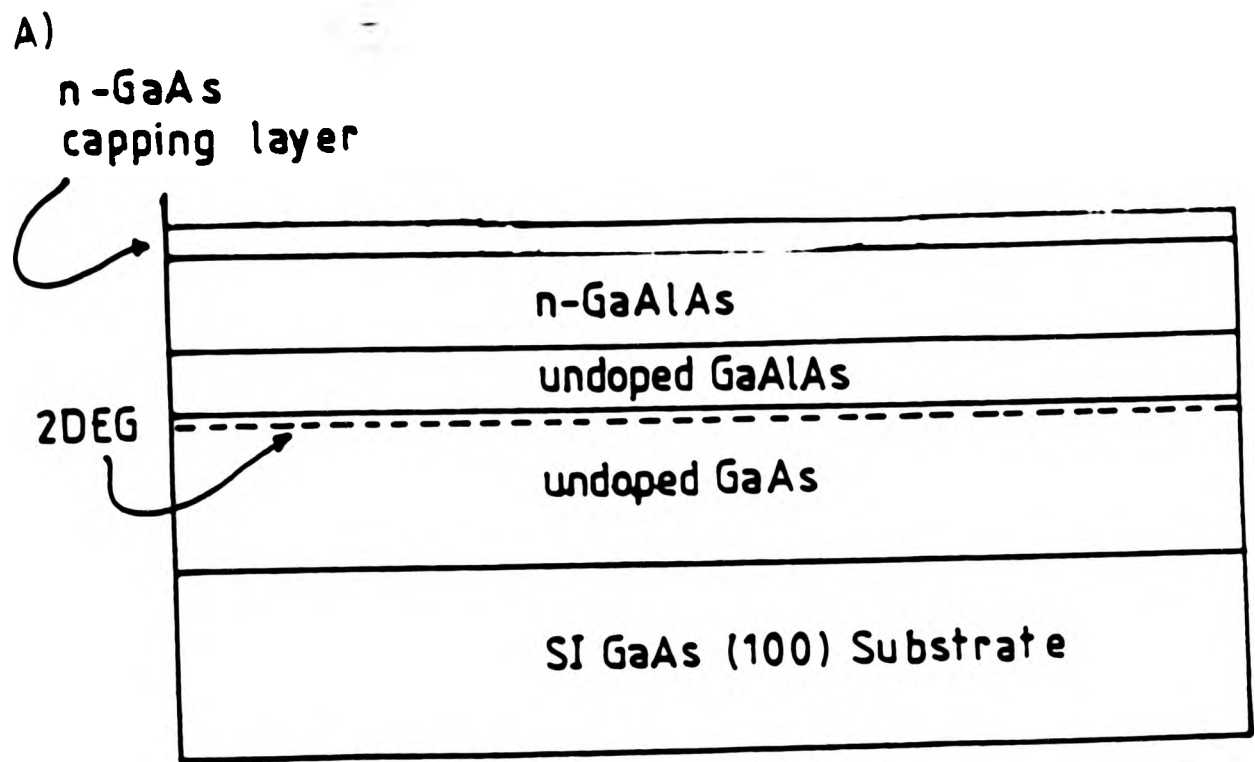


FIGURE 8.7: Layer sequence (A) and band diagram (B) for a HEMT structure.

devices, the fundamental physics of transport properties in two-dimensional electron gases provides a wealth of interesting phenomena, particularly at low temperature and high magnetic fields. In high mobility samples, with long scattering times, electrons are able to perform complete orbits in a magnetic field before being scattered. Such motion modifies the electron density of states giving rise to Landau levels. Since the electron transport properties are largely determined by the density of states, the Landau levels modify the resistivity of the material. Crucially, the Hall resistivity is quantised in units of h/e^2 independent of sample size. This provides a route to the standard ohm expressible in terms of fundamental constants only. It seems to be the case that the best samples for studying this Quantum Hall Effect (QHE) are those that possess only moderately enhanced mobilities and significant interfacial disorder. In samples with the very highest mobilities, purity and crystallinity, cooperative electron effects dominate and conduction is via apparently fractionally charged particles (12). The experimental measurement and theoretical description of these effects and the explanation of the role of disorder and impurities is currently an area of vigorous activity in solid state physics.

Figure 8.8 shows a SIMS profile (9) through a HEMT structure doped with selenium. The Al and Se traces have comparably abrupt profiles and comparison of the half-height points reveals an undoped spacer layer thickness of 85Å which compares with the intended value of 87.5Å. Although the reason for the sloping of the Se profile in the doped GaAlAs region is unknown, the required structure is realised.

Loughborough Consultants Limited

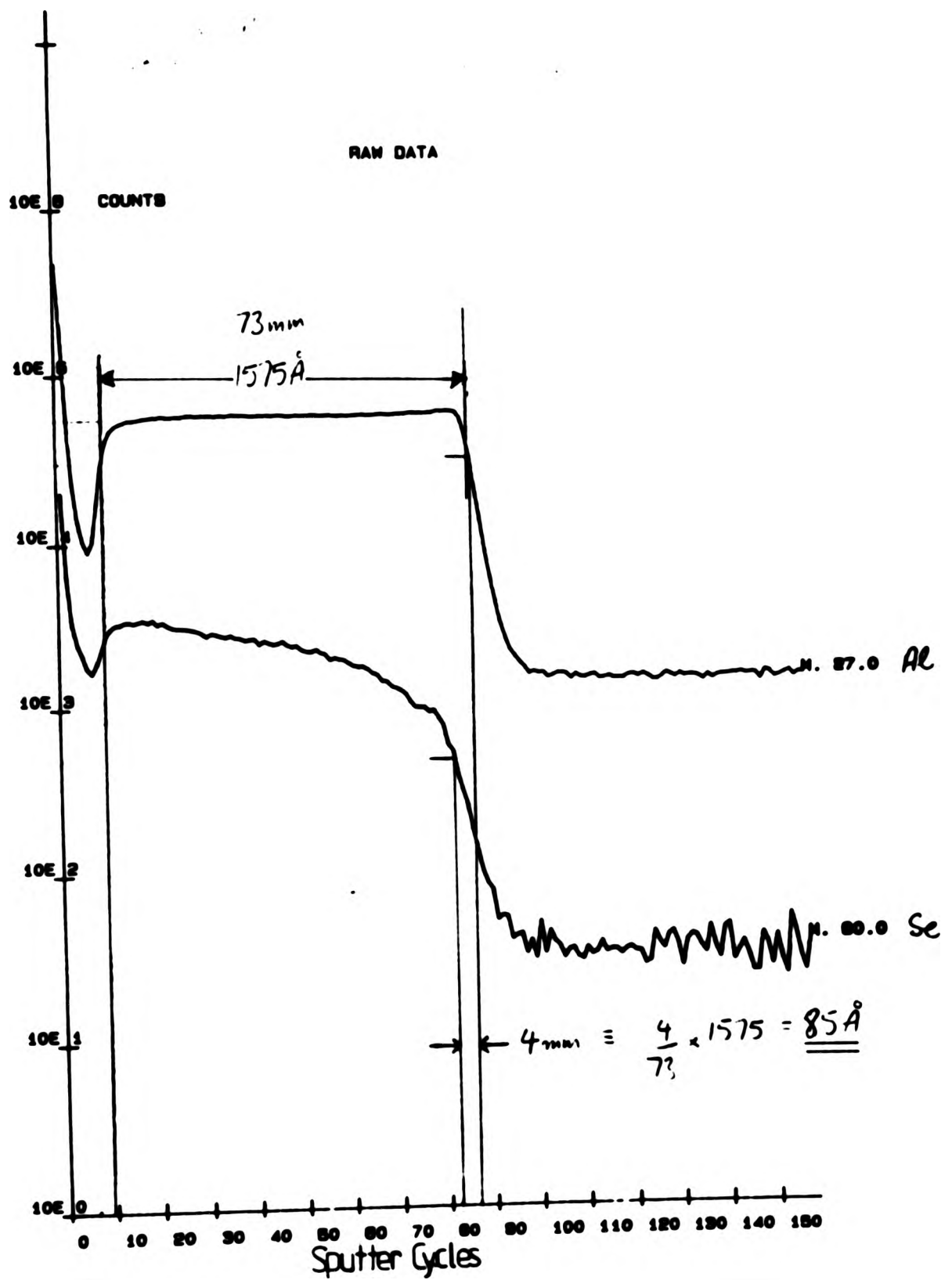


FIGURE 8.8: SIMS profile through a selenium-doped HEMT structure.

Figure 8.9 shows the electron mobility versus temperature for a number of sulphur and selenium doped HEMTs grown with different undoped spacer layer thicknesses. Also shown are the results of Stormer et al (19) who used silicon as the dopant. The initial rise as temperature is reduced is due to the suppression of phonon scattering. For 3-D samples at low temperatures, where phonon scattering is reduced, one would expect a $T^{1.5}$ dependence characteristic of ionised impurity scattering. Since the ionised impurities and the electrons are separated in the HEMT structure, the suppression of this dependence and the existence of a plateau in mobility are characteristic of 2-D structures. The higher mobilities at the largest spacer layer thicknesses are due to the enhancement of this separation (19). Figure 8.10 illustrates this different behaviour of mobility as a function of temperature in 3-D and 2-D systems (21).

Several modulation sulphur doped GaAs-GaAlAs heterostructures have been grown and supplied to various establishments for studies of 2-D effects (13). One particular sample MB397, whose structure was shown in figure 8.7, has been subject to detailed examination at the Cavendish Laboratory, Cambridge, along with similar silicon doped structures grown in the same system (14-17). For example, the Quantum Hall Effect is illustrated in figure 8.11 for a gated Hall bar sample of MB397 (14). The quantisation of the Hall resistivity is clearly apparent in the nearly step-like transition from plateau to plateau. Measurement at high frequency reveals the suppression of the integral quantisation and the appearance of fractionally quantised states, characteristic of mutual interaction between electrons. Silicon-doped samples show similar behaviour (15). Further samples of this material have been processed by

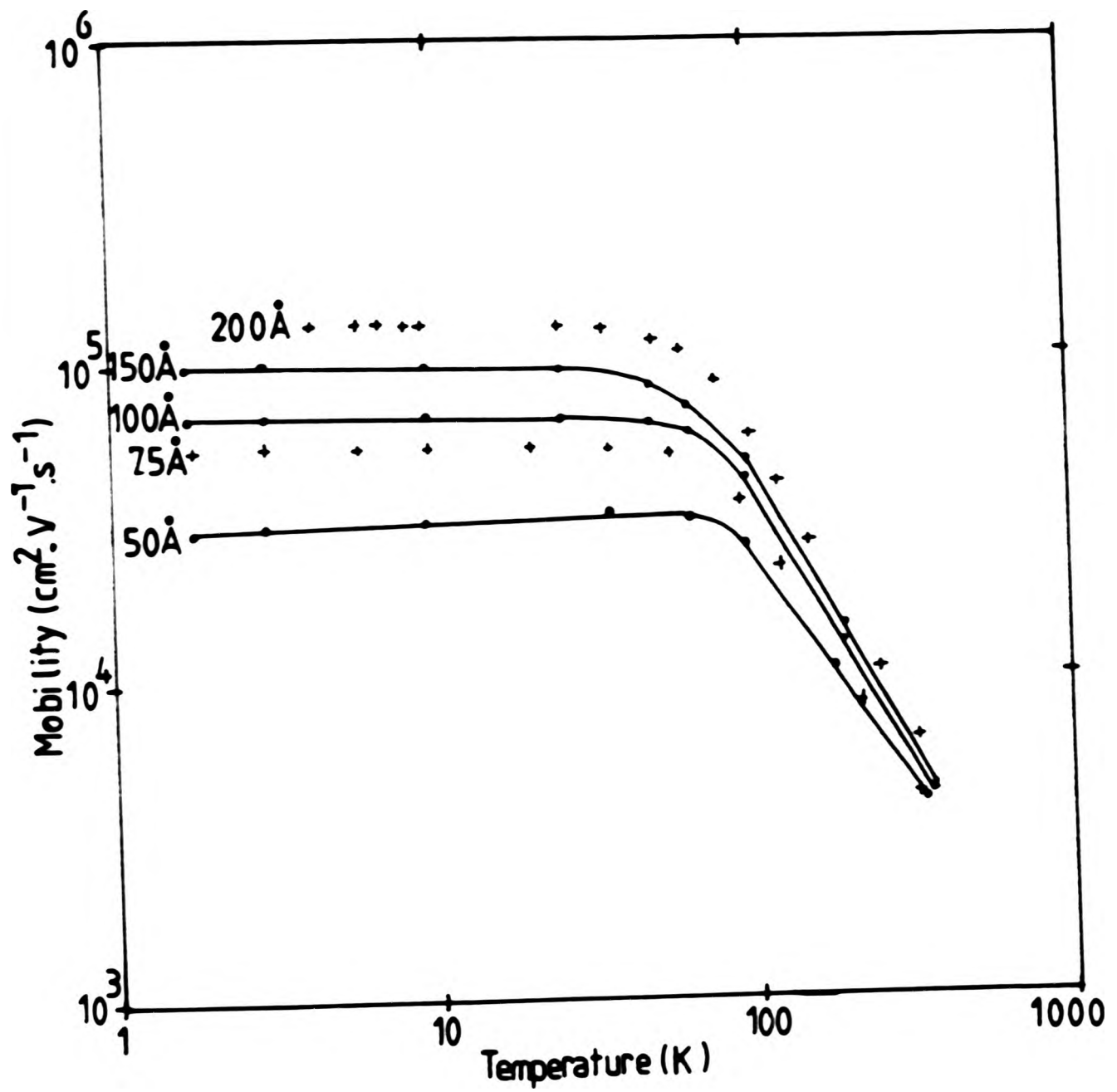


FIGURE 8.9: Electron mobility vs. temperature for a series of HEMTs with different undoped spacer layer thicknesses. Solid lines from reference (19), + :- our data.

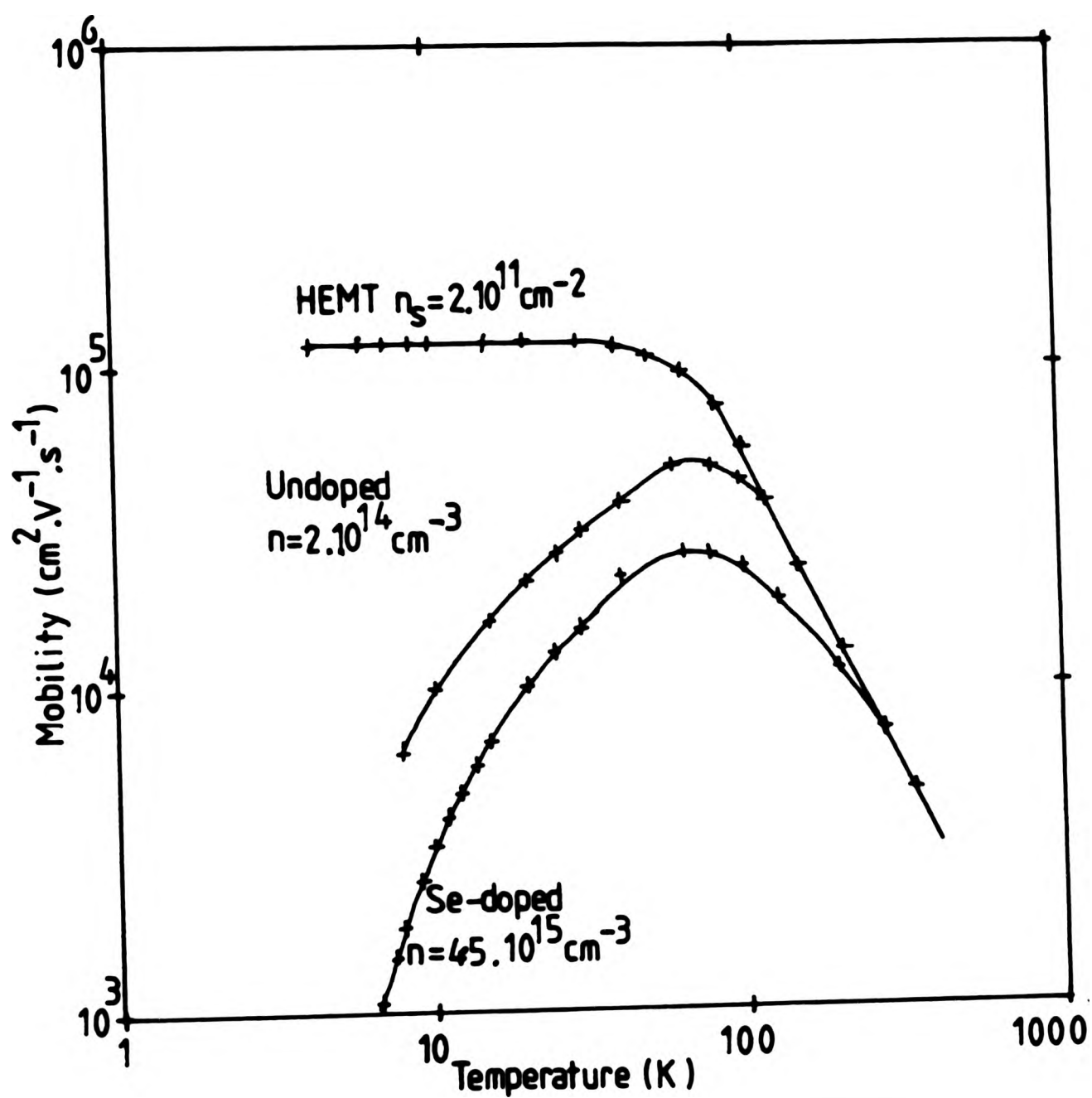


FIGURE 8.10: Comparison of the behaviour of electron mobility as a function of temperature for 2-D and 3-D samples.

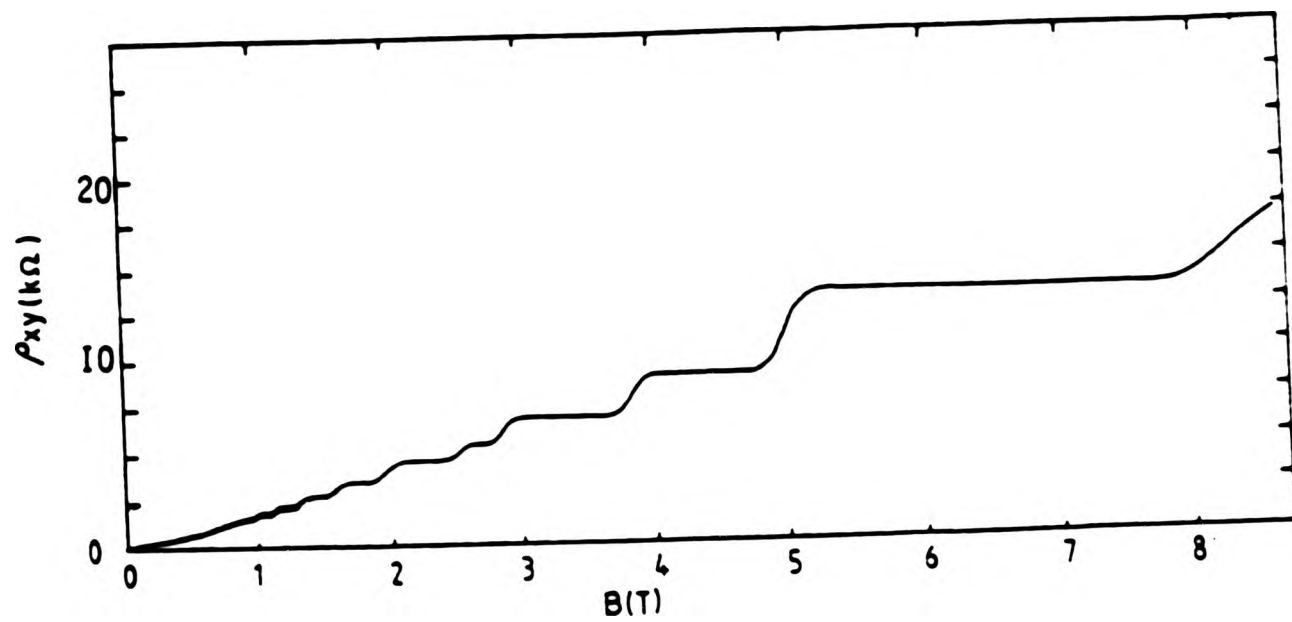


FIGURE 8.11: The Quantum Hall Effect in a sulphur doped HEMT. Hall resistivity is plotted against magnetic field. From reference (14).

electron beam lithography to produce HEMT FETs where the device size is reduced in two dimensions (16,17,18). Figure 8.12 shows a micrograph of a HEMT-FET with a 50nm gate stripe. Measurements on this device have revealed behaviour characteristic of 1-dimensional conduction (16,17).

8.6: Postscript on DX centres.

In chapter 1, we commented on the possibility of reducing the effect of the DX centre in AlGaAs by the use of chalcogen dopants to getter arsenic vacancies. Fundamental studies of transport properties, such as those outlined above, have failed to reveal any substantial differences between silicon or chalcogen doped material grown under similar conditions. In particular, the degree of carrier freeze-out and persistent photoconductivity is similar for both sulphur and silicon doped HEMTs as depicted in Table 8.1 (21).

This behaviour is consistent with more recent theories on the nature of DX centres in the light of its constancy of behaviour across MBE, LPE and MOVPE-grown AlGaAs doped with Te, Se, Si, Sn or S (22), especially so since the observation of persistent photoconductivity and the DX centre in GaAs and AlGaAs under hydrostatic pressure (23,24).

Current models of the DX centre are expressed mostly in terms of the interaction between substitutional donors and the multi-valley conduction band structure of GaAs and AlGaAs, rather than by invoking donor vacancy complexes (23-27).

GaAs/GaAlAs HEMT-FET

molecular beam epitaxy: e-beam lithography

position of
gate stripe

30 μm

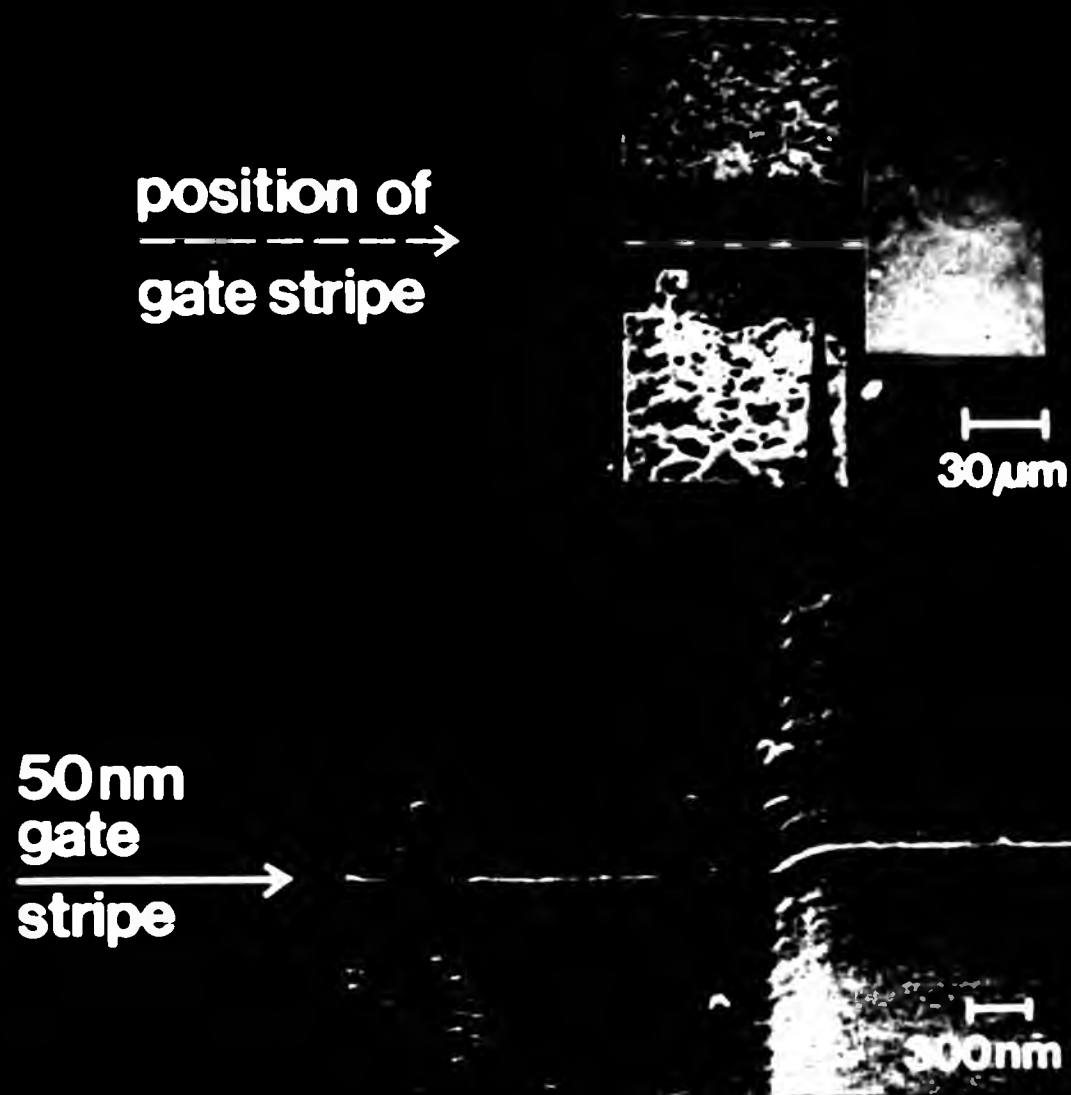
50 nm
gate
stripe →

300 nm

(British Telecom Research Laboratories
and Cambridge University)

GaAs/GaAlAs HEMT-FET

molecular beam epitaxy: e-beam lithography



(British Telecom Research Laboratories
and Cambridge University)

	Temp.	Electron Concentration (cm^{-2})		Electron Mobility ($\text{cm}^2\text{V}^{-1}\text{s}^{-1}$)	
		Dark	Light	Dark	Light
		MB397(S)	10K	1.9×10^{11}	2.2×10^{11}
	300K	4×10^{11}	4.5×10^{11}	6000	6000
MB458(Si)	10K	4.2×10^{11}	5.6×10^{11}	1.6×10^5	1.8×10^5
	300K	7.5×10^{11}	7.5×10^{11}	5800	5800

The enhanced carrier concentration and mobility under illumination persisted in both samples for approximately 2.5 hours.

TABLE 8.1: Comparison of persistent photoconductivity in sulphur and silicon doped HEMT structures.

8.7: Conclusions.

In this chapter we have shown that, despite the non-ideal incorporation behaviour of S and Se at elevated growth temperatures, a wide range of GaAs/GaAlAs structures may be grown successfully S and Se doped with properties comparable to those conventionally Si-doped. In several instances, enhanced performance (varactor and low-loss waveguide) and new phenomena (HEMTs) have been observed.

In the next chapter, we draw some general conclusions about chalcogen doping in MBE and suggest some areas for further work.

8.8: References.

- 1) D.V.Morgan and P.J.Tasker, University of Leeds.
- 2) A.J.N.Houghton, Proceedings of the European Conference on Optical Communication, ECOC82, Cannes, Sept. 1982, pp226-230.
- 3) A.J.N.Houghton, D.A.Andrews, G.J.Davies and S.Ritchie, Optics Comms., 46, 164, (1983).
- 4) A.J.N.Houghton, P.M.Rodgers and D.A.Andrews, Electronics Letters, 20, 479, (1984).
- 5) D.A.Andrews, E.G.Scott, A.J.N.Houghton, P.M.Rodgers and G.J.Davies, J.Vac.Sci.Tech., B3, 813, (1985).
- 6) A.Y.Cho, H.C.Casey, C.Radice and P.W.Foy, Electronics Letters, 16,72, (1980).
- 7) Broad Area Laser fabrication and characterisation by J.Regnault, R4, BTRL.
- 8) GRINSCH = Graded Refractive Index Separate Confinement Heterostructure.
- 9) SIMS carried out by Loughborough Consultants Ltd and Charles Evans and Associates.
- 10) F.Capasso, Surface Science, 142, 513, (1984).
- 11) T.Mimura, S.Hiyamizu, T.Fujii and K.Nanbu, Jpn.J.Appl.Phys.,19, L225, (1980).
- 12) R.J.Nicholas, Phys.Bull., 37, 116, (1986).
- 13a) M.Pepper, Cavendish Laboratory, Cambridge University. Quantum Hall Effect measurements, (14-17).
- 13b) L.Eaves, University of Nottingham. Ballistic transport.
- 13c) A.Hartland, National Physical Laboratory. Resistance standards (20).
- 13d) M.Chamberlain, University of Nottingham. Far infra-red transient photoconductivity.
- 14) C.McFadden, A.P.Long, H.W.Myron, M.Pepper, D.Andrews and

- G.J.Davies. J.Phys.C, 17, L439, (1984).
- 15) C.McFadden, A.P.Long, H.W.Myron, M.Pepper, D.Andrews and G.J.Davies. J.Vac.Sci.Tech., B3, 639, (1985).
- 16) T.J.Thornton, M.Pepper, H.Ahmed, D.Andrews and G.J.Davies., Phys.Rev.Lett., 56, 1198, (1986).
- 17) T.J.Thornton, M.Pepper, H.Ahmed, D.Andrews and G.J.Davies., Electronics Letters, 22, 247, (1986).
- 18) G.J.Davies and D.A.Andrews, British Telecom Technology Journal, 3, 59, (1985).
- 19) H.L.Stormer, Surface Science, 142, 130, (1984).
- 20) A.Hartland, G.J.Davies and D.R.Wood, IEEE Transactions on Instrumentation and Measurement, IM-34, 309,(1985).
- 21) Mobility measurements as a function of temperature performed by D.R.Wood, R3.1.1, BTRL.
- 22) E.F.Schubert and K.Ploog, Phys.Rev.B., 30, 7021, (1984).
- 23) M.Mizuta, M.Tachikawa, H.Kukimoto and S.Minomura, Jap.J.Appl.Phys., 24, L143, (1985).
- 24) M.Tachikawa, T.Fujisawa, H.Kukimoto, A.Shibata, G.Oomi and S.Minomura, Jap.J.Appl.Phys., 24, L893, (1985).
- 25) E.Yamaguchi, Jap.J.Appl.Phys., 25, L643, (1986).
- 26) N.Iwata, Y.Matsumo, T.Baba and M.Ogawa, Jap.J.Appl.Phys., 25, L399, (1986).
- 27) Y.Ashizawa and M.O.Watanabe, Jap.J.Appl.Phys., 24, L883, (1985).

9.1: Conclusions and Suggestions.

High purity and chalcogen-doped GaAs has been grown in a diffusion-pumped MBE system and has mobility and photoluminescence properties comparable with those from Si-doped GaAs grown in ion-pumped systems. The lack of any deleterious effects attributable to the use of diffusion pumps confirms their value in MBE systems, especially in those cases where high gas loads have to be handled (e.g. in gas source MBE where arsine and phosphine are used).

Earlier calculations indicating that S and Te should be incorporated into GaAs under MBE conditions have been extended to include Se with similar conclusions. The calculations have been further extended to include S, Se and Te in InP and the predictions for this system discussed in conjunction with the limited experimental MBE data available.

Electrochemical sulphur and selenium Knudsen cell have been demonstrated as versatile and highly controllable sources of n-type dopant for MBE growth of GaAs and GaAlAs alloys. At low growth temperatures, S and Se incorporate into both matrices in a simple manner with no evidence for anomalous diffusion, segregation or electrical activation* properties. At higher growth temperatures (>590°C for S and >620°C for Se) some reevaporation of the dopant is observed during growth and is attributed to the formation of volatile Ga₂S and Ga₂Se. This loss may be overcome however by increasing the incident S or Se flux or by increasing the arsenic overpressure. The behaviour

* See pp 70-71.

has been modelled successfully in terms of the competition between two reactions.

1) The reaction of S or Se with arsenic vacancies to give incorporation of the chalcogen onto the arsenic sublattice as a donor in the normal way. This reaction is known to proceed unhindered at low growth temperatures.

2) The formation of the volatile gallium chalcogenides Ga_2S and Ga_2Se , the kinetics of which reaction are mediated by the stoichiometry of the growing GaAs surface.

A thermodynamic framework has been described in which the equilibria between the MBE species and the solid and gaseous Ga chalcogenides are calculated. These calculations predict that the volatile species Ga_2S and Ga_2Se should form under any practical MBE growth conditions so the successful doping of GaAs with S and Se must be due to a kinetic barrier to their formation.

Similar calculations for the aluminium sulphides suggest that they should have much lower equilibrium vapour pressures under MBE conditions so loss of sulphur from GaAlAs alloys is still believed to occur via the formation of Ga_2S , albeit progressively reduced by the dilution of surface Ga atoms by the presence of increasing Al concentrations in these alloys.

The calculation for the aluminium selenides predicts borderline pressures comparable with the incident Se pressures. Depending on whether their formation is kinetically hindered or not, the doping efficiency of GaAlAs with Se may be lower than for S at high temperatures. The experimental position is presently unclear in this high temperature regime for Se and would

benefit from further work.

The doping study presented here has relied heavily on electrochemical C-V and SIMS measurements on grown layers. As such they only give indirect information on the doping chemistry. This is a consequence of performing the experiments in a production-oriented MBE system. More detailed information on the kinetics of the processes governing dopant incorporation during growth might be obtained from a modulated beam mass spectrometry study in the manner of Joyce et al (1). Although the impinging and reevaporating dopant fluxes are much smaller than the matrix element fluxes they studied, refinement of the technique might allow direct identification of the reevaporating species as Ga₂S or Ga₂Se.

In practical terms, for GaAs selenium is probably the preferred chalcogen dopant due to the higher growth temperature achievable before the onset of reevaporation. Sulphur is likely to be more profitably applied to GaAs/GaAlAs heterostructures, especially HEMTs where GaAs growth temperatures may be used. In this case it is likely that the upper limit for electron concentration using Si doping could be exceeded by the use of sulphur with beneficial results for power devices and fast HEMTs (2).

There are other material systems to which electrochemical generation of chalcogen dopants might be profitably applied. Sulphur and selenium have high solid solubility in InP and both enable high carrier concentrations to be achieved ($>10^{19}\text{cm}^{-3}$). Apart from the electrical properties, the benefits of these high concentrations in pinning dislocations in bulk InP growth

are well known (3). Successful intentional (and unintentional) sulphur doping of InP has been achieved in MBE (4) using an electrochemical source and morphological improvements have been observed in highly S-doped layers.

Sulphur and selenium have also been used successfully as donors in GaInAs and AlInAs layers grown lattice matched to InP (5), although the narrow range of temperatures and arsenic overpressures in which these materials have good electrical and optical properties make it difficult to perform doping chemistry studies in the same way as for GaAs. However, the successful doping of these materials with S and Se is consistent with the predictions from the GaAs and InP materials systems.

The antimonide alloy system however is a prime candidate for the application of electrochemical chalcogen generation of donors in MBE. Silicon is decidedly amphoteric in GaSb producing p-type, closely compensated material. This property also persists in GaAsSb alloys with less than 80% GaSb. Similar difficulties exist with Al-containing antimonides (6). Selenium incorporation and n-type doping has been achieved by the use of PbSe compound sources, but the incorporation is complicated both by dopant loss (presumably as Ga_2Se) and the interaction with Pb (7). Although it would be valuable to study all the chalcogens in this system with electrochemical generation, the work presented in this thesis would suggest that, in Al-containing alloys at least, sulphur may be the most useful.

It seems likely however that silicon will continue to be used as the main n-type dopant for GaAs/GaAlAs structures. The disadvantages outlined in chapter 1 have largely been overcome

or sidestepped. Sulphur or selenium are only likely to be used where their specific properties (e.g. high carrier concentrations or non-amphoteric behaviour) are required or where the benefits of electrochemical generation are sought (e.g. in the hyperabrupt varactor of chapter 8). Where such needs arise however, this study provides the basis for such use. Similarly, where S or Se might be applied in new materials systems, in the antimonides for example, the foundation for further experimental and theoretical studies has been laid.

9.2: References.

- 1) B.A.Joyce and C.T.Foxon, *J.Cryst.Growth*, 31, 122, (1975).
- 2) N.Thomas, R4.2.2. BTRL, private communication.
- 4) A. Iliadis, K.A.Prior, C.R.Stanley, T.Martin and G.J.Davies, *J.Appl.Phys.*, 60, 213, (1986).
- 3) L.Suchow, *Mat.Res.Bull.*, 17, 1401, (1982).
- 5) T.M.Kerr, PhD.Thesis, Glasgow University, (1984).
- 6) T.M.Kerr, T.D.Maclean, J.D.Grange and D.I.Westwood, *J.Vac.Sci.Technol.*, B3, (1985).
- 7) T.D.Maclean, T.M.Kerr, D.I.Westwood, C.E.C.Wood, D.F.Howell and R.J.Nicholas, Submitted to *J.Appl.Phys.*, (1986).

CHAPTER 10: PUBLICATIONS.

Many aspects of the work presented in this thesis have been the subject of papers published by the author. A complete collection of those which fall within the period of registration are listed below and may be found in the pages following.

Chapter 4.

The contribution of SIMS to the characterisation of III-V semiconductor layers grown by molecular beam epitaxy. G.D.T.Spiller and D.A.Andrews, *Vacuum*, 36, 991, (1986).

Chapter 6.

The influence of growth conditions on sulphur incorporation in GaAs grown by molecular beam epitaxy. D.A.Andrews, R.Heckingbottom and G.J.Davies, *J.Appl.Phys.*, 54, 4421, (1983).

The influence of growth conditions on selenium incorporation in GaAs grown by molecular beam epitaxy. D.A.Andrews, M.Y.Kong, R.Heckingbottom and G.J.Davies, *J.Appl.Phys.*, 55, 841, (1984).

Chapter 7.

The influence of growth conditions on sulphur and selenium incorporation in $\text{Ga}_{1-x}\text{Al}_x\text{As}$ grown by molecular beam epitaxy.

D.A.Andrews, R.Heckingbottom and G.J.Davies, J.Appl.Phys., 60, 1009, (1986).

Chapter 8.

Low-loss optical waveguides in MBE-grown GaAs/GaAlAs heterostructures. A.J.N.Houghton, D.A.Andrews, G.J.Davies and S.Ritchie, Optics Communications, 46, 164, (1983).

Electron transport across depleted region of a fine-gate GaAs:AlGaAs heterojunction FET. T.J.Thornton, M.Pepper, H.Ahmed, D.A.Andrews and G.J.Davies, Electronics Letters, 22, 247, (1986).

One-dimensional conduction in the 2-D electron gas of a GaAs-AlGaAs heterojunction. T.J.Thornton, M.Pepper, H.Ahmed, D.A.Andrews and G.J.Davies, Phys.Rev.Lett., 56, 1198, (1986).

Frequency-enhanced fractional quantisation in GaAs-GaAlAs heterojunctions. C.McFadden, A.P.Long, H.W.Myron, M.Pepper, D.A.Andrews and G.J.Davies, J.Phys.C: Solid State Phys., 17, L439, (1984).

The contribution of SIMS to the characterization of III-V semiconductor layers grown by molecular beam epitaxy

G D T Spiller and D A Andrews, *British Telecom Research Laboratories, Martlesham Heath, Ipswich IP5 7RE, UK*

Secondary ion mass spectrometry (SIMS) is widely used in the analysis of semiconductor layers and devices, such as those fabricated by molecular beam epitaxy (MBE). The need for controllably-doped, high purity, single crystal layers with thicknesses from over a μm down to a few atomic layers, places considerable demands on the growth technique and on the assessment methods used to characterize the layers. This paper describes how SIMS is being used for trace level profiling of dopants and impurities and for matrix element profiling in MBE layers. The profiling of very thin layered (multi-quantum well) structures is also considered.

1. Introduction

Secondary ion mass spectrometry (SIMS), with the ability to detect many elements at concentrations between 1 part in 10^6 and 10^9 in thin layers (less than $0.1 \mu\text{m}$ thick), finds many applications in the characterization of semiconductor layers and devices. The high depth resolution (less than a few nanometres under ideal conditions) makes SIMS well suited to the assessment of multi-layer structures, which may contain a number of different matrices.

The recent demands for microwave and opto-electronic devices with progressively thinner, planar, epitaxial layers with extremely abrupt compositional and doping profiles, has stimulated the development of advanced crystal growth techniques, such as molecular beam epitaxy (MBE)¹. Devices including photodetectors, lasers and field effect transistors (FETs)² have been fabricated from InP and ternary and quaternary materials such as GaInAs and GaInAsP in the technologically-important long wavelength range $1.3\text{--}1.6 \mu\text{m}^3$. Structures such as multi-quantum wells (MQWs)⁴ and high electron mobility transistors (HEMTs) with individual layer thicknesses of less than 5 nm have also been grown by MBE.

This paper highlights a number of ways in which SIMS has contributed to the characterization of epitaxial layers (epilayers) grown by MBE. The high sensitivity of SIMS makes it ideally suited to the profiling of deliberately-introduced n- and p-type dopants, incorporated to tailor the device properties, at concentrations of less than $1 \times 10^{16} \text{cm}^{-3}$ to greater than $1 \times 10^{19} \text{cm}^{-3}$. The ability to identify unintentional impurities at similar concentrations is also an important quality. Electrochemical profiling⁵ is used routinely to measure the net carrier concentration in the epilayers and this usually gives the first indication if an electrically-active impurity (dopant or trap) is present, or if the dopant has not been incorporated as expected. SIMS can then be used to identify the impurity (independent of its electrical behaviour), or produce the depth of distribution of the dopant. A

valuable approach in identifying impurities is the growth of test structures designed to yield the maximum information from the SIMS analysis of a single specimen.

The problems involved in profiling structures with very thin layers (less than 10 nm) are also considered: the atomic mixing which results from the sputtering process in SIMS³ makes the analysis of these structures difficult. High resolution techniques such as transmission electron microscopy are, however, already making a substantial impact in this area⁶.

2. Experimental

2.1. SIMS background. In the analysis of semiconductor materials it is important to obtain the lowest detection limits for elements which are electrically-active as n- or p-type dopants, while retaining the depth resolution required to analyse multi-layer specimens. Practical detection limits depend on many factors, of which the choice of primary ion beam and the presence of mass interferences and instrumental background signals are the most important.

Reactive primary ions, such as caesium and oxygen, are commonly used to enhance secondary ion yields, thereby improving detection limits⁷. For many n-type dopants in III-V materials, such as Si, S, Se, and Te and common impurities such as C and O, the lowest detection limit is obtained with caesium primary ions (detecting negative secondary ions): detection limits with argon or oxygen may be higher by orders of magnitude. Oxygen profiling is used to enhance the positive ion yield of elements such as Be, Fe and Al.

Molecular ions, often formed from a combination of matrix and residual gas atoms, can interfere with the detection of elemental ions at the same integral mass. Although these 'mass interferences' can be discriminated against by energy filtering or by high mass resolution⁸, the detection limit of elements will be affected and impurity signals may be wrongly assigned. The unambiguous

identification of impurities and profiling of dopants is helped if more than one isotope can be profiled: the signals should be present in the correct isotopic ratio if there are no mass interferences. This does not guarantee, however, that the signal arises from the specimen and is not an instrumental background: while background signals from the vacuum such as C and O are expected, others such as sulphur can also occur. In some cases, it is also useful to compare with a sample known to contain a low concentration of the element of interest.

2.2. SIMS analyses. The SIMS analyses reported here were carried out in a Cameca IMS 3F⁹ equipped with caesium and oxygen ion sources. Primary energies between 5–15 keV were used in most cases, although energies down to 1.5 keV were used in the profiling of multi-quantum well structures (see section 4). Typical primary beam currents were 1 μA for O_2^+ and 0.1 μA for Cs^+ , giving sputter rates of several $\mu\text{m h}^{-1}$. Rastered areas were 250 or 500 μm^2 square, with an area between 35 and 150 μm^2 square being analysed. Detection limits routinely achieved were $1\text{--}5 \times 10^{15} \text{ cm}^{-3}$ for Si, S and Be, $1\text{--}10 \times 10^{16} \text{ cm}^{-3}$ for C and O, and less than $1 \times 10^{14} \text{ cm}^{-3}$ for Se and Te. Energy filtering was not used in the examples given here (matrices GaAs, GaInAs and GaAlAs). The problem of mass interferences in III-V materials is more severe in the analysis of InP, due to the presence of the intense low mass P^- ion.

Concentration scales were derived by comparison with ion implanted reference specimens. For convenience, these were not usually run at the same time as the unknown specimen and care was needed to ensure that experimental conditions were reproduced¹⁰. The concentrations are expected to be accurate to better than $\pm 50\%$, considering both experimental errors and possible dose inaccuracies in the implanted reference materials. Depth scales were usually derived from a surface profilometer ('Dektak') measurement of the analysis crater.

2.3. MBE growth. Molecular beam epitaxy¹ is, in essence, a vacuum evaporation process but with two main differences: the vacuum is ultra-high (pressures $< 10^{-10}$ torr) and the product of the evaporation is single crystal. Molecular beams, generated from thermal Knudsen evaporation sources, interact on a heated crystalline substrate to produce epitaxial layers. Each source contains either a dopant or one of the elements that comprise the compound to be grown. As the process name implies, the transport of material from the sources across the vacuum to the substrate takes place under conditions of molecular flow. The interposition of a simple line-of-sight mechanical shutter between each source and the substrate interrupts the beam and allows different layer compositions to be achieved by switching between sources. Shutter operating times are significantly shorter than the monolayer deposition time ($\sim 1\text{s}$) resulting in potentially extremely sharp interfaces.

The layers described in this work were grown in a VG Semicon Ltd V80H or MB288 machine. Both are standard commercial instruments and are used routinely in this laboratory for the growth of device-quality layers in both GaAs and InP-based material systems. The layers were grown using well-established substrate preparation techniques and growth conditions¹¹. Typical growth temperatures were 500–680°C depending on the material.

3. Results

3.1. Dopant profiling. One of the advantages of growing epilayers over using bulk substrates is that the required dopants (n- or p-type) can be incorporated into the layers during growth. In order that the concentration of dopants may be controlled, it is necessary to calibrate the sources. For example, Se doping in MBE may be accomplished using an electrochemical cell¹² in which the flux depends on the applied potential. Figure 1(a) shows a Se 'doping staircase' in GaAs, for six different cell voltages. Two different Se isotopes ($m_e = 78$ and 80) were used to ensure the unambiguous identification of the dopant (each profile has been corrected for the isotopic abundance). By comparing the Se concentration measured using SIMS with the cell voltage, a calibration curve (Figure 1(b)) may be obtained.

A potential problem in any crystal growth technique involving high growth temperatures (necessary to ensure good crystalline quality) is diffusion of dopants during growth. Figure 2 shows a depth profile through a GaInAs FET structure. Two highly p-type (Be-doped, $\sim 5 \times 10^{18} \text{ cm}^{-3}$) layers are grown with an n-type (Si-doped, $\sim 10^{16} \text{ cm}^{-3}$) layer in between. The SIMS depth profile shows that a small amount of Be has diffused into the n-channel from the lower layer, resulting in electrical compensation of the Si dopant, a problem that may be solved by a correct choice of growth conditions. The lack of Be diffusion from the top Be-doped layer is probably due to the shorter time at the growth temperature, compared with the lower layer.

3.2. Impurity identification. The ability to grow epilayers of high intrinsic purity, containing less than 0.1 ppm ($< 5 \times 10^{15} \text{ cm}^{-3}$) of electrically-active impurities, is an essential quality of any crystal growth technique. However, impurities can arise either from the equipment itself (particularly in view of the high source (up to 1100 C) and substrate temperatures employed) or from starting materials used to grow the epilayers. SIMS is used routinely to

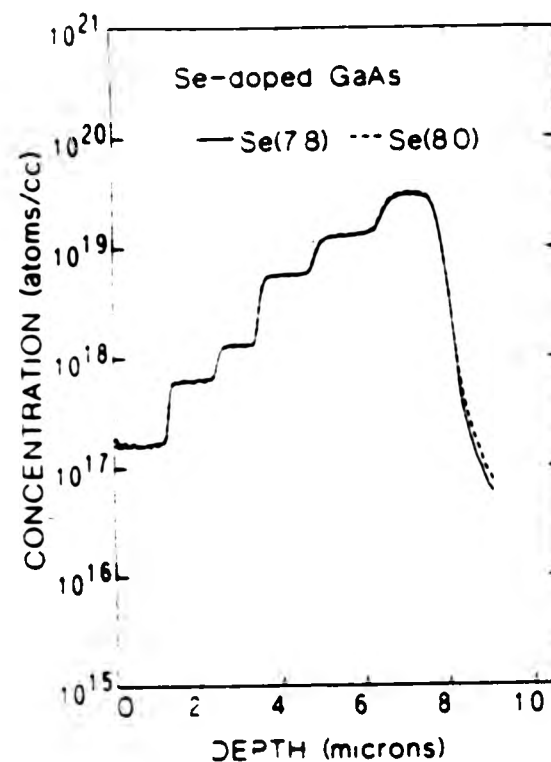


Figure 1(a). SIMS depth profile of Se 'staircase' in GaAs, showing six doping levels corresponding to Se-cell voltages of 180 (closest to surface), 200, 210, 230, 240 and 250 mV. The two Se isotopes produce almost indistinguishable profiles. (Analysis conditions 14.5 keV Cs^+ ions, detecting Se^- .)

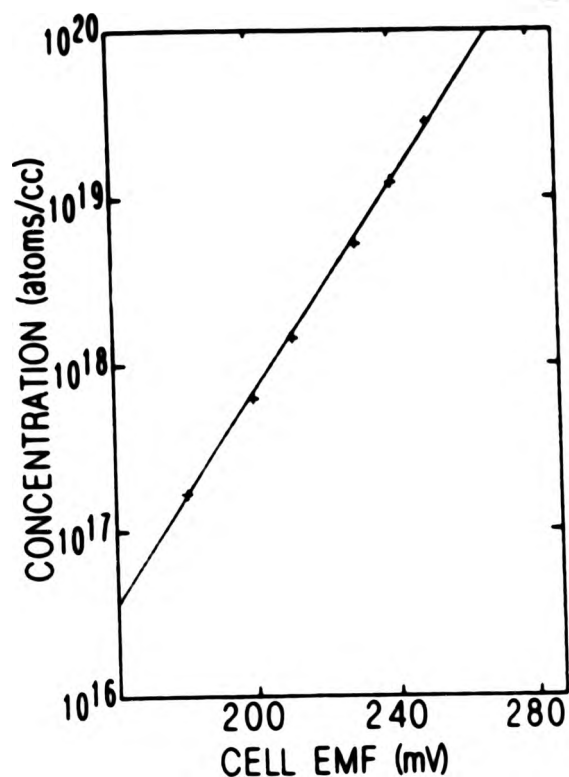


Figure 1(b). Se-cell calibration graph derived from the data in Figure 1(a).

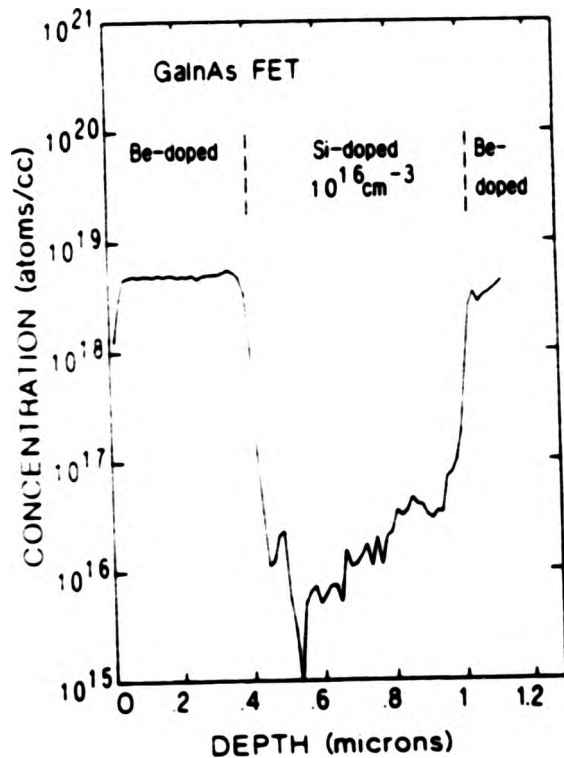


Figure 2. Beryllium depth profile through a GaInAs FET structure, showing Be diffusion from the lower layer into the middle Si-doped channel. (Analysis conditions 8 keV O_2^+ primary ions, detecting Be^+ .)

identify impurities in epilayers, but the crystal grower must then identify and eliminate the source of the impurity.

Figure 3 shows a depth profile through a GaAs test structure grown to test for the presence of impurities in the arsenic. Previous experience had shown a dependence of residual carrier concentration on the supplier of the As source material and also on the batch number¹³. In one particular case, in which a residual n-type carrier concentration of $\sim 10^{18} \text{ cm}^{-3}$ was obtained, wet chemical analysis showed Te to be present at comparable levels¹⁴. A four layer test structure was grown at different excess As fluxes in each layer to highlight the dependence of the doping concentration on the As source temperature. The SIMS profiles clearly show the

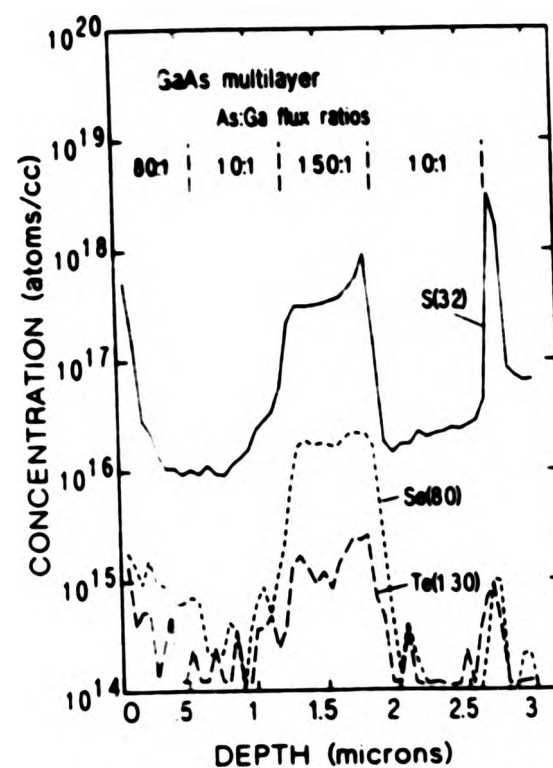


Figure 3. GaAs four-layer structure grown to test for the presence of impurities in the arsenic starting material. The As/Ga flux ratios were 10 (nearest the substrate), 150, 10 and 80. The SIMS profile clearly shows S, Se and Te (in decreasing concentration) in the '150' layer. (Se is also detected in the '80' layer; the S here may be masked by the higher background signal). Two isotopes were detected for each element producing identical results: only one isotope is shown in each case for clarity. The substrate-epilayer interface is marked by the prominent S 'spike'. (Analysis conditions 14.5 keV Cs^+ primary ions, detecting negative secondary ions.)

presence of S, Se and Te in the layer grown at the highest As overpressure, indicating an impure batch of arsenic. The elements were present in decreasing concentrations ($S > Se > Te$), as expected from the relative volatility of these elements. Sulphur has also been identified as an impurity in MBE InP in a similar experiment¹⁵.

The volatile chalcogens S, Se and Te are not routinely screened by material suppliers, and even at the detection limit of conventional spectrographic techniques (typically 1 ppm, $\sim 5 \times 10^{16} \text{ cm}^{-3}$), it is evident that these elements can still pose a problem in semiconductor applications. The identification of these elements as important trace impurities highlights the need for more sensitive screening of arsenic (and possibly other elements) by materials suppliers. While SIMS could be used after the growth of layers, analysis of the starting material by new high sensitivity techniques such as glow discharge mass spectrometry¹⁶ would be a more satisfactory approach.

3.3. Matrix element profiling. Although the main strength of SIMS lies in its ability to detect low concentrations of elements, in some situations it is a valuable technique for rapid depth profiling of matrix elements. Techniques such as Auger electron spectroscopy (AES)⁵, in combination with sputter profiling, are capable of detecting concentrations in excess of 1%, but profiling rates are often several times slower than those routinely achieved with SIMS. (This arises not from a fundamental limitation of the technique, but from the low current density ion guns conventionally fitted to AES profiling systems.) However, quantitative profiling of matrix elements ($> 1\%$) with SIMS is complicated by the non-linear relationship between concentration and ion yield at

these relatively high concentrations. Nevertheless, qualitative data is often adequate in these instances.

Figure 4 shows an Al profile through a 8 μm thick $\text{Ga}_{1-x}\text{Al}_x\text{As}/\text{GaAs}$ multilayer sample. Successive layers with $x = 0.2, 0.05$ and 0 were grown at each of three different substrate temperatures. A problem was suspected with the shutter on the Al source, which may have resulted in some of the later layers not containing Al. SIMS profiling quickly showed that all the layers were present and that the problem had occurred after the completion of growth. Such rapid confirmation that the intended structure had been grown prevented the possible waste of subsequent device processing time.

4. Profiling of low dimensional structures

There is considerable interest at the moment in 'low dimensional structures' (LDS), in which the layer thicknesses are sufficiently small (less than 50 nm) that bulk properties are altered. Technological interest arises from the ability to vary the bandgap in multi-quantum well (MQW) structures by varying the layer thickness¹, opening up the possibility of producing a wide range of high performance opto-electronic devices for telecommunications applications. MQWs comprise many (up to 100) alternate layers of two different matrices, such as $\text{GaAlAs}/\text{GaAs}$ or GaInAs/InP .

SIMS analyses of such structures is problematical, even for matrix elements, because of the relocation of atoms that occurs during any sputtering process, resulting in a loss of depth resolution. The extent of this 'collisional mixing' depends on the penetration depth of the primary ion¹⁷ and is therefore dependent on the primary beam energy, angle of incidence and mass of the primary ion. In general, this effect will be reduced for low beam energies, glancing angles of incidence and heavy primary ions. In

addition, recoil implantation (knock-on of atoms in the sample by the incident ions³) and chemical segregation (caused by the use of reactive primary ions¹⁸), may also occur, producing a further broadening of the profile.

Experimentally, the primary beam parameters may not be independently variable: in particular, in the Cameca IMS 3F, the presence of a high extraction field in front of the sample either retards or accelerates the incoming ion (depending on the relative polarity of the specimen and primary ion), resulting in a variation of the angle of incidence with energy. Furthermore, the lowest practical beam energy is about 1.5 keV (net), at which the glancing angle of incidence produces an increasingly elliptical beam which is difficult to focus. The situation is better in quadrupole-based instruments, which use a low extraction field¹⁹. This allows low energies (less than 1 keV) to be achieved and decouples the energy and angle of incidence. These may then be freely varied to give the optimum depth resolution. Although high extraction field instruments, such as the Cameca IMS 3F allow more rapid, high sensitivity profiling of samples than quadrupole-based instruments, the latter instruments may be better suited to studies requiring high depth resolution.

The performance of the Cameca IMS 3F under low energy O_2^+ profiling conditions is shown in Figure 5. The Al profile from a 11 nm $\text{Ga}_{0.7}\text{Al}_{0.3}\text{As}/8$ nm GaAs MQW (after profiling through 0.1 μm of GaAs) is shown at 8.0, 2.0 and 1.5 keV (net). The energy per incident oxygen atom is half of these values. The corresponding angles of incidence are estimated to be 39, 64 and 90° to the normal respectively. The improvement in depth resolution with decreasing energy is clearly seen. The peak-to-trough ratio increases from 2 at 8.0 keV to 100 at 1.5 keV, while the depth resolution, defined here as 10-90% on the trailing slopes improves from 4.7 nm at 2.0 keV to 2.9 nm at 1.5 keV (the value at 8.0 keV cannot be defined in this way). These values correspond to $dz/z = 4.7$ and 2.9% respectively at 100 nm beneath the surface.

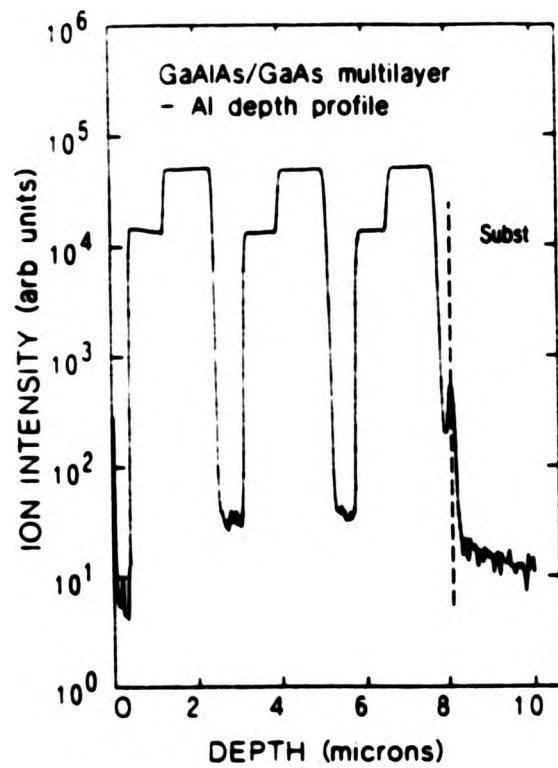


Figure 4. Al depth profile from a $\text{Ga}_{1-x}\text{Al}_x\text{As}$ multilayer sample. Three layers with $x = 0.2, 0.05$ and 0 respectively were grown at each of three different substrate temperatures (550, 650 and 750°C nearest surface). A thin GaAs layer was grown first, which can be seen between the small spike at the substrate-epilayer interface (probably caused by a yield enhancement of Al due to interfacial oxygen) and the first Al containing layer. The total profiling time was about 90 min. (Analysis conditions 8 keV O_2^+ , detecting Al^+ .)

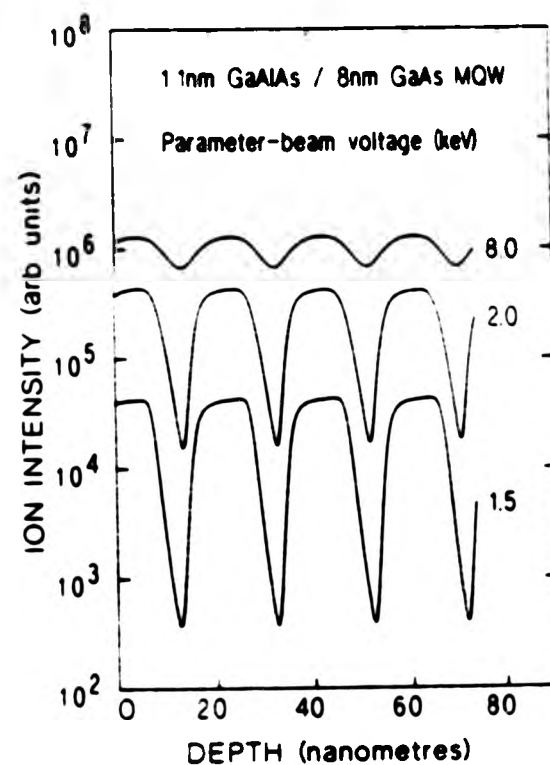


Figure 5. Depth profiles from an 11 nm $\text{Ga}_{0.7}\text{Al}_{0.3}\text{As}/8$ nm GaAs multi-quantum well structure recorded using O_2^+ primary ions at three different energies (after profiling through 100 nm of GaAs). The corresponding angles of incidence are approximately 39, 64 and $\sim 90^\circ$ to the normal. The improvement in depth resolution with decreasing energy is readily apparent.

5. Summary

This paper has given a number of illustrative examples of the way in which SIMS contributes to the characterization of semiconductor epilayers. Although the principles of SIMS are straightforward, the reliable application of the technique requires an appreciation of the problems which may arise from mass interferences and background signals. An awareness of the factors affecting detection limits is essential so that the best values may be obtained.

It is evident that the value of SIMS data is greatly enhanced if the profiles are provided to the crystal grower in a quantitative form: a correlation between electrical performance and dopant or impurity concentration can then be quickly established. The technique is substantially devalued in this area if only qualitative data is supplied. Furthermore, the value of growing special test structures, specifically for SIMS depth profiling, has been demonstrated.

The use of SIMS as a means of rapid matrix profiling has been shown. However, the profiling of LDSs is still a problem area and more work is required to explore the feasibility of using SIMS to analyse these structures.

Acknowledgements

Acknowledgement is made to the Director of Research of British Telecom for permission to publish this paper and to the Department of Trade and Industry for partial funding of this work

under the Joint Opto-Electronics Research Scheme (JOERS). We would also like to thank Dr E G Scott for the results in Figure 2.

References

- ¹ G J Davies and D A Andrews. *Br Telecom Technol J.* 3, 59 (1985).
- ² E G Scott, D Wake, A W Livingstone, D A Andrews and G J Davies. *J Vac Sci Technol.* B3, 816 (1985).
- ³ A Y Chu. *Thin Solid Films.* 100, 291 (1983).
- ⁴ T Ambridge, J L Stevenson and M Redstall. *J Electrochem Soc.* 127, 223 (1980).
- ⁵ S Hofmann. *Surface Interface Analysis.* 2, 143 (1980).
- ⁶ M R Taylor, M Hockly, D A Andrews and G J Davies. *Inst Phys Conf Ser.* 76, 295 (1985).
- ⁷ H A Storms, K F Brown and J D Stein. *Analyt Chem.* 49, 2023 (1977).
- ⁸ R J Blattner and C A Evans. *Scanning Electron Microscopy.* IV, 55 (1980).
- ⁹ M Lepareur. *Revue Thomson-CSF.* 12, 225 (1980).
- ¹⁰ G D T Spiller and T Ambridge. *Secondary Ion Mass Spectrometry—SIMS V, Proc V Int Conf, Washington* (Edited by A Benninghoven, R J Colton, D S Simons and H W Werner). Springer Series in Chemical Physics, Vol 4, p 127. Springer, Berlin (1985).
- ¹¹ G J Davies, D A Andrews and R Heckingbottom. *J appl Phys.* 52, 7214 (1981).
- ¹² D A Andrews, M Y Kong, R Heckingbottom and G J Davies. *J appl Phys.* 55, 841 (1984).
- ¹³ G J Davies and D A Andrews. *J Phys D.* 17, L143 (1984).
- ¹⁴ Chemical analysis by Johnson Matthey Chemicals Ltd, Royston, England.
- ¹⁵ T Martin, C R Stanley, A Iliadis, C R Whitehouse and D E Sykes. *Appl Phys Letts.* 46, 994 (1985).
- ¹⁶ J W Coburn and E Kay. *Appl Phys Letts.* 19, 350 (1971).
- ¹⁷ W Vandervorst and F R Shepherd. *Appl Surface Sci* (in press).
- ¹⁸ W Vandervorst, J Remmere, F R Shepherd and M L Swanson. ref 10, p 288 (1985).
- ¹⁹ K Wittmaack. *Surface Sci.* 89, 668 (1979).

The influence of growth conditions on sulfur incorporation in GaAs grown by molecular beam epitaxy

D. A. Andrews, R. Heckingbottom, and G. J. Davies
British Telecom Research Laboratories, Martlesham Heath, Ipswich IP5 7RE, United Kingdom

(Received 22 December 1982; accepted for publication 17 March 1983)

An electrochemical sulfur cell has been used as a source of donors for molecular beam epitaxy grown GaAs. The galvanic cell is Pt/Ag/AgI/Ag₂S/Pt. The electrical and optical properties of the films grown in the substrate temperature range 550–590 °C are good. However, at substrate temperatures above 600 °C the incorporation rate of sulfur is much reduced. The reduction in the incorporation rate is explained on the basis of the competing reactions (1) the incorporation of sulfur into the GaAs matrix and (2) the formation of volatile Ga₂S. A detailed discussion of the incorporation at elevated substrate temperatures and with varying As₄/Ga ratio is presented. It is also demonstrated that if the substrate temperature is reproducibly known then the electrochemical cell can be used to introduce intricate doping profiles into epitaxial GaAs. A hyperabrupt varactor diode has been fabricated as an example.

PACS numbers: 68.55. + b, 81.15.Ef

INTRODUCTION

The Group IV elements Sn, Ge, and Si have been used almost exclusively for donor impurity incorporation in molecular beam epitaxy (MBE) grown GaAs. However, the incorporation of these elements into the growing layers is not straightforward, and some complications occur in practice. Tin shows marked segregation at the surface,¹ and for this reason it is difficult to achieve abrupt changes in doping profile. Germanium shows the amphoteric behavior^{2,3} implicit in all Group IV elements. Silicon, which appears the most promising,⁴ also demonstrates its amphoteric nature at concentrations in excess of 5×10^{18} cm⁻³.⁵ Furthermore, it requires a high temperature source which makes it particularly sensitive to unintentional impurities generated at the source and its surrounds.⁶

The other major source of intentional donor impurities is the Group VI elements, Se and Te. These have received little attention until recently which probably arises from two causes. The first is a misconception that high vapor pressure materials are unsuitable for incorporation into MBE grown layers. However, it has recently been shown⁷ that strong interaction between the Group VI impurities and the GaAs host lattice is sufficient to ensure effective doping. The second is the practical problem that during bake-out most of the Group VI charge would be lost from the Knudsen cell. Recent work has illustrated experiments to overcome this latter point. Wood⁸ used "captive sources" in the form of the chalcogenides PbS and PbSe to obtain donor impurity incorporation. The lead was found not to be incorporated in detectable amounts. Collins *et al.*^{9,10} have used SnTe in a similar manner to obtain controlled donor incorporation. However, at elevated substrate temperatures (> 850 K) surface segregation of both the Sn and Te was observed. Davies *et al.*¹¹ described a novel method of incorporating S into GaAs using an electrochemical cell. This cell utilized the galvanic cell Pt/Ag/AgI/Ag₂S/Pt. When an EMF is applied across the cell, with the positive pole at the Ag₂S then the stoichiometry of the Ag₂S is altered, from silver sulfide coexisting with metallic silver at one extreme to silver sulfide coexisting

with liquid sulfur at the other. Within this range of nonstoichiometry the chemical potentials and therefore the activities of both silver and sulfur atoms in the silver sulfide vary with stoichiometry. Thus changing the cell EMF changes the gas phase pressure of sulfur over the cell. Then provided the cell is kept at some modest temperature, i.e., 473 K, sulfur molecules S_x where $2 < x < 8$ effuse from the cell. In the regime in which we chose to work the sulfur species was S₂ which predominates by 3–4 orders of magnitude over the next most abundant species, S₃.¹²

The primary advantage of this cell is its fast time constant, which was shown to be ~ 1 s. This is fast when compared with MBE growth rates (~ 6 Å s⁻¹) and with conventional thermal Knudsen cells. Thus one can consider introducing, in a facile manner, complicated doping profiles with very sharp interfaces into the growing layer with just one cell.

This paper reports an extension of that work which examines the effect of substrate temperature variation and As₄/Ga flux changes on the incorporation of sulfur atoms into MBE grown GaAs. The impetus for the work is the improved crystal quality that can be obtained at elevated temperatures (> 850 K for GaAs and > 950 K for GaAlAs). Thus it becomes necessary to investigate the incorporation behaviour of S₂ molecules in GaAs at these temperatures.

EXPERIMENT

The experimental work was carried out in a Vacuum Generators MB288 three chamber MBE system which has been described previously.¹¹ The sulfur doped GaAs epitaxial layers were grown on both *n* type (Si doped) and semi-insulating (Cr-doped and undoped) GaAs substrates. Substrate preparation was carried out immediately before loading the substrate into the MBE system using chemical treatments similar to those described in the literature.¹¹ After loading, the substrates were outgassed in the preparation chamber at 775 K until the pressure in the chamber fell to $< 1 \times 10^{-9}$ torr. The substrates were then transferred to the growth chamber, where they were heated to ~ 880 K in

an arsenic flux to desorb the surface oxide layer. This "in situ" cleaning procedure left the GaAs surface free of C and O contamination, within the limits of sensitivity of Auger Electron Spectroscopy (AES). Growth rates of $1 \mu\text{m h}^{-1}$ were used throughout the S doping experiments.

The electrical and optical properties of the resulting layers are described elsewhere.¹³

RESULTS AND DISCUSSION

A. Sulfur doping results

The effect of varying the substrate temperature (T_s) during growth is shown in Fig. 1. The sulfur flux was kept constant throughout the epitaxial growth by applying an EMF of 155 mV to the electrochemical cell.¹¹ This corresponds to a flux of S_2 molecules of 5.2×10^9 molecules $\text{cm}^{-2} \text{s}^{-1}$ arriving at the substrate surface. $J_{\text{As}}/J_{\text{Ga}}$ was kept constant at 2:1 whilst T_s was increased in four steps from 590 °C (863 K). It is evident from the C-V profile¹⁴ that there is a decrease in carrier concentration with increasing substrate temperature. Secondary Ion Mass Spectroscopy (SIMS)¹⁵ bears out the result that this is due to a decrease in the sulfur atom concentration. We believe that the mechanism responsible for this decrease in sulfur atom concentration with increasing T_s is the increased desorption of Ga_2S from the growing layer at high substrate temperatures. A similar result was obtained when repeating this experiment but with a lower incident S_2 flux of 5.2×10^8 molecules $\text{cm}^{-2} \text{s}^{-1}$, i.e., at a cell EMF of 135 mV.

The incorporated concentration can be plotted as a function of reciprocal substrate temperature so that the activation energy for desorption can be calculated. This is shown in Fig. 2. Also shown in this figure are the data extracted from the work of Collins *et al.* on SnTe incorporation.¹⁰ It can be seen that the temperature dependence of Te incorporation (measured by SIMS) into GaAs exactly mirrors that of S incorporation. The activation energy is the same in both cases, $\sim 70 \text{ k cal mole}^{-1}$ over the same temperature range. It is clear that the high and very different vapor pressures of the two elements, at the substrate temperature, are not relevant to the situation at the GaAs surface.

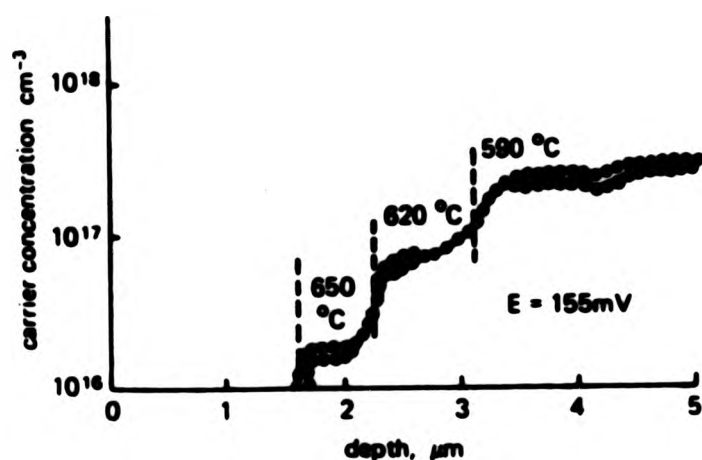


FIG. 1. A C-V depth profile of a four layer S-doped GaAs film. The figure shows the decrease in S incorporation with increasing substrate temperature (T_s).

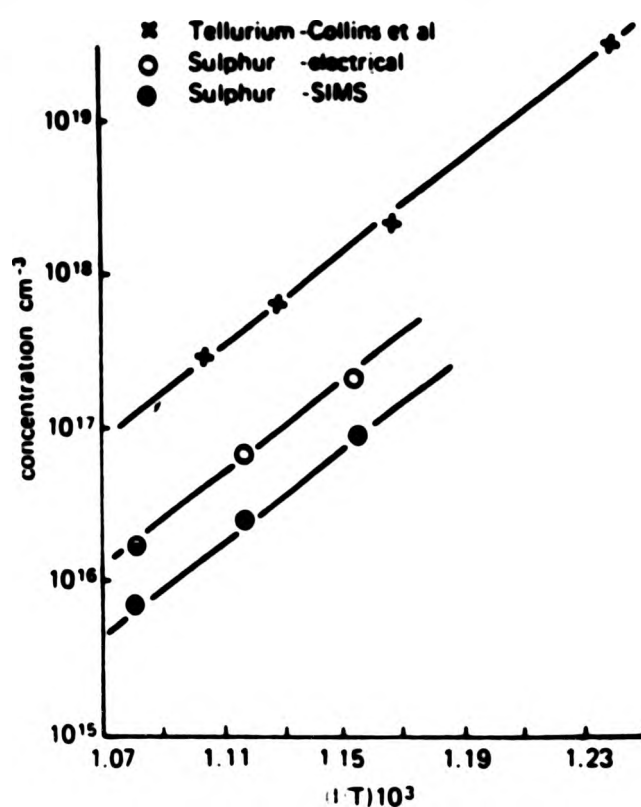


FIG. 2. Incorporated concentration of dopant vs reciprocal temperature. O-S-doping (this work) X-Te doping (Collins *et al.*).

The desorption of sulfur from GaAs over this elevated temperature range can be partially offset by increasing the As_4 :Ga ratio. This is shown in Fig. 3 where the substrate temperature was kept constant at 615 °C (888 K), the sulfur flux was also constant at $5.2 \cdot 10^9$ molecules $\text{cm}^{-2} \text{s}^{-1}$ whilst the As_4 :Ga ratio was varied from 1.5:1 to 9.3:1 in four steps. As can be seen from Fig. 3 increasing the As_4 :Ga ratio increases the incorporation concentration of sulfur. Again this exactly mirrors Collins data for Te from SnTe.

B. Thermodynamic framework

The desired doping reaction



where $\text{S}_2(\text{g})$ is diatomic gas phase sulfur, V_{As} is an arsenic vacancy in GaAs, S_{As}^+ is an ionized sulfur atom on an arsenic site in GaAs and e is an electron in the conduction band of GaAs, has been considered earlier.⁷ It was shown, by consid-

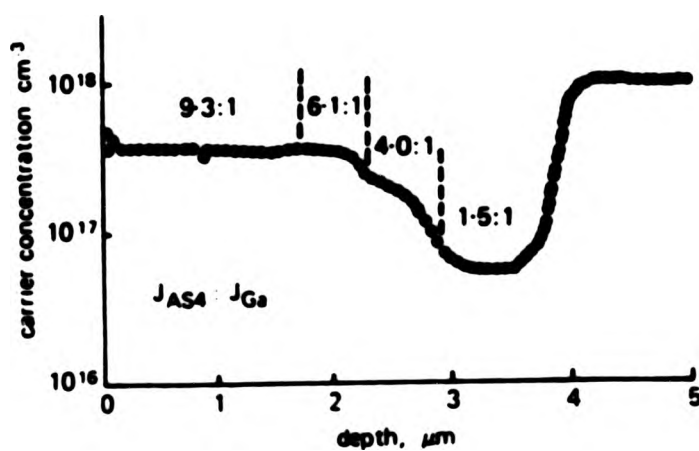


FIG. 3. A C-V depth profile of a four layer S-doped GaAs film where the As_4 :Ga beam flux ratio was changed as indicated in the figure. $J_{\text{S}_2} = 5.2 \cdot 10^9$ mol. $\text{cm}^{-2} \text{s}^{-1}$, $T_s = 888 \text{ K}$.

ering the standard dependence of $|V_{As}|$ on $P_{As}^{1/4}$ and the observed dependence on sulfur in the gas phase from VPE, that

$$[S_{As}^+] = K P_{S_2}^{1/2} P_{As_4}^{-1/4}, \quad (2)$$

were P_{S_2} and P_{As_4} are the pressures in atmospheres of species S_2 and As_4 in the gas phase, $[S_{As}^+]$ is the concentration in cm^{-3} of S_{As}^+ in GaAs and K is the equilibrium constant. Substituting $P_{As_4} = 2 \times 10^{-6}$ torr we obtain $P_{S_2} = 3.19 \times 10^{-19}$ torr for a useful doping of $[S_{As}^+] = 2 \times 10^{18} cm^{-3}$ at 560 °C (833 K). Thus, based on reaction (1) any typical MBE beam pressure would lead to the incorporation of S as a dopant. In order to grow a layer with the above doping level therefore, the flux of S_2 should be simply 5×10^{-5} that of Ga—typically $P_{Ga} = 5 \times 10^{-11}$ torr for $P_{Ga} = 1 \times 10^{-6}$ torr.

In the earlier paper the competing reaction



was considered briefly. It was clear from existing results⁸ that it was not an important consideration at 560 °C. The present work indicates that sulfur loss is, however, most important at higher temperatures and reaction (3) therefore requires closer analysis. First it is noted that strictly speaking Ga in GaAs should be considered. However in MBE, conditions are very close to the Ga liquidus of GaAs and consideration of Ga (l)—or gallium liquid—is a very good approximation, well within the accuracy required.¹⁶ The details of the approach including a check on the self-consistency of the method are given in the Appendix.

Reaction (3) then gives

$$K_3 = P_{Ga_2S} / P_{S_2}^{1/2}. \quad (4)$$

Taking literature values^{17,18} we obtain $K_3 = 9.22 \times 10^{10} atm^{1/2}$ at 560 °C. Substituting the value of $P_{S_2}^{1/2}$ in equilibrium with $[S_{As}^+] = 2 \times 10^{18} cm^{-3}$ gives $P_{Ga_2S} = 1.89 atm$.

Quite clearly therefore, thermodynamically all the sulfur should be converted to Ga_2S even at 560 °C. There should be virtually no doping, so any observed doping must be due to a kinetic barrier preventing reaction (3) proceeding. It should also be noted that K_3 changes very little over the experimental range studied and is $2.50 \times 10^{10} atm^{1/2}$ at 650 °C. There is therefore no thermodynamic explanation for the observed changes in doping efficiency in this temperature range.

There is just one final aspect to be considered at this stage. It may be argued that as $[S_{As}^+]$ should not actually be formed, it should not be used to calculate the value of $P_{S_2}^{1/2}$ to be substituted in Eq. (4). One may start with the beam pressure instead (5×10^{-11} torr) and assume it is all converted to P_{Ga_2S} (1×10^{-10} torr). Using this value in Eq. (3) we obtain the corresponding value of $P_{S_2}^{1/2}$ leading to $[S_{As}^+] = 1.53 \times 10^5 cm^{-3}$. This approximation is therefore excellent with all but $\approx 1 \times 10^{-12}$ of the available sulfur following the assumed route.

In order to understand more about the sulfur doping reaction therefore, the kinetic barrier to loss of Ga_2S must be examined in more detail.

C. Kinetic model

It is evident from Fig. 2 that when the incorporated

concentrations of S and Te are plotted as a function of reciprocal temperature they have the same temperature dependence. The calculated activation energy for the desorption process in both cases is $\sim 70 k cal mole^{-1}$. This is a similar temperature dependence to that reported by Panish¹⁹ for the border between different RHEED patterns on the GaAs (100) surface as a function of As_2/Ga ratio, e.g., the GaAs (2×4) As stabilized surface to the GaAs (3×1) As stabilized surface. It is tempting to speculate that the rate determining step for all three processes is the loss of arsenic from the surface layer.²⁰ Particularly so, as in both cases the effect of increasing substrate temperature on doping can be partially offset by increasing the As_2/Ga ratio as is shown in Fig. 3. Collins *et al.* observed a similar behavior for Te incorporation from SnTe with a variation of As_2/Ga . They, however, suggested that the increase in Te incorporation for increasing As_2/Ga ratio was the opposite to what might be expected from thermodynamic point defect models. This would be true if the incorporation reaction were the only important one. We suggest that the effect on the competing loss reaction is the dominant one. Thus the loss of arsenic at elevated temperatures not only leads to the formation of new surface structures but also leads to an increasing surface Ga population free to bond to dopant atoms via a much lower energy transition state and so to a loss of volatile species such as Ga_2S or $(GaTe)_2$. Therefore, increasing the As_2/Ga ratio decreases the free Ga surface population available to bond to the Group VI dopant atoms. Thus we have the situation that, as we increase the substrate temperature to $\sim 850 K$, we see a change in the relative rates of the two competing reactions (1) the incorporation of sulfur into the GaAs matrix and (2) the formation of Ga_2S . At temperatures below 850 K the kinetic barrier to reaction (2) reduces the formation of Ga_2S to a negligible amount, allowing reaction (1), where no kinetic barriers have been detected, to dominate.

D. Application to varactor fabrication

Despite this increasing loss of sulfur with increasing temperature we are able to demonstrate the usefulness of the electrochemical cell in the MBE growth of GaAs provided the substrate temperature is known reproducibly. Figure 4 shows a range of doping levels achieved over a large number of growth runs even when working in a region where there is some loss of sulfur. As is implicit from this figure a straight line relationship holds between applied EMF and incorporated S concentration from levels of $N_D - N_A \sim 1 \times 10^{15} cm^{-3}$ to $3-4 \times 10^{18} cm^{-3}$. At high doping levels ($\sim 3-4 \times 10^{18} cm^{-3}$) a deviation from the straight line is observed. This is approaching the value for the solid solubility limit for S in GaAs as observed by other workers using different crystal growth techniques.²¹

A more practical demonstration of the versatility of the electrochemical cell is evident in the fabrication of a test hyperabrupt varactor for use as a narrow band microwave tuner. The epilayer was grown at 880 K. The C-V profile through the varactor structure is shown in Fig. 5. As can be seen the plot shows four separate regions which exactly match the required theoretical profile. From the air/semiconductor interface there is (1) a region of constant doping

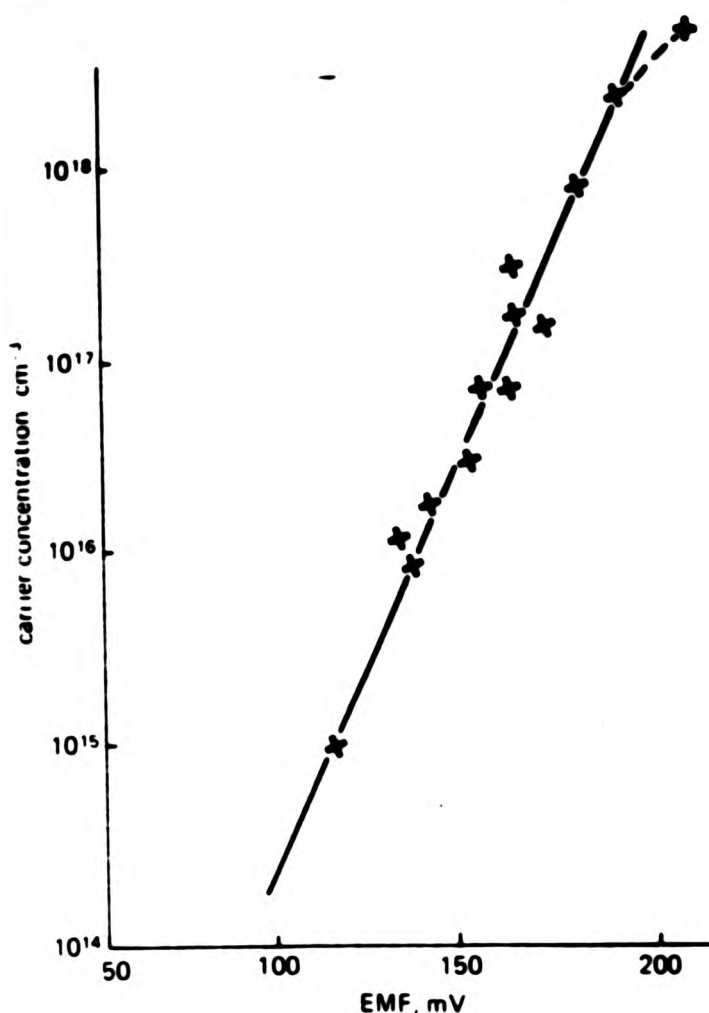


FIG. 4. Plot of carrier concentration of S doping in GaAs (measured by C-V method) as a function of applied EMF to the electrochemical cell. $T_s = 880$ K.

level whose thickness is calculated to deplete out when contacted to, (2) an exponential region with exponent of $-3/2$, (3) a plateau region in carrier concentration, and (4) a hyperabrupt change to an n^+ buffer region. The complete structure

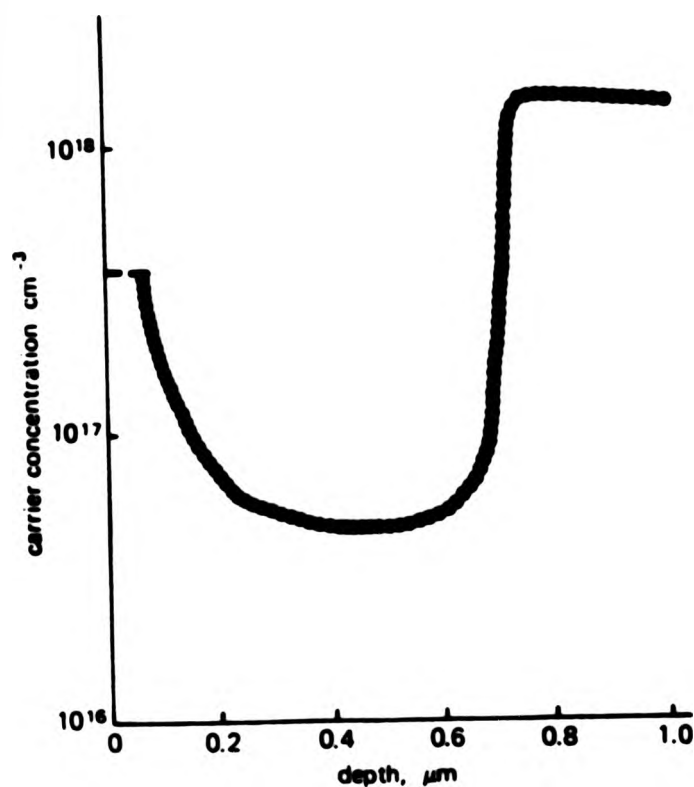


FIG. 5. A C-V depth profile through a test hyperabrupt varactor structure. $T_s = 880$ K. See text for further comment.

was generated with just one dopant cell, a task that would be difficult with conventional thermal Knudsen cells. Devices fabricated from these layers were large, $80 \mu\text{m}$ in diameter with an associated capacitance of ~ 4 pF. However, when measured in the 2–18 GHz region the devices showed promising results, the series resistance of the device was $< 1 \Omega$ most of which is spreading resistance in the substrate. The epilayer resistance was estimated to be $\sim 0.2 \Omega$. The capacitance ratio $C_{0.3}/C_{V_{\text{MAX}}}$ was measured to be 14:1 whilst the corresponding maximum voltage swing V_{MAX} was 10 V.

CONCLUSIONS

In conclusion, we present an examination of the variation in incorporation rate of sulfur atoms in MBE grown GaAs with increasing substrate temperature. An increasing loss of sulfur is observed at temperatures in excess of 850 K. This reduction in incorporation rate is explained on the basis of two competing reactions: (1) the incorporation of S into the GaAs host matrix and (2) the formation of the volatile species Ga_2S . Increasing the As_4/Ga ratio partially offsets the effects of increasing the substrate temperature. This lends support to the hypothesis that it is an increasing loss of arsenic from the GaAs growing surface that dominates the rate determining step. We also demonstrate, from the fabrication of a hyperabrupt varactor diode structure, that the electrochemical cell can still be used to introduce intricate doping profiles into epitaxial GaAs even in this higher temperature (> 850 K) range.

ACKNOWLEDGMENTS

The authors would like to thank D. V. Morgan and P. J. Tasker, Leeds University, for fabricating the varactor diodes and making the device results available to us. Acknowledgment is also made to the Director of Research, British Telecom for permission to publish this paper.

APPENDIX

A. Thermodynamic calculations

It is important to check the validity of the thermodynamic estimates and the approximations involved in the method wherever possible. One such check can be made by comparing the calculated sulfur pressures corresponding to given doping levels of S in GaAs with the lowest pressure of sulfur in equilibrium with the Ga_2S_3 phase. This value of course represents the saturation solubility of S in GaAs and experimental data on this point is available.

First, the calculation of sulfur doping levels should be assessed. In an earlier paper⁷ values were obtained in the following way. Experimental sulfur doping levels were taken from typical VPE work²² using the $\text{Ga}/\text{AsCl}_3/\text{H}_2/\text{H}_2\text{S}$ system. Standard thermochemical data¹⁸ was used to convert to the $\text{Ga}/\text{As}/\text{S}$ system relevant to MBE. Crucially, the same point defect model used to explain the VPE pressure dependence (and activity dependence in Te doping by LPE) was used as the basis for the significant extrapolation needed to calculate results in MBE conditions. The following results were obtained:

Concentration 2.2×10^{16} , 2.2×10^{17} , 2.2×10^{18} , and 2.2×10^{19}

$[S_{As}^*]$, cm^{-3}

Equilibrium value 4.2×10^{-26} , 4.2×10^{-24} , 4.2×10^{-22} , and 4.2×10^{-20}

P_s , atm.

These results may now be compared with the stability of $\text{Ga}_2\text{S}_3(s)$ calculated from the equation



which gives

$$K_A = P_s^{-3/2} \quad (\text{A2})$$

Standard thermochemical data^{17,18} for reaction A1 yields the value $K_A = 2.02 \times 10^{30} \text{ atm}^{-3/2}$ at 560 °C, leading to $P_s = 6.25 \times 10^{-21} \text{ atm}$. The calculated solubility limit for $[S_{As}^*]$ in GaAs is thus $8.49 \times 10^{18} \text{ cm}^{-3}$. Although there is still some uncertainty about the exact position experimentally²¹ it is in the region of $1 \times 10^{19} \text{ cm}^{-3}$. The agreement is thus extremely good, and to some degree fortuitous, as the simple two term expressions used for free energy throughout the calculations is more approximate than this. However, the essential validity of the method is undoubtedly demonstrated.

One final point also deserves comment. The beam pressure of $P_s = 6.58 \times 10^{-14} \text{ atm}$ should not cause formation of Ga_2S_3 under MBE conditions, even at 560 °C where the formation of Ga_2S_3 is kinetically hindered. It would if this beam impinged on the same GaAs surface for long enough, but during growth the chemical potential of S in the growing layer is reduced by the finite amount of S present, i.e., by the kinetic limit on the supply rate. The effective chemical potential is given by $[S_{As}^*]$, which at the above beam pressure is

$2 \times 10^{18} \text{ cm}^{-3}$, and so below the solubility limit. The thermodynamic treatment must be applied to the growing layer of course, as this is where the same (substrate) temperature obtains for all species.

¹A. Y. Cho and J. R. Arthur, *Prog. Solid State Chem.* **10**, 157 (1975).

²K. Ploog, A. Fischer, and H. Kuzel, *Appl. Phys.* **18**, 353 (1979).

³R. Heckingbottom and G. J. Davies, *J. Cryst. Growth* **98**, 644 (1980).

⁴A. Y. Cho, *J. Appl. Phys.* **46**, 1733 (1975).

⁵Y. G. Chai, R. Chow, and C. E. C. Wood, *Appl. Phys. Lett.* **39**, 800 (1981).

⁶E. H. C. Parker, R. A. Kubak, R. M. King, and J. D. Grange, *J. Phys. D* **14**, 1853 (1981).

⁷R. Heckingbottom, C. J. Todd, and G. J. Davies, *J. Electrochem. Soc.* **127**, 444 (1980).

⁸C. E. C. Wood, *Appl. Phys. Lett.* **33**, 770 (1978).

⁹D. M. Collins, *Appl. Phys. Lett.* **38**, 67 (1979).

¹⁰D. M. Collins, J. N. Miller, Y. G. Chai, and R. Chow, *J. Appl. Phys.* **53**, 3010 (1982).

¹¹G. J. Davies, D. A. Andrews, and R. Heckingbottom, *J. Appl. Phys.* **52**, 7214 (1981).

¹²H. Rickert, *Physics of Electrolytes*, edited by J. Hladik (Academic, New York, 1972), Vol. 2, p. 519.

¹³G. J. Davies and D. A. Andrews, *Vacuum* (unpublished).

¹⁴T. Ambridge, J. L. Stevenson and R. M. Redstall, *J. Electrochem. Soc.* **127**, 222 (1980).

¹⁵SIMS analysis performed by Charles Evans and Associates, San Mateo, California.

¹⁶J. R. Arthur, *J. Phys. Chem. Solids* **28**, 2257 (1967).

¹⁷O. M. Uy, D. W. Muenow, P. J. Ficalora, and J. L. Margrave, *Trans. Faraday Soc.* **64**, 2998 (1968).

¹⁸O. Kubaschewski and C. B. Alcock, *Metallurgical Thermochemistry*, 5th Ed. (Pergamon, London 1979), p. 268.

¹⁹M. B. Panish, *J. Electrochem. Soc.* **127**, 2729 (1980).

²⁰R. Heckingbottom, G. J. Davies and K. A. Prior, 2nd IUPAP/UNESCO Semiconductor Symposium, Trieste, 1982 (to be published in *Surf. Sci.*).

²¹E. Venhoff, M. Maier, K. H. Bachem, and P. Balk, *J. Cryst. Growth*, **53**, 598 (1981).

²²M. A. Savva, *J. Electrochem. Soc.* **123**, 1498 (1976).

The influence of growth conditions on selenium incorporation in GaAs grown by molecular beam epitaxy

D. A. Andrews, M. Y. Kong,^{a)} R. Heckingbottom, and G. J. Davies
British Telecom Research Laboratories, Martlesham Heath, Ipswich, IP5 7RE, United Kingdom

(Received 14 September 1983; accepted for publication 10 November 1983)

An electrochemical cell Pt/Ag/AgI/Ag₂Se/Pt has been used as a highly controllable source of Se₂ for *n*-type doping of GaAs grown by molecular beam epitaxy (MBE). Se is incorporated with 100% efficiency under all normal MBE conditions up to growth temperatures of 620 °C. Above this temperature doping is still possible but with reduced efficiency. The general behavior is similar to that already reported for sulfur doping, with the added advantage that doping can be extended to temperatures some 30 °C higher in the case of Se. Chemical analysis has confirmed that when doping efficiency is reduced, it is due to actual loss of Se. Thermodynamic analysis indicates that loss as Ga₂Se is to be expected under all conditions studied, so successful doping is due to kinetic barriers to this loss reaction. Excess As₄ is shown to hinder the loss of Ga₂Se even further.

PACS numbers: 61.70.Tm, 81.15.Ef, 82.80. — d

I. INTRODUCTION

The search for *n*-type dopants for molecular beam epitaxy (MBE) of GaAs and other III-V compound semiconductors has, until recently, led almost exclusively to the use of the group IV elements Sn, Ge, and Si. In practice, however, these elements have turned out to be less than ideal. Tin has a less than straightforward incorporation behavior¹; germanium shows the amphoteric nature intrinsic to all the group IV dopants,^{2,3} and silicon, although the best behaved and most commonly used of the group, still shows amphoteric character, particularly at high doping levels.⁴ Silicon also has an inconveniently low vapor pressure that demands the use of high temperature sources with a corresponding susceptibility to the unintentional generation of other impurities from the source and its surrounds.⁵

The other potential source of *n*-type dopants lies in group VI of the periodic table. The chalcogens, S, Se, and Te, are widely used in GaAs technology but have been neglected in MBE for two main reasons. The first is a belief that materials with a high vapor pressure at MBE growth temperatures are intrinsically unsuitable. However, it has recently been shown⁶ that the strong interaction between the group VI atoms and the GaAs host lattice is sufficient to ensure incorporation. The second reason is the practical problem of containing the volatile group VI elements during UHV system bakeout. One solution to this problem that has been pursued is the use of chalcogenide captive sources such as PbS, PbSe, SnTe, and SnSe₂,⁷⁻⁹ where the chalcogen vapor pressure is reduced in compound form from its elemental value. However, Sn and Te both show surface segregation at the high growth temperatures necessary for the production of the highest quality GaAs, even when incorporated from a compound source.⁸ Of the others, SnSe₂ shows most promise although its evaporation behavior does display some peculiarities.⁹

A novel, alternative approach has been developed in our laboratories by Davies *et al.*,¹⁰ whereby sulfur is incorporated into GaAs by the electrolysis of a sulfide electrolyte. The combination of this electrochemical cell with a Knudsen cell yields a highly controllable, low temperature (200 °C) source of sulfur dimers with a fast response time (1 s), giving significant advantages over thermal elemental and captive sources in terms of flexibility and molecular beam composition.

Using this source, we have characterized the incorporation behavior of S into GaAs (Ref. 11) and have suggested that loss of sulfur from the growing surface can occur via the evaporation of the volatile species Ga₂S at high temperatures or low arsenic overpressures. We have also demonstrated that the electrochemical sulfur source permits the facile production of high performance GaAs devices with complicated doping profiles.

In this paper, the study of the group VI dopants is extended to the electrochemical generation of Se and the characterization of its incorporation into GaAs as a function of selenium flux, growth temperature, and arsenic overpressure.

II. EXPERIMENT

The experiments were conducted in a Vacuum Generators MB288, three-chamber MBE system which has been described elsewhere.¹⁰ Selenium doped GaAs epitaxial layers were grown simultaneously on *n*⁺ (Si-doped) and undoped GaAs substrates which were prepared using well-established chemical treatments.¹⁰ After loading into the system, the substrates were outgassed in the preparation chamber at 450 °C and transferred to the growth chamber when the pressure had fallen below 10⁻⁹ Torr. Subsequent heating to 610 °C in an arsenic flux resulted in desorption of the surface oxide, leaving contamination-free, highly ordered surfaces as determined by reflection high energy electron diffraction (RHEED) and Auger electron spectroscopy (AES). Growth rates were typically between 1 and 2 μm h⁻¹.

^{a)} On leave from the Institute of Semiconductors, Chinese Academy of Sciences, Beijing, China.

A. The electrochemical selenium cell

The electrochemical sulfur source has been described in detail elsewhere¹⁰ and is easily modified to produce selenium vapor by replacing the Ag_2S electrolyte with Ag_2Se .¹²

Briefly, an electrochemical cell $\text{Pt}/\text{Ag}_2\text{Se}/\text{AgI}/\text{Ag}/\text{Pt}$ was constructed by pressing a pellet of Ag_2Se powder onto a pellet of AgI powder. The AgI has a negligible electronic conductivity and acts as an Ag^+ ion conductor between the Ag_2Se and the Ag electrode. By varying the emf across the cell, the full stoichiometric range of the Ag_2Se phase may be accessed and the activity of the selenium in this compound controlled. Therefore, the equilibrium vapor pressure of Se over Ag_2Se may be varied by several orders of magnitude, from the Se-rich boundary (Ag_2Se in equilibrium with liquid Se) to the silver-rich boundary (Ag_2Se in equilibrium with Ag). Combining this electrochemical cell with a conventional Knudsen effusion enclosure results in a highly controllable, pure source of selenium dimers.¹⁵

The operation of the selenium source is identical to that of the sulfur source except for the following points. Since elemental selenium is less volatile than sulfur, the selenium source has to be operated at a slightly higher temperature to achieve the same fluxes. A temperature of 300 °C was sufficient and permitted doping levels of $2 \times 10^{18} \text{ cm}^{-3}$ to be achieved with ease. It should be noted that this is still a desirably low temperature. Care must also be taken in exploring the composition range of Ag_2Se as a function of temperature as it possesses several phases, and it is possible to trespass into regimes where elemental selenium is precipitated in the selenide. This can result in irreversible deterioration in the characteristics of the electrochemical cell.

B. Material properties

Uniformly doped layers with carrier concentrations in the range $2 \times 10^{15} < \text{Nd-Na} < 2 \times 10^{18} \text{ cm}^{-3}$ showed excellent electrical properties and morphology. Mobilities of $6350 \text{ cm}^2 \text{ V}^{-1} \text{ s}^{-1}$ and $25000 \text{ cm}^2 \text{ V}^{-1} \text{ s}^{-1}$, at 300 and 77 K, respectively, were achieved for $\text{Nd-Na} = 8 \times 10^{15} \text{ cm}^{-3}$. Surface morphology was in general excellent with defect densities of the order of 10^3 cm^{-2} , comparable with the etch pit densities of the substrates used.

Figure 1 shows a combined carrier concentration and

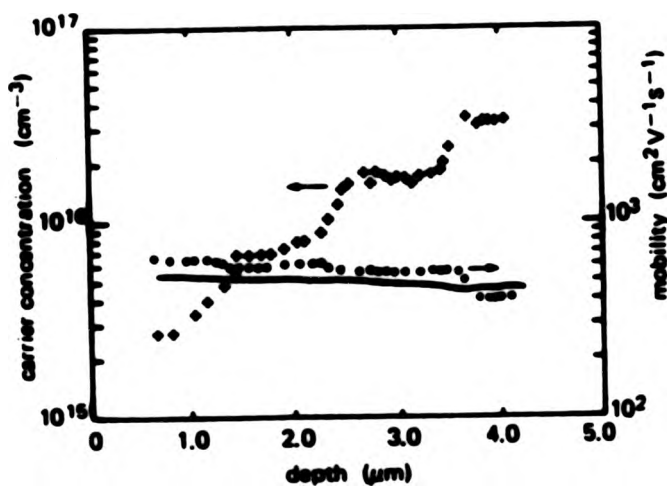


FIG. 1. A combined C-V and Hall mobility depth profile of a four-layer Se-doped GaAs film. The crosses show the local carrier concentration, the circles the local Hall mobility, and the solid line the sheet mobility.

Hall mobility profile through a GaAs layer grown with a four-step selenium staircase doping profile. The layer was grown on an undoped substrate and fabricated into the familiar Van der Pauw mesa for mobility measurement. The measurement technique¹³ makes use of an electrolytic Schottky contact to give controlled dissolution of the layer and a depth profile of the local carrier concentration (upper curve), local Hall mobility (middle curve), and sheet mobility (lower curve). The changes in carrier concentration are clearly resolved and are reflected in the local mobility curve. On the other hand, the sheet mobility reveals little information thus highlighting the utility of the modulation technique for extracting local information.

III. RESULTS

The effect of varying the substrate temperature (T_s) during the growth of Se-doped layers is shown in Fig. 2. The selenium flux was kept constant by applying a fixed emf to the electrochemical cell. The arsenic to gallium flux ratio ($J_{\text{As}_4}/J_{\text{Ga}}$) was kept constant at 2.7:1 while T_s was increased in four steps from 580 °C at the interface to 690 °C at the surface. The grown layer was electrochemically C-V profiled using a British Telecom Profile Plotter¹⁴ to reveal the carrier concentration as a function of depth.

It is readily apparent that there are two domains of behavior. At or below 620 °C, the carrier concentration is a very weak function of growth temperature, while above 620 °C it decreases with increasing T_s . That this is due to a decreasing selenium atom concentration is borne out by results from secondary ion mass spectrometry (SIMS).¹⁵

In a separate experiment, a selenium-doped layer was grown at a T_s where Se loss was observed and the effect of varying the arsenic overpressure during growth studied. At a T_s of 660 °C and a nominal doping level of $4 \times 10^{17} \text{ cm}^{-3}$ (assuming unity sticking coefficient), $J_{\text{As}_4}/J_{\text{Ga}}$ was varied in four steps from 4.2:1 to 1.5:1. It may be seen from Fig. 3 that selenium loss is suppressed at the higher arsenic overpressures. The dips in the profile at the changes in overpressure are believed to be due to the dynamic response of the arsenic effusion cell. Although the temperature response of the effusion cell is critically damped the flux response measured by the moveable ion gauge shows some overshoot, presumably due to temperature gradients within the cell.

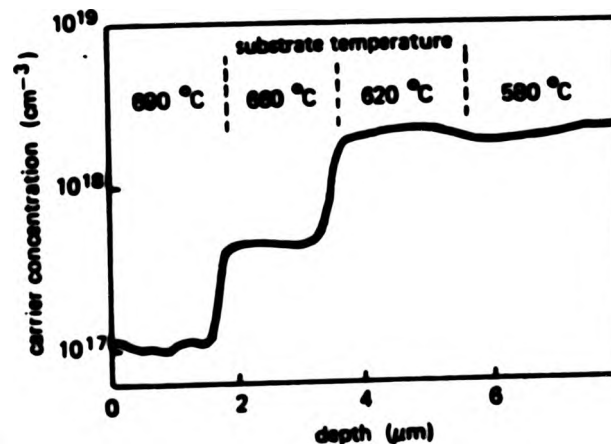


FIG. 2. A C-V depth profile of a four-layer Se-doped GaAs film. The figure shows the decrease in Se incorporation with increasing temperature.

A. The electrochemical selenium cell

The electrochemical sulfur source has been described in detail elsewhere¹⁰ and is easily modified to produce selenium vapor by replacing the Ag_2S electrolyte with Ag_2Se .¹²

Briefly, an electrochemical cell $\text{Pt}/\text{Ag}_2\text{Se}/\text{AgI}/\text{Ag}/\text{Pt}$ was constructed by pressing a pellet of Ag_2Se powder onto a pellet of AgI powder. The AgI has a negligible electronic conductivity and acts as an Ag^+ ion conductor between the Ag_2Se and the Ag electrode. By varying the emf across the cell, the full stoichiometric range of the Ag_2Se phase may be accessed and the activity of the selenium in this compound controlled. Therefore, the equilibrium vapor pressure of Se over Ag_2Se may be varied by several orders of magnitude, from the Se-rich boundary (Ag_2Se in equilibrium with liquid Se) to the silver-rich boundary (Ag_2Se in equilibrium with Ag). Combining this electrochemical cell with a conventional Knudsen effusion enclosure results in a highly controllable, pure source of selenium dimers.¹⁵

The operation of the selenium source is identical to that of the sulfur source except for the following points. Since elemental selenium is less volatile than sulfur, the selenium source has to be operated at a slightly higher temperature to achieve the same fluxes. A temperature of 300 °C was sufficient and permitted doping levels of $2 \times 10^{18} \text{ cm}^{-3}$ to be achieved with ease. It should be noted that this is still a desirably low temperature. Care must also be taken in exploring the composition range of Ag_2Se as a function of temperature as it possesses several phases, and it is possible to trespass into regimes where elemental selenium is precipitated in the selenide. This can result in irreversible deterioration in the characteristics of the electrochemical cell.

B. Material properties

Uniformly doped layers with carrier concentrations in the range $2 \times 10^{15} < \text{Nd-Na} < 2 \times 10^{18} \text{ cm}^{-3}$ showed excellent electrical properties and morphology. Mobilities of $6350 \text{ cm}^2 \text{ V}^{-1} \text{ s}^{-1}$ and $25000 \text{ cm}^2 \text{ V}^{-1} \text{ s}^{-1}$, at 300 and 77 K, respectively, were achieved for $\text{Nd-Na} = 8 \times 10^{15} \text{ cm}^{-3}$. Surface morphology was in general excellent with defect densities of the order of 10^3 cm^{-2} , comparable with the etch pit densities of the substrates used.

Figure 1 shows a combined carrier concentration and

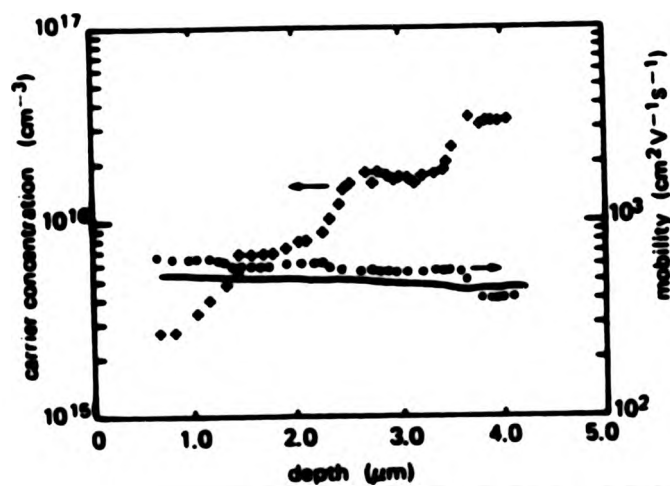


FIG. 1. A combined C-V and Hall mobility depth profile of a four-layer Se-doped GaAs film. The crosses show the local carrier concentration, the circles the local Hall mobility, and the solid line the sheet mobility.

Hall mobility profile through a GaAs layer grown with a four-step selenium staircase doping profile. The layer was grown on an undoped substrate and fabricated into the familiar Van der Pauw mesa for mobility measurement. The measurement technique¹³ makes use of an electrolytic Schottky contact to give controlled dissolution of the layer and a depth profile of the local carrier concentration (upper curve), local Hall mobility (middle curve), and sheet mobility (lower curve). The changes in carrier concentration are clearly resolved and are reflected in the local mobility curve. On the other hand, the sheet mobility reveals little information thus highlighting the utility of the modulation technique for extracting local information.

III. RESULTS

The effect of varying the substrate temperature (T_s) during the growth of Se-doped layers is shown in Fig. 2. The selenium flux was kept constant by applying a fixed emf to the electrochemical cell. The arsenic to gallium flux ratio ($J_{\text{As}_4}/J_{\text{Ga}}$) was kept constant at 2.7:1 while T_s was increased in four steps from 580 °C at the interface to 690 °C at the surface. The grown layer was electrochemically C-V profiled using a British Telecom Profile Plotter¹⁴ to reveal the carrier concentration as a function of depth.

It is readily apparent that there are two domains of behavior. At or below 620 °C, the carrier concentration is a very weak function of growth temperature, while above 620 °C it decreases with increasing T_s . That this is due to a decreasing selenium atom concentration is borne out by results from secondary ion mass spectrometry (SIMS).¹⁵

In a separate experiment, a selenium-doped layer was grown at a T_s where Se loss was observed and the effect of varying the arsenic overpressure during growth studied. At a T_s of 660 °C and a nominal doping level of $4 \times 10^{17} \text{ cm}^{-3}$ (assuming unity sticking coefficient), $J_{\text{As}_4}/J_{\text{Ga}}$ was varied in four steps from 4.2:1 to 1.5:1. It may be seen from Fig. 3 that selenium loss is suppressed at the higher arsenic overpressures. The dips in the profile at the changes in overpressure are believed to be due to the dynamic response of the arsenic effusion cell. Although the temperature response of the effusion cell is critically damped the flux response measured by the moveable ion gauge shows some overshoot, presumably due to temperature gradients within the cell.

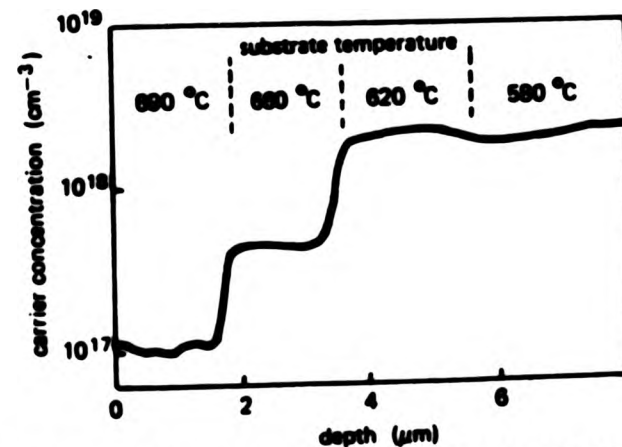


FIG. 2. A C-V depth profile of a four-layer Se-doped GaAs film. The figure shows the decrease in Se incorporation with increasing temperature.

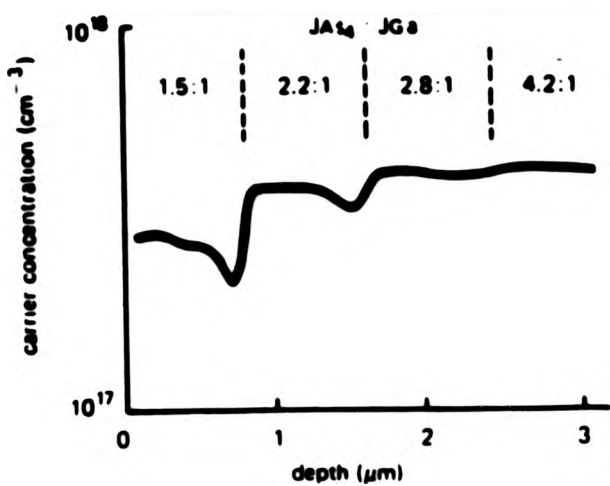


FIG. 3. A C-V depth profile of a four-layer Se-doped GaAs film where the $J_{As_4}:J_{Ga}$ beam flux ratio was changed as indicated in the figure.

In a further experiment, the incorporation of selenium into GaAs was investigated as a function of arriving Se flux. A growth temperature of 560 °C was used, with a $J_{As_4}:J_{Ga}$ ratio of 3.5:1 and the electrochemical cell driving emf varied in four steps from 180 to 230 mV. The resulting depth profile is shown in Fig. 4 and the carrier concentration plotted against emf in Fig. 5.

Theoretical considerations predict an exponential relationship between the flux and the applied emf.¹⁶ This is clearly borne out by the straight line behavior of the logarithmic plot in Fig. 5. Moreover, the relationship holds true up to the highest doping level of $2.5 \times 10^{18} \text{ cm}^{-3}$. This contrasts with the result of Smith *et al.*,⁹ who find a drop in apparent incorporation efficiency above 10^{17} cm^{-3} when selenium is incorporated by noncongruent evaporation of SnSe_2 from a conventional Knudsen cell. This deviation is then probably due to some peculiarity in the evaporation behavior of SnSe_2 rather than any intrinsic property of selenium.

Since the staircase profile shows flat trends and steep risers, we have no evidence for segregation or diffusion of

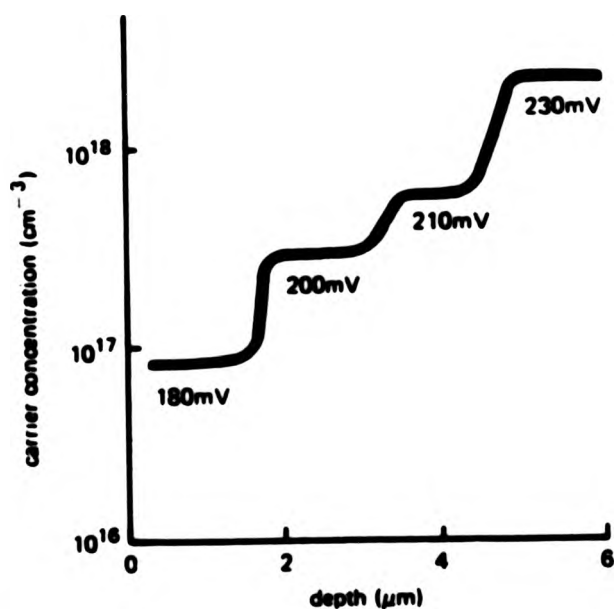


FIG. 4. A C-V depth profile of a four-layer Se-doped GaAs film where the emf applied to the electrochemical Se source is varied as indicated in the figure. $T_s = 560 \text{ }^\circ\text{C}$, $J_{As_4}:J_{Ga} = 3.5:1$.

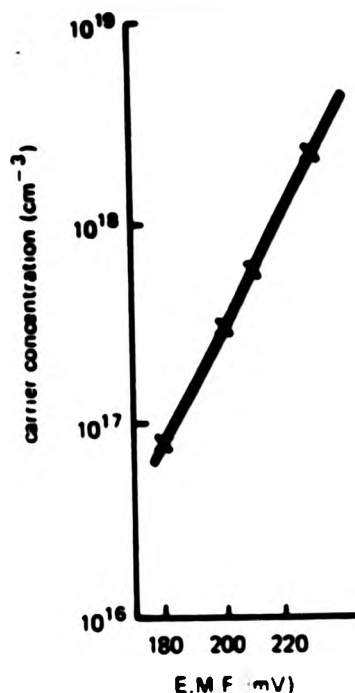


FIG. 5. Plot of carrier concentration via Se doping of GaAs as a function of Se cell emf.

selenium within the resolution of the electrochemical profiling technique.

The temperature dependence of the incorporation behavior of the common chalcogen dopants S, Se, and Te into MBE GaAs is summarized in Fig. 6. The sulfur and selenium data are our own and the tellurium data is drawn from the work of Collins *et al.*⁸ In this figure, reciprocal substrate temperature is plotted along the horizontal axis and donor concentration on the vertical axis. Sulfur and tellurium both exhibit very similar behavior, and the activation energy for desorption derived from the slope of the high temperature portion of the graph is identical for both at 70 kcal mol^{-1} .

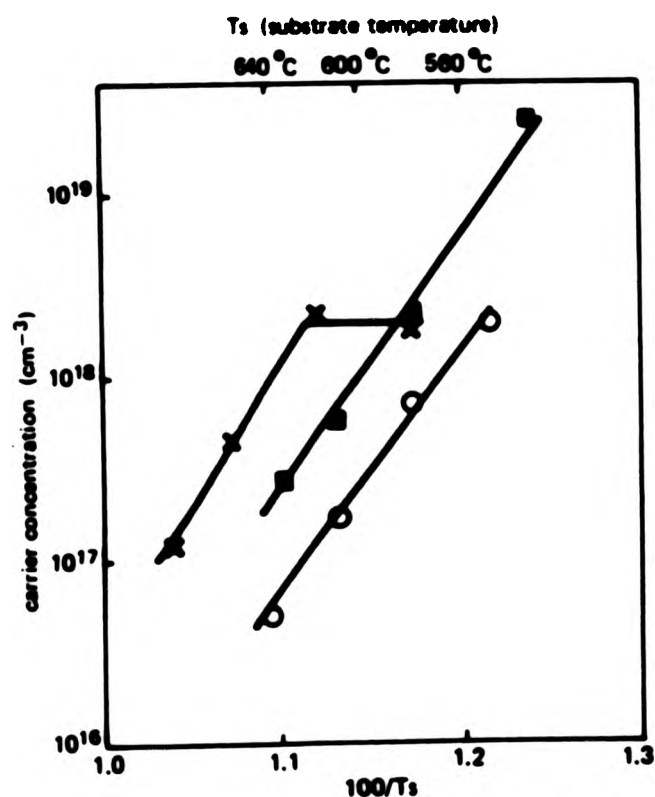


FIG. 6. Incorporated dopant concentration vs reciprocal substrate temperature. \circ —S; \times —Se (C-V data from this work); \blacksquare —Te (SIMS data from Collins *et al.*).

Sulfur does in fact show a plateau region at slightly lower temperatures than those plotted, and desorption is negligible below 570 °C. The range of temperatures depicted in Fig. 6 is that in which the best quality GaAs has been grown, and it is clear that selenium is the only chalcogen dopant to show a plateau within this technologically important range. This plateau extends to almost 630 °C. Beyond this region, selenium is lost from the growing surface in much the same manner as sulfur and tellurium and with a similar activation energy. This being so, it is still possible to achieve useful doping levels in this loss region simply by applying an increased dopant flux, as was demonstrated for sulfur.¹¹

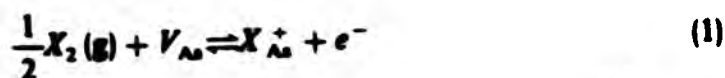
It should be noted that the rather high growth temperatures and reduced arsenic overpressures necessary to induce selenium loss place the growing surface very close to becoming gallium rich. The RHEED pattern from such surfaces is generally rather diffuse, certainly well away from the As-rich (2×4) pattern and more characteristic of the (3×1) phase.

It is clear from the above that selenium, generated as dimers from the electrochemical effusion source, is incorporated in a facile manner over a useful range of MBE growth parameters. It is only in the extremes of high substrate temperatures and reduced arsenic overpressures that the incorporation efficiency is reduced.

IV. DISCUSSION

It has been shown by Heckingbottom *et al.*⁶ that clear predictions as regards doping behavior can be made on the basis of thermodynamic calculations. These calculations stem from a consideration of the energetics of chemical processes and can therefore offer firm conclusions as to whether a particular reaction is possible or not. In particular, they show that the interaction between the GaAs lattice and the group VI dopants S, Se, and Te is strong enough to ensure their incorporation under MBE conditions.

Thus the reaction



[where X is S, Se, or Te, (g) indicates the gas phase, V_{As} is an arsenic vacancy in GaAs, X_{As}^+ an ionized atom on an arsenic site in GaAs and e^- an electron in the conduction band of GaAs] is well to the right under MBE conditions. At the time of this study⁶ the only experimental work⁷ indicated that there were no loss reactions of significance at a growth temperature of 560 °C and this possibility was not pursued further. Later work¹¹ showed however that at slightly higher growth temperatures the loss of sulfur from the growing surface becomes significant. A wider survey of likely competing reactions showed that



[where Ga(l) represents liquid gallium which is a good approximation to Ga in MBE grown GaAs since growth conditions are close to the Ga liquidus of the GaAs solid phase] should lead to the loss of virtually all the sulfur from the growing surface under all normal MBE growth conditions.

Thus, at 560 °C, to obtain a dopant concentration $[S_{As}^+] = 2 \times 10^{18} \text{ cm}^{-3}$ would require an equilibrium pressure $P_{Ga_2S} \sim 1.89 \text{ atm}$, quite inaccessible in MBE.

A similar analysis of the tendency to form Ga_2Se by the reaction analogous to Eq. (2) is possible using the data of Uy *et al.*¹⁷ and Kubaichewski and Alcock.¹⁸ For a beam equivalent pressure of $5 \times 10^{-11} \text{ Torr}$ [enough to give a doping level of $2 \times 10^{17} \text{ cm}^{-3}$ via reaction (1)] and a growth temperature of 560 °C, the equilibrium pressure of Ga_2Se is 0.28 Torr. At higher growth temperatures, this pressure would be even higher. Thus, as with sulfur, no useful doping should be possible except for an effective kinetic barrier to reaction (2).

In view of the apparent similarities with the doping with tellurium shown in Fig. 6, it is interesting to calculate that the comparable pressure of Ga_2Te (the majority gas phase species¹⁷) is $\sim 1.5 \times 10^{-7} \text{ Torr}$ so that even here less than one part per thousand of the Te would be incorporated as dopant except for the kinetic barrier to reevaporation. Figure 6 effectively shows the activation energy of this kinetic barrier to reaction (2). It is clear that it is similar for Se to that reported previously^{8,11} for Te and S at $\sim 70 \text{ kcal/mol}$ suggesting a common reaction mechanism. As was suggested earlier^{11,19} when considering sulfur doping, the temperature dependence is similar to that reported by Panish²⁰ for As loss from the GaAs surface. Additionally, as shown for Se doping in Fig. 3, increasing the As_4/Ga flux ratio increases the amount of Se incorporated, establishing that the concentration of surface arsenic plays a key role in hindering the loss reaction for all the chalcogens.

The selenium results show quite clearly however that not all aspects of the situation can be explained in terms of the Ga-As system. The preexponential factor is least for the Se case, leading to the lowest actual loss rate of the three chalcogens under otherwise similar conditions (though the Te results are not strictly comparable due to the interaction with Sn at the growing surface⁸). The explanation for this difference is not known. It is noted that Se, being adjacent to As in the periodic table of elements, is likely to be accommodated in the GaAs lattice with less strain than S or Te, but there is insufficient data to pursue this possibility more quantitatively. What is clear is the technological importance of this difference. Se can, as a result, be used as a dopant quite straightforwardly at the higher growth temperatures and low ($\sim 2:1$) As_4/Ga flux ratios consistent with the growth of the highest quality GaAs layers.

V. CONCLUSION

Selenium from a beam of Se_2 has been used successfully to dope MBE GaAs. The selenium is incorporated in a facile manner, and with effectively 100% efficiency under all conditions allowing successful growth of GaAs, up to growth temperatures of 620 °C. Above this temperature, incorporation at useful levels can still be achieved but an increased loss of selenium is observed. This loss is interpreted in terms of the competition between the incorporation reaction and the formation of volatile Ga_2Se which is increasingly favored as the growth temperature and hence surface gallium concentration is increased. Reducing this gallium concentration by

increasing the arsenic overpressure results in a reduced loss of selenium, thus supporting the postulate that it is the arsenic concentration on the GaAs surface that dominates the kinetics of the loss reaction.

Selenium, therefore, shows a great similarity to sulfur and tellurium in its incorporation behavior into MBE GaAs, but with an enhanced stability at the high temperatures desirable for the best GaAs growth. In this respect it is probably the most ideal group VI dopant for GaAs, and in combination with its generation from an electrochemical effusion source offers a most versatile, well-behaved doping technique with low temperatures in the source, a fast response time (1 s) and simple dimeric beam composition.

ACKNOWLEDGMENTS

The authors would like to thank D. Wood and C. J. Allen for the mobility profile. Acknowledgment is made to the Director of Research, British Telecom for permission to publish this paper.

- ¹A. Y. Cho and J. R. Arthur, *Prog. Solid State Chem.* **10**, 157 (1975).
²K. Ploog, A. Fischer, and H. Kunzel, *Appl. Phys.* **18**, 353 (1979).
³R. Heckingbottom and G. J. Davies, *J. Cryst. Growth* **50**, 644 (1980).

- ⁴Y. G. Chai, R. Chow, and C. E. C. Wood, *Appl. Phys. Lett.* **39**, 800 (1981).
⁵E. H. C. Parker, R. A. Kubick, R. M. King, and J. D. Grange, *J. Phys. D.* **14**, 1853 (1981).
⁶R. Heckingbottom, C. J. Todd, and G. J. Davies, *J. Electrochem. Soc.* **127**, 444 (1980).
⁷C. E. C. Wood, *Appl. Phys. Lett.* **33**, 770 (1978).
⁸D. M. Collins, J. N. Miller, Y. G. Chai, and R. Chow, *J. Appl. Phys.* **53**, 3010 (1982).
⁹R. S. Smith, P. M. Ganser, and H. Eason, *J. Appl. Phys.* **53**, 9210 (1982).
¹⁰G. J. Davies, D. A. Andrews, and R. Heckingbottom, *J. Appl. Phys.* **52**, 7214 (1981).
¹¹D. A. Andrews, R. Heckingbottom, and G. J. Davies, *J. Appl. Phys.* **54**, 4421 (1983).
¹²Lancaster Synthesis Ltd., Morecambe, Lancashire, UK.
¹³T. Ambridge and C. J. Allen, *Electron. Lett.* **15**, 648 (1979).
¹⁴T. Ambridge, J. L. Stevenson, and R. M. Reddell, *J. Electrochem. Soc.* **127**, 222 (1980).
¹⁵SIMS analysis by Charles Evans and Associates, San Mateo, California, USA.
¹⁶H. Rickert, *Physics of Electrolytes*, edited by J. Hindik (Academic, New York, 1972), Vol. 2, p. 519.
¹⁷O. M. Uy, D. W. Musnow, P. J. Ficalora, and J. L. Margrave, *Trans. Faraday Soc.* **64**, 2998 (1968).
¹⁸O. Kubaschewski and C. B. Alcock, *Metallurgical Thermochemistry*, 5th ed. (Pergamon, London, 1979).
¹⁹R. Heckingbottom, G. J. Davies, and K. A. Prior, *Surf. Sci.* **132**, 375 (1983); *Proceedings of the 2nd IUPAP/UNESCO Semiconductor Symposium, Trieste (1982)*.
²⁰M. B. Panish, *J. Electrochem. Soc.* **127**, 648 (1979).

The influence of growth conditions on sulfur and selenium incorporation in $\text{Ga}_{1-x}\text{Al}_x\text{As}$ grown by molecular-beam epitaxy

D. A. Andrews, R. Heckingbottom, and G. J. Davies

British Telecom Research Laboratories, Martlesham Heath, Ipswich IP5 7RE, United Kingdom

(Received 20 August 1985; accepted for publication 8 April 1986)

An electrochemical cell $\text{Pt}/\text{AgI}/\text{Ag}_2\text{X}/\text{Pt}$ ($\text{X} = \text{S}, \text{Se}$) has been used as a highly controllable source of chalcogen dimers for n -type doping of $\text{Ga}_{1-x}\text{Al}_x\text{As}$ grown by molecular-beam epitaxy (MBE). The incorporation behavior has been investigated as a function of alloy composition, growth temperature, and arsenic overpressure. At low temperatures, $< 600^\circ\text{C}$, sulfur and selenium are incorporated into $\text{Ga}_{1-x}\text{Al}_x\text{As}$ in a facile manner. At higher temperatures, where loss of chalcogen dopant from GaAs has previously been observed, sulfur shows an enhanced stability in the aluminum-containing alloys. Excess As_4 is shown to hinder the loss further. The behavior is modelled in terms of the relative stabilities of the volatile and involatile gallium and aluminum chalcogenides under MBE growth conditions.

I. INTRODUCTION

The group VI dopants S, Se, and Te have received increased attention in recent publications concerned with the growth of GaAs by molecular-beam epitaxy.¹⁻³ This renewed interest stems from two origins. Firstly, the group VI elements do not exhibit amphoteric behavior in III-V growth, unlike the group IV elements.⁴ Secondly, the low-source temperatures required for doping with the group VI elements imply a high beam purity.

Evaporation from the elements themselves has proved incompatible with UHV techniques; their high vapor pressures at typical bakeout temperatures imply that much of the group VI charge would be lost from the source. Some practical solutions involve the use of "captive sources" in the form of the lead chalcogenides PbS and PbSe ,¹ with the incorporation of the Pb being negligible. SnTe has been used in a similar manner, but at elevated substrate temperatures ($> 570^\circ\text{C}$), surface segregation of both Sn and Te was observed.³ A novel method for the incorporation of S and Se into GaAs has been described⁶ using the electrolysis of a solid-state silver chalcogenide electrolyte. A change in the programming EMF applied to the cell produces a corresponding change in the chalcogen vapor pressure over the electrolyte. Then provided the cell is kept at some modest temperature (200°C), chalcogen dimers (S_2 or Se_2) are produced in the molecular beam. These dimeric species predominate by 3-4 orders of magnitude over the next most abundant species S_3 .

It has been shown⁷ that at elevated growth temperatures ($> 600^\circ\text{C}$) the incorporation efficiency of the group VI element is reduced. It has also been shown that by increasing the As_4 overpressure during growth, the loss of dopant may be suppressed. This study has been extended to the incorporation of group VI dopants in $\text{Ga}_{1-x}\text{Al}_x\text{As}$. Layers of this material, of high crystalline quality and high purity, are obtained at growth temperatures some 100° higher than for typical GaAs growths. It might therefore seem that this increase in growth temperature would preclude the successful incorporation of group VI dopants in MBE $\text{Ga}_{1-x}\text{Al}_x\text{As}$. This paper reports for the first time the use of an electrochemical cell as a source of S and Se dopant incorporation in $\text{Ga}_{1-x}\text{Al}_x\text{As}$.

II. EXPERIMENT

The experiments were carried out in a vacuum generators MB288 three-chamber MBE system using substrate cleaning and growth techniques described previously.⁶ Two multilayer structures were grown to investigate the incorporation behavior of sulfur in $\text{Ga}_{1-x}\text{Al}_x\text{As}$. The first was designed to explore a range of Al concentrations ($x = 0.03, 0.075, \text{ and } 0.15$) and growth temperatures for a fixed incident sulfur and arsenic flux. The second explored Al concentration and $\text{As}_4/\text{total group III flux}$ ratio at fixed sulfur flux and growth temperature. The sulfur flux used corresponded to an intended doping level of $n = 2 \times 10^{17} \text{ cm}^{-3}$.

The resulting layers were analyzed by secondary ion mass spectrometry (SIMS).⁸ The changes in Al concentration were used as markers in the SIMS depth profile for the expected response in the sulfur concentration. These complicated structures were unsuitable for accurate analysis by electrochemical $C-V$ profiling, but measurements on bulk layers doped between 1×10^{17} and $1 \times 10^{18} \text{ cm}^{-3}$ produced a factor of 2 agreement between the SIMS concentrations and electrical activity.

III. RESULTS

Figures 1 and 2 show the growth sequence and SIMS profile of the substrate temperature experiment, respectively. There is an overall curvature to the sulfur depth profile, which is believed to be due to an instrumental effect in the SIMS measurement (possibly caused by drifting of the mass peak corresponding to sulfur), but the changes stimulated by the steps in the aluminum profile and the growth temperature, and synchronous with them, are of most interest. At 550°C the addition of aluminum to GaAs to form $\text{Ga}_{0.85}\text{Al}_{0.15}\text{As}$ has no effect on the SIMS mass 34 or 32 sulfur signal. There are two possible effects that might be expected; a change in the rate of any sulfur loss and a change in the yield of ionized species from the SIMS process due to the change in the aluminum content of the $\text{Ga}_{1-x}\text{Al}_x\text{As}$ and the subsequent matrix effects. The lack of any observed change in the ion count rate argues strongly for both no change in sulfur loss and no change in SIMS yield for sulfur 32 and 34 species for $\text{Ga}_{1-x}\text{Al}_x\text{As}$ ($x < 0.15$). The alternative expla-

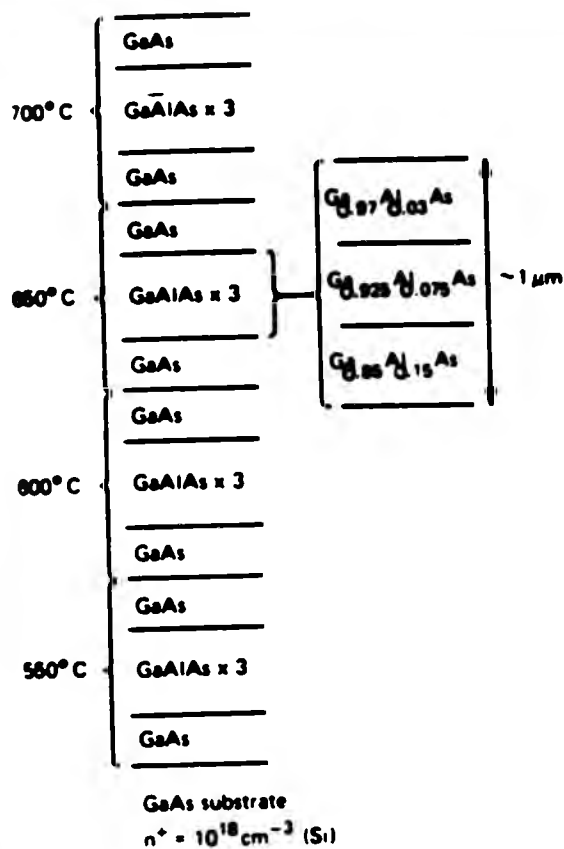


FIG. 1. Growth sequence for the study of sulfur incorporation in $\text{Ga}_{1-x}\text{Al}_x\text{As}$ as a function of x and growth temperature.

nation is that the change in any sulfur loss rate is exactly balanced by a change in the SIMS sensitivity as the elemental composition of the $\text{Ga}_{1-x}\text{Al}_x\text{As}$ is changed. This seems an unlikely coincidence.

In the GaAs region where the temperature was raised from 550 to 600 °C, a small sulfur loss is observed at the higher temperature. This loss is completely suppressed at the initiation of the $\text{Ga}_{0.85}\text{Al}_{0.15}\text{As}$ layer and remains undetectable down to the lowest aluminum concentration of $\text{Ga}_{0.97}\text{Al}_{0.03}\text{As}$. The loss reappears, however, in the GaAs layer grown before the temperature was raised to 650 °C. At

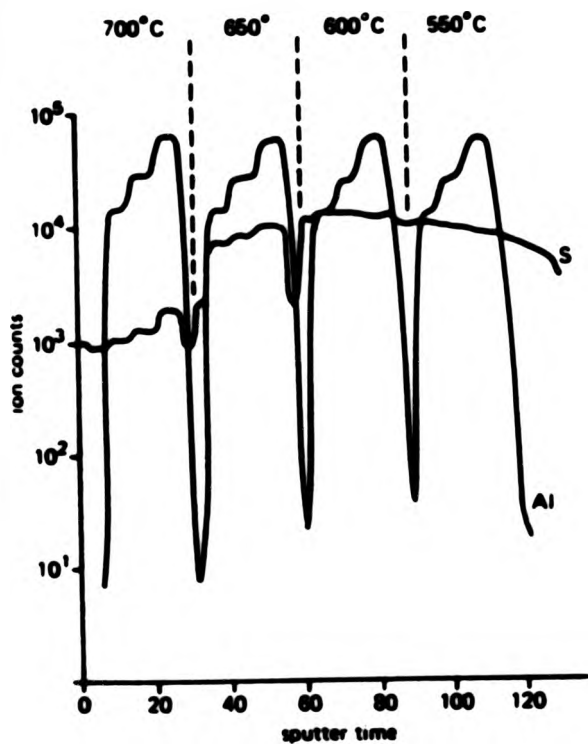


FIG. 2. SIMS depth profile of the structure illustrated in Fig. 1.

this higher temperature, the sulfur loss from the GaAs becomes much more significant but is again suppressed by the addition of aluminum to form $\text{Ga}_{0.85}\text{Al}_{0.15}\text{As}$. This time, however, there is still some residual loss from the $\text{Ga}_{1-x}\text{Al}_x\text{As}$ which becomes greater as x is reduced. Note again that the degree of sulfur loss is identical for the two GaAs layers grown at the same temperature on either side of the $\text{Ga}_{1-x}\text{Al}_x\text{As}$ layers. As the temperature is raised further to 700 °C, less than 10% of the sulfur remains in the GaAs. This figure may be smaller, as the background level for the SIMS machine is unknown. At this elevated temperature, the addition of Al results in a much smaller but still significant suppression of the sulfur loss. These results are summarized in Fig. 3, where the sulfur ion count signal is plotted against AlAs content for the different growth temperatures. At 550 °C the signal is independent of aluminum content corresponding to no loss. At 600 °C approximately 15% of the arriving sulfur is lost from GaAs, and this is reduced to an unmeasurable amount in the case of $\text{Ga}_{0.97}\text{Al}_{0.03}\text{As}$. At 650 °C the doping efficiency was of the order of 15% of the value at 550 °C for GaAs rising rapidly to 50% for $\text{Ga}_{0.97}\text{Al}_{0.03}\text{As}$ and more slowly to 75% for $\text{Ga}_{0.85}\text{Al}_{0.15}\text{As}$. At 700 °C, the suppression of sulfur loss was more gradual. The doping efficiency rose from of the order of 5% in GaAs to 15% in $\text{Ga}_{0.85}\text{Al}_{0.15}\text{As}$. This loss seems severe, but extrapolation suggests that the doping efficiency could rise towards 50% at these higher growth temperatures for the higher aluminum content of layers used in many devices such as lasers and HEMTs where $\text{Ga}_{0.7}\text{Al}_{0.3}\text{As}$ is commonly used.

Figures 4 and 5 show the grown structure and the corresponding SIMS profile for the investigation of the effects of the arsenic overpressure on sulfur loss from $\text{Ga}_{1-x}\text{Al}_x\text{As}$. A growth temperature of 650 °C was used, corresponding to a region where sulfur loss had been observed to take place from the previous experiment. Starting from the substrate, GaAs were grown at 600 °C under an arsenic overpressure

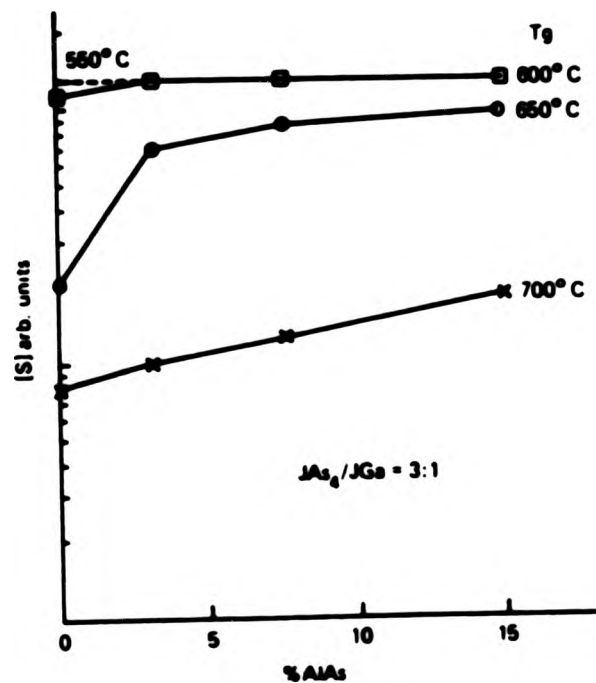


FIG. 3. Incorporated sulfur concentration in $\text{Ga}_{1-x}\text{Al}_x\text{As}$ as a function of x and growth temperature.

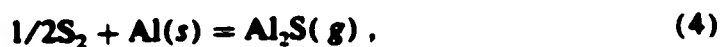
lies well to the right under all practical MBE conditions with equilibrium pressures $P(\text{Ga}_2\text{X})$ of 1.9, 3.7×10^{-4} , and 2×10^{-10} atm for $\text{X} = \text{S}, \text{Se},$ and Te , respectively.¹⁰ These pressures were calculated for an intended doping level of $2 \times 10^{18} \text{ cm}^{-3}$ and are not accessible in the MBE regime, except perhaps for Te , where fewer than one Te atom in a thousand are predicted to be incorporated. In addition, the equilibrium between the gaseous and solid forms of the gallium chalcogenides favors loss, and the reaction



also lies well to the right with an equilibrium pressure $P(\text{Ga}_2\text{S})$ of the order of 2×10^{-2} atm at 600°C .

In the above, formation of volatile Ga_2S is identified as a possible route for the loss of sulfur. The equilibrium with Ga_2S_3 is used to determine the stability of any Ga_2S so formed. However, it is not suggested that the sulfur is actually present in GaAs as Ga_2S_3 , except at the solubility limit, only that in considering the equilibria between the sulfide species, Ga_2S_3 is a convenient analogy for the sulfur environment for which thermochemical data are readily available. The calculations are therefore strictly only valid at the solubility limit (hence the choice of a high doping level), and at lower concentrations the activity of the Ga_2S_3 would be reduced. However, the predictions regarding the formation of Ga_2S are sufficiently strong that they remain valid over a wide range of doping. It should be emphasized that the sulfide equilibria are concerned with the loss route, and the actual incorporation reaction is still believed to be governed by Eq. (1) via the interaction with arsenic vacancies, notwithstanding the analogy with Ga_2S_3 .

The situation is somewhat different for the interaction of sulfur with AIAs. Firstly, there are at least three species of gaseous aluminum sulfide for which thermodynamic data are available: $\text{AlS}(g)$, Al_2S_2 , and $\text{Al}_2\text{S}(g)$. Although the following is described in terms of $\text{Al}_2\text{S}(g)$ for purposes of comparison with $\text{Ga}_2\text{S}(g)$, the other species produce very similar equilibrium pressures. Rewriting Eq. (2) for aluminum produces



and substitution of standard thermochemical data^{11,12} reveals that for a doping level of $2 \times 10^{18} \text{ cm}^{-3}$, the equilibrium Al_2S pressure is of the order of 8×10^{-12} atm at 600°C , rising to 2.3×10^{-10} atm at 750°C , which compares with the incident PS_2 of 6×10^{-14} atm.

Although these pressures are many orders of magnitude lower than for the gallium chalcogenides, they still predict a borderline doping efficiency of the order of less than 0.1%.

The key difference between the predicted behavior of sulfur incorporation in AIAs and GaAs becomes clear when the aluminum analogue of reaction (3) is considered. Whereas $\text{Ga}_2\text{S}_3(s)$ (sulfur in the GaAs lattice) is unstable with respect to the gaseous form $\text{Ga}_2\text{S}(g)$, Al_2S_3 (sulfur in the AIAs lattice) is predicted to be stable under MBE conditions of pressure and temperature. Hence, the reaction



lies substantially to the left with a predicted $P(\text{Al}_2\text{S})$ less than 1.71×10^{-18} atm at 600°C . This is much less than the

corresponding figure for $P(\text{Ga}_2\text{S})$ of 2×10^{-2} atm.

Although the values of the predicted pressures are not necessarily precise due to the uncertainty in the thermodynamic data and the simple two-term approximation used for the free-energy calculations, there is a clear difference in the predicted behavior for the relative stabilities of the gallium and aluminum chalcogenides. It seems likely, therefore, that the observed difference in the doping behavior between GaAs and $\text{Ga}_{1-x}\text{Al}_x\text{As}$ is strongly related to these relative stabilities.

Therefore, although the incorporation of sulfur into GaAs is only possible due to a kinetic barrier to the formation of volatile Ga_2S , the equivalent loss reactions are not favored for the interaction of sulfur with AIAs, and the behavior in this case may be explained from purely thermodynamic considerations without recourse to hindered kinetics.

In considering the behavior for $\text{Ga}_{1-x}\text{Al}_x\text{As}$, we may model the GaAs and AIAs components separately, since they have little heat of mixing and the activity coefficients for GaAs and AIAs are near unity.¹³ The aluminum activity therefore scales as x , the concentration of the AIAs component. However, the predicted difference in behavior is strong enough (16 orders of magnitude) that between 600 and 700°C sulfur should be incorporated even for $\text{Ga}_{1-x}\text{Al}_x\text{As}$ very dilute in AIAs ($x \ll 1$), where the activity of the Al is much reduced. However, our data suggest that something slightly different is happening in practice. At low AIAs concentrations ($< 10\%$), some sulfur continues to be lost. It is assumed that this loss occurs as Ga_2S and, of course, in the limit of zero aluminum content this is indeed so. High crystal quality implies significant atom mobility in the growing surface layer, and there will therefore be competition for the sulfur atoms in this layer between the free aluminum and gallium atoms. Although the reaction is heavily in favor of bonding to the aluminum in the lattice (leading to incorporation), for low Al concentrations there is a higher probability that a sulfur atom will encounter two Ga atoms with the subsequent options of incorporation or kinetically hindered desorption as Ga_2S in the same way as for GaAs . Higher overpressures of As_4 therefore increase the sulfur doping efficiency by suppressing the loss reaction through control of the surface arsenic and hence gallium concentrations. The balance between the various thermodynamically allowed reaction pathways is critically dependent on the details of the surface kinetics. A simple model, requiring a sulfur atom to have two Ga-atom nearest neighbors for Ga_2S formation, would predict an incorporation efficiency proportional to $1 - (1 - x)^2$, where x is the AIAs mole fraction. This has approximately the correct form but takes no account of surface diffusion. Further modelling would require a wider experimental database to elucidate the kinetics in more detail, but the situation for $\text{Ga}_{1-x}\text{Al}_x\text{As}$ is clearly intermediate between GaAs and AIAs.

For the case of selenium, we have shown that it exhibits an excess of stability over sulfur at elevated growth temperatures when used to dope MBE GaAs .¹⁰ This is believed to be due to a kinetic barrier to the formation of $\text{Ga}_2\text{Se}(g)$ in the same way as for sulfur. In fact, $\text{Ga}_2\text{Se}_3(s)$ is predicted to be less stable with respect to $\text{Ga}_2\text{Se}(g)$ under MBE conditions

than $\text{Ga}_2\text{S}_3(s)$ is with respect to $\text{Ga}_2\text{S}(g)$, so the apparent enhanced stability remains largely unexplained.

In considering the incorporation of selenium in AIAs, calculation shows that Al_2Se_3 (selenium in the AIAs lattice) is barely stable at 600 °C and at $2 \times 10^{18} \text{ cm}^{-3}$ doping, and significant decomposition to volatile Al_2Se is expected. Thus, for the reaction



the equilibrium pressure of Al_2Se is predicted to be of the order of $3.1 \times 10^{-14} \text{ atm}$, comparable with the incident selenium flux ($P_{\text{Se}_2} = 6 \times 10^{-14} \text{ atm}$). The successful incorporation of Se in $\text{Ga}_{1-x}\text{Al}_x\text{As}$ alloys therefore probably depends on the existence of kinetic barriers in the same way as for incorporation into GaAs.

Preliminary results indicate that selenium may be incorporated successfully into $\text{Ga}_{0.75}\text{Al}_{0.25}\text{As}$ at GaAs growth temperatures ($\sim 600 \text{ °C}$) in HEMT structures. However, data at higher temperatures and other compositions are limited, but indicate that incorporation may be less reliable. Unfortunately, we are unsure whether this was due to the chemical effects predicted above or simply a deterioration in the electrochemical selenium cell which failed while this was being investigated.

V. CONCLUSIONS

An electrochemical cell has been used to dope $\text{Ga}_{1-x}\text{Al}_x\text{As}$ successfully with sulfur and selenium. At low temperatures, $< 600 \text{ °C}$, the behavior is facile, as for GaAs. Above this temperature, loss of chalcogen dopant was observed and is believed to be due to the formation of the volatile gallium chalcogenides Ga_2S and Ga_2Se , which are the stable species under MBE conditions. Successful doping of GaAs is therefore believed to be due to the existence of a kinetic barrier to their formation, possibly mediated by the surface gallium population.^{7,10}

For sulfur doping of AIAs, simple thermodynamic calculations predict that the volatile aluminum sulfides are unstable with respect to the solid form Al_2S_3 (sulfur in the AIAs lattice) under MBE conditions between 600 and 700 °C. The dopant loss route postulated for sulfur doping in GaAs is therefore not favored for AIAs. The experimental observations reveal an enhanced stability of sulfur in $\text{Ga}_{1-x}\text{Al}_x\text{As}$ ($x < 0.15$), where the loss is increasingly suppressed at higher values of x . This is interpreted in terms of competition for sulfur between mobile Ga and Al surface atoms with the options of desorption as Ga_2S or incorporation in the AIAs lattice.

The calculations for selenium show a less clear difference between Se incorporation in GaAs and AIAs. In particular, Al_2Se_3 is predicted to have a borderline stability under MBE conditions, and the behavior for $\text{Ga}_{1-x}\text{Al}_x\text{As}$ may not be very different to that for GaAs. However, further work is needed in this area.

For growth of $\text{Ga}_{1-x}\text{Al}_x\text{As}$ at elevated temperatures, sulfur would appear to be the preferred chalcogen dopant, while for devices such as HEMTs, where GaAs growth temperatures are more usual,¹⁴ both have been used successfully in this laboratory.

In cases where the chalcogen dopants are chosen for their nonamphoteric behavior in preference to group IV dopants such as silicon, in the antimony-containing III-V alloys, for example,¹⁵ the above comments regarding the choice of chalcogen dopant for aluminum-containing alloys may be particularly relevant.

ACKNOWLEDGMENT

Acknowledgment is made to the Director of Research, British Telecom, for permission to publish this paper.

APPENDIX

Thermodynamic calculations

In this appendix, the reactions considered are listed together with the pressures predicted. The method of calculation is already covered in the literature.^{7,9,10}

The conditions assumed for the calculations are as follows:

- (i) Growth temperature = 600 °C for comparison with typical GaAs growth temperatures;
- (ii) $P_{\text{X}_2} = 6 \times 10^{-14} \text{ atm}$ ($\text{X} = \text{S, Se}$) for $2 \times 10^{18} \text{ cm}^{-3}$ doping;
- (iii) $[\text{M}] \sim 1$ [$\text{M} = \text{Ga}(l), \text{Al}(s)$] since MBE growth takes place near the liquidus;
- (iv) $[\text{M}_2\text{X}_3] \sim 1$: The doping level of $2 \times 10^{18} \text{ cm}^{-3}$ is assumed to be close to the solid solubility of the chalcogen dopant in GaAs and AIAs.

These conditions were chosen since they allow the activities of the solid components to be approximated to unity and in some respects are a calculational device, since practical growth under these conditions would almost certainly produce poor morphology material. However, they do allow comparisons to be drawn between the different material systems. It should be emphasized that the calculated values are order-of-magnitude estimates only, relying as they do on a simple two-term evaluation of the free-energy change.

Gallium sulfide reactions

- (1) $2\text{Ga}(l) + 1/2\text{S}_2(g) = \text{Ga}_2\text{S}(g) \dots\dots P_{\text{Ga}_2\text{S}} = 7 \text{ atm.}$
- (2) $2\text{Ga}(l) + 3/2\text{S}_2(g) = \text{Ga}_2\text{S}_3(s) \dots\dots P_{\text{S}_2} = 4.5 \times 10^{-19} \text{ atm.}$
- (3) $\text{Ga}_2\text{S}(g) + \text{S}_2(g) = \text{Ga}_2\text{S}_3(s) \dots\dots P_{\text{Ga}_2\text{S}} = 8.5 \times 10^{-19} \text{ atm.}$
- (4) $4\text{Ga}(l) + \text{Ga}_2\text{S}_3(s) = 3\text{Ga}_2\text{S}(g) \dots\dots P_{\text{Ga}_2\text{S}} = 2 \times 10^{-2} \text{ atm.}$

Gallium selenide reactions

- (5) $2\text{Ga}(l) + 1/2\text{Se}_2(g) = \text{Ga}_2\text{Se}(g) \dots\dots P_{\text{Ga}_2\text{Se}} = 4.4 \times 10^{-3} \text{ atm.}$

- (6) $2\text{Ga}(l) + 3/2\text{Se}_2(g) = \text{Ga}_2\text{Se}_3(s) \dots P_{\text{Se}_2} = 4.6 \times 10^{-16} \text{ atm.}$
 (7) $\text{Ga}_2\text{Se}(g) + \text{Se}_2(g) = \text{Ga}_2\text{Se}_3(s) \dots P_{\text{Ga}_2\text{Se}} = 2.9 \times 10^{-6} \text{ atm.}$
 (8) $4\text{Ga}(l) + \text{Ga}_2\text{Se}_3(s) = 3\text{Ga}_2\text{Se}(g) \dots P_{\text{Ga}_2\text{Se}} = 4.1 \times 10^{-4} \text{ atm.}$

Aluminum sulfide reactions

- (9) $2\text{Al}(s) + 1/2\text{S}_2(g) = \text{Al}_2\text{S}(g) \dots P_{\text{Al}_2\text{S}} = 8 \times 10^{-12} \text{ atm.}$
 (10) $2\text{Al}(s) + 3/2\text{S}_2(g) = \text{Al}_2\text{S}_3(s) \dots P_{\text{S}_2} = 2.4 \times 10^{-27} \text{ atm.}$
 (11) $\text{Al}_2\text{S}(g) + \text{S}_2(g) = \text{Al}_2\text{S}_3(s) \dots P_{\text{Al}_2\text{S}} = 6.5 \times 10^{-32} \text{ atm.}$
 (12) $4\text{Al}(s) + \text{Al}_2\text{S}_3(s) = 3\text{Al}_2\text{S}(g) \dots P_{\text{Al}_2\text{S}} = 1.7 \times 10^{-18} \text{ atm.}$

Aluminum selenide reactions

- (13) $2\text{Al}(s) + 1/2\text{Se}_2(g) = \text{Al}_2\text{Se}(g) \dots P_{\text{Al}_2\text{Se}} = 4.4 \times 10^{-3} \text{ atm.}$
 (14) $2\text{Al}(s) + 3/2\text{Se}_2(g) = \text{Al}_2\text{Se}_3(s) \dots P_{\text{Se}_2} = 2.1 \times 10^{-22} \text{ atm.}$
 (15) $\text{Al}_2\text{Se}(g) + \text{Se}_2(g) = \text{Al}_2\text{Se}_3(s) \dots P_{\text{Al}_2\text{Se}} = 1.1 \times 10^{-22} \text{ atm.}$
 (16) $4\text{Al}(s) + \text{Al}_2\text{Se}_3(s) = 3\text{Al}_2\text{Se}(g) \dots P_{\text{Al}_2\text{Se}} = 3.1 \times 10^{-14} \text{ atm.}$

¹C. E. C. Wood, *Appl. Phys. Lett.* **33**, 770 (1978).

²D. M. Collins, *Appl. Phys. Lett.* **35**, 67 (1979).

³Jiang De-Shang, Y. Makita, K. Ploog, and H. J. Queisser, *J. Appl. Phys.* **53**, 999 (1982).

⁴K. Ploog, A. Fischer, and H. Kunzel, *Appl. Phys.* **18**, 353 (1979).

⁵D. M. Collins, J. N. Miller, Y. G. Chai, and R. Chow, *J. Appl. Phys.* **53**, 3010 (1982).

⁶G. J. Davies, D. A. Andrews, and R. Heckingbottom, *J. Appl. Phys.* **52**, 7214 (1981).

⁷D. A. Andrews, R. Heckingbottom, and G. J. Davies, *J. Appl. Phys.* **54**, 4421 (1983).

⁸SIMS analysis performed by Loughborough Consultants, Ltd. United Kingdom.

⁹R. Heckingbottom, C. J. Todd, and G. J. Davies, *J. Electrochem Soc.* **127**,

444 (1980).

¹⁰D. A. Andrews, M. Y. Kong, R. Heckingbottom, and G. J. Davies, *J. Appl. Phys.* **55**, 841 (1984).

¹¹K. C. Mills, *Thermodynamic Data for Inorganic S, Se, and Te Compounds* (Butterworths, London, 1974).

¹²O. Kubaschewski and C. B. Alcock, *Metallurgical Thermochemistry*, 5th ed. (Pergamon, London, 1979).

¹³R. Heckingbottom, Proceedings of the Third International Conference on MBE, San Francisco, CA, 1984, in *J. Vac. Sci. Technol. B* **3**, 572 (1985).

¹⁴G. Weimann and W. Schlapp, *Appl. Phys. Lett.* **46**, 411 (1985).

¹⁵T. M. Kerr, T. D. McLean, D. I. Westwood, J. D. Medland, and C. E. C. Wood, Presented at the 3rd European Workshop on MBE at Aussois, France, March, 1985.

LOW-LOSS OPTICAL WAVEGUIDES IN MBE-GROWN GaAs/GaAlAs HETEROSTRUCTURES

A.J.N. HOUGHTON, D.A. ANDREWS, G.J. DAVIES and S. RITCHIE

British Telecom Research Labs, Martlesham Heath, Ipswich IP5 7RE, UK

Received 25 April 1983

GaAs/Ga_{0.96}Al_{0.04}As epitaxial heterostructure material grown by MBE has been used to fabricate low-loss single-mode optical waveguides. The waveguides are rib structures, formed by ion-beam-milling, and have measured propagation losses at $\lambda = 1.15 \mu\text{m}$ as low as 1.9 dB cm^{-1} .

1. Introduction

There is increasing interest in guided wave optical devices, as a result of the expansion in the use of optical fibres in telecommunication systems and cable TV networks. Devices such as directional coupler switches, phase modulators and interferometric amplitude modulators can be made in both semiconductor materials and dielectrics but a particular attraction of semiconductor devices is their potential for monolithic integration with light sources (lasers) and detectors. However, discrete semiconductor devices have a reputation for high optical loss, compared to similar dielectric devices. This loss has been attributed in part to the presence of free carriers [1] and it has been argued that in high purity low-doped semiconductor material the waveguide losses could be comparable to those in dielectric waveguides. We report here the fabrication of single-mode rib waveguides in GaAs/GaAlAs heterostructures grown by molecular beam epitaxy (MBE), which is a growth technique highly suited to integrated optics applications because it can provide large area multilayer heterostructures with precise dimensional and compositional control. These guides have lower optical propagation loss than any two-dimensional semiconductor waveguides hitherto reported. The guide structures are similar to those used previously for directional couplers and other devices [1].

2. Experimental details

The material growth was carried out in a Vacuum Generators MB288, three chamber MBE system which has been described previously [2]. The n⁺ GaAs substrates were Si doped. Substrate preparation was carried out immediately before loading the substrate into the MBE system using chemical treatments similar to those described in the literature [2]. After loading, the substrates were outgassed in the preparation chamber at 720 K until the pressure in that chamber fell to $< 1 \times 10^{-9}$ torr. The substrates were then transferred to the growth chamber, where they were heated to 880 K in an arsenic flux to absorb the surface oxide layer. This provided an As-stabilized surface, reconstructed to give a streaked C(2 × 4) RHEED pattern. This "in-situ" cleaning procedure left the GaAs surface free of C and O contamination, within the limits of sensitivity of Auger Electron Spectroscopy (AES).

The waveguide structure consists of GaAs and Ga_{0.96}Al_{0.04}As layers grown in the following sequence (fig. 1). A 1.2 μm thick n⁺ GaAs buffer layer, $N_D - N_A = 8 \times 10^{17} \text{ cm}^{-3}$, was grown first, followed by 2.3 μm thick Ga_{0.96}Al_{0.04}As, $N_D - N_A = 5 \times 10^{17} \text{ cm}^{-3}$. On top of these was grown the guiding medium which was low-doped GaAs, ($n \approx 1 \times 10^{15} \text{ cm}^{-3}$), 1.5 μm thick.

The substrate temperature was kept at 873 K for the GaAs layers and 963 K for the GaAlAs layers whilst the growth rate was $2 \mu\text{m hour}^{-1}$ for GaAs. Layer thicknesses and doping were measured using an

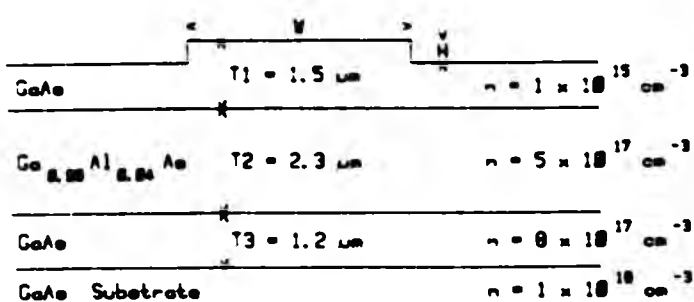


Fig. 1. Material layer structure: thicknesses and doping.

Electrochemical Profile Plotter (Polaron Ltd). Al percentages were measured by both photovoltaic and cathodoluminescence methods, and found to be 4% by both methods.

In all cases the layers were doped with sulphur, generated using an electrochemical cell. This cell which utilizes the galvanic cell Pt/Ag/AgI/Ag₂S(or SE)/Pt, has been used to produce S and Se for dopant incorporation in GaAs and GaAlAs [2]. A change in EMF changes the gas phase pressure of sulphur or selenium over the cell and hence produces a change in doping level. The main advantage of this cell is its fast time constant, which was shown to be ~1 s.

The rib waveguides were fabricated by defining photoresist stripes of widths between 2 μm and 15 μm on the semiconductor material. The ribs were then formed by ion-beam-milling (Ar⁺, 500 eV, normal incidence). The waveguide ends were cleaved and

guiding was observed by end-fire coupling of a TE-polarised He-Ne laser beam ($\lambda = 1.15 \mu\text{m}$) through X 45 microscope objectives (NA = 0.54) into the rib guides. The output laser beam was detected by an IR TV camera and, for loss measurements, a Ge photodiode.

3. Waveguide measurements

Loss measurements were made using a "sample-in, sample-out" procedure. Conventionally, such measurements are made by sequentially cleaving one sample to a series of shorter lengths. However, it was found, for the low-loss guides reported here, that variations in coupling efficiency between different guides could be larger than the propagation loss. The procedure adopted was therefore to make a series of measurements on very short guides (for which the propagation loss could be neglected) and on the longest guides available, for which the propagation loss was a maximum.

Loss measurements on two samples are shown in table 1. Sample A comprised several rib guides (fig. 1), width $W = 5 \mu\text{m}$ with a rib height of 0.4 μm. All guides were single-mode. Sample B had stripes of 2, 4, 6 and 15 μm width, with a rib height H of 0.2 μm. The 2 μm and 4 μm stripes were single moded (losses shown in table 1). The 6 μm stripes had two lateral modes and

Table 1
Insertion loss measurements [loss in dB]

Sample A (stripewidth 5 μm)				Sample B (stripe width 2, 4 μm)			
Guide length	1.	3.8		Guide length	1.	7.4	
= 0.75 mm	2.	5.4	4.1 AV	= 1.0 mm	2.	7.8	7.7 AV
	3.	3.4			3.	7.8	
Guide length	1.	5.8		Guide length	1.	10.2	
= 7.75 mm	2.	5.7	5.6 AV	= 13.5 mm	2.	10.0	10.1 AV
	3.	5.4			3.	10.2	
Propagation loss				Propagation loss			
= $\frac{5.6 - 4.1}{0.775 - 0.075} \text{ dB cm}^{-1}$				= $\frac{10.1 - 7.7}{1.35 - 0.10} \text{ dB cm}^{-1}$			
= 2.1 dB cm ⁻¹				= 1.9 dB cm ⁻¹			

3 or 4 modes were observed in the 15 μm stripes. The mode spot size (intensity) was 10 $\mu\text{m} \times 3 \mu\text{m}$, to the $1/e^2$ points, for the 5 μm wide ribs. To improve matching to this elliptical mode profile, the input beam profile was tailored by passing it through a slit.

The total measured insertion loss can be divided into coupling loss from mismatch between the guided mode profile and incident laser beam profile, reflection losses at the air-GaAs interfaces, and propagation loss. For a plane wave incident on an air-GaAs interface ($n = 3.45$ at 1.15 μm), the reflection coefficient is ~ 1.5 dB at each end of the guide. For short guides, multiple reflections at the interfaces need to be taken into account; the effective loss at the output face may be less than 1.5 dB and as low as ~ 1.1 dB, depending on the relative phase of the reflected light. This loss can in principle be reduced to a very low value by evaporating an Al_2O_3 dielectric layer onto the cleaved facets to form a $\lambda/4$ anti-reflection coating.

For sample A in table 1 it can be seen that for short guides, most of the measured insertion loss can be accounted for by reflection loss, suggesting that end-fire coupling efficiencies $> 80\%$ were achieved. These high coupling efficiencies reinforce the conclusions of recent studies of coupling between fibres and LiNbO_3 waveguides [3] that under the right circumstances there is no fundamental barrier to achieving very efficient coupling to planar guided wave devices. It was found in this work, however, that careful positioning of the lenses relative to guides was required to achieve high coupling efficiencies. The variation in insertion loss seen between different guides could be in most cases attributed to the quality of the cleaved facets.

Table 1 also shows that we have been able to fabricate waveguides of length up to 13.5 mm, with measured losses as low as 1.9 dB cm^{-1} . A series of careful measurements consistently produced values of propagation loss in the range 1.7 dB cm^{-1} to 2.1 dB cm^{-1} . The lowest loss measurements previously reported for semiconductor waveguides is 2.3 dB cm^{-1} , for a hybrid

oxide-GaAs epitaxial structure grown by VPE [4]. The results presented here are of especial interest because they are on MBE-grown material. This growth technique is very suitable for growing multilayer structures, for example for optimised directional coupler designs. Preliminary measurements on three-layer structures, with $\sim 0.5 \mu\text{m}$ of GaAlAs ($\text{Al} \approx 20\%$) as the top layer, indicate that absorption due to metal electrodes on top of rib structures can also be substantially reduced.

We expect that in integrated optical circuits, devices and interconnecting waveguides will typically have lengths in the range 1 mm to 5 mm. The propagation loss of $< 2 \text{ dB cm}^{-1}$ demonstrated here, indicates that device losses of < 1 dB are thus attainable in semiconductors.

Acknowledgements

We wish to thank R.M. Redstall and B. Wakefield for characterisation of the grown material and P.J. Smith and P.N. Woolnough for provision of ion milling facilities. Acknowledgement is made to the Director of British Telecom Research Labs for permission to publish this letter.

References

- [1] A.J.N. Houghton, Proc. European Conf. on Optical communication, ECOC '82, Cannes, Sept. 1982, pp. 226-230.
- [2] G.J. Davies, D.A. Andrews and R. Heckingbottom, J. Appl. Phys. 52 (1981) 7214.
- [3] R.C. Alferness, V.R. Ramaswamy, S.K. Korothy, M.D. Divino and L.L. Bull. IEEE J. Quantum Electron. QE-18 (1982) 1807.
- [4] F.J. Leonberger, C.O. Bozler, R.W. McClelland and I. Melngailis, Appl. Phys. Lett. 38 (1982) 313.

ELECTRON TRANSPORT ACROSS DEPLETED REGION OF A FINE-GATE GaAs : AlGaAs HETEROJUNCTION FET

Indexing terms Semiconductor devices and materials, Electron transport

The low-temperature characteristics of a depleted GaAs : AlGaAs heterojunction FET with gate length of 1000 Å and width 10 µm show that the current is initially space-charge-limited. The onset of velocity saturation is observed as the source-drain bias is increased. The structure in the differential of resistance is attributed to the emission of optic phonons by hot electrons.

We have fabricated GaAs : AlGaAs heterojunction FETs with gate lengths of 1000 Å. The heterojunction was grown by molecular beam epitaxy and consisted of 1500 Å AlGaAs grown on 1 µm of GaAs on a semi-insulating substrate. The initial structure was a 100 µm × 10 µm mesa defined by optical lithography and wet etching with source and drain contacts provided by Au : Ge : Ni diffusions. A 30 kV electron beam was used to expose a fine line in the PMMA resist, and AuPd gate metal was deposited by lift-off. Analysis of Shubnikov-de Haas oscillations yielded a carrier concentration of $4 \times 10^{11} \text{ cm}^{-2}$ and a mobility of $200000 \text{ cm}^2 \text{ V}^{-1} \text{ s}^{-1}$. The resistance between source and drain was 800 Ω at 4.2 K in the absence of an applied gate voltage, and the application of a negative gate voltage produced a strong increase in resistance to hundreds of kilohms, indicating that the portion of channel beneath the gate was totally dominating the device conductivity. We will therefore assume in our discussion that this portion of the device is the active element. At 4.2 K the application of a small source-drain voltage across a highly

depleted channel produced a rapid drop in resistance as shown in Fig. 1. The I/V relation in Fig. 2 shows the low-voltage nonohmic behaviour passing into an ohmic region. The low-voltage portion is shown in detail in Fig. 3 in the form $I \propto V^2$, and it is seen that a linear relation is found which deviates at higher voltages. This V^2 dependence indicates that space-charge-limited conduction occurs because of the injected charge dominating the characteristic.

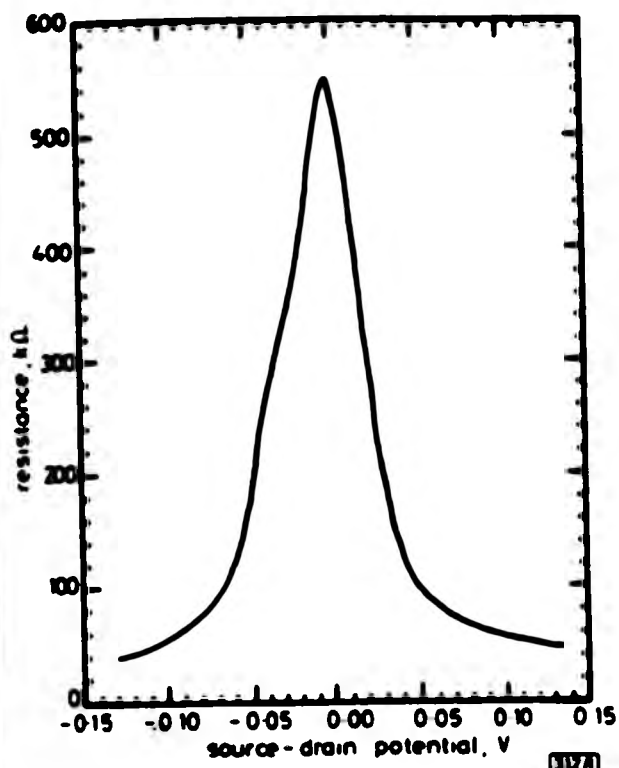


Fig. 1 Channel resistance as a function of source-drain voltage $V_g = -1.5$ V

The expression for the space-charge-limited current is¹

$$I = \frac{9}{4} \epsilon_0 A \mu \frac{V^2}{d^3}$$

where μ is the channel mobility, d the channel length, ϵ the dielectric constant of GaAs, ϵ_0 the permittivity of free space and A is the cross-sectional area of the channel. The linear region of Fig. 3 gives a value of $\mu/d^3 = 160 \times 10^{17} \text{ m}^{-1} \text{ V}^{-1} \text{ s}^{-1}$. We note that the $I \propto V^2$ regime is dependent on a constant mobility and that an increase in mobility with electron temperature would explain the deviation in Fig. 3. This increase is expected as we estimate the carrier concentration to be $\approx 10^{18} \text{ cm}^{-2}$, and the electron gas is non-degenerate at these very small values. Hence the mobility is temperature-dependent, being determined by scattering from impurities in the AlGaAs and at the AlGaAs-GaAs interface.

Returning to Fig. 2, we associate the ohmic regime with the onset of velocity saturation; here only the injected carrier concentration varies with V and the electron velocity is independent of voltage. Assuming that the saturation drift velocity is

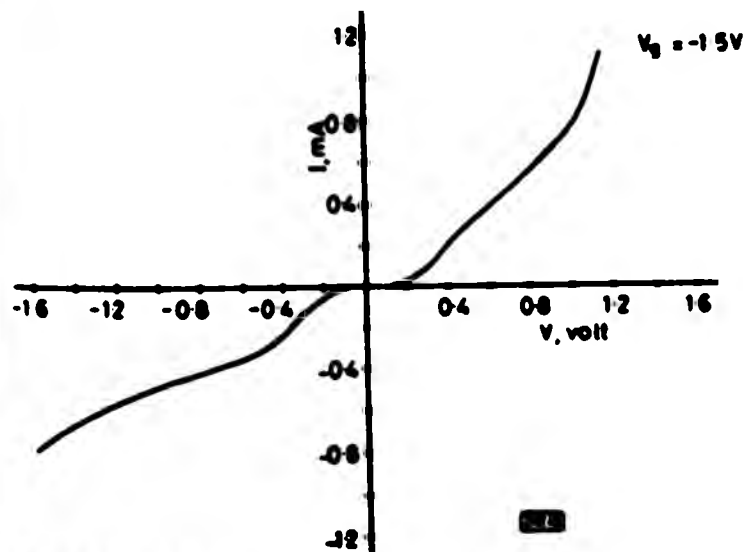


Fig. 2 Current-voltage characteristics of a strongly depleted channel

$2 \times 10^7 \text{ cm s}^{-1}$ and using the value of μ/d^3 obtained from Fig. 3, we calculate $\mu = 1000 \text{ cm}^2 \text{ V}^{-1} \text{ s}^{-1}$ and $d = 1800 \text{ \AA}$.

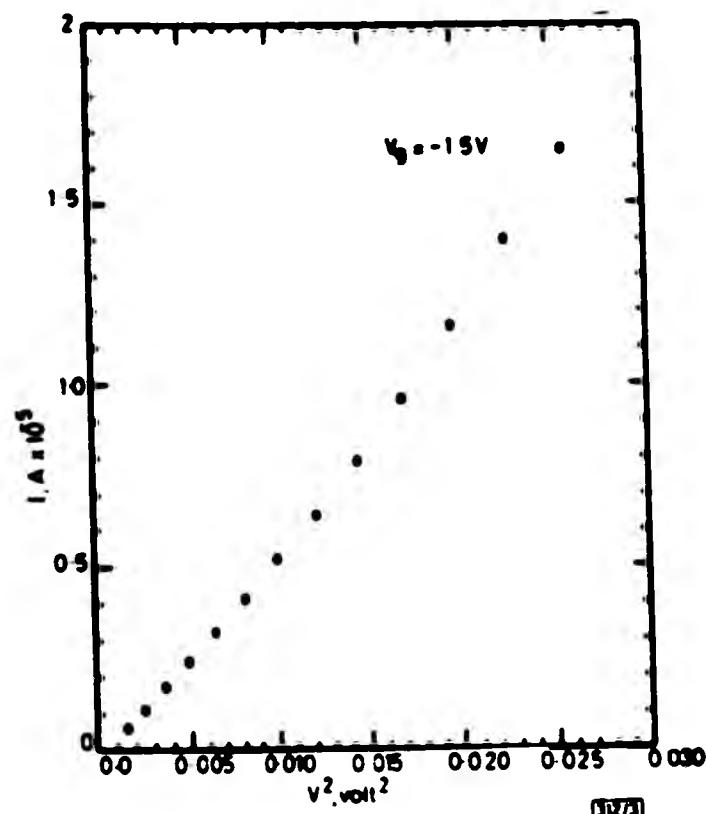


Fig. 3 Low-voltage results shown in detail in the form $I \propto V^2$

The increase in d above the gate length of 1000 \AA arises from the fringing field of the gate across the 1500 \AA of AlGaAs. The value of the mobility is enormously reduced compared to the initial value of $2 \times 10^5 \text{ cm}^2 \text{ V}^{-1} \text{ s}^{-1}$, which we attribute to the lack of carrier screening of charges within the AlGaAs. As a final comment on Fig. 2, we suggest that the rise in current at

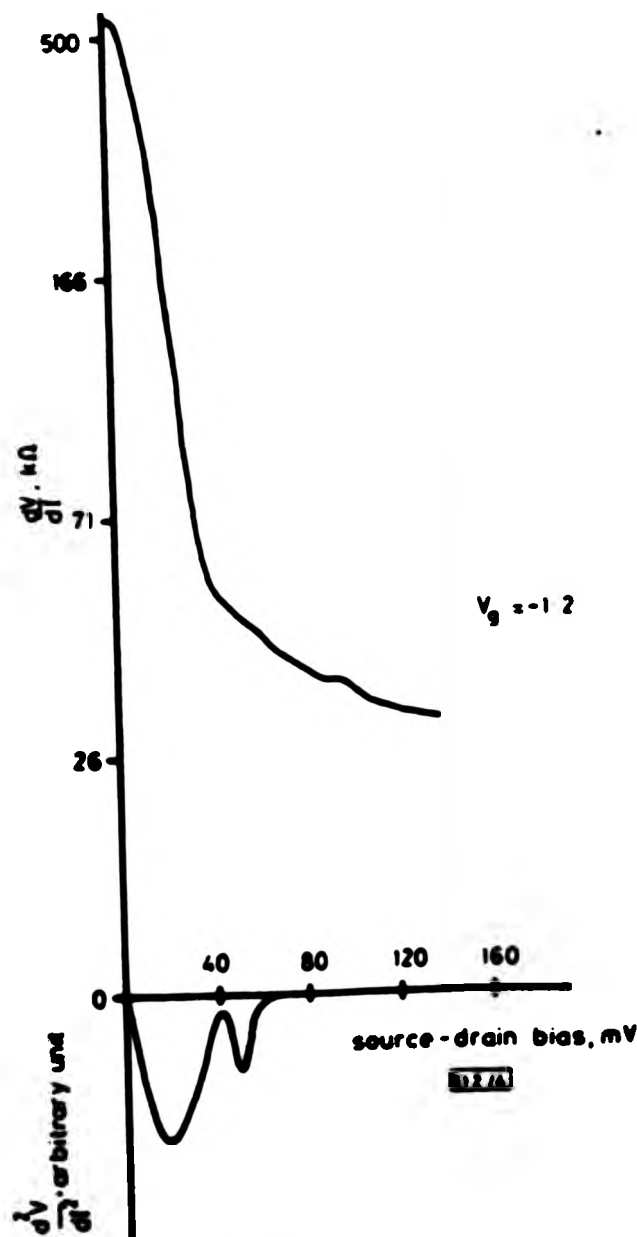


Fig. 4 First and second differential of resistance as a function of source-drain bias

the highest values of voltage may be due to carrier flow moving away from the interface and, possibly, impact ionisation of electrons in traps in the GaAs or AlGaAs.

We have measured the first and second differential of resistance as a function of source-drain voltage, and this is shown in Fig. 4. The principal feature is the structure at 40 mV and 85 mV. We suggest that this corresponds to phonon emission, as has been observed earlier in point-contact spectroscopy² and modulated structures.³ The structure arises because some electrons do not lose energy until the optic phonon threshold (36 meV) is reached; they then emit an optic phonon, and the consequent reduction in their energy corresponds to a reduced contribution to the current. However, we cannot exclude the possibility that a number of electrons have travelled across ballistically without suffering elastic collisions. The increase in energy of the structure, approximately 10% above the LO phonon energy, may be due to a small voltage drop near the ends of the channel where electron-electron scattering prevents carrier heating. We could not observe structure at an energy of three times the LO phonon energy as has been seen in other systems.³

Acknowledgments: This work was supported by the UK Science & Engineering Research Council, and T. J. Thornton acknowledges a CASE studentship with GEC.

T. J. THORNTON
M. PEPPER*
H. AHMED

17th January 1986

*Camdenish Laboratory
Cambridge, CB3 0HE, United Kingdom*

D. ANDREWS
G. J. DAVIES

*British Telecom Research Centre
Martlesham Heath, Ipswich, IPS 7RE, United Kingdom*

* Also with GEC Hirst Research Centre, Wembley, Middx. HA9 7PP, United Kingdom

References

- 1 MOTT, N. F., and GURNEY, R. W.: 'Electronic processes in ionic crystals' (Oxford University Press, 1940), pp. 167-172
- 2 PEPPER, M.: 'Ballistic injection of electrons in metal-semiconductor junctions: I. Phonon spectroscopy and impurity enhanced inelastic scattering in n⁺ silicon', *J. Phys. C: Solid-State Phys.*, 1980, 13, pp. L709-L716
- 3 HICKMOTT, T. W., SOLOMON, P. M., FANG, F. F., STERN, F., FISCHER, R., and MORKOC, H.: 'Sequential single-phonon emission in GaAs-AlGaAs tunnel junctions', *Phys. Rev. Lett.*, 1984, 52, pp. 2053-2056
- 4 PEPPER, M.: 'Ballistic injection of electrons in metal semiconductor junctions: II. Phonon spectroscopy of aluminium', *J. Phys. C: Solid-State Phys.*, 1980, 13, pp. L717-L719

One-Dimensional Conduction in the 2D Electron Gas of a GaAs-AlGaAs Heterojunction

T. J. Thornton

Cavendish Laboratory, Cambridge CB3 0HE, United Kingdom

M. Pepper

Cavendish Laboratory, Cambridge CB3 0HE, United Kingdom, and GEC Hirst Research Centre, Wembley, Middlesex, United Kingdom

H. Ahmed

Cavendish Laboratory, Cambridge CB3 0HE, United Kingdom

and

D. Andrews and G. J. Davies

British Telecom Research Centre, Martlesham, Ipswich, United Kingdom

(Received 17 September 1985)

We present results on the transport properties of the 2D electron gas in a narrow channel formed by the split gate of a GaAs-AlGaAs heterojunction field-effect transistor. There are both quantum-interference and interaction corrections to the conductivity. We find that the temperature dependence of the phase relaxation length is in agreement with a recent theory based on scattering by electromagnetic fluctuations. Beyond the regime of quantum interference the conductivity varies with temperature as T^2 .

PACS numbers: 71.55.Jv, 72.20.Jv, 73.40.Lq

There has recently been considerable experimental interest in one-dimensional quantum interference (weak localization) and interaction effects.¹⁻⁵ Quantum-interference corrections in a two-dimensional electron gas become one dimensional when the phase coherence length, L_0 , exceeds the width of the sample, W . The correction, expressed as a conductance per unit length δG , is given by

$$\delta G = -e^2 L_0 / \pi \hbar. \quad (1)$$

When L_0 exceeds the localization length diffusive behavior will not occur as carriers are strongly localized⁶ and conduction will proceed by hopping. If the overlap of electron states is small then transport is due to (phonon-assisted) variable-range hopping.

Thouless⁷ suggested that if the overlap is significant the hops are caused by electron-electron collisions. The diffusion coefficient, D , is given by $L_0^2 / 12\tau_{in}$ where L_0 is the localization length and τ_{in} the electron-electron scattering time. Therefore the conductivity will vary as τ_{in}^{-1} . It is well known that if $k_F l > 1$ the Landau-Baber T^2 behavior of τ_{in} is augmented by diffusion corrections with a weaker dependence on temperature. However, if electrons are strongly localized then these corrections may not apply and τ_{in} will vary as T^{-2} . Recently it has been suggested⁸ that if the localization is one dimensional, a phonon-assisted hopping process could give a conductivity varying as T^2 , provided the energy difference between hopping sites is less than the thermal energy

kT .

Negative magnetoresistance is found in the regime of quantum interference; in one dimension the theoretical relation is⁹

$$\delta G(B) = \frac{-e^2}{\pi \hbar} \left(\frac{1}{L_0^2} + \frac{W^2}{3L_c^4} \right)^{-1/2}, \quad (2)$$

where W is the width of the conducting region and L_c is the cyclotron radius, $(\hbar/eB)^{1/2}$. Equation (2) arises from the change in the effective length scale and is due to the perturbation of the wave function by the magnetic field; it is only valid for $L_c > W$. Significant decrease of L_c below W results in 2D localization behavior; analogous 3D and 2D behavior has been discussed elsewhere,¹⁰ as has the behavior of $G(B)$ in the presence of spin-orbit coupling and spin-flip scattering.¹¹

In addition to quantum interference the electron-electron interaction produces a conductivity correction which is one dimensional when $(\hbar D/kT)^{1/2} > W$, where k is Boltzmann's constant. The interaction correction to the conductivity can be written

$$\delta G = (-e^2 g_{1D} / \pi \hbar) (\hbar D / 2kT)^{1/2}, \quad (3)$$

where g_{1D} is the 1D interaction parameter and D is the Boltzmann value of diffusion coefficient.^{12,13} To first order the quantum-interference and interaction corrections are additive¹⁴ when both are weak.

In this Letter we present results on one-dimensional

conduction in narrow conducting channels in GaAs-AlGaAs heterojunctions. We find both the interference and interaction corrections together and, from the negative magnetoresistance, we confirm the existence of a recently predicted 1D electron-electron scattering mechanism.¹⁵⁻¹⁷ Further narrowing of the channel results in the loss of these corrections and the conductance decreases as T^2 , and a positive magnetoresistance is found. Eventually with even more narrowing a transition to variable range hopping is found.

The samples used were GaAs-AlGaAs heterojunctions, the carrier concentration was $4.0 \times 10^{11} \text{ cm}^{-2}$, and the mobility at 4.2 K was $2 \times 10^5 \text{ cm}^2 \text{ V}^{-1} \text{ sec}^{-1}$. The samples were in the form of Hall bars with Au-Ge-Ni Ohmic contacts. A gold gate of 700-Å thickness was fabricated on the 1500-Å thick AlGaAs with a small gap 15 μm long and 0.6 μm wide between the two halves, as in the inset of Fig. 1. The gates were fabricated by electron-beam lithography with use of PMMA positive resist. By application of a negative voltage to the two gates, the underlying GaAs is depleted of electrons and current flows through the narrow region not covered by gate metal. Further increase in the negative gate voltage results in a reduction in the width of the conducting channel until it is removed. The action of the gate is similar to the squeezing action of the P^+ regions in Si accumulation layers used previously.^{18,19} However, the problem of gate overlap onto source and drain regions (which can give activated conduction at low temperatures) is removed here and the gate voltage now acts to narrow

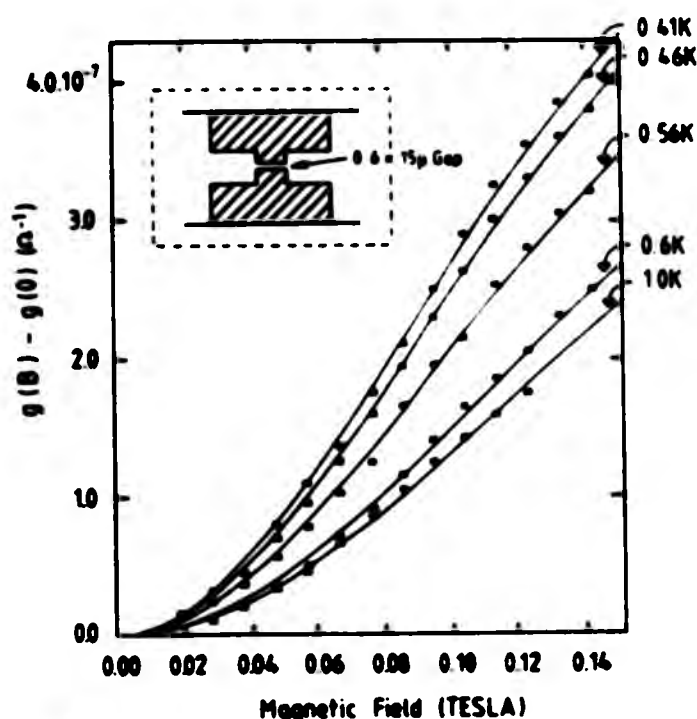


FIG. 1. The values of conductance as a function of magnetic field, indicated by crosses. The lines indicate the best fit of Eq. (2) at each temperature. Inset: The gate defining the narrow channel in the underlying heterojunction.

the conducting channel rather than to offset the squeezing action of the P^+ regions in the metal-oxide-semiconductor device. In the absence of a gate voltage, the device resistance was 700 Ω at 1.3 K, and when the gate voltage was such as to induce the one-dimensional behavior discussed later the device resistance was greater than $10^5 \Omega$. High-magnetic-field Shubnikov-de Haas measurements indicated that the carrier concentration remained constant as the channel width was reduced.

Conductance and magnetoconductance measurements were carried out below 1.2 K. The field across the channel was always less than 1 V/m to avoid electron heating. Figure 1 illustrates the increase in conductance induced by a magnetic field with -1.2 V on the gate. The results of Fig. 1 did not fit the 2D expression²⁰ whereas an excellent fit was obtained by use of Eq. (2). We note that it is not necessary to introduce spin-orbit coupling into the theoretical expression in order to obtain agreement with theory. In 2D the spin-orbit coupling in GaAs heterojunctions is only significant at very low temperatures and very low magnetic fields.²¹ Analysis of a number of temperatures between 1.0 and 0.4 K yielded a constant value for the width of the conducting channel of $450 \text{ \AA} \pm 10\%$ and a temperature-dependent L_0 which is plotted in Fig. 2; this figure will be discussed later.

From the values of L_0 in Fig. 2, it is possible to obtain the value of δG due to quantum interference [Eq. (1)]. This was always small compared to G , having a maximum value of just over 20% at 0.41 K. In order to investigate the correction due to the electron-electron interaction we have added δg to the conductance g for each temperature and plotted the resultant value against $T^{-1/2}$, as shown in Fig. 3. A linear relation is

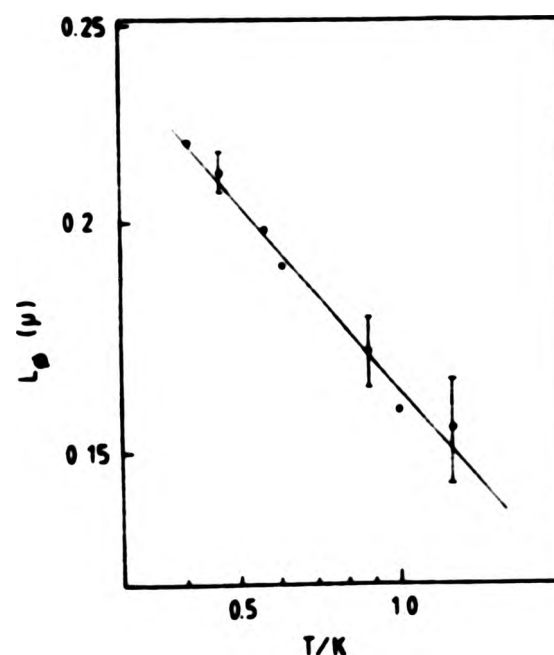


FIG. 2. The phase relaxation length plotted against temperature on a log-log scale.

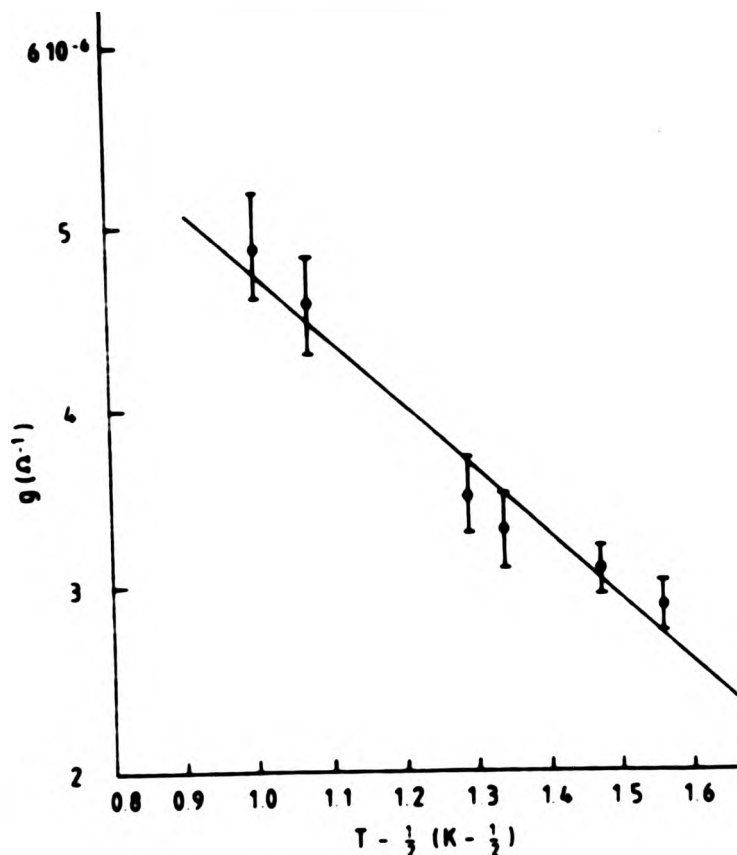


FIG. 3. The conductance after addition of the quantum-interference correction, plotted against $T^{-1/2}$.

found which gives a value of D of $660 \text{ cm}^2 \cdot \text{sec}^{-1}$ for an interaction parameter of 1.35 appropriate to this carrier concentration.¹³ If we assume the two-dimensional density of states for GaAs, this Boltzmann value of D gives a value of $g_B \approx 8.9 \times 10^{-6} \Omega^{-1}$ for a value of width of conducting channel of 450 Å. This is in satisfactory agreement with the value of $8.3 \times 10^{-6} \Omega^{-1}$ derived by extrapolation to zero $T^{-1/2}$. At all values of temperature the interaction length scale, $(\hbar D/kT)^{1/2}$, is considerably greater than the sample width. However, it is surprising that the $T^{-1/2}$ law is found for such large changes in conductance. The values of magnetic field were such that $g\mu B < kT$ and the interaction correction was not significantly enhanced.

We now consider the temperature dependence of the inelastic length shown in Fig. 2. The power of temperature for the best fit is -0.35 ± 0.06 which agrees with recent predictions that in 1D the dominant scattering of electrons is a low-energy process arising from electromagnetic fluctuations.¹⁵⁻¹⁷ The fluctuations dominate over the disorder correction unlike the 2D situation where the disorder correction is strong giving a T^{-1} dependence of the phase relaxation time.²² Altshuler *et al.* predict a phase relaxation length L_0 given by¹⁵

$$L_0 = (DgL\hbar^2/2e^2kT)^{1/3}, \quad (4)$$

where L is the sample length. If we assume the Boltzmann values of D and g derived from the inter-

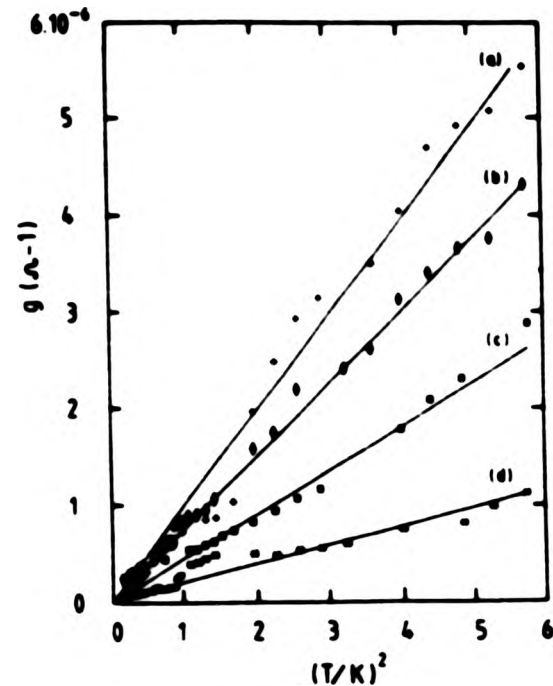


FIG. 4. The conductance for a number of gate voltages plotted against T^2 . (a) $V_g = -1.210$, (b) $V_g = -1.215$, (c) $V_g = -1.220$, (d) $V_g = -1.225$. The error in g is approximately 5%.

action behavior, Eq. (4) predicts that $L_0 = 5.6 \times 10^{-5} T^{-1/3} \text{ cm}$ in reasonable agreement with the experimental result of $1.6 \times 10^{-5} T^{-1/3} \text{ cm}$.

Decreasing the gate voltage in steps of 0.02 V resulted in the introduction of a strong temperature dependence as shown in Fig. 4. These results are consistent with the T^2 behavior discussed earlier. A further feature of this regime was a strong positive magnetoresistance at low fields, of magnitude 30% for $B = 0.1 \text{ T}$. This behavior may indicate that a shrinkage of the wave function is lowering the conductance. Further reduction in the channel width results in hopping with an exponential dependence on temperature, i.e., phonon-assisted hopping. However, the experimental range was too limited for us to establish the precise power of temperature.²³ It is seen from Fig. 4 that the conductance shows oscillations about the T^2 line. We do not have an explanation for this but, in a similar manner to oscillations which occur as a function of carrier concentration, the effect may be related to the small number of conducting electrons $[N(E_F)kTLW]$. At the lowest temperatures this number can be of the order of unity.

In conclusion, these results show that the magnetic separation of quantum interference and interaction corrections can be achieved in 1D as well as 2D.²⁴⁻²⁶ We have also found the existence of a recently predicted mechanism of electron phase relaxation and the transition from diffusive transport to hopping.

This work was supported by the Science and Engineering Research Council and in part by the European Research Office of the U.S. Army. One of us

(T.J.T.) acknowledges a CASE studentship with GEC. We have enjoyed many discussions on this topic with Professor Sir Nevill Mott, K.-F. Berggren, M. Kaveh, D. J. Thouless, Dr. C. C. Dean, D. J. Newson, C. G. Smith, and R. P. Upstone. Two of us (D.A. and G.J.D.) thank the Director of Research of British Telecom Research Laboratories for permission to publish this paper.

-
- ¹J. C. Licini, G. J. Dolan, and D. J. Bishop, *Phys. Rev. Lett.* **54**, 1585 (1985).
- ²K. K. Choi, D. C. Tsui, and S. C. Palmateer, *Phys. Rev. B* **32**, 5540 (1985).
- ³P. Santhanau, S. Wind, and D. E. Prober, *Phys. Rev. Lett.* **53**, 1179 (1984).
- ⁴M. Laviro, P. Averbuch, H. Godfrin, and R. E. Rapp, *J. Phys. (Paris) Lett.* **44**, L1021 (1983).
- ⁵R. G. Wheeler, K. K. Choi, A. Goel, R. Wisnieff, and D. E. Prober, *Phys. Rev. Lett.* **49**, 1674 (1982).
- ⁶M. Kaveh, *J. Phys. C* **18**, 4165 (1985).
- ⁷D. J. Thouless, *Solid State Commun.* **34**, 683 (1980).
- ⁸B. Movaghar, to be published.
- ⁹B. L. Altshuler and A. G. Aranov, *Pis'ma Zh. Eksp. Teor. Fiz. [JETP Lett.]* **33**, 499 (1981).
- ¹⁰C. McFadden, D. J. Newson, M. Pepper, and N. J. Mason, *J. Phys. C* **18**, L383 (1985).
- ¹¹P. Santhanam, S. Wind, and D. E. Prober, *Phys. Rev. Lett.* **53**, 1179 (1984).
- ¹²K. K. Choi, D. C. Tsui, and S. C. Palmateer, to be published.
- ¹³B. L. Altshuler and A. G. Aranov, *Solid State Commun.* **46**, 429 (1983).
- ¹⁴P. A. Lee and T. V. Ramakrishnar, *Rev. Mod. Phys.* **57**, 287 (1985).
- ¹⁵B. L. Altshuler, A. G. Aranov, and D. E. Khyelnitsky, *J. Phys. C* **15**, 7367 (1982).
- ¹⁶E. L. Altshuler, B. L. Altshuler, and A. G. Aranov, *Solid State Commun.* **54**, 617 (1985).
- ¹⁷W. Eiler, *J. Low Temp. Phys.* **56**, 481 (1984).
- ¹⁸C. C. Dean and M. Pepper, *J. Phys. C* **17**, 5663 (1984).
- ¹⁹C. C. Dean and M. Pepper, *J. Phys. C* **15**, L1287 (1982).
- ²⁰S. Hikami, A. I. Larkin, and Y. Nagaoka, *Prog. Theor. Phys.* **63**, 707 (1980).
- ²¹S. Kawaji, K. Kuboki, H. Shigeno, T. Naibu, and J. Wakabayashi, in *Proceedings of the Seventeenth International Conference on the Physics of Semiconductors*, edited by D. J. Chadi and W. A. Harrison (Springer, New York, 1985), p. 413.
- ²²R. A. Davies and M. Pepper, *J. Phys. C* **16**, L353 (1983).
- ²³A. B. Fowler, A. Hartstein, and R. A. Webb, *Phys. Rev. Lett.* **48**, 196 (1982).
- ²⁴M. J. Uren, R. A. Davies, and M. Pepper, *J. Phys. C* **13**, L985 (1980).
- ²⁵M. J. Uren, R. A. Davies, M. Kaveh, and M. Pepper, *J. Phys. C* **14**, 5737 (1981).
- ²⁶D. J. Bishop, R. C. Dynes, and D. C. Tsui, *Phys. Rev. B* **26**, 773 (1982).

LETTER TO THE EDITOR

Frequency-enhanced fractional quantisation in GaAs-GaAlAs heterojunctions

C McFadden†, A P Long†, H W Myron‡, M Peppert§, D Andrews|| and G J Davies||

† Cavendish Laboratory, University of Cambridge, Madingley Road, Cambridge CB3 0HE, UK

‡ Physics Department, University of Nijmegen, Netherlands

§ G E C Hirst Research Centre, Wembley, Middlesex

|| British Telecom Research Centre, Martlesham Heath, Ipswich

Received 23 March 1984

Abstract. We report the observation of fractional quantisation obtained by increasing the frequency of measurement; this is found up to a Landau index of 10. The result is coincident with the suppression of integer quantisation and is interpreted as indicating a transition from a liquid state to a solid state behaviour as the time scale of measurement is reduced.

Previous work has established that varying the frequency of measurement has a pronounced effect on the measurement of the quantum Hall effect (QHE) (Pepper and Wakabayashi 1983, Wakabayashi *et al* 1983, Long *et al* 1984). This arises from the QHE being a manifestation of localisation in the Landau level. If states at the centre of the level are weakly localised, plateaux of quantum Hall resistance are not found at DC. However, if the frequency of measurement is increased, then when the amplitude of the drift path of the centre of the orbit is less than the localisation length, the plateaux of quantised Hall resistance become apparent. The frequency-aided delocalisation occurs first at the centre of the Landau level where localisation is weakest. Further increase in frequency delocalises states in the tails of the Landau levels, thus destroying a necessary condition for the observation of the QHE. The exact increase in frequency necessary for the observation of this effect depends on the localisation length, i.e. disorder, and hence will be sample-dependent. Previous work (Pepper and Wakabayashi 1983) has indicated that the maximum observable localisation length is the sample length, which acts as a cut-off. The previous work showed that increasing the frequency removed the plateau by delocalising tail states, and the quantised value was only found when E_t was between empty and full Landau levels—the condition for the quantisation in the absence of localisation. The essential feature of the 'frequency effect' is that when the sample is in the plateau condition the velocity of the centre of the orbit is eF/B , where F is the electric field and B is the magnetic field. However, if a number of carriers are localised then the velocity is correspondingly increased to maintain the quantisation of Hall resistance; this can result in a considerable increase in the velocity as a substantial proportion of the carriers can be localised. In the samples used in our experiments, the degree of localisation was such that the velocity enhancement was not more than a factor of three. A

typical velocity of electrons in the plateau of the ground Landau level is 10^2 cm s^{-1} , at a frequency of 10 MHz; this gives a drift length of 150 \AA . In the tails of the levels, rough estimates of the diffusivity D suggest that the diffusion length in a frequency ω can be decreased considerably using the MHz region of frequencies. This is particularly effective as the localisation lengths are long. Accordingly we would expect the AC conductivity to be less dependent on scattering and disorder and be more dependent on the electron-electron interaction than it would under DC conditions. We therefore investigated the possibility of using the effect of frequency to observe the fractional quantum Hall effect (Tsui *et al* 1982, Stormer *et al* 1983, Laughlin 1983).

The samples used in this experiment were MBE-grown modulation-doped GaAs-GaAlAs heterojunctions in the form of gated Hall bars, 1.9 mm long and 0.2 mm wide. The mobility μ and carrier concentration n_s could be continuously varied between $120000 \text{ cm}^2 \text{ V}^{-1} \text{ s}^{-1}$ at $n_s = 5 \times 10^{11} \text{ e}^- \text{ cm}^{-2}$ and $50000 \text{ cm}^2 \text{ V}^{-1} \text{ s}^{-1}$ at $n_s = 2.7 \times 10^{11} \text{ e}^- \text{ cm}^{-2}$. Lock-in techniques were used to measure only the in-phase component of current from a matched current monitoring resistor and the two-terminal

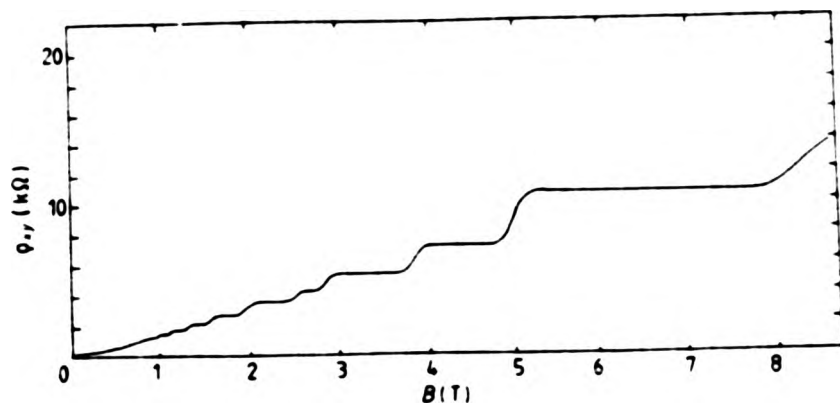


Figure 1. The quantum Hall effect (ρ_{xx} versus B) at $f = 80 \text{ Hz}$, $T = 280 \text{ mK}$, $V_g = -0.2 \text{ V}$.

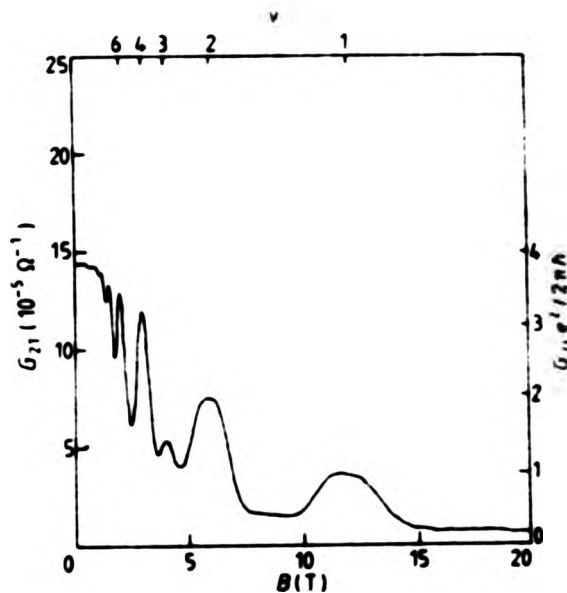


Figure 2. The two-terminal conductance G_{2T} versus magnetic field at $f = 80 \text{ Hz}$, $T = 1.4 \text{ K}$, $V_g = +0.2 \text{ V}$. The Landau level filling factor ν is shown on the top scale whilst the expected values of G_{2T} are shown on the right-hand side.

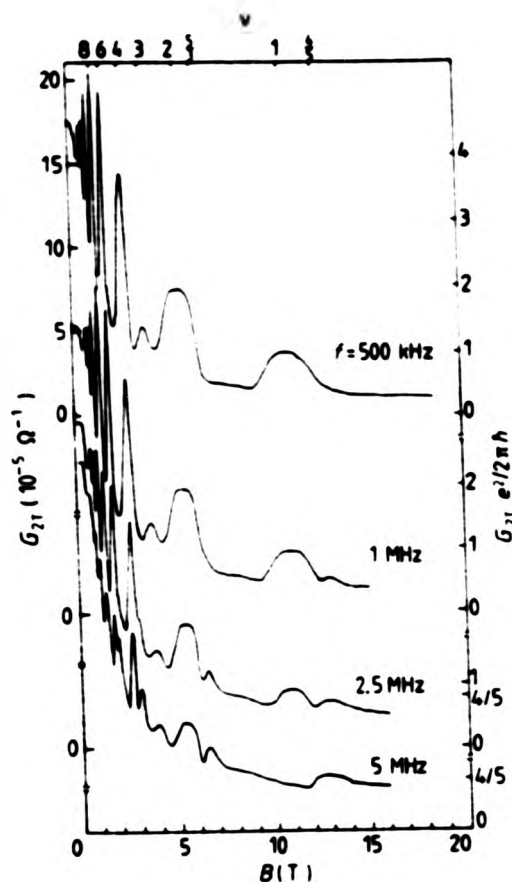


Figure 3. The two-terminal conductance G_{2T} versus magnetic field at $T = 1.4$ K, $V_g = 0.0$ V and $f = 500$ kHz to 5 MHz. $n_s = 2.7 \times 10^{11}$ cm $^{-2}$ and $\mu = 5.5$ m 2 V $^{-1}$ s $^{-1}$. The Landau level filling factor ν is shown on the top scale whilst the expected values of G_{2T} are shown in multiples of $e^2/2\pi h$.

conductance method of measurement was used (Fang and Stiles 1983, Powell *et al* 1984). Our method of measurement eliminated the role of gate capacitance but we experienced cable loss; here we compensated for the loss at those frequencies where it occurred. The frequency-dependent magnetoconductance oscillations were measured at $T = 1.4$ K in fields up to 20 T.

An example of the DC quantum Hall effect obtained at 280 mK is shown in figure 1. As seen, the integer plateaux are very broad down to $i = 2$; the field available was not high enough to observe the $i = 1$ plateau. Figure 2 shows the high-field two-terminal conductance obtained at 1.4 K and 80 Hz. Here the $i = 1$ and 2 plateaux are observable but the higher temperature prevents a clear plateau for $i = 3$, which is a spin-split state. In figure 2 we have indicated the expected positions of the plateaux and it is clear that there is no additional structure. Figure 3 shows G_{2T} plotted against magnetic field for frequencies up to 5 MHz. At frequencies up to 1 MHz the $i = 1$ and $i = 2$ plateaux have their expected values and additional structure appears at a filling factor $\nu = \frac{1}{2}$. With further increase in frequency the $i = 2$ plateau remains flat up to 2.5 MHz but falls in value. This is due to cable loss and we find that the loss increases linearly with frequency and can be modelled by a parasitic capacitance of 0.8 pF. This enables us to extract the two-terminal device conductance G_{2T} . It is clear the fractional quantisation is present at filling factors $\nu = \frac{1}{2}$ and $\nu = \frac{3}{2}$, the structure at $\frac{1}{2}$ being a plateau at the correct value of conductance at 5 MHz. A distinct feature of the result is the collapse of the $i = 1$ integer

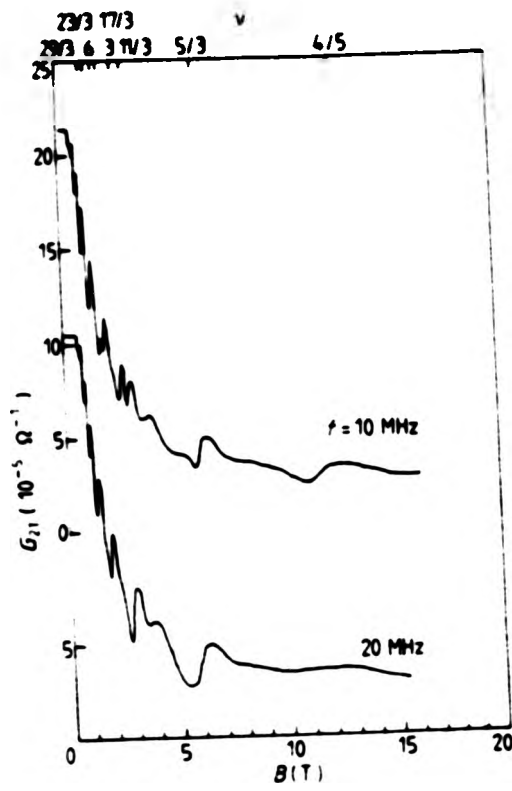


Figure 4. The two-terminal conductance G_{2T} versus magnetic field at $T = 1.4$ K, $V_g = 0.0$ V and $f = 10$ and 20 MHz. The Landau level filling factors ν are shown on the top scale.

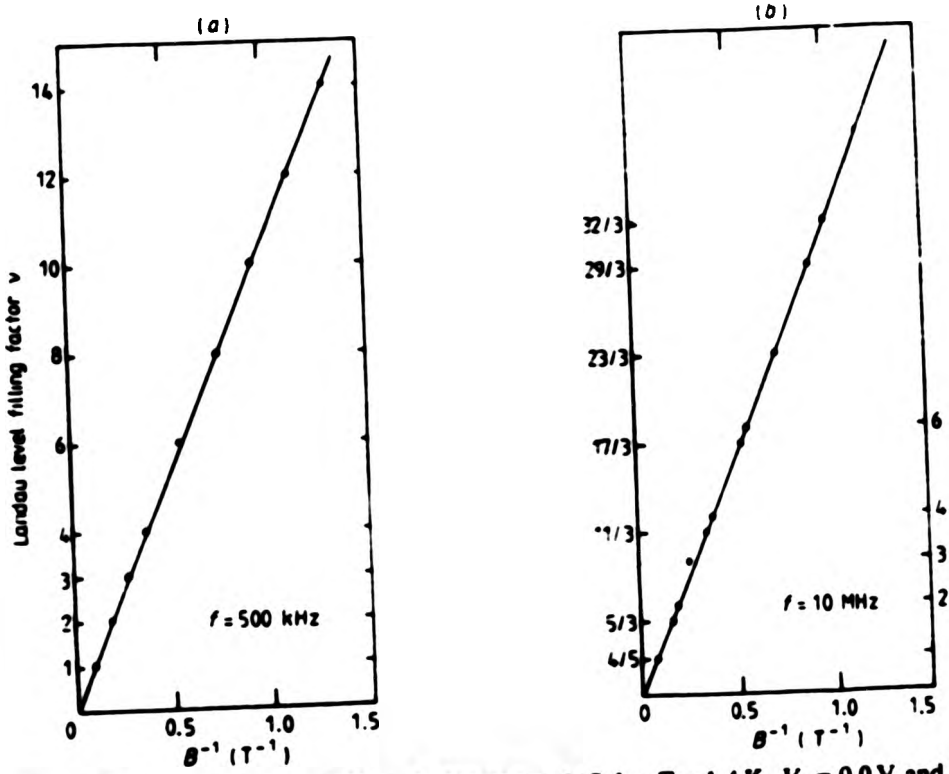


Figure 5. The Landau level filling factor versus $1/B$ for $T = 1.4$ K, $V_g = 0.0$ V and $f = 500$ kHz (a) and $f = 10$ MHz (b).

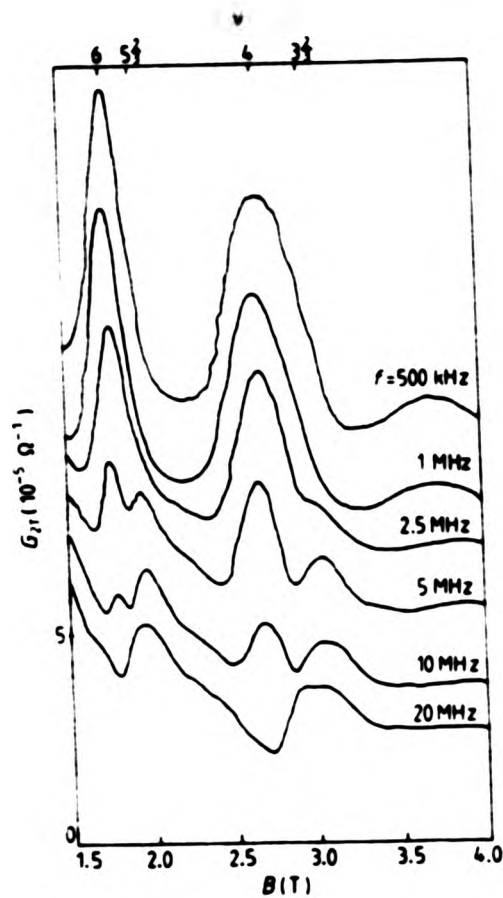


Figure 6. The two-terminal conductance versus magnetic field between 1.5 and 4.0 T indicates the emergence of the $\frac{5}{2}$ and $\frac{3}{2}$ peaks and the coincident suppression of the integer peaks $i = 6$ and $i = 4$. The graphs have been offset for clarity; for exact values refer to figures 3 and 4

plateau; this has disappeared at 5 MHz and becomes a minimum at higher frequencies. At frequencies higher than 2.5 MHz the $i = 2$ plateau starts to disappear and becomes a minimum. At 10 MHz there is evidence of further structure (figure 4) but this is not analysed here. Increasing the frequency to 20 MHz results in a pronounced minimum at $i = 2$; appreciable loss was found at this frequency preventing analysis of lower-order structure.

The frequency was found to have a pronounced effect on higher-order Landau levels. The principal structure was always at the $\frac{3}{2}$ filling factors and this was apparent up to $\nu = \frac{3}{2}$ which occurred at a magnetic field of 1 T. Figures 5(a) and (b) show the Landau level indexation at frequencies of 500 kHz and 10 MHz. It is seen that at low frequencies only integer quantisation is present but at higher frequencies the fractions are dominant. It is noticeable that when an integer peak appears strongly localised, and does not reach a quantised value at low frequency, it is not significantly affected by frequency and persists when other integers have disappeared. This is most pronounced for odd integers, which being spin-split are the weakest, and is exemplified by the persistence of the $i = 3$ peak. Figure 6 illustrates the progressive decline of the $i = 4$ and 6 integer peaks and the appearance of the $\frac{5}{2}$ and $\frac{3}{2}$ peaks.

We have investigated these effects as a function of carrier concentration n_s , which is varied by the gate voltage. The enhancement of the fractions and decrease of the integer peaks by frequency is most pronounced as n_s decreases; this is despite the decrease in

mobility. Presumably the frequency is minimising the disorder element and the reduction in n_s is increasing the relative importance of the interaction for a given filling factor.

We now turn to a discussion of the main points of this work, namely the frequency-induced appearance and enhancement of the fractional quantisation and coincident decrease and collapse of integer quantisation. The essential feature of the experiment is that the diffusion length of the electrons is smaller than the localisation length. The drift length of the extended electrons is small and we therefore remove the role of localisation lengths greater than this. We expect, as in Si, the conversion of the quantised plateau to a peak as frequency is increased. However, the results go beyond this and the integer quantisation disappears and then becomes a minimum. We conclude that this is the result of electron interactions which are also producing the fractional quantisation. The frequency is enhancing the liquid state and the interaction. Our measurement is monitoring the response of the electrons over a short period of time ($1/\omega$) and it appears as if the entire Landau level does not conduct for very short intervals of time (10^{-8} s). The observation of an insulating state when the time is short suggests that when E_f is between Landau levels the system behaves as a pinned solid and is an insulator. As the time increases the liquid state becomes apparent, giving conduction, and the integer quantisation reappears. It is the liquid motion itself which gives diffusion and conduction.

We therefore conclude that at very short intervals of time, or insignificant disorder, conventional (integer Landau level) magnetic quantisation will not be observed. The only quantisation apparent will be at fractional values and transport is totally dominated by mutual interactions of electrons.

The results suggest that in any Landau level the interaction increases as the filling factor increases. Thus the integer disappears and the $\frac{1}{2}$ occupancy is favoured over $\frac{1}{3}$ etc. There is a complicated relation between disorder, interactions and frequency. The disorder and localisation give a plateau based on the interaction-induced fractional gap. Increasing the frequency enhances the gap, but also minimises the plateau by reducing the disorder-induced localisation. Therefore we expect the system will behave as a solid at sufficiently high frequencies and for all values of carrier concentration.

We have enjoyed many discussions with Dr J Wakabayashi and Dr D Woods. This work was supported by SERC and in part by the European Research Office of the US Army. We acknowledge a NATO travel grant. C McFadden and A P Long acknowledge SERC grants. C McFadden also acknowledges a GEC (CASE) studentship. We are grateful to the technical staff of the High Magnetic Field Laboratory, University of Nijmegen for their assistance.

References

- Fang F F and Stiles P J 1983 *Phys. Rev. B* **27** 6487
 Laughlin R B 1983 *Phys. Rev. Lett.* **50** 1395
 Long A P, Myron H and Pepper M 1984 *J. Phys. C: Solid State Phys.* **17** L433-8
 Pepper M and Wakabayashi J 1983 *J. Phys. C: Solid State Phys.* **16** L113-7
 Powell T, Dean C C and Pepper M 1984 *J. Phys. C: Solid State Phys.* **17** L359-64
 Störmer H L, Chang A, Tsui D C, Hwang J C, Gossard A C and Weigmann W 1983 *Phys. Rev. Lett.* **50** 1953-5
 Tsui D C, Störmer H L and Gossard A C 1982 *Phys. Rev. Lett.* **48** 1159
 Wakabayashi J, Myron H and Pepper M 1983 *Physica* **117B**, **118B** 691-3

Attention is drawn to the fact that the copyright of this thesis rests with its author.

This copy of the thesis has been supplied on condition that anyone who consults it is understood to recognise that its copyright rests with its author and that no quotation from the thesis and no information derived from it may be published without the author's prior written consent.

D75209/87

END